UNIVERSITÀ
DEGLI STUDI
DI PADOVA

UNIVERSITA' DEGLI STUDI DI PADOVA

DIPARTIMENTO DI BIOLOGIA

SCUOLA DI DOTTORATO DI RICERCA IN BIOSCIENZE E BIOTECNOLOGIE

INDIRIZZO: BIOTECNOLOGIE

CICLO XXV

microRNAs and breast cancer: a genomic study reveals miR-148b as a major coordinator of tumor progression

Direttore della Scuola: Ch.mo Prof. Giuseppe Zanotti

Coordinatore d'indirizzo: Ch.mo Prof. Giorgio Valle

Supervisore: Ch.mo Prof. Gerolamo Lanfranchi

Dottorando: Cristiano De Pittà

INDEX

ABSTRACT

Abstract

Breast cancer is a multistep disease controlled by a wide spectrum of genetic and epigenetic changes occurring within a cell as well as environmental influences; and it is the most common malignancy in women worldwide, often fatal because of metastasis dissemination. Aberrant miRNA expression can influence several gene networks and pathways implicated in tumorigenesis and metastasis formation.

To unravel the role of miRNAs during breast cancer progression we investigated miRNA expression in 77 ductal breast carcinoma biopsies and 17 mammoplasties by microarray analysis. Sixteen differentially expressed miRNAs were identified comparing patients with or without disease relapse, within 72 months from surgery. This signature correlates with survival and/or distinguishes tumor subtypes in different datasets.

Among them, miR-148b, down-regulated in aggressive breast tumors, was found to be a major coordinator of malignancy. In fact, it is able to oppose various steps of tumor progression when overexpressed in cell lines by influencing invasion, survival to *anoikis*, extravasation, lung metastasis formation, and chemotherapy response. miR-148b controls malignancy by coordinating a novel pathway involving over 130 genes and, in particular, it directly targets players of the integrin signaling, such as ITGA5, ROCK1, PIK3CA/p110α, and NRAS, as well as CSF1, a growth factor for stroma cells.

Our findings reveal the importance of the identified 16 miRNAs for disease outcome predictions and suggest a critical role for miR-148b in the control of breast cancer progression.

RIASSUNTO

Il tumore al seno è una malattia multifattoriale controllata sia da un ampio spettro di variazioni genetiche ed epigenetiche che si verificano all'interno di una cellula, sia da fattori ambientali. E' sicuramente la neoplasia più diffusa tra le donne di tutto il mondo ed è spesso fatale a causa della diffusione metastatica. Recentemente è emerso che l'espressione aberrante dei miRNA può influenzare il comportamento di diverse reti genetiche e *pathway* biologici implicati nel processo tumorigenico e nella formazione di metastasi.

Per meglio comprendere il ruolo dei miRNA, durante la progressione tumorale, abbiamo definito il loro profilo trascrizionale, utilizzando una piattaforma *microarray*, in settantasette pazienti affetti da carcinoma mammario duttale e diciassette mammoplastie (controlli sani). Abbiamo identificato sedici miRNA differenzialmente espressi in grado di discriminare i pazienti che presentano, o meno, recidiva dopo 72 mesi dall'intervento chirurgico. E' interessante notare come l'espressione di questo gruppo di miRNA correla con la sopravvivenza dei pazienti e sia in grado di distinguere sottotipi tumorali in altri *dataset* di espressione.

All'interno di questo gruppo è stato identificato il miR-148b, sottoespresso nei pazienti con prognosi più infausta, che si è dimostrato essere uno dei principali coordinatori del processo metastatico. In particolare questo miRNA, una volta sovraespresso nelle linee cellulari, è in grado di bloccare la formazione di metastasi influenzando l'invasività, la sopravvivenza delle cellule tumorali nel torrente circolatorio (*anoikis*), la fuoriuscita dai vasi sanguigni, la formazione di metastasi polmonari e la risposta alla chemioterapia. Abbiamo dimostrato che il miR-148b coordina l'azione di 130 geni e, in particolare, regola direttamente l'espressione di vari membri della via di segnalazione mediata dalle integrine tra cui ITGA5, ROCK1, PIK3CA/p110α e NRAS, così come CSF1, che è un fattore di crescita delle cellule stromali.

I nostri dati dimostrano il valore prognostico dei 16 miRNA identificati e suggeriscono un ruolo critico del miR-148b nel controllo del processo metastatico in pazienti affetti da carcinoma mammario.

1. INTRODUCTION

1.1 Breast cancer biology and classification

Breast cancer is a heterogeneous disease characterized by a collection of breast tumor subtypes that have diverse histopathologies, genetic and genomic variations, and clinical outcomes [Bertucci & Birnbaum, 2008, Vargo-Gogola & Rosen, 2007]. It is the most common malignancy in women worldwide, often fatal because of metastasis dissemination [Jemal *et al.*, 2010]. The transformation of breast epithelial cells in a metastatic breast cancer is due to epigenetic and genetic changes and aberrant interactions within the microenvironment such as described in Figure 1. During this multistage process, control of proliferation, survival, differentiation and migration become deregulated, and aberrant tumor–stromal cell interactions facilitate this process (Figure 1).

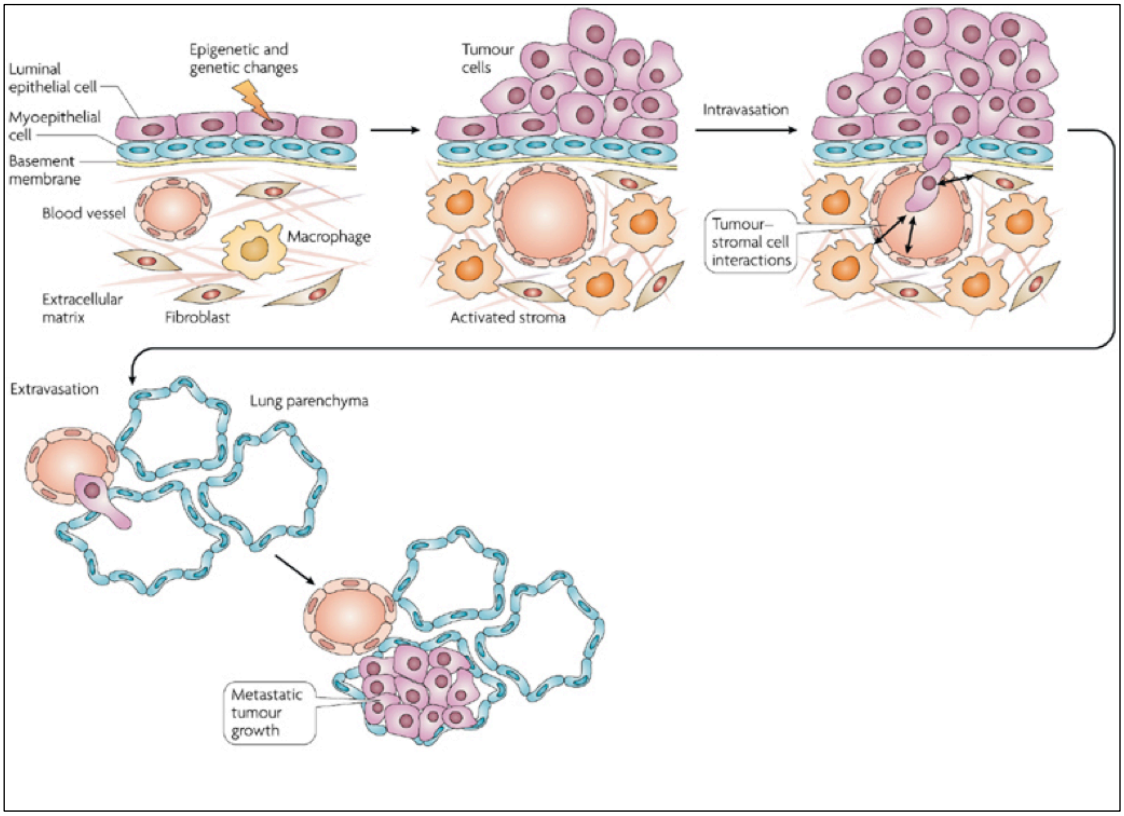

Figure 1. Schematic representation of the breast cancer formation and progression. In order to form metastases, cancer cells must invade the basement membrane, enter the vasculature (intravasate), survive in the absence of adhesion, exit the vasculature (extravasate) and establish a new tumour in a foreign microenvironment (Reprinted and modified from Vargo-Gogola & Rosen, 2007).

Fortunately, the mortality is decreasing in most western countries, because of mass mammography screening, frequent use of post-surgery chemotherapy and/or hormone therapy and the recent introduction of new drugs [Siegel *et al*., 2012].

Clinical and pathological parameters, including tumor size, lymph node involvement, histological grade and age [Dunnwald *et al.*, 2007], are routinely employed to categorize patients with breast tumors in order to assess prognosis and to determine the appropriate therapy. The additional use of molecular tumor markers, such as the receptors for estrogens (ER) and progesterone (PR) or the ERBB2 gene, significantly enhances the ability to stratify patients according to risk and better allows the appropriate therapy tailoring [Colozza *et al*., 2005]. The HER2 gene (ErbB2, commonly referred to as HER2/*neu*) is a newer biological marker routinely tested in all breast cancer tumors [Harris *et al*., 2007; Harari & Yarden, 2000].

The combination of morphological and molecular markers provides better clinical results than the use of single approaches. The combination of these two methodologies has been successfully applied to group patients in different categories of risk such as the St. Gallen criteria [Goldhirsch *et al*., 2009], the NIH consensus criteria [Eifel *et al*., 2000] the Nottingham Prognostic Index [Galea *et al*., 1992]. However, since patients with similar combinations of features may often have different clinical outcomes, it is necessary to identify new ways to classify the disease.

In recent years, protein-coding gene expression profiles have been used to improve breast cancer classification allowing to identify at least five subtypes of invasive ductal carcinoma that constitute approximately 80% of all breast cancers: Luminal A and Luminal B (both estrogen receptor positive, ER+); Basal (ER-); ERBB2 (HER2 overexpressing); and normal-like [Sorlie *et al*, 2001]. Specific clinical features, responses to treatment and prognosis have been observed to correspond to the various subgroups in agreement with the concept that breast cancer is not a single disease. Furthermore, the expression of certain gene sets, defined as “signatures”, appeared to have a prognostic and/or predictive role for patients [Sotiriou & Piccart, 2007]. Interestingly, microarray expression profiling of the tumor-associated stroma derived from breast cancer patients reveals characteristic expression signatures associated with metastatic outcome demonstrating the critical roles of stromal cells in enabling the malignant behavior of carcinoma cells [Finak *et al*., 2008].

Recently many studies have demonstrated the central role of microRNAs (miRNAs) in the establishment and progression of human tumors. A pioneering investigation for miRNA levels in human tumors showed that miRNA expression, which is globally downregulated in tumours compared to normal tissues, could classify human cancers more accurately than mRNA expression profiles, according to developmental lineage and differentiation status [Lu *et al.*, 2005].

1.2 miRNA definition, biogenesis and mechanism of action

miRNAs are a class of small non-coding RNAs (~22 nucleotides (nt) in length) that negatively regulate protein-coding gene expression post-transcriptionally by targeting mRNAs, mostly at the 3′ untranslated region (3′-UTR), and triggering either translational repression or RNA degradation [Bartel, 2004; Bartel, 2009]. MicroRNA genes represent approximately 1% of the genome of different species, and each of them has hundreds of different conserved or non-conserved targets. It has been estimated that about 30% of the genes are regulated by at least one microRNA. According to their genomic localization, microRNAs can be classified in: exonic microRNAs located in non-coding transcripts, intronic microRNAs located in non coding transcripts, and intronic microRNA located in protein-coding trancripts [Kim & Nam, 2006].

MicroRNAs are transcribed, by RNA polymerase II, as long primary transcripts characterized by hairpin structures (pri-microRNAs) and containing typical mRNA features such as cap structures and poly(A) tail. The pri-microRNAs are processed in the nucleus by RNAse III enzyme, Drosha, and the double-stranded-RNA-binding protein, Pasha, into 70-100-nucleotide pre-miRNAs, which fold into imperfect stem-loop structures. These nucleotide hairpin pre-miRNA precursors are exported into the cytoplasm by the RAN GTP-dependent transporter exportin5 and undergo further processing by another RNAse III enzyme, Dicer, which leads to the formation of a 22-nucleotide miRNA duplex that is incorporated into the multiprotein/RNA complex called "Multiprotein RNA-Induced-Silencing Complex" (RISC) (Figure 2) [Kim *et al*., 2009]. According to thermodynamic properties, one strand of the duplex, named miRNA* species (star miRNA; many publications refer to the two strand pair as miRNA-3p/miRNA-5p, referring to the direction of the functional miRNA), gets degraded whereas the other strand represents the mature miRNA and negatively regulates its target genes through partial complementarity (2-8 nt, “seed region”) to the

3'-UTR [Filipowicz *et al*., 2008]. However increasing evidence points to essential roles for star-microRNAs (miRNA*), which are usually expressed at much lower levels respect to mature miRNAs [Bhayani *et al*., 2012; Mah *et al*., 2010].

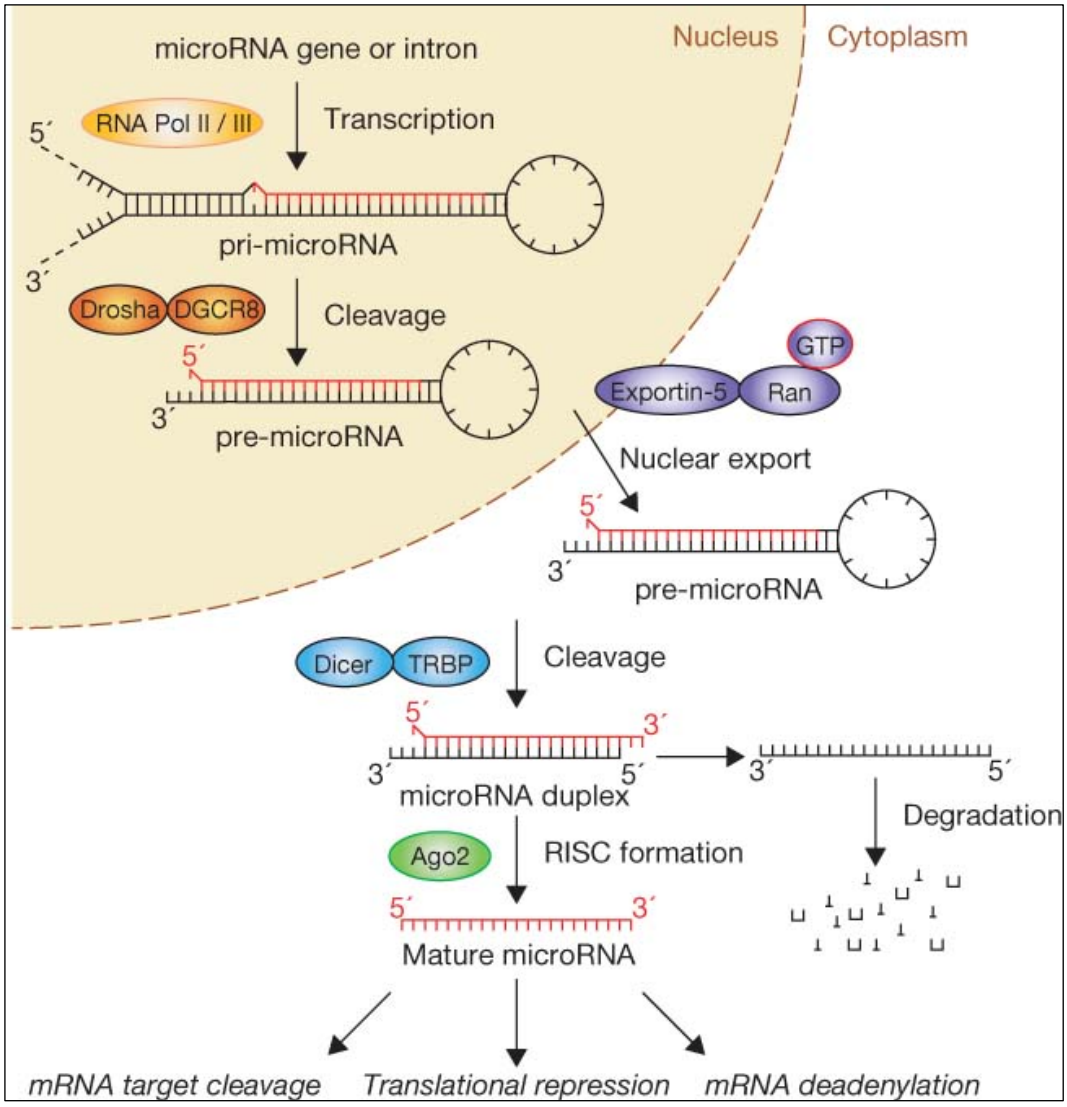

Figure 2. Biogenesis and mechanism of action of miRNAs. (Reprinted from Winter *et al*., 2009)

1.3 miRNAs biological role and expression

miRNAs have a primary impact on animal development and clearly animals cannot live without miRNAs [Alvarez-Garcia & Miska, 2005]. MicroRNAs are further implicated in a variety of important biological processes including differentiation [Landgraf *et al*., 2007], apoptosis [Leonardo *et al*., 2012], fat metabolism [Poy *et al*., 2007], viral infection [Stern-Ginossar *et al*., 2007] and pathological processes, such as tumorigenesis [Voorhoeve & Agami, 2006; Wiemer, 2007; Cho, 2007; Zhang et *al*., 2007; Hammond, 2007]. Since a single miRNA can pleiotropically influence the expression of multiple genes, miRNAs have obvious diagnostic value, as showed for tumour classification [Calin *et al*., 2005; Subramanian *et al*., 2008]. The first evidence of the involvement of miRNAs in human cancer derives from analysis of the 13q14 deletion in human chronic lymphocytic leukemia (CLL) which revealed that the only genes present within the deleted region where two miRNAs, miR-15a and miR-16-1. The same genes were found to be down regulated in 50% to 60% of human CLL [Calin *et al*., 2002].

The first study describing a microRNA signature of breast carcinoma was published in 2005. The authors have identified 13 microRNAs able to discriminate tumors and normal tissues with an accuracy of 100%. Recent studies demonstrated that breast cancers can be classified into specific tumor pathological phenotypes (ER, PR, proliferation, stage, metastasis, ERBB2) as well as subtypes (Luminal A or B, Basal-like, ERBB2+ and Normal-like) based on their miRNA expression profiles [Blenkiron *et al.*, 2007; Enerly *et al*., 2011]. Thus, it seems essential to combine miRNA and protein-coding gene expression analyses to obtain information for prognosis and cancer treatment.

microRNAs, recently named “metastamiRs”, have been demonstrated to have a crucial role not only in controlling the primary tumor growth by regulating pathways involved in cell cycle and proliferation, but also to be determinant in modulating migration, invasion and the interaction with the microenvironment, mechanisms related to the acquisition of a more aggressive phenotype and promoting the onset of the metastatic process [Hurst *et al*., 2009].

1.4 microRNAs and the Invasion-Metastasis Cascade in breast cancer

Metastases are characterized by a series of successive cell-biology events, which are collectively named the invasion-metastasis cascade. During this process epithelial cells in primary tumors: **1)** invade locally through surrounding extracellular matrix (ECM), **2)** enter into the lumina of blood vessels (intravasation), **3)** disseminate systematically by surviving transport through the blood circulation, **4)** arrest at distant organ sites, **5)** exit the vessel lumina and enter into the parenchyma of distant tissues (extravasation), **6)** survive in these foreign microenvironments in order to form micrometastases, and **7)** reinitiate their proliferative programs at metastatic sites generating macroscopic and clinically detectable neoplastic formations (metastatic colonization) [Valastyan & Weinberg, 2011].

1) Local invasion:

Local invasiveness is the first step in the metastatic process allowing tumor cells, previously well encapsulated in primary tumors, to escape these confines and to invade the surrounding stroma and adjacent normal tissue parenchyma. So, cancer cells have to breach the basement membrane (BM), a specialized ECM that provides a physical barrier between the epithelial and stroma compartments of various tissues (see Figure 1). After the degradation of BM by matrix metalloproteinases (MMP) whose actions are frequently hyper-activated during the malignant progression, cancer cells can invade the stroma as cohesive multicellular units ("collective invasion") or as individual cells via two different programs known as "mesenchymal invasion" and "amoeboid invasion" [Valastyan & Weinberg, 2011]. Interestingly, an important property of breast cancer cells is represented by the dynamic plasticity to interconvert between above described invasion programs.

Numerous miRNAs have been found to affect the local invasiveness of breast cancer cells. For example miR-10b promotes the invasion via suppression of its target HoxD10 and the consequent upregulation of RhoC activity [Valastyan, 2012]. MiR-31 inhibits breast cancer invasion via concomitant suppression of key effectors of both mesenchymal (such as integrin α5) and amoeboid (such as RhoA) invasion programs [Valastyan *et al*., 2009]. MiR-21 is able to inhibit the expression of the MMP antagonist tissue inhibitor of metalloproteinase-3 (TIMP3) enhancing the invasive potential of

breast cancer cells [Song *et al*., 2010]. Conversely, miR-29b can suppress invasiveness through the inhibition of MMP2 expression, while miR-31 can post-transcriptionally suppress MMP16 levels [Valastyan *et al*., 2009].

In order to proceed in the process of stromal invasiveness, cancer cells have acquired a cell-biological program known as epithelial mesenchymal transition (EMT), which involves dissolution of adherent and tight junctions and a loss of cell polarity, dissociates the cells within epithelial cell sheets into individual cells that exhibit multiple mesenchymal attributes, including a great invasiveness. Recently, it has been demonstrated that the miR-200 family regulate EMT programs. MiR-200 members promote an epithelial phenotype suppressing the expression of the ZEB1 and ZEB2 transcription factors, which organize entrance into a mesenchymal state. Acting in the opposite direction, ZEB1 and ZEB2 are also able to transcriptionally repress miR-200 family members, thereby establishing a double-negative-feedback loop that maintains cells into either the epithelial or mesenchymal state [Thiery *et al*., 2009, Korpal & Kang, 2008]. In addition to the miR-200 family, other miRNAs have been found to control the EMT, such as the E-cadherin-targeting miR-9 and the ZEB1- and ZEB2 suppressing miR-205 [Valastyan, 2012]. Furthermore, miR-103/107 family promotes the EMT by suppressing Dicer expression and so dampening the activity of miR-200 family miRNAs [Martello *et al*., 2010].

2) Intravasation:

The term intravasation describes the cellular events that allow locally invasive cancer cells to enter into the lumina of lymphatic or blood vessels. The hematogenous circulation appears to represent the major mechanism by which metastatic carcinoma cells disperse systematically [Valastyan & Weinberg, 2011]. The mechanics of intravasation are likely to be strongly influenced by the structural features of tumor-associated blood vessels. In fact, cancer-associated vessels are tortuous, leaky, and continuously in a state of reconfiguration. The weak interactions between the endothelial cells of tumor-associated microvessels are likely to facilitate intravasation.

Currently, only miR-21 is known to promote intravasation, at least *in vitro* assays, controlling the expression of the programmed cell death-4 (PDCD4). There some evidences that miR-9 expression leads to the activation of vascular endothelial

growth factor (VEGF) signaling, whereas miR-205 antagonizes VEGF-mediated transduction events [Valastyan, 2012].

3) Survival in the circulation:

Once tumor cells have successfully intravasated into the lumina of blood vessels, they are able to disseminate widely through the venous and arterial circulation. Circulating tumor cells (CTC) must survive a variety of stresses in order to reach distant organ sites. For example, in the absence of cellular adhesion to ECM components, epithelial cells are susceptible to a form of apoptotic cell death known as *anoikis*. Furthermore, CTCs are subjected to the damage caused by hemodynamic shear forces and predation by cells of the innate immune system, specifically natural killer cells [Valastyan & Weinberg, 2011].

There are some evidences that miRNAs play an important role in regulating the capacity of CTCs to survive through the vasculature. For example miR31 triggers *anoikis* responses by the suppression of ITGA5, RDX and RhoA and similarly miR-7 controls the expression of EGFR [Webster *et al*., 2009]. Also miR-155, that is a well-characterized controller of immune system responsiveness, could be important in facilitating the dissemination of tumor cells in the systemic circulation [Tili *et al*., 2009].

4) Arrest at distant organ site:

Two alternative models have been proposed to explain how circulating tumor cells decide where to arrest. According to the first model, this arrest is due to the layout of the vasculature and size restrictions imposed by blood vessel diameters. In contrast, the second model considers that CTCs are able to recognize particular distant organ sites thanks to specific ligand-receptor interactions [Valastyan & Weinberg, 2011].

At present, not a single miRNA has yet been described to influence the capacity of CTCs to lodge in the microvessels of distant organ sites.

5) Extravasation:

The term extravasation is defined as the escape of tumor cells from the vessel lumina into the tissue parenchyma of a distant organ. Recently, Taverna's group has elucidated the role of miR-214 during the extravasation step modulating the expression of integrin α3 (ITGA3) and the transcription factor AP2 gamma (TFAP2C) [Penna *et al*., 2011]. A recent study has also demonstrated the involvement of miR-31 in the extravasation process by modulating the expression of ITGA5 and RhoA [Valastyan *et al*., 2009].

6) Micrometastasis formation:

In order to produce micrometastases, extravasated tumor cells have to survive in the new microenvironment that they found in the parenchyma of distant tissues but this microenvironment is very different from that present in the site of primary tumor formation. Indeed, cancer cells must rapidly adapt to this new stroma in order to survive and to produce a new neoplastic formation.

MiRNAs play a fundamental role in controlling the initial survival of cancer cells in the parenchyma of a distant organ. For example the miR-15/16 and miR-34 families modulate the expression of the anti-apoptotic factor B-cell lymphoma-2 (Bcl-2) suppressing aggressive cell behavior.

7) Metastatic colonization:

This process is characterized by the initial survival of disseminated cancer cells as micrometastases and their capacity to generate macroscopic metastatic formations. Metastatic colonization represents a highly organ-specific process that is mainly dependent on the particular microenvironmental context of the distant organ site that the disseminated tumor cells are colonized. Definitely, the metastatic colonization represents the rate-limiting step of the invasion-metastasis cascade because only subpopulations of the neoplastic cells, present within a tumor, possess a self-renewal capability [Valastyan & Weinberg, 2011].

Several miRNAs have been implicated in the regulation of metastatic colonization. For example, it has been demonstrated the anti-metastatic role of miR-31 in breast cancer by modulating the expression of ITGA5 and RDX that are genes

involved in cell survival and proliferation [Valastyan *et al*., 2009]. Similarly, miR-126 arrests the metastatic colonization of breast tumor cells in lung and bone by the disruption of recruitment of endothelial cells to metastatic nodules and the consequent inhibition of neo-angiogenesis process [Png *et al*., 2011]. Furthermore, there are various evidences that the miR-200 family opposes self-renewal in breast cancer cells via the suppression of EMT-controlling transcription factors ZEB1 and ZEB2, but also through modulation of BMI1, Sox2 and Klf4. However, other studies have demonstrated that miR-200 family is able to promote metastatic colonization by the suppression of Sec23a [Valastyan, 2012].

1.5 Therapeutical role of miRNAs

An important consideration in the design of antimetastatic agents is that cancer patients frequently have already significant numbers of disseminated tumor cells, at the diagnosis, in their blood, bone marrow and distant organ sites. Indeed, an effective tumor therapy have to be able of impairing the proliferation and survival of already disseminated cancer cells rather than only trying to block the escape of these cells from primary tumors [Braun *et al*., 2005; Pantel *et al*., 2008, Valastyan & Weinberg, 2011].

For this reason therapeutic agents directed against miRNAs that solely impact initial dissemination events, such as miR-10b antagonists, will only have modest effects on patient outcome respect to agents targeting miRNAs involved in the metastatic colonization [Ma *et al*., 2010]. In fact, recent studies have demonstrated that reactivation of miR-31, which is involved in breast tumor dissemination, leads to a marked metastatic regression in mice. Similarly, reintroduction of miR-15a/16–1 induces apoptosis in leukemic MEG01 cells and inhibits tumor growth *in vivo* in a xenograft model [Calin *et al*., 2008], whereas the inhibition of oncogenic miR-21 with antisense oligonucleotides generates a pro-apoptotic and antiproliferative response *in vitro* in different cellular models, and reduces tumor development and metastatic potential *in vivo* [Si *et al.*, 2007]. Furthermore, microRNAs could also alter the sensitivity to radiotherapy, as recently reported by Slack's group [Weidhaas *et al*., 2007] that used anti-miR-34 as a radiosensitizing agent in p53-mutant breast cancer.

These pre-clinical studies are definitely interesting, but effective delivery and stability into target tissues remains a major technical problem for microRNA-based therapy, including the applications of antagomirs and synthetic microRNA duplexes.

Fortunately, a number of recent technological advances have improve the delivery of relatively stable species of miRNA therapeutical agents, such as chemically modified antimiR oligonucleotides (AMOs), locked nucleic acid (LNA)-oligonucleotides and microRNA sponges, via the bloodstream of mammals [Iorio *et al*., 2011].

1.6 Aim of this work

In our work, we investigated the relationship between altered miRNA expression and breast cancer metastasis by analyzing miRNA levels in a cohort of patients characterized by different disease relapse. We identified a signature of 16 miRNAs that is able to discriminate patients with bad prognosis (Relapse positive) respect to patients with a better clinical outcome (Relapse negative).

Among the deregulated miRNAs, miR-148b, down-regulated in more aggressive breast tumors, was able to predict survival *per se* and to coordinate tumor cell growth and progression as well as chemotherapy-induced apoptosis via a novel pathway involving over 130 genes such as the adhesion receptor ITGA5 and its downstream players ROCK1, PIK3CA/p110alpha, NRAS as well as CSF1. Among them ITGA5, ROCK1, PIK3CA/p110alpha and CSF1 were found to be direct targets of miR-148b. Our findings underline the relevance of the identified relapse-signature for patient prognosis and suggest a critical role for miR-148b in breast cancer progression.

2. MATERIALS & METHODS

2.1 Cell culture

Human MDAMB231, 4175 TGL [Minn *et al*., 2005], MCF7, T47D and mouse 4T1, cells were maintained in standard conditions: Dulbecco's Modified Eagle's Medium containing 10 mM Glutamax and 4.5 g/mL glucose (DMEM Glutamax™, GIBCO Invitrogen Life Technologies, Carlsbad, CA), supplemented with 10% heat-inactivated FCS (Biochrom AG, Berlin, DE), 1 mM sodium pyruvate, 25 mM HEPES pH 7.4 and 100 mg/mL gentamycin (all from GIBCO Life Technologies, Carlsbad, CA).

2.2 Patients and Samples

77 frozen tumor specimens were selected from the Tumor Bank of the Department of Obstetrics and Gynecology, University of Turin, obtained from patients who underwent primary surgical treatment between 1988 and 2001 at a median age of 54 years (25-82 age). Eligibility criteria were the following: diagnosis of invasive breast cancer, all T and N stages, no distant metastasis at diagnosis (M0), complete clinical-pathological data and updated follow up for at least 72 months and up to 100 months. All patients were treated with radical modified mastectomy or quadrantectomy and axillary dissection plus breast irradiation. High-risk node-negative and node-positive patients received adjuvant treatments (generally 6 cycles of CMF, 600 mg/m^2 cyclophosphamide, 40 mg/m^2 Metotrexate, 600 mg/m^2 5-Fluorouracil) and/or 20 mg tamoxifen daily for 5 years in ER+ cases. Patient stage distribution was assessed as prescribed by the Union for International Cancer Control (UICC) clinical staging guidelines, and tumor grading was performed as described previously [Simpson *et al*., 2000]. As normal breast controls 17 frozen mammoplastic reductions were included in the screening (provided from dr. C. Brisken, EPFL, Lausanne, Switzerland). Appropriate ethical approval was obtained for this study.

2.3 Reagents and antibodies

***miR precursors and inhibitors**:*

Pre-miR miRNA Precursor Molecules–Negative Control 1, miRNA precursors hsa-miR-148b (PM10264) and hsa-miR-214 (PM12124). Anti-miR miRNA Inhibitor–Negative Control 1, and miRNA inhibitor hsa-miR-148b (AM10264) were from Ambion (Austin, TX, USA).

***miR detection**:*

TaqMan miRNA assays: hsa-miR-148b (ID: 000471), hsa-miR-187 (ID: 000487), hsa-miR-365 (ID: 001020), hsa-miR-10a (ID: 000387), has-miR-19a (ID: 000395), hsa-miR-342-3p (ID: 002260), hsa-miR-214 (ID: 002306), hsa-RNU44 (ID: 001094), and U6 snRNA (ID: 001973) were from Applied Biosystems (Foster City, CA, USA).

***Extracellular matrix (ECM)**:*

Collagen IV and fibronectin were from Sigma-Aldrich (St. Louis, MO, USA).

***Apoptosis reagents**:*

FITC-conjugated annexin V was provided by Boehringer Mannheim (Indianapolis, IN, USA). PE-conjugated annexin V was provided by BD Biosciences (Bedford, MA, USA). Tetramethylrhodamine methyl ester (TMRM) was provided by Molecular Probes (Invitrogen, Life Technologies). Paclitaxel (Onco-Tain brand) was from Mayne Pharma (Melbourne, Australia), cisplatin was from Ebewe Italia Srl. (Rome, Italy), and doxorubicin was from Sigma-Aldrich.

RNAi:

si-ITGA5 (Hs_ITGA5_5 siRNA) and All Stars Negative Control siRNA were purchased from Qiagen (Stanford, CA, USA).

Primary antibodies:

Anti-N-RAS mAb F155, anti-hsp90 mAb F-8, anti-ROCK1 pAb H-85, and anti-actin pAb I-19 were from Santa Cruz Biotechnology (Santa Cruz, CA, USA). Anti-PIK3CA (4255) was from Cell Signaling Technology (Danvers, MA, USA). Anti-ITGA5 pAb

RM10 was kindly provided by G. Tarone (University of Torino, Turin, Italy) [Tarone *et al*., 1993]. Anti-CSF1 mAb M01-1A9 was from Abnova (Taipei, Taiwan), and anti-α-tubulin mAb B5-1-2 was from Sigma-Aldrich.

Secondary antibodies:

Goat anti-mouse and goat anti-rabbit HRP-conjugated IgG were from Santa Cruz Biotechnology. All antibodies were used at the producer's suggested concentrations. Matrigel used for in vivo tumor growth experiments (BD Matrigel Basement Membrane Matrix High Concentration) was from BD Biosciences.

Primers:

RT-PCR assays (Qiagen) employed in this study are listed in Table 1. Cloning oligonucleotides employed in this study are listed in Supplemental Table 1.

QuantiTect Primer ID	Assay ID
COPZ1	QT00087024
CSF1	QT00035224
CTSA	QT00087381
CXCL5	QT00203686
DYRK2	QT01011073
GRB2	QT00065289
ITGA5	QT00080871
MMP15	QT00014063
NRAS	QT00076874
NRP1	QT00023009
PIK3CA	QT00014861
ROCK1	QT00034972
RRN18S	QT00199367

Table 1. RT-PCR assays employed in this study

2.4 Plasmid Construction and lentiviral infections

Luciferase reporter vectors containing the partial 3'-UTR of the indicated miR-148b target genes were generated following PCR amplification of the 3'-UTR from human cDNA and cloned into the Firefly Luciferase reporter pMIR-Report™ vector (Ambion, Life Technologies). When indicated the 3'-UTRs were mutagenized at the miR-148b recognition site/s using the QuickChange Site- Directed Mutagenesis kit (Stratagene, Agilent Technologies) according to the manufacturer's instructions. miR-148b-sensor was obtained by annealing, purifying and cloning short oligonucleotides containing three perfect miR-148b binding sites into the *Spe*I and *Hind*III sites of the pMIR-Report™ vector.

The human **pre-miR-148b** sequence (a 306 bp fragment containing the pre-miR sequence) was amplified from genomic DNA, extracted from MDAMB231 cells, and cloned into pLemiR-tRFP (Open Biosystems) vector to obtain pLemiR-148b (still containing tRFP) vector. The human **pre-miR-187** sequence (a 251 bp fragment containing the pre-miR sequence) was amplified from genomic DNA, extracted from MDAMB231 cells, and cloned into pWPT (AddGene) vector to obtain pWPT-miR-187 vector. Stable cell lines were generated by lentiviral infection. Lentiviruses were produced by calcium phosphate transfection of 293T cells with 20 μg of specific vector together with 15 μg packaging (pCMVdR8.74) and 6 μg envelope (pMD2.G-VSVG) plasmids in, according to Trono's lab protocol (http://tronolab.epfl.ch). Supernatant was harvested 48h post-transfection, filtered with 0.45 μm filters, diluted and used to infect 3.5×10^5 cells in 6-well plates, in presence of 8 μg/mL Polybrene (Sigma-Aldrich).

ITGA5 overexepression was obtained by transfecting pEGFP-N3-ITGA5 expression vector (plasmid 15238, AddGene) [Laukaitis *et al*., 2001].

2.5 Total RNA isolation from tissues or cells

After surgical removal, tumor samples were macro-dissected by pathologists, quickly frozen and stored at –80°C. Total RNA was isolated with Concert Cytoplasmic RNA Reagent (Invitrogen, Life Technologies) from 20 to 50 mg tumor tissues, according to the manufacturer's guidelines. Frozen tumors were placed in this reagent and homogenized using a ball mill (MM200, Retsch, Dusseldorf, Germany). The suspension was centrifuged at 14,000 x g for 5 min at 4°C, then lysed with 0.1 ml of 10% SDS followed by 0.3 ml of 5M Sodium chloride and 0.2 ml of chloroform per ml of reagent. The lysate was centrifuged at 14,000 x g for 15 min at 4°C and the upper aqueous phase was removed and combined with 0.8 volume of isopropyl alcohol for 10 min at room temperature. The total RNA was recovered by centrifugation washed with 75% ethanol and finally dissolved in RNAse-free water.

Total RNA from normal samples or cells in culture was isolated with TRIzol® Reagent (Invitrogen Life Technologies). Each frozen tissue sample was homogenized in the denaturing lysis solution using an ULTRA TURRAX® T50 Basic homogenizer (IKA) followed by acid-phenol:chloroform extraction according to the manufacturer's guidelines.

RNA quantitation was performed using the NanoDrop-1000 spectrophotometer (Nanodrop, Wilmington, DE, USA). Total RNA integrity and the content of miRNAs (percentage, %) in each sample were assessed by capillary electrophoresis using the Agilent Bioanalyzer 2100 with the RNA 6.000 Nano and the Small RNA Nano LabChips respectively (Agilent Technologies, Palo Alto, CA, USA). Only total RNA samples with an RNA Integrity Number (R.I.N.) ≥ 6 and the miR percentage $< 30\%$ were used for miRNA microarray analysis.

2.6 miRNA and gene expression profiles

miRNA expression profiles were carried out using the "Human microRNA Microarray kit (V2)" (Agilent Technologies), that allows the detection of 723 known human (miRBase v.10.1) and 76 human viral miRNAs. Each slide contains eight individual microarrays, with ~15.000 features each, including 48 negative controls, used to estimate fluorescence background and background variance. Each miR was targeted by 16-20 array-probes of different sizes. Total RNA (200 ng) was labeled with pCp Cy3, according to the Agilent's protocol and unincorporated dyes were removed with MicroBioSpin6 columns (BioRad, Hercules, CA) [Wang *et al*., 2007]. Probes were hybridized at 55°C for 22 hours using the Agilent's hybridization oven that is suited for bubble-mixing and microarray hybridization processes. Slides were washed by Agilent Gene expression wash buffer 1 and 2 and scanned using an Agilent microarray scanner (model G2565CA) at 100% and 5% sensitivity settings.

Gene expression profiling was performed with the "Whole Human Genome Oligo Microarray" (Agilent Technologies) consisting of ~41.000 (60-mer) oligonucleotide probes, which span conserved exons across the transcripts of the targeted full-length genes. Each slide contains four individual microarrays, each with about 44.000 features. 800 ng of total RNA were labeled with "Agilent One-Color Microarray-Based Gene Expression protocol" according to the manufacturer's instructions. The synthesized cDNA was transcribed into cRNA and labeled with cyanine 3-labelled nucleotide. Labeled cRNA was purified with RNeasy Mini columns (Qiagen). The quality of each cRNA sample was verified by total yield and specificity calculated with NanoDrop ND-1000 spectrophotometer measurements (Nanodrop). 1.65 μg of labeled cRNA were used in each reaction and the hybridization was carried out at 65°C for 17 hours in an hybridization oven rotator (Agilent Technologies). The arrays were washed by Agilent Gene expression washing buffers and Stabilization and Drying Solution as suggest by the supplier. Slides were scanned on an Agilent microarray scanner.

Agilent Feature Extraction software version 10.5.1.1 was used for image analysis of both miRNA and gene expression arrays. Raw miRNA and gene expression data are available in the U.S. National Center for Biotechnology Information Gene Expression Omnibus (GEO, http://www.ncbi.nlm.nih.gov/geo) database with the Accession N. GSE26666.

2.7 Statistical analysis

2.7.1 Statistical analysis of miRNA and gene expression data

Inter-array normalization of expression levels was performed with cyclic Lowess for miR experiments and with quantile for gene expression profilings [Bolstad *et al*., 2003; Risso *et al*., 2009] in order to correct possible experimental distortions. Normalization function was applied to expression data of all experiments and then values of spot replicates within arrays were averaged. Furthermore, Feature Extraction Software provides spot quality measures in order to evaluate the quality and the reliability of the hybridization. In particular, flag "glsFound" (set to 1 if the spot has an intensity value significantly different from the local background, 0 otherwise) was used to filter out unreliable probes: flag equal to 0 will be noted as "not available (NA)". So, in order to make more robust and unbiased statistical analyses, probes with a high proportion of NA values were removed from the dataset. 40% of NA was used as threshold in the filtering process, obtaining a total of 237 available human miRNAs and 31.315 available human genes.

Principal Component Analysis (PCA), cluster analysis and profile similarity searches were performed with Multi Experiment Viewer version 4.5.1 (tMev) of the TM4 Microarray Software Suite [Saeed *et al*., 2006]. To perform differential gene expression analysis the level of each miRNA was calculated as $\log_2$ (tumor sample/mammoplastic reduction median). The identification of differentially expressed genes and miRNAs was performed with two class-Significance Analysis of Microarray (SAM) algorithm [Tibshirani *et al*., 2002] with default settings. SAM uses a permutation-based multiple testing algorithm and identifies significant genes and miRNA with variable false discovery rates (FDR). This can be manually adjusted to include a reasonable number of candidate genes with acceptable and well-defined error probabilities. All heath maps were obtained by tMeV software using an unsupervised two-dimensional hierarchical clustering approach with average linkage method and Pearson correlation.

2.7.2 Statistical analyses of biological samples

Data are presented as means ± SEM or SD, and 2-tailed Student's t test was used for comparison analysis, with value of $P < 0.05$ considered to be statistically significant. Box and whisker plots were prepared based on Liu (2008). The bottom and top of the box are, respectively, the first (bottom) and third (top) quartile; the line in the middle corresponds to the median, and circles label outliers.

2.7.3 Statistics for survival analysis

In collaboration with dr. P. Provero (MBC, University of Turin), survival association analyses were performed using the SPSS 18.0 statistical software (SPSS Inc.) and the Bioconductor suite of software tools (http://www.bioconductor.org). The receiver operating characteristic (ROC) method [Zweig & Campbell, 1993] was used to categorize samples according to miRNA or mRNA expression. Kaplan-Meier survival curves were used to estimate time-to-event models in the presence of censored cases. Risk differences between the two groups were assessed using the Mantel-Haenszel log-rank test [Mantel, 1966].

Survival analysis was carried out in both univariate and multivariate setting using Cox's proportional hazard model [Gill, 1982]. ITGA5 survival association was evaluated in GSE2034 [Wang *et al*., 2005]; gene expression values were calculated as described previously [Damasco *et al*., 2011], and results were divided into two categories according to gene expression levels.

2.7.4 Analysis of human breast cancer data sets

Blenkiron (2007) and Enerly (2011) miR expression values and sample phenodata were obtained respectively from GSE7842 and GSE19536 (GEO database, NCBI) and from the supplementary materials of these publications.

2.8 Target Prediction and Pathway Analysis

The TargetScan 5.1 algorithm [Lewis *et al*., 2005] was used to predict miR targets. The Ingenuity Pathways Knowledge Base (http://www.ingenuity.com/) is currently the world's largest database of knowledge on biological networks, with annotations organized by experts. We exploited this database to look for enrichments in

specific pathways among the relapse (or other categories) associated miRNA putative targets. The negative Log_{10} of the *P*-value indicates enrichment significance in pathways analysis. The *P*-value is calculated with the right-tailed Fisher's Exact Test. Ingenuity networks are scored based on the number of Network Eligible Molecules they contain. The network Score is based on the hypergeometric distribution and is calculated with the right-tailed Fisher's Exact Test. The score is the negative log of this *P*-value.

2.9 qRT-PCR for miRNA or mRNA detection

miRNA microarray result validations and miRNA detection for *in vitro* experiments were performed by the TaqMan® miRNA Assay kit (Applied Biosystems) [Chen *et al*., 2005]. Briefly, each RT reaction (15 µl) contained 10 ng of total purified RNA, 5X stem-loops RT primer, 1X RT buffer, 0.25 mM each of dNTPs, 50U MultiScribe™ reverse transcriptase and 3.8U RNAse inhibitor. The reactions were incubated in a Thermal Cycler (Applied Biosystems) in 0.2 ml PCR tubes for 30 min at 16°C, 30 min at 42°C, followed by 5 min at 85°C, and then held at 4°C. The resulting cDNA was quantitatively amplified in 40 cycles on an ABI 7500 Real-Time PCR System, using TaqMan Universal PCR Master Mix and Taqman MicroRNA Assays. For each real-time PCR reaction three replicates of each sample and endogenous control were amplified.

For mRNA detection, 1 µg of DNAse-treated RNA (DNA-free™ kit, Ambion) was retrotranscribed with RETROscript™ reagents (Ambion, Austin, TX) and qRT-PCRs were carried out using gene-specific primers, by a 7900HT Fast Real Time PCR System (standard settings) at the Molecular Biotechnology Centre (University of Torino).

As endogenous normalizers of the expression, RNU44 small nucleolar RNA or of 18S ribosomal RNA were chosen for miRNA or mRNA detection, respectively. The relative expression levels between samples were calculated using the comparative delta Ct (threshold cycle number) method ($2^{-\Delta\Delta Ct}$) [Livak & Schmittgen, 2001]. In the case of tumor samples, the median expression for miRNA or mRNA was used across samples as calibrator; while for cell lines the control sample was the reference point [Bookout & Mangelsdorf, 2003].

2.10 *In vitro* analysis

2.10.1 Transient transfections of pre-miRs, anti-miRs, siRNAs or plasmids

To obtain transient anti-miR, pre-miR, or siRNA expression, cells were plated in 6-well plates at 30-50% confluency and transfected 24h later using RNAiFect (QIAGEN) reagent, according to manufacturer's instructions, with 75 nM anti-miR, 40 nM pre-miR or 100 nM siRNA.

For ITGA5 overexpression, 80% confluent cells were transfected with the pEGF-ITGA5 vector using Lipofectamine^{TM}2000 (Invitrogen Life, Technologies), according to manufacturer's instructions. Cells were tested for miRNA or protein-coding gene overexpression/knockdown 24h, 48h or 72h later.

2.10.2 Invasion and transendothelial migration assays

To measure invasion 5x10^4 MDA-MB-231, 4175 TGL or 4T1 cells were seeded in serum-free media in the upper chambers of cell culture inserts (transwells) with 8 μm pore size membrane (24-well format, Becton Dickinson) pre-coated with 10μg/mL fibronectin, or 4 μg/well growth factor reduced Matrigel (Becton Dickinson), or in the upper chambers of BioCoat™ Matrigel Invasion Chambers with 8μm pore size membrane (Becton Dickinson, NJ). The lower chambers were filled with complete growth media. After 18-20 h, the migrated cells present on the lower side of the membrane were fixed with methanol, stained with haematoxylin and eosin (Diff-Quik, Medion Diagnostics) and photographed using an Olympus IX70 microscope.

For transendothelial migration assay 10^5 HUVECs-GFP were seeded in complete medium in the upper part of transwell inserts with 5.0 μm pore size membrane (24-well format, Costar, Corning) coated with fibronectin at 5 μg/cm^2, and grown for 72h, till confluence. Then, 5x10^4 MDAMB231 cells were labeled with CellTracker™ Orange CMRA (Molecular Probes, Invitrogen Life Technologies), according to the manufacturer's instructions and seeded in HUVEC's complete medium onto the HUVEC-GFP monolayer on the upper side of the transwell. 20h later the HUVEC-GFP monolayer was photographed using Zeiss Axiovert 200M microscope. Then, HUVECs and non transmigrated cells were removed and the red-fluorescent cells that migrated on the lower side of the membrane were fixed in 4% paraformaldhyde and photographed using Zeiss AxioObserver microscope with ApoTome Module. Invasion and

transendothelial migration were evaluated by measuring the area occupied by migrated cells using the ImageJ software [Collins, 2007].

2.10.3 Adhesion and proliferation assays

$5x10^4$ cells/well were seeded onto 5 μg/mL collagen IV or 10μg/mL fibronectin or 5 μg/mL laminin (all from Sigma-Aldrich) precoated 96-well plates, for 1h at 37°C. Cells were washed thoroughly to remove non-adherent cells, fixed with methanol and stained with haematoxylin and eosin (Diff-Quik, Medion Diagnostics). Wells were photographed using Olympus IX70 microscope and the area occupied by the adherent cell was measured by using the ImageJ software [Collins, 2007].

$5x10^3$ cells/well were plated in 96-well plates in complete medium and starved for 24h. Complete medium was then added and cells were allowed to grow for 1, 2, 3, 4 days, fixed with 2.5% glutaraldehyde and stained with 0.1% crystal violet. The dye was solubilized using 10% acetic acid and optical density measured directly in plates using a Microplate Reader Mithras LB940 (Berthold Technologies, GmbH) at 570 nm wavelength [Kueng *et al*., 1989].

2.10.4 Anoikis analysis and apoptosis assays

Cells were plated on a 2% agarose pad in serum-free medium for 48h, collected, washed in PBS buffer, resuspended in 10 mM Hepes, 150 mM NaCl, 5 mM $CaCl_2$ buffer containing FITC conjugated Annexin-V (Bender MedSystems, GmbH) and 200 nM tetramethyl-rhodamine-methyl-7ester (TMRM, Molecular Probes, Invitrogen) and incubated at 37° C for 15 minutes. Flow cytometry analysis was carried out by using a FACS Calibur flow cytometer (Becton Dickinson). Data acquisition was performed using CellQuest software (Becton Dickinson) and data analysis with WinMDI software (version 2.8, Scripps Institute, CA). Results were displayed in bidimensional plots, with gates indicating the percentages of healthy and apoptotic populations [Rasola & Geuna, 2001].

In order to trigger apoptosis, 72 h after miR transfection, cells were plated at 45.000/cm^2 density, grown in complete medium with or without Paclitaxel (PTX) 5 μM, Cisplatin (CDDP) 100 μM or Doxorubicin (DOXO) 1 μM for 24 or 48h. After apoptosis induction cells were washed once in phosphate-buffered saline (PBS) and detached by trypsinization. Labeling and analysis was performed as in anoikis analysis.

2.11 Luciferase assays

$15x10^4$ cells were co-transfected with 50 ng of the pMIR-Report™ (Ambion) Firefly Luciferase constructs containing the wild type or mutant/deleted 3'-UTRs of the indicated miR-148b potential target genes and 20 ng of pRL-TK Renilla Luciferase normalization control (Promega), using LipofectamineTM2000 (Invitrogen Life Technologies). Lysates were collected 48h after transfection and Firefly and Renilla Luciferase activities were measured with a Dual- Luciferase Reporter System (Promega, Madison, WI).

2.12 Protein preparation and Immunoblotting

Total protein extracts were extracted from cultured cells or from frozen breast tumor specimens. A boiling buffer containing 0.125 M Tris/HCl, pH 6.8 and 2.5% sodium dodecyl sulphate (SDS) was used. 25 μg proteins were separated by SDS polyacrylamide gel electrophoresis (PAGE) and electroblotted on to polyvinylidene fluoride (PVDF) membranes (Bio-Rad). Membranes were blocked in 5% BSA Tris buffered saline (TBS)-Tween buffer (137 mM NaCl, 20 mM Tris/HCl, pH 7.6, 0.1% Tween-20) for 1h at 42 °C, then incubated with appropriate primary and secondary antibodies in 1% BSA TBS-Tween buffer, respectively overnight at 4 °C and for 1h at room temperature and visualized by enhanced chemiluminescence (ECL®, Amersham Biosciences).

2.11 *In vivo* analysis (Prof. D. Taverna)

2.11.1 *In vivo* tumor and metastasis assays

6-weeks-old female NOD/SCID IL2Rγnull mice [Quintana *et al*., 2008] were injected in the mammary gland fat pad with $6x10^6$ 4175 TGL cells transduced with pLemiR-148b or pLemiR-empty vectors, expressing Turbo-Red Fluorescent Protein (tRFP) in 1:1 medium/matrigel (BD Biosciences). Tumor growth was monitored every 3 days. Mice were dissected 12 days after injection and tumor weight was evaluated. Spontaneous metastasis formation was also evaluated in these mice, lungs were dissected and photographed using a Leica MZ16F fluorescence stereomicroscope; red-fluorescent metastatic foci were analyzed in the fresh total lungs using the ImageJ software [Collins, 2007]. Three representative pictures of the whole lung per mouse were considered.

Total lungs were formalin-fixed, cut in small pieces and paraffin-embedded, sectioned and haematoxylin & eosin (H&E)-stained. Micrometastases were photographed on specimens, with an Olympus BH2 microscope, on at least three different sections. Alternatively, lung metastases formation was evaluated in 14 weeks old female immunocompetent BALB/c mice injected via tail vein with $5x10^5$ 4T1 cells either transfected with pre-miR-148b or negative controls. Lungs were dissected 5 days after injections, formalin-fixed, cut in small pieces and paraffin-embedded, sectioned and haematoxylin & eosin (H&E)-stained. For 4T1 cells, micrometastases were evaluated on specimens, with an Olympus BH2 microscope, on at least three different sections using the ImageJ software [Collins, 2007].

2.11.2 *In vivo* extravasation assay

7-weeks-old female CD1 nude mice (Charles River Laboratories, Wilmington, MA) were injected via tail vein with $1.6x10^6$ MDAMB231 cells transduced with pLemiR-148b or pLemiR-empty vectors, previously labeled with CellTracker™ Orange CMRA (Molecular Probes, Invitrogen, Life Technologies) and resuspended in PBS. 2h or 48h later mice were sacrified and 4% paraformaldeyde was injected in the trachea. Total lungs were dissected and photographed using a Leica MZ16F fluorescence stereomicroscope and red fluorescent cells were counted 48h following injections using

the ImageJ software [Collins, 2007]. Lungs were included in freezing resin (OCT Killik, Bio-Optica, IT) and cryostat-cut in 4 μm thick sections.

For immunohistochemistry staining of blood vessels, samples were blocked in 5% bovine serum albumin (Sigma-Aldrich) for 1h, incubated with anti CD31 primary antibody (1:100 dilution) overnight and anti-rat secondary antibody conjugated with biotin for 1 hour at room temperature (1:100 dilution) (Dako). Peroxidase was developed with DAB (ABC kit Vectastain PK-6100 from Vector Labs, Burlingame, CA). Specimens were examined and photographed using a Zeiss AxioObserver microscope with the ApoTome Module.

3. RESULTS

3.1 microRNA expression profiling in breast cancer

In a retrospective study, we analyzed miRNA expression in 77 primary human breast ductal tumors as well as 17 mammoplastic reductions (Table 3), using microarrays (Agilent Human miRNA Microarray V2) and a Two-class Significance Analysis of Microarray (SAM).

Characteristics		N	%
Tumor samples			
Number of patients		77	
Age (years)	median range	54 25-82	
Tumor Stage	1 2 3 4	20 51 3 3	26 66.2 3.9 3.9
Tumor Grade	1 2 3 Unknown	4 35 33 5	5.2 45.4 42.8 6.5
LN	Positive Negative	44 33	57.1 42.9
ER*	Positive Negative	53 24	68.8 31.2
PR*	Positive Negative	42 35	54.5 45.4
Subtype**	Luminal ERBB2** Basal	53 14 10	68 18 12
Relapse (at least 72 months)	yes ER+ ER - no ER+ ER -	41 25 16 36 28 8	53.2 61*** 39*** 46.7 78*** 22***
Normal samples			
Number of patients		17	
Age (years)	median range	43 20-67	

Table 3. N: number; %: percentage, LN: Lymph node status, ER: Estrogen receptor status, PR: Progesterone receptor status. * ER and PR are defined positive when tumors contain more than 10 fmol of receptors/mg proteins or less than 10% positive tumor cells. **Samples were classified according to ERBB2 mRNA level combined to ER and PR status. ***Percentage refers to the total of relapsing or not relapsing samples.

In particular, when we compared patients with (Relapse, n=41) or without (No Relapse, n=36) disease relapse, within at least 72 months from surgery, 16 differentially expressed miRNAs (FDR=16%) were identified and expressed as Fold changes (FCs) or levels, relative to the median of the healthy controls (log2 tumors/controls) (Figure 3A and 3B).

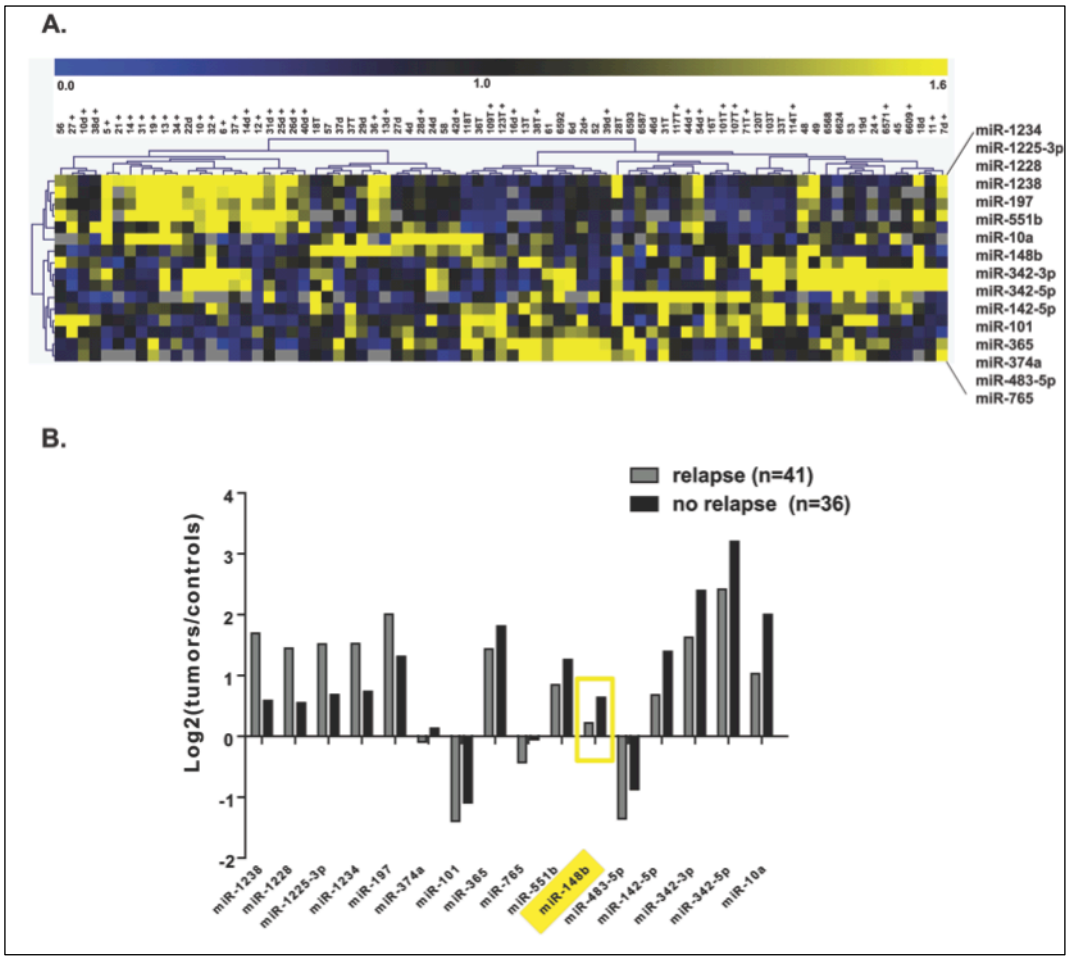

Figure 3. Expression of 16 miRNAs in Relapse positive (+) or negative (-) primary cancers. **(A)** Clustering (Pearson correlation, average linkage) for the 16 most modulated miRNAs considering relapsing (n=41) *versus* not relapsing (n=36) tumors. The heatmap represents relative miRNA levels referring to the median expression across all samples; row: miRNAs; column: tumors. **(B)** Graph showing the levels of expression of the 16 most modulated miRNAs expressed as averaged levels (Log2) in R+ or R- tumor samples *versus* mammoplastic reductions (controls). SAM two classes, False Discovery Rate (FDR): 16%.

Instead, when ER or PR positive (+) or negative (-) tumors were compared, respectively 29 (FDR=14%) and 56 (FDR=9.30%) differentially expressed miRNAs were found, as presented in Supplemental Figures S1 and S2.

Microarray data validation was performed by qRT-PCR analysis for miR-148b, miR-365, miR-10a and miR-342-3p (Figure 4) for R+/R- or ER+/ER samples (n=10 per group). The expression values obtained with quantitative RT-PCR for all tested miRNAs were in agreement with microarray results (Gene Expression Omnibus Series No. GSE26666).

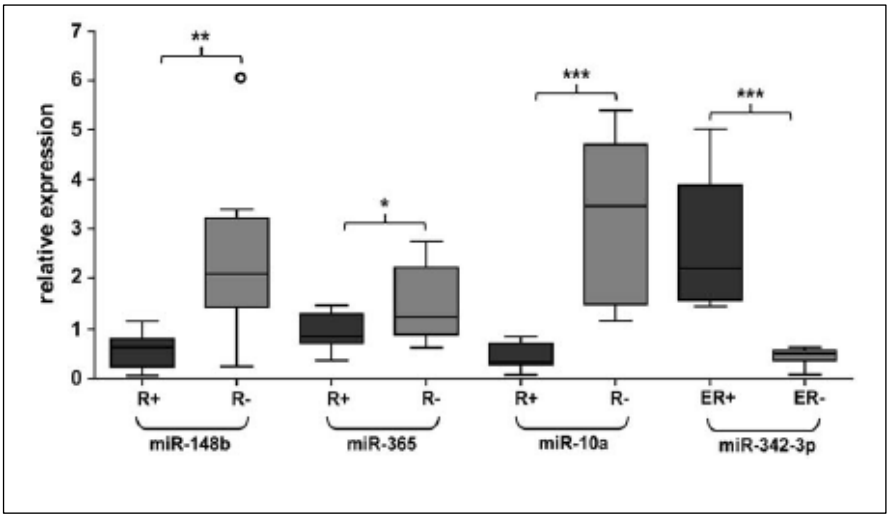

Figure 4. Validation of the miRNA microarray analysis results by qRT-PCR.
miRNA expression levels were represented by box-and-whisker plots. Normalized qRT-PCR data were expressed as fold changes (FC) relative to the median expression for each group of patients. U44 RNA was used for normalization. R, relapse; ER, Estrogen Receptor; +, positive; -, negative. N=10 tumor samples per group. *P<0.05; **P<0.01; ***P<0.001.

By using the 16-relapse associated miRNAs together as a whole (as a group), we were able to identify two groups of patients with different overall (OS, *P*-value=0.018) and disease-free (DFS, *P*-value=0.016) survival, independently of the lymph node (LN) status (Cox proportional-hazards regression model, *P*-value=0.015) in our study. The same was found when certain individual specific miRNAs were used, for instance miR-148b, downregulated in relapsing tumors (OS, *P*-value=0.027; DFS, *P*-value=0.036). However, a correlation with survival was not found when our 16-relapse associated miRNAs were used as a whole for two other available public datasets [Blenkiron *et al*., 2007; Enerly *et al*., 2011]. These studies refer to around 100 patients each; the primary tumors were used to measure mRNA and miRNA expression with the goal to identify

tumor subtypes. Importantly, in these datasets, our group of 16-relapse associated miRNAs was able to identify tumor subtypes and to separate more (ERBB2+ or Basal-like) *versus* less (Luminal A/B) aggressive cancers (Figure 5, compare black *versus* gray symbols), based on the breast cancer classification in Sorlie *et al*. (2001). Moreover, our 16-miRNA signature could also predict survival, in our cohort, when only Luminal tumors (n=53) were considered (DFS, *P*-value=0.0097). In conclusion, we identified 16-relapse associated miRNAs that could be used in the clinics to identify tumor subtypes and to predict disease outcome.

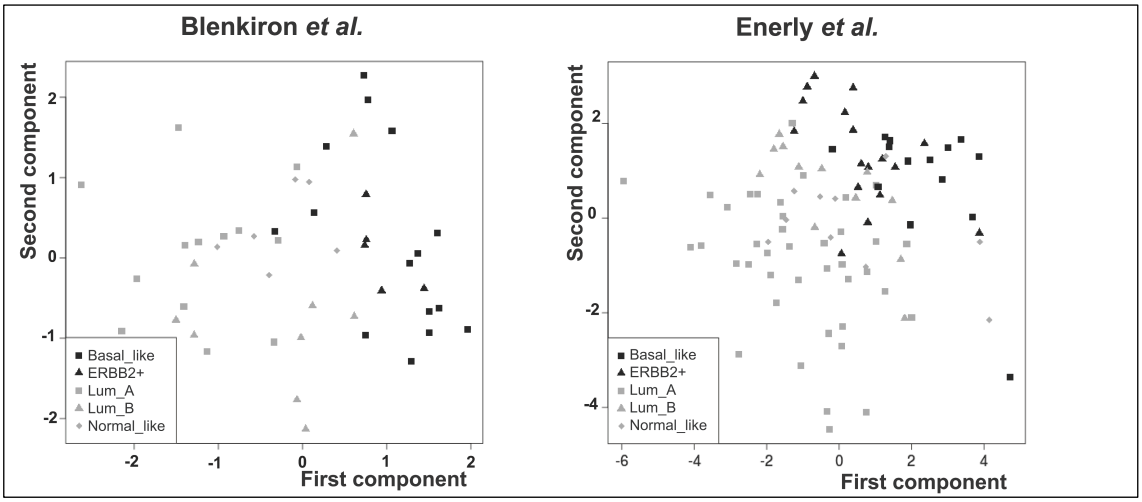

Figure 5. Tumor subtype identification.
Principal Component Analysis (PCA) plots for tumor subtypes using all 16 miRNAs in Blenkiron *et al*. (2007) and Enerly *et al*. (2010) datasets. Basal_like: Basal; ERBB2+: ERBB2 positive; Lum_A: Luminal A; Lum_B: Luminal B; Normal_like: normal like breast cancer.

3.2 The biological function of miR-148b

A detailed bioinformatics analysis was carried out for the putative targets of the 16-relapse associated miRNAs, as predicted by TargetScan 5.1, using Ingenuity Pathways Analysis (IPA) in order to identify pathways and functions in which each miRNA was involved (Figure 6). This analysis, together with literature searches, let us to conclude that miR-148b has the potential to coordinate a very high number of pathways relevant for breast cancer and that its function has still to be elucidated.

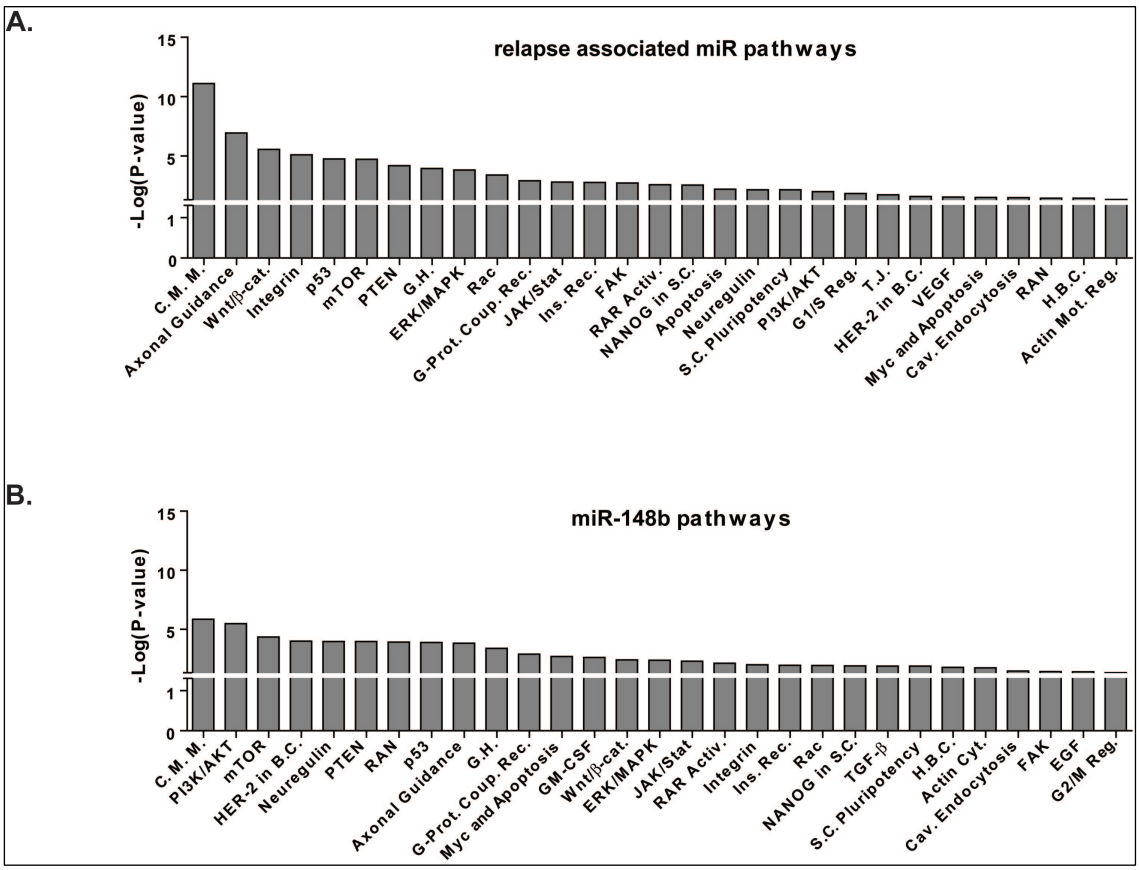

Figure 6. Pathway enrichment for relapse-associated or miR-148b putative targets.
Pathway analysis was performed for relapse-associated **(A)** or miR-148b **(B)** putative targets using the Ingenuity Pathway Analysis Systems (http://www.ingenuity.com) and enrichments were accepted when $P<0.05$ (Fisher test). Abbreviations: CMM: Cancer Molecular Mechanisms; Wnt/β-cat: Wnt/β-catenin; GH: Growth Hormone; G-Prot Coup Rec: G-Protein Coupled Receptor; Ins Rec: Insulin Receptor; RAR Activ: RAR Activation; NANOG in SC: Role of NANOG in stem cell; SC Pluripotency: Stem Cell Pluripotency; G1/S Reg: G1/S Checkpoint Regulation; T.J: Tight Junction; HER-2 in BC: HER-2 in Breast Cancer; Myc Apoptosis: Myc Mediated Apoptosis; Cav Endocytosis: Caveolar-mediated Endocytosis; HBC: Hereditary Breast Cancer Signaling; Actin Mot Reg: Actin-based Motility Regulation; Actin Cyt: Actin Cytoskeleton; G2/M Reg: G2/M Checkpoint Regulation.

3.2.1 Analysis of miR-148b expression

With this in mind, we investigated the biological role of miR-148b in neoplasia by modulating (up or down) its expression in MDAMB231, 4175 TGL, 4T1, T47D and MCF7 mammary tumor cell lines with a different level of malignancy (independently of ER, PR and ERBB2 expression) [Holliday & Speirs, 2011]. We first analyzed miR-148b expression in several mammary epithelial cell lines (human and mouse) by qRT-PCR. Low miR-148b expression was found in the human SKBR3, MDAMB468, MDAMB231 cell lines and in the mouse 4T1 mammary tumor cells. Instead, intermediate or high levels of expression were identified in the human HBL100, MCF10A, MCF12A, MCF7, T47D, MDAMB435, MDAMB453, BT474 cell lines and in 66cl4 mouse tumor cells (Figure 7).

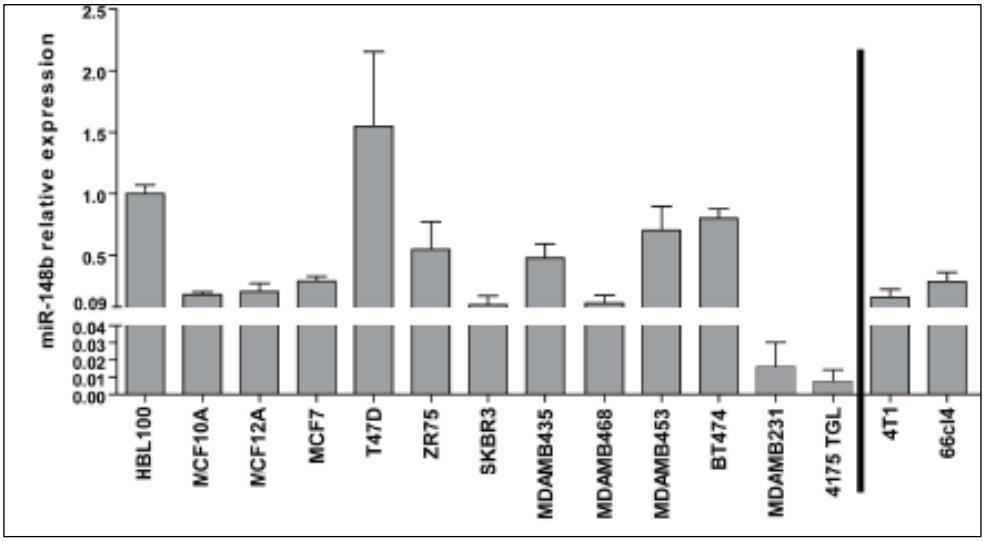

Figure 7. miR-148b expression levels in breast cancer cell lines.
miR-148b expression was evaluated for the indicated human or mouse tumor cell lines by qRT-PCR analysis. Results were normalized on U44 RNA levels and presented as Fold Changes (FC) of mean±SD relative to miR-148b expression in HBL100 cells.

On the basis of these results we decided to study the biological role of miR-148b in the human T47D, MCF7, MDAMB231, 4175 TGL cell lines and the mouse 4T1 cell in which it was easier to over-express (MDAMB231, 4175 TGL and 4T1) or down-modulate (T47D, MCF7) miR-148b (Figure 8A).

Transient modulations were obtained using miR-148b precursors or inhibitors or negative controls (pre-miR-148b, anti-miR-148b, or pre-control or anti-control) and evaluated 48h or 72h post-transfection for expression and biology (Figure 8B and 8C). Instead, for stable expression, cells were transduced with pLemiR-empty or pLemiR-

148b overexpressing lentivirus vectors and selected with puromycin as pools; expression evaluation is shown in Figure 8C.

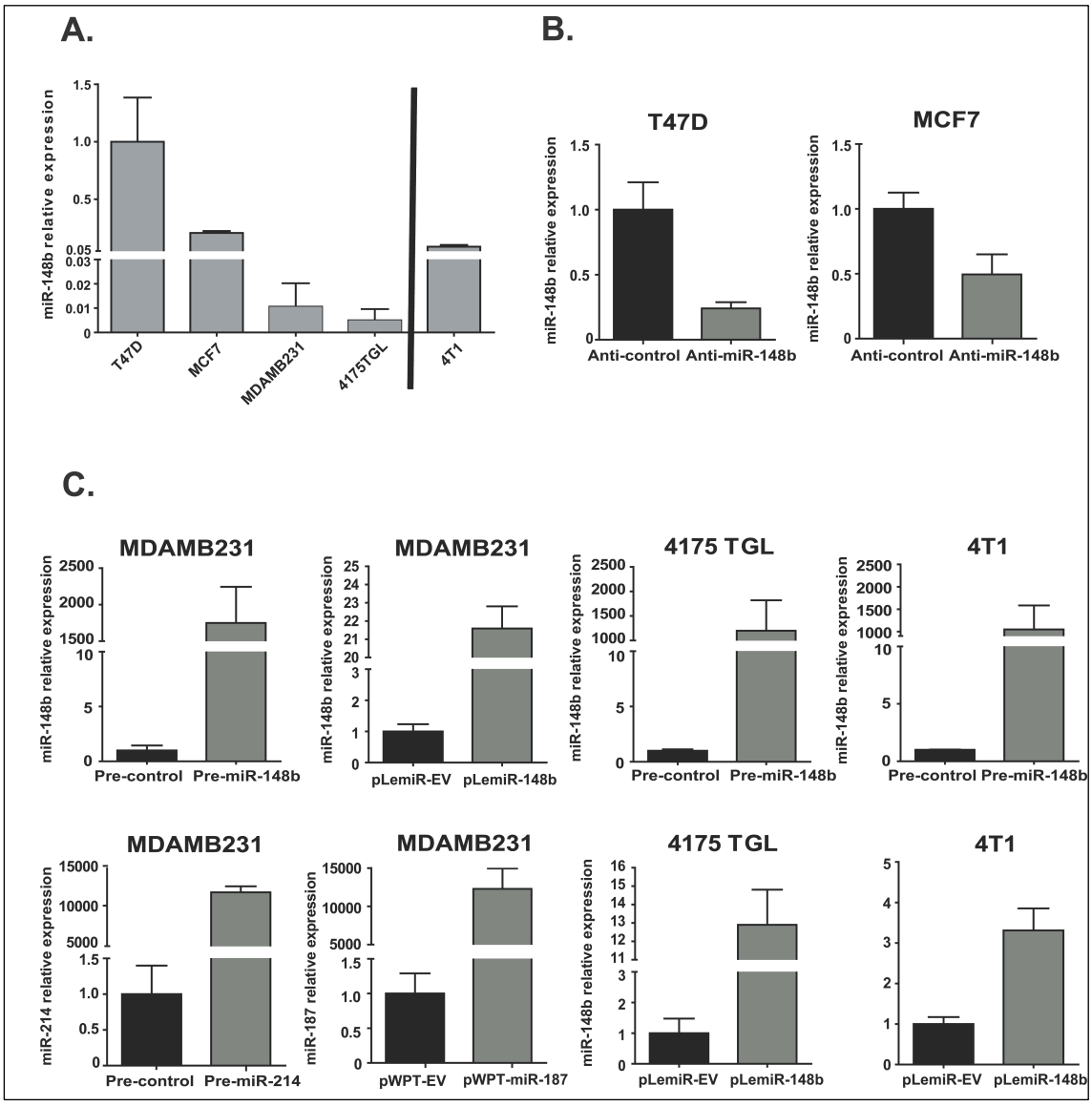

Figure 8. Analysis of miRNA expression. (A) miR-148b expression was evaluated for the indicated human or mouse tumor cell lines by qRT-PCR analysis. **(B)** qRT-PCRs were performed to evaluate miR-148b expression levels in MCF7 or T47D cells transiently transfected with miR-148b inhibitors or negative controls (anti-miR-148b or anti-control). **(C)** qRT-PCR were performed to evaluate miR-148b, miR-214 and miR-187 expression levels in MDAMB231, 4175 TGL or 4T1 cells transiently transfected with the indicated miR-precursors or negative controls (pre-miR-148b, pre-miR-214 or control) or stably transduced with pLemiR-empty (pLemiiR-EV) or pWPTempty (pWPT-EV) or miR-148b (pLemiR-148b) or miR-187 (pWPT-miR-187) overexpressing vectors. Results were normalized on U44 RNA levels and presented as Fold Changes (FC) of mean±SD relative to miR-148b expression in T47D cells **(A)** or to controls **(B, C)**. Representative overexpressions/downmodulations are shown.

3.2.2 miR-148b involvement in tumor cell growth, invasion and adhesion

In vitro proliferation was not affected or only slightly modulated up to 4 days for MDAMB231, 4175 TGL and 4T1 cells in stable or transient conditions (Figures 9A). However, tumors derived from transduced pLemiR-148b 4175 TGL cells grew significantly less compared to controls (pLemiR-EV) when analyzed up to 12 days following injection in the fat pad of immunocompromised NOD/SCID IL2Rγ^{null} mice (see below). When invasion through Fibronectin or Matrigel was evaluated by transwell assays for the same cell lines, reduced cell movement was observed in presence of miR-148b overexpression compared to controls (Figures 9B). However, no effect was observed when cells were transduced with pWPT-miR-187 (negative control) lentivirus overexpression vectors compared to controls (pWPT-EV or pre-control) (Figures 9B). Instead, increased cell invasion was observed when miR-214 was overexpressed in these cells (Figure 9B) such as previously demonstrated by Penna *et al*. (2011).

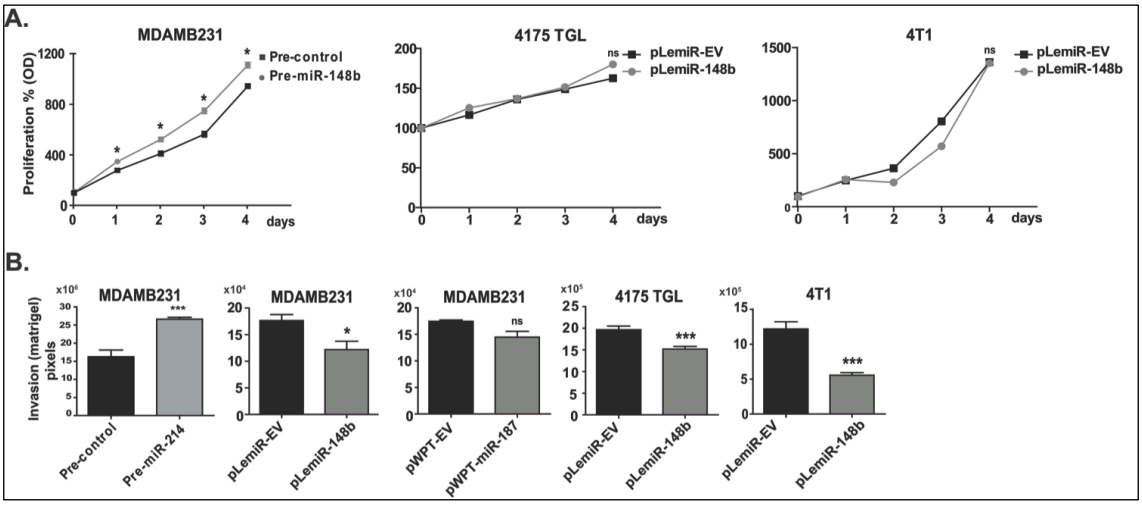

Figure 9. miR-148b involvement in tumor cell growth and invasion.
MDAMB231 or 4175 TGL or 4T1 cells transiently transfected with miR-148b or miR-214 precursors their negative controls (pre- or control) or stably transduced with pLemiR-EV (empty) or pWPT-EV (empty) or pLemiR-148b or pWPT-miR-187 overexpression vectors were used to analyze proliferation **(A)** or invasion **(B)**. Results are shown as mean±SD of the increased percentage (%) of proliferation, measured by optical density (OD) at 1-4 days **(A)** or as area covered by matrigel-invading **(B)** or adherent cells. Two or three independent experiments were performed in triplicate and representative results are shown. *P<0.05; **P<0.01; ***P<0.001.

When cell adhesion was investigated, increased adhesion on fibronectin and collagenIV was found for MDAMB231 cells overexpressing miR-148b compared to controls. Conversely, downmodulation of miR-148b in MCF7 and T47D cells led to decreased adhesion (Figure 10).

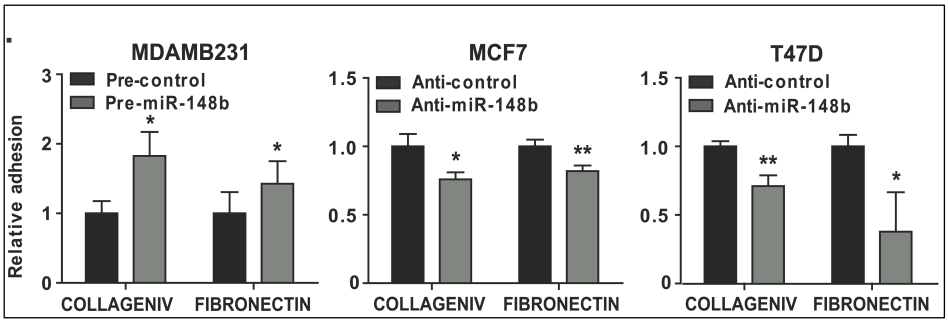

Figure 10. miR-148b involvement in tumor cell adhesion.
MDAMB231 or MCF7 or T47D cells transiently transfected with miR-148b precursor or inhibitor or their negative controls (pre- and anti-miR-148b or control) were used to analyze adhesion on collagenIV or fibronectin. Results are shown as mean±SD of the area covered by adherent cells. Adhesion of miRNA-modulated cells is shown relative to controls. Two or three independent experiments were performed in triplicate and representative results are shown. *P<0.05; **P<0.01; ***P<0.001.

3.2.3 miR-148b impairs metastasis formation

In collaboration with the Taverna's group (MBC, University of Turin) in order to study the role of miR-148b in *in vivo* metastasis formation we injected miR-148b-overexpressing (pre-miR-148b) 4T1 cells, in the tail vein of female BALB/c syngeneic mice and analyzed dissemination in lungs. A significant reduction in the number of lung colonies or area occupied by the lesions was found five days post-injections compared with controls as measured in H&E stained sections (Figure 11A). More relevantly, when red fuorescent pLemiR-148b-transduced 4175 TGL cells, were injected orthotopically in NOD/SCID IL2Rγ^{null} mice and primary tumors formed (Figure 11B), a striking reduction of malignant cell dissemination from the primary tumors to the lungs was observed compared to controls (Figure 11B). Quantitation refers to the red fluorescent metastatic foci (number/area) in the lungs, 12 days post-injection (Figures 11B) and H&E sections are shown (Figure 11B). Similar results were obtained with pLemiR-148b-transduced 4T1 cells (not shown). Importantly when similar experiments were previously performed with miR-214-overexpressing 4T1 cells, increased dissemination was observed (Penna *et al*., 2011).

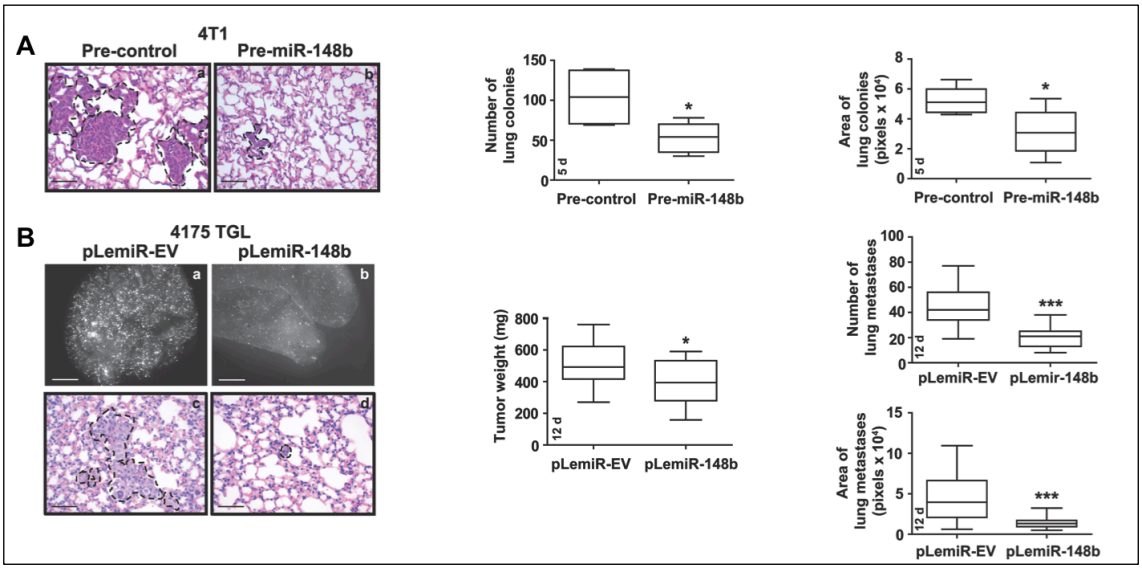

Figure 11. miR-148b impairs metastasis formation in mice.
A) 4T1 cells transiently transfected with miR-148b precursors or their negative controls (pre-miR-148b or control) were used to evaluate lung colony formation in BALB/c mice, 5 days after tail vein injection.
B) Alternatively 4175 TGL cells stably transduced with pLemiR-EV or pLemiR-148b overexpression vectors were injected in the mammary gland fat pad of NOD/SCID/IL2Rg^{null} mice and primary tumor growth as well as metastasis formation in the lungs analyzed 12 days post-injection. Two independent experiments were performed, results pooled together (n= 10 mice/group) and shown as box and whisker plots for primary tumor weights **(B)** or number (or area) of microscopic colonies **(A)** or metastasis **(B)** in the lungs. Tumor cell dissemination was evaluated in H&E-stained sections at day 5 **(A)** or as fluorescent lesions in the whole lung at day 12 **(B)**. Representative H&E stainings are shown. Scale bars: 60 µm (A; B*c*, B*d*), 2 mm (B*a*, B*b*). *P<0.05; **P<0.01; ***P<0.001.

Based on this, we assessed the involvement of miR-148b in extravasation and survival in the blood circulation, two essential steps of the metastatic dissemination. To investigate extravasation *in vivo*, red fluorescent pLemiR-148b transduced MDAMB231 cells were injected in the tail vein of immunocompromised mice and cell seeding/extravasation in the lung was evaluated 2h or 48h post-injection. A high percentage of cells lodged in the lung at 2h (within the vessels or outside) in presence or absence of miR-148b. However, extravasation was highly reduced for miR-148b overexpressing cells compared to controls, as quantitation of the area occupied by metastatic cells showed (Figures 12A and 12B). Vessels were labeled for CD31 in Figure 12C.

To investigate survival in the blood circulation, we evaluated apoptosis in miR-148b-overexpressing MDAMB231 cells kept without serum and with or without

(anoikis) adhesion for 48h, by cytofluorimetric analyses and reduced survival was observed compared to controls (Figure 12C), suggesting a potential role for miR-148b in tumor cell intraluminal viability and initial survival.

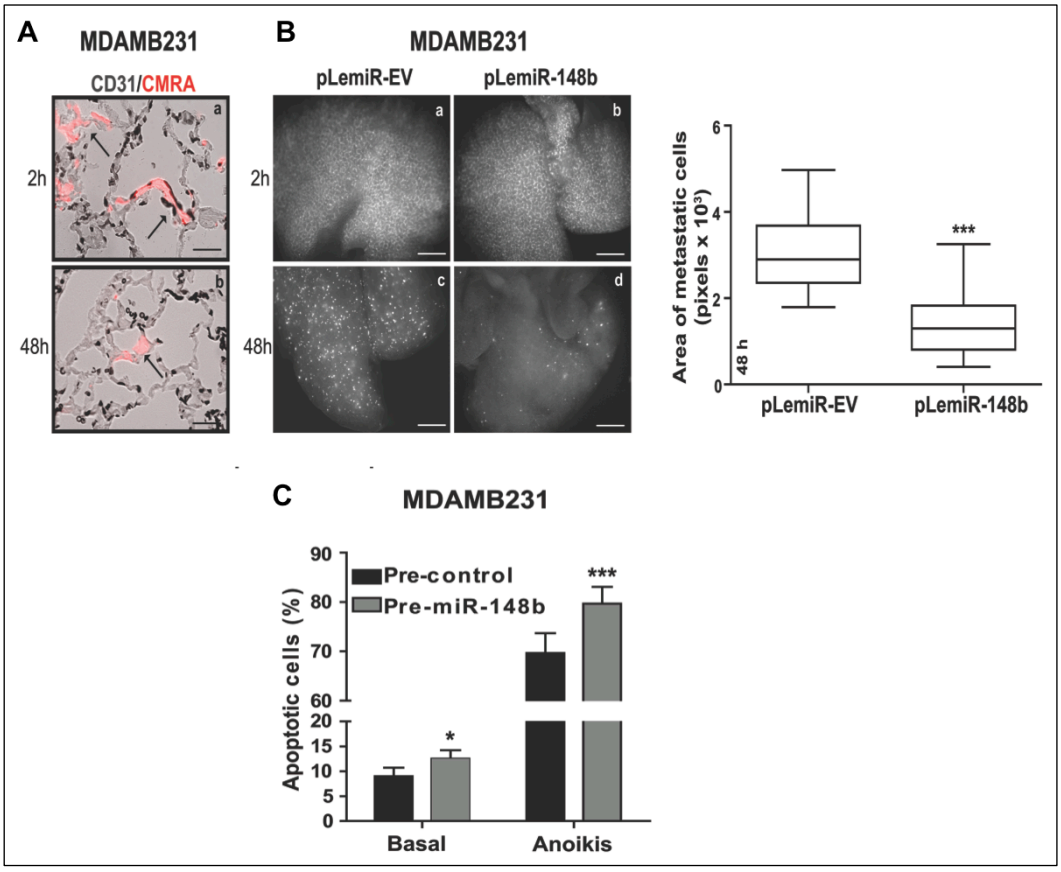

Figure 12. miR-148b impairs metastasis formation in mice by affecting extravasation and survival.

A, B) *In vivo* seeding/extravasation assays following tail vein injections in nude mice of red fluorescent MDAMB231 cells, stably transduced with pLemiR-EV or pLemiR-148b overexpression vectors. **A)** Representative fields of lung sections 2h or 48h post-injections, stained for CD31 (black) and containing red fluorescent MDAMB231 cells. No cells were found in the vessels at 48h. **B)** Red fluorescent cells in the whole lungs 2h or 48h post-injection (a-d); on the right, quantitation of the red fluorescent cells (area) at 48h (c and d) for n=8 mice/group. Scale bars: 2 mm (B), 120 µm (B*a*), 30 µm (C*b*).

C) MDAMB231 cells transfected with miR-148b precursors or their negative controls (pre-miR-148b or control) were grown in presence or absence (*anoikis*) of attachment and without serum for 48h**.** The percentage (%) of apoptotic cells was evaluated by TMRM and AnnexinV-FITC stainings in a FACS analysis. ^{High}TMRM-^{Low}AnnexinV: healthy cells; ^{Low}TMRM-^{High}AnnexinV: apoptotic cells. Three independent experiments were performed in duplicate and pooled quantitations are shown as mean±SEM. *P<0.05; **P<0.01; ***P<0.001.

All these experiments strongly suggest that miR-148b is involved in metastatic cell dissemination by controlling tumor growth and cell survival in anoikis but mostly by inhibiting cell escaping through the endothelial cells of the vessels.

3.2.4 miR-148b expression enhances chemotherapy-induced apoptosis

Considering the relevance of chemotherapy response for tumor progression, we analyzed the response to Paclitaxel, Doxorubicin, Cis-Platin following 24h or 48h-treatment in miR-148b-overexpressing (MDAMB231, 4175 TGL, 4T1) or downmodulated (T47D) cells by cytofluorimetric analyses. A significant modulation in cell survival was found for all cell lines and treatments compared to controls (Figures 13) favoring a positive role for miR-148b in chemotherapy response.

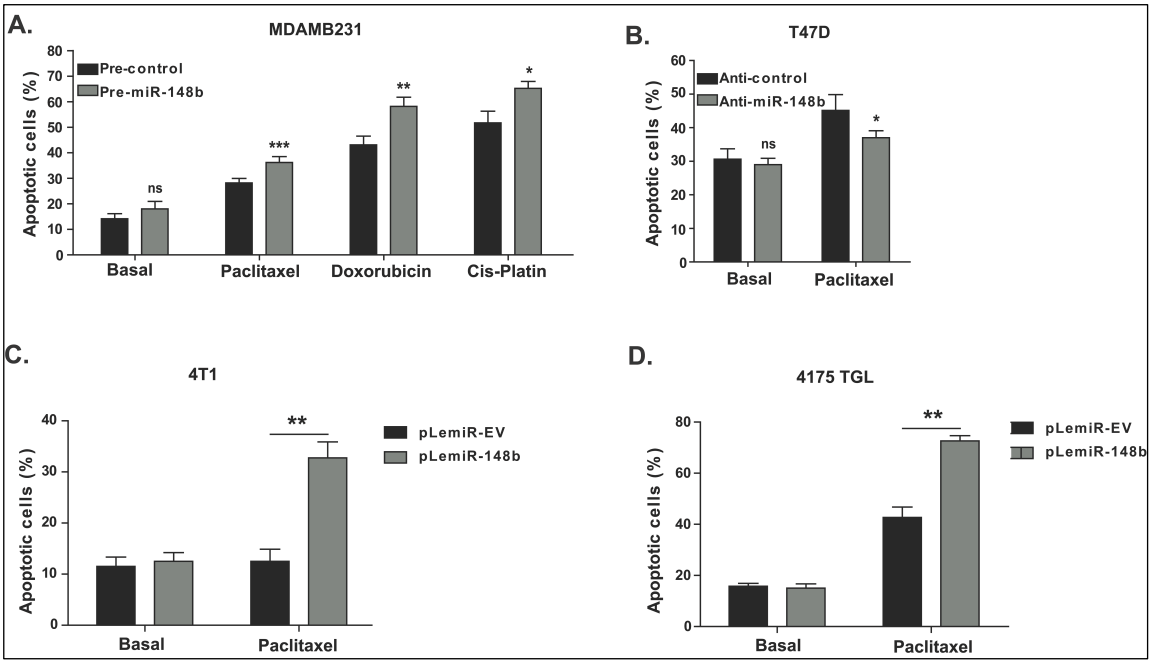

Figure 13. miR-148b affects chemotherapy-induced apoptosis.
MDAMB231 **(A)** or T47D **(B)** or 4T1 **(C)** cells transfected with miR-148b precursors or inhibitors or their negative controls (pre- and anti-miR-148b or control) or 4175TGL **(D)** cells stably transduced with pLemiR-EV or pLemiR-148b overexpression vectors were grown in complete medium with or without Paclitaxel or Doxorubicin or Cis-Platin for 24h or 48h**.** The percentage (%) of apoptotic cells was evaluated by TMRM and AnnexinV-FITC stainings in a FACS analysis. ^{High}TMRM-^{Low}AnnexinV: healthy cells; ^{Low}TMRM-^{High}AnnexinV: apoptotic cells. Three independent experiments were performed in duplicate and pooled quantitations are shown as mean±SEM. *P<0.05; **P<0.01; ***P<0.001.

3.3 Identification of miR-148b target genes

To identify direct or indirect miR-148b modulated genes, miR-148b overexpressing MDAMB231 cells were first used to perform gene expression analysis by microarrays. 129 differentially expressed genes (49 up-regulated and 80 down-regulated) were found, considering a 1.5 fold change (FC) and a 16% false discovery rate (FDR) (Supplemental Table S2). qRT-PCR analysis was used to validate expression of the non-modulated *NRAS*, *ROCK1*, *PI3KCA*, *COPZ1*, *GRB2*, *CXCL5* and of the differentially expressed *DYRK2*, *CSF1*, *CTSA*, *ITGA5*, *MMP15*, *NRP1* (Figure 14).

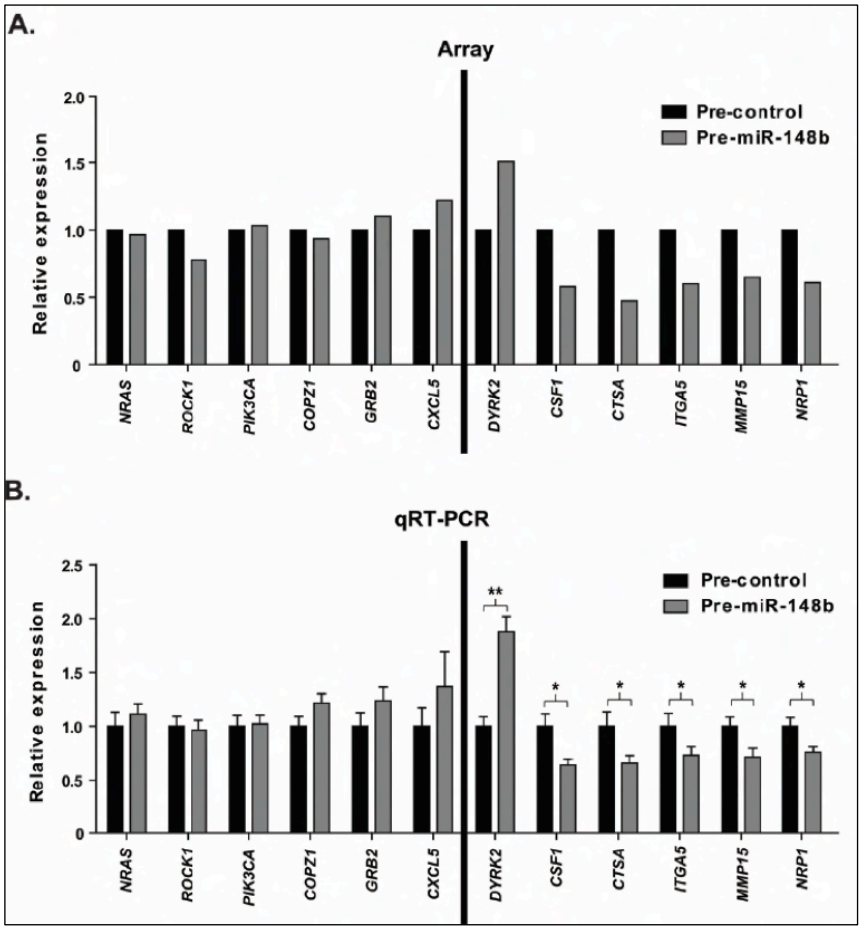

Figure 14. Validation of the protein-coding microarray analysis results.
A) MDAMB231 cells transfected with miR-148b precursors or negative controls (pre-miR-148b or control) were used to perform a whole-genome microarray analysis 48h post-transfection. Results are displayed as gene expression Fold Changes (FC) referring to controls, for 12 chosen proteincoding genes. **B)** Validations of the same 12 genes were performed by qRTPCR analysis; results were normalized on 18S ribosomal RNA and calculated as gene expression FC (mean±SD) referring to the negative controls **(B)**; n=3; on the right: differentially expressed genes; on the left: no differential expression. *P<0.05; **P<0.01; ***P<0.001.

By crossing these results with putative miR-148b targets (TargetScan 5.1) twenty common genes (19 down and 1 up) were found and are shown in Figure 15. Among them Integrin alpha 5 (ITGA5), known to modulate apoptosis, adhesion, migration/invasion [Mierke *et al.*, 2011; Desgrosellier *et al.*, 2010] and Colony stimulating factor 1 (CSF1), involved in tumor-stroma interactions [Abraham *et al.*, 2010; Aharinejad *et al.*, 2004]

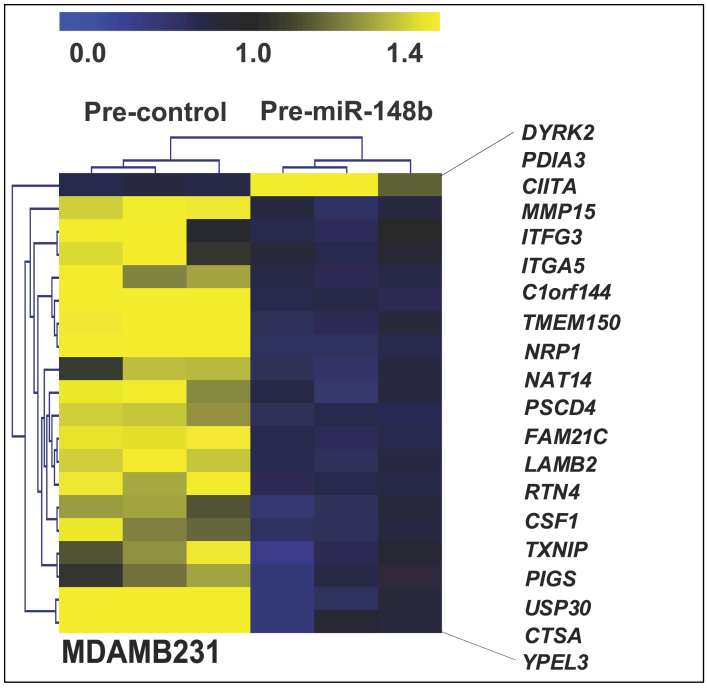

Figure 15. Microarray analysis of miR-148b over-expressing cells
MDAMB231 cells transfected with miR-148b precursors (pre-miR-148b or pre-control) analyzed 48h post-transfection were used to perform microarray analysis. Clustering (Pearson correlation, average linkage) was performed for 20 putative miR-148b targets. Heatmap represents relative gene expression referring to the median across all samples; row: protein-coding gene; column: cell preparation.

Using TargetScan predictions for an Ingenuity Pathway Analysis (IPA) analysis, Granulocyte-Macrophage Colony-Stimulating Factor (GM-CSF) and Integrin pathways were identified as statistically significant (Figure 16). Therefore, we investigated the plausible direct regulation of these pathways by miR-148b and their involvement in breast tumor progression.

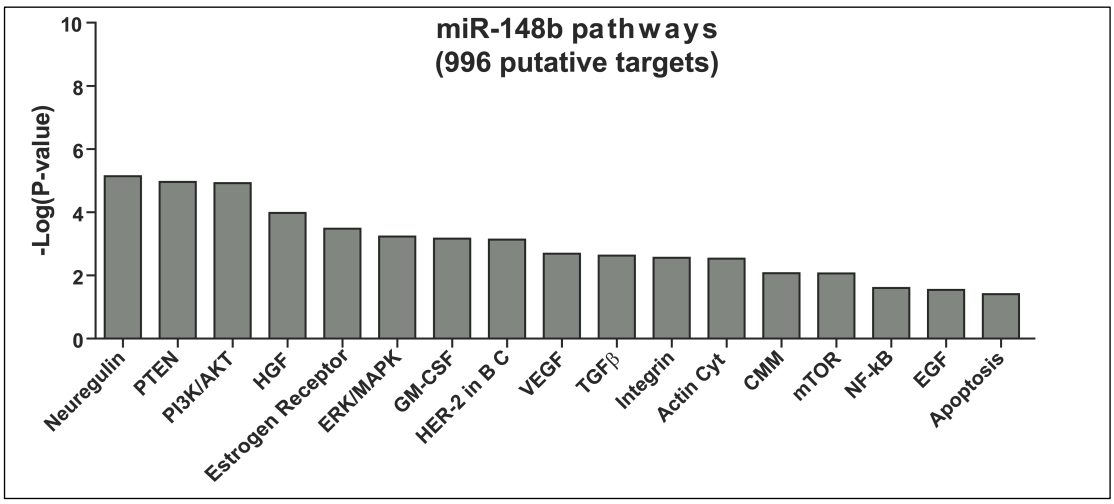

Figure 16. Pathway enrichments obtained using the Ingenuity Pathway Analysis Systems. First TargetScan 5.1 algorithm (non-conserved) was used to predict miR-148b miR targets (996) and then Ingenuity Pathway Analysis was performed to identify miR-148b modulated pathways. 63 pathways related to tumorigenesis and cancer aggressiveness were found and a selection of them is shown here together with the negative Log 10 of the p-value, - Log10 (P-value) with $P<0.05$ (Fisher test). CMM, Cancer Molecular Mechanisms; BC, Breast Cancer.

3.3.1 miR-148b modulates multiple genes of the integrin pathway

Protein expression was evaluated for ITGA5 and its downstream players, Rho-associated, coiled-coil containing protein kinase 1 (ROCK1), PI3-kinase p110 subunit alpha (PI3KCA/p110α), Neuroblastoma RAS viral (v-ras) oncogene homolog (NRAS) (predicted targets) and for CSF1 in miR-148b overexpressing MDAMB231 or 4175TGL cells by Western Blot (WB) analysis and strong reductions were found compared to controls (Figures 17).

Instead, when miR-148b was downmodulated in MCF7 cells, increased levels of ITGA5 proteins were observed (Figure 17). Interestingly, ROCK1, PI3KCA/p110α and NRAS were not modulated at the mRNA level (Figure 14).

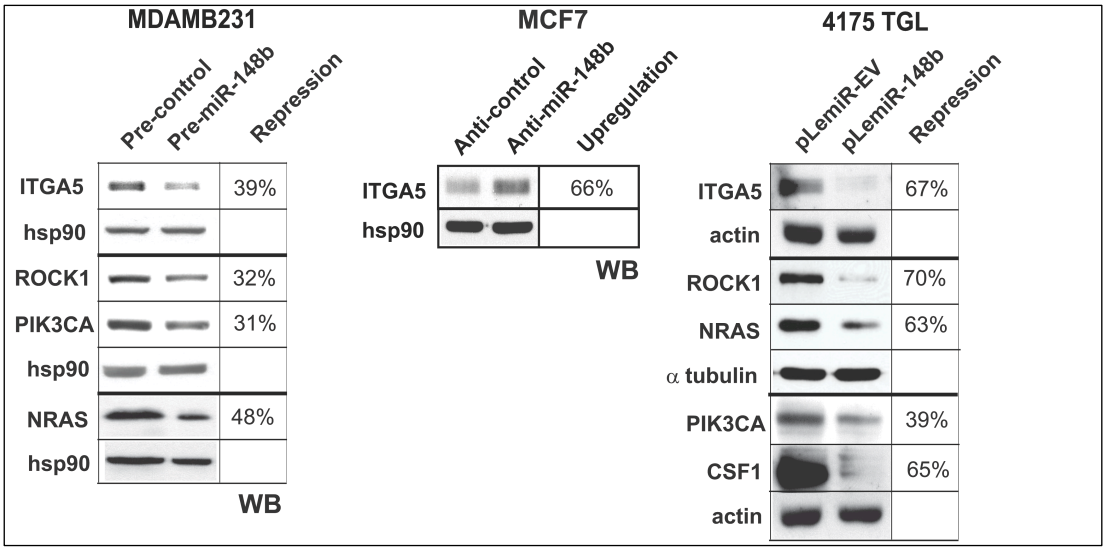

Figure 17. miR-148b modulates multiple genes.
MDAMB231 or MCF7 cells transfected with miR-148b precursors or inhibitors or their negative controls (pre- and anti-miR-148b or pre- and anti-control) analyzed 48h post-transfection or 4175TGL cells stably transduced with pLemiR-EV or pLemiR-148b overexpression vectors were used to perform Western Blot (WB) analysis for five putative miR-148b targets, ITGA5, ROCK1, p110α (PIK3CA), NRAS and CSF1. Protein expression was calculated relative to controls, following miR-148b-overexpression or down-modulation, normalized on the indicated loading controls (hsp90/actin/atubulin) and expressed as repression percentages (%). Three independent experiments were performed with independent protein preparations and representative results are shown.

Direct modulation of miR-148b on its targets, was proven by performing luciferase assays in miR-148b-overexpressing or control MDAMB231 cells transfected with reporter vectors containing wild type or mutated 3'-UTRs (Figures 18A and B). As positive control, a miR-148b-sensor construct was used (Figure 18A). Importantly, when we evaluated miR-148b target expression on a subset of R+/R- human tumors, differential expression was found (Figure 18C).

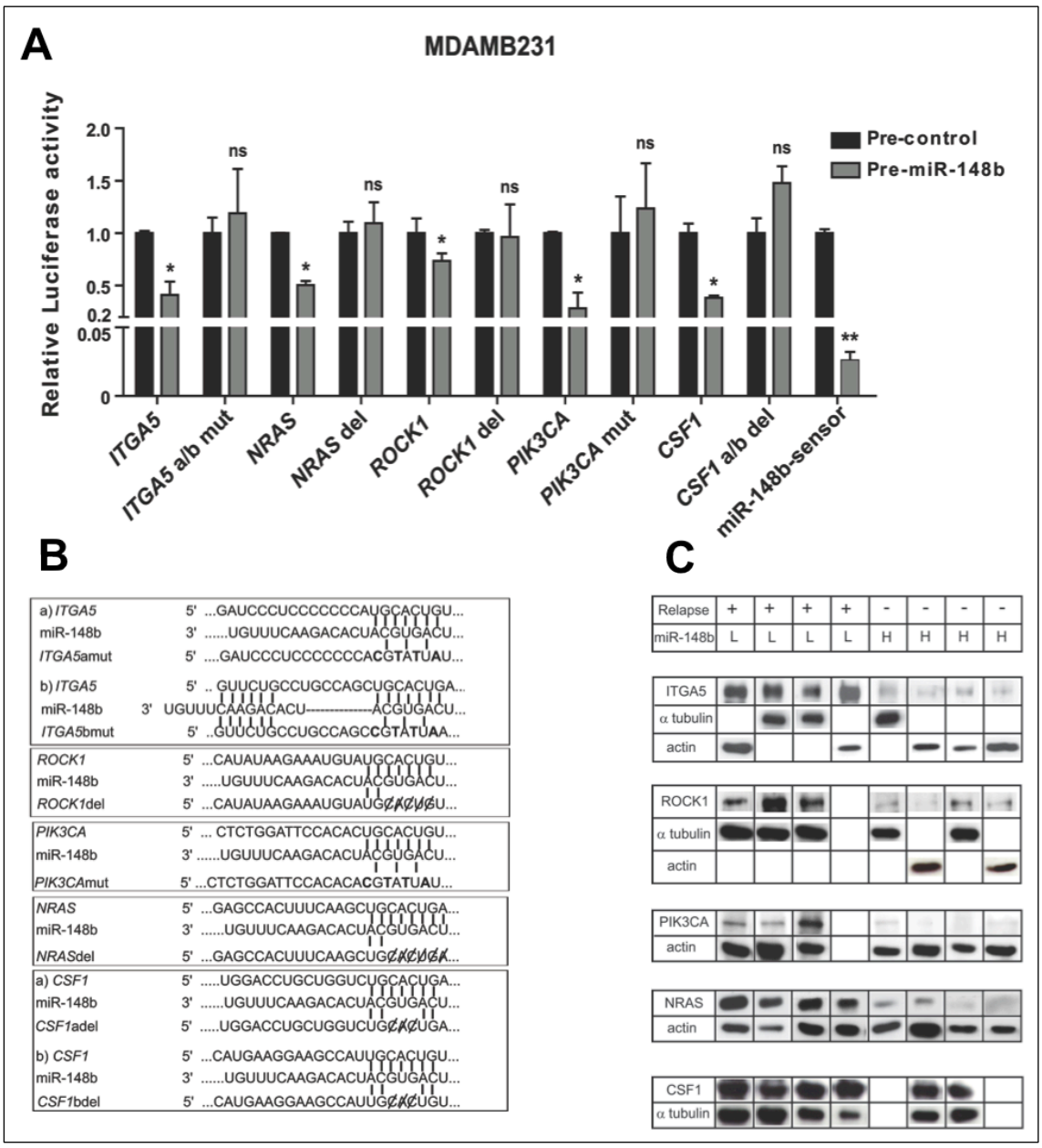

Figure 18. Luciferase array and analysis of miR-148b modulated genes in human tumors.
A-B) MDAMB231 cells transfected with miR-148b precursors (pre-miR-148b or pre-control) analyzed 48h post-transfection were used to perform Luciferase assays (A) in cells transfected with reporter constructs containing wild type or mutant 3'-UTRs (B) for the indicated genes or a synthetic sequence including three perfect miR-148b binding sites (sensor). Results are shown as mean±SEM of Firefly Luciferase activity relative to controls, normalized on Renilla Luciferase activity. mut=mutation; del=deletion; a/b: a and b binding sites. In (A) results of three independent experiments are pooled together. *P<0.05; **P<0.01; ***P<0.001.
C) Proteins were extracted from relapsing or not relapsing primary breast tumors and Western Blot (WB) analysis was performed for the direct miR-148b targets, ITGA5, ROCK1, PIK3CA, NRAS, and CSF1. miR-148b expression is indicated as low (L) or high (H), according to previous microarray and/or qRT-PCR analyses. αtubulin or actin were used as loading controls.

Relevantly, when the 23 predicted and modulated miR-148b target genes were used in Ingenuity System Analysis to look for gene connections the "*Cell-To-Cell Signaling and Interaction, Tissue Development, Cellular Movement*" network was identified (Figure 19A, Ingenuity score=22). Giving the relevance of the integrin pathway in our investigations, we evaluated the possibility that the upstream player, ITGA5, can be used to predict survival in a large microarray dataset of human breast tumor [Wang *et al*., 2005]. Performing hierarchical clustering and Kaplan-Meier analyses, referring to ITGA5 median expression, disease-free survival (DSF) was predicted (Figure 19B). This, together with similar results reported in Nam *et al*. (2009), suggests that repression of ITGA5 correlates with better clinical outcome and can be used as a prognostic marker.

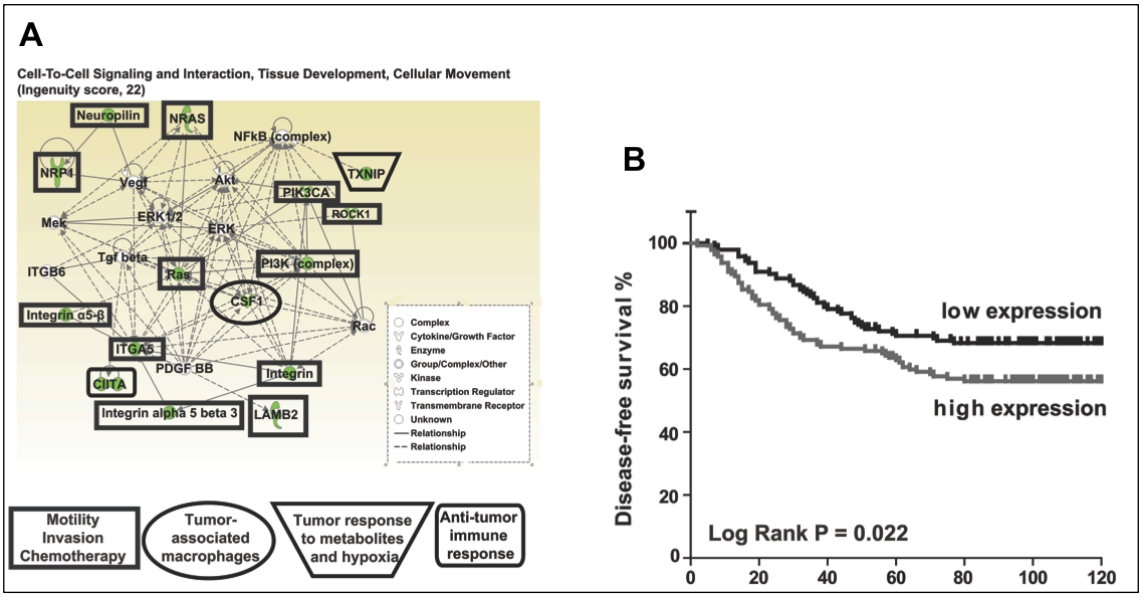

Figure 19. Analysis of miR-148b modulated genes by Ingenuity Systems Analysis.
A) 20 miR-148b down-modulated genes identified in the microarray analysis (Figure 15) plus the three direct targets, ROCK1, PIK3CA and N-RAS, were used to perform an Ingenuity Systems Analysis searching for gene connections; the "*Cell-To-Cell Signaling and Interaction, Tissue Development, Cellular Movement*" functional network was generated. Ingenuity score 22: negative Log10 of the *P*-value. Gene products are represented as nodes and biological relationships between two nodes as a line. Continuous lines indicate direct interactions, while dashed lines represent indirect connections. Shapes of nodes symbolize functional classes of gene products (see figure legend). The green symbols represent down-regulations, while the white symbols indicate genes absent in the input but related with the dataset used. **(B)** Kaplan-Meier analyses of the probability of disease-free survival of breast cancer patients based on ITGA5 expression (median) in Wang *et al*., 2005 dataset for 286 breast tumor samples. *P* value was calculated using the Log Rank test.

3.3.2 Downmodulation of ITGA5 accounts for miR-148b chemotherapy response

The impact of the integrin signaling on cell survival and chemotherapy response was evaluated in absence of serum and adhesion (anoikis) or in presence of Paclitaxel. When ITGA5 was silenced with siRNAs in MDAMB231 cells, reduction in cell survival was observed in anoikis conditions and for Paclitaxel-treated cells *versus* controls (Figure 20A). Instead, when ITGA5 (cDNA lacking its 3'-UTR) was overexpressed (pEGFP-ITGA5), together with pre-miR-148b, in MDAMB231 or MCF7 cells (Figure 20B) and cells were kept in presence of Paclitaxel, the effect of miR-148b on cell death (Figure 13) was abolished. To note that, in Figure 20B, only the difference (delta) observed comparing presence or absence of miR-148b is considered.

ITGA5 and miR-148b levels were evaluated by qRT-PCR analysis (Figure 20A-C). From these results, we can conclude that ITGA5 directly controls, at least partially, miR-148b-driven apoptosis in *anoikis* conditions and in presence of Paclitaxel.

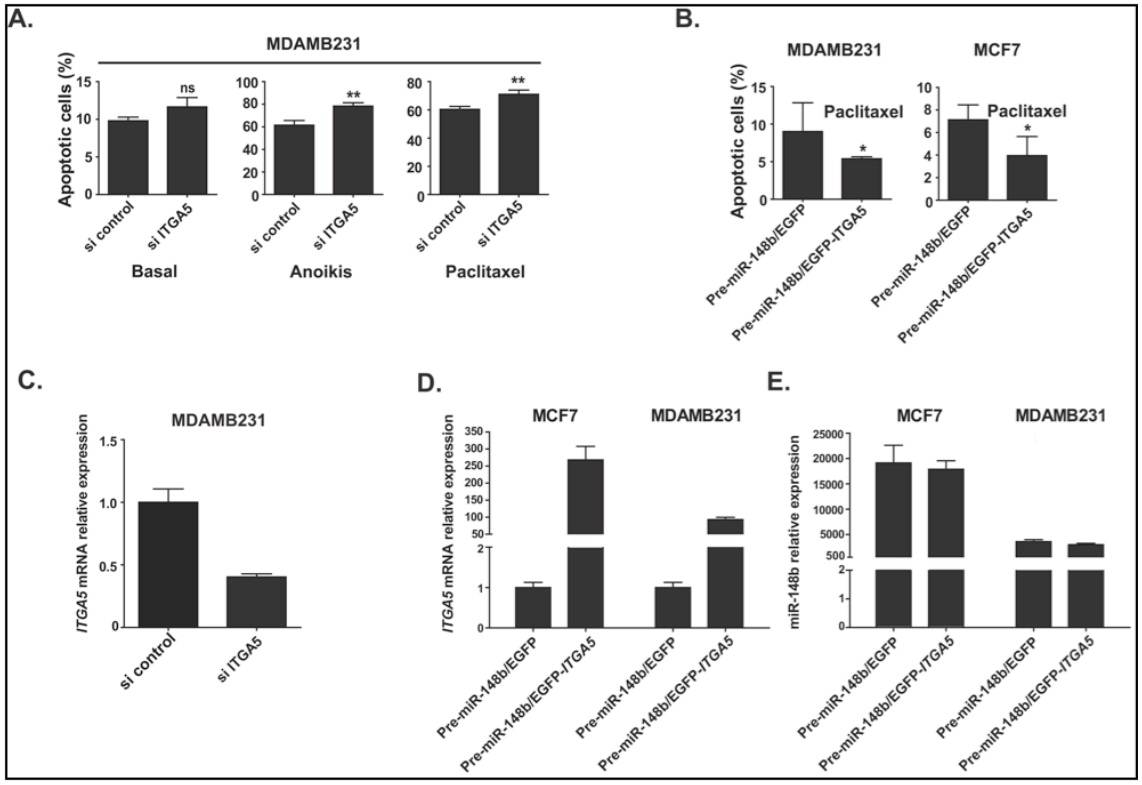

Figure 20. miR-148b-mediated down-modulation of ITGA5 leads to increased chemotherapy-induced apoptosis.

A) Basal or *anoikis*- or Paclitaxel- induced apoptosis was evaluated in MDAMB231 cells transiently transfected with ITGA5-targeting or negative control siRNAs (si ITGA5 or control). **B)** Alternatively, MDAMB231 or MCF7 cells were first transfected with miR-148b precursors or their negative controls (pre-miR-148b or pre-control) and then transfected again (24h later) with empty EGFP or EGFP-ITGA5 overexpressing vectors. No 3'-UTR is present for ITGA5 cDNA. Then cells were treated with Paclitaxel and apoptosis evaluated 48h later. Cell death was measured by TMRM and AnnexinV-FITC **(A)** or AnnexinV-PE stainings **(B)** by FACS analysis. **(A)** ^{High}TMRM-^{Low}AnnexinV: healthy cells; ^{Low}TMRM-^{High}AnnexinV: apoptotic cells. **(B)** ^{Low}AnnexinV: healthy cells; ^{High}AnnexinV: apoptotic cells. Two or three independent experiments were performed in duplicate and pooled quantitations shown as mean±SD. **C, D, E)** qRT-PCR analyses were performed to evaluate ITGA5 mRNA or miR-148b expression for the cells shown Figure 20. Two independent experiments were performed in triplicate, and a representative one is shown. *P<0.05; **P<0.01.

ITGA5 and miR-148b levels were evaluated by qRT-PCR analysis (Figure 21A-C). From these results, we can conclude that ITGA5 directly controls, at least partially, miR-148b-driven apoptosis in *anoikis* conditions and in presence of Paclitaxel.

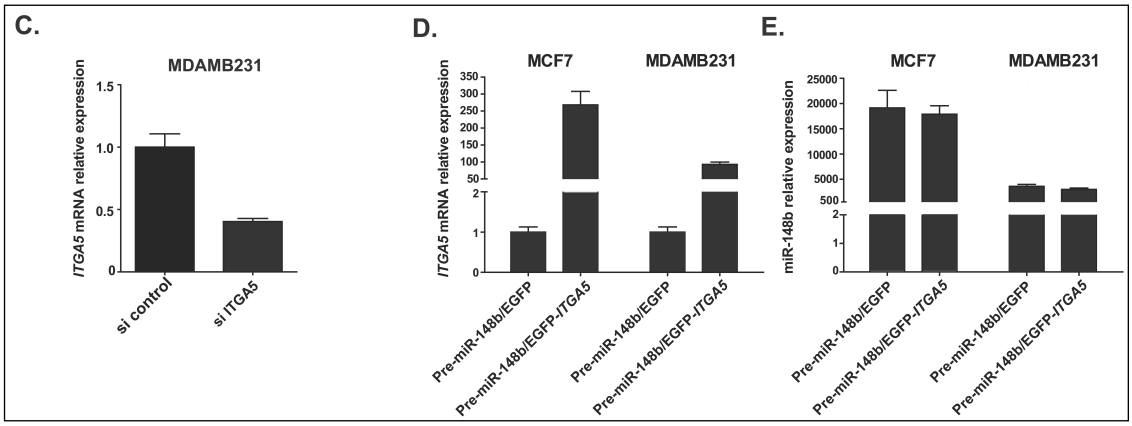

Figure 21. Evaluation of ITGA5 expression values by qRT-PCR.

4. DISCUSSION

In this work we identified a group of 16 miRNAs that associate with bad prognosis in our breast cancer patient cohort (Relapse positive) and we revealed the function of miR-148b as a metastasis suppressor in mice as well as its molecular mechanism of action.

The identification of a group of miRNAs able to identify primary tumor subtypes is highly relevant for the clinics. In fact, it represents a potent molecular tool that clinicians can use at the time of surgery to attempt the most appropriate therapy for every patient. The strength of this tool is further marked by the fact that single components of the signature, for instance miR-148b, can predict tumor outcome individually. Relevantly, low levels of miR-148b were previously observed in Basal-like [Enerly *et al*., 2011] and ERBB2+/ER-/PR- [Mattie *et al*., 2006] breast tumors suggesting its involvement in malignancy.

Our functional experiments with metastatic cells, strongly suggest that miR-148b exerts its metastasis-suppressing role mostly by controlling cell movement. In fact, while it is true that ectopic expression of miR-148b in malignant tumor cells leads to decreased tumor growth, this effect is modest and not sufficient to justify the much more pronounced control of metastasis dissemination. On this line, increased miR-148b levels lead to stronger adhesion and *anoikis* and reduce invasion *in vitro*. Moreover, *in vivo*, miR-148b strongly reduces extravasation and lung colonization shortly after injection of the cells in the blood circulation, when proliferation has no time to play a major role. Overall, it is well accepted that miRNAs have pleiotropic functions and therefore can act in independent events such as tumor formation and progression via the activation/repression of a selective and rate-limiting cascade of specific genes [Blenkiron *et al*., 2007; Ma & Weinberg, 2008; Valastyan *et al*., 2010; Tavazoie *et al*., 2008].

Of the over 130 genes modulated by miR-148b, many are known to be relevant in tumor progression; among them, cathepsin A (CTSA*)*, neuropilin 1 (NRP1*)*, colony stimulating factor 1 (CSF1), matrix metallopeptidase 15 (MMP15*)* and integrin alpha 5 (ITGA5), all suppressed by miR-148b. By focusing on the ITGA5 signaling, we found that not only ITGA5, but also Rho-associated, coiled-coil containing protein kinase 1 (ROCK1), PI3-kinase p110 subunit alpha (PI3KCA/p110α), Neuroblastoma RAS viral (v-ras) oncogene homolog (NRAS) are directly downregulated by miR-148b,

suggesting a specific control for this miRNA on a pathway known to be involved in metastasis dissemination and chemotherapy response. In fact, ITGA5 and ROCK1 were previously found to be highly expressed in malignant breast tumors and are known to increase tumor growth or progression [Nam *et al*., 2009; Valastyan *et al*., 2009, Taverna *et al*., 2001; Liu *et al*., 2009; Lane *et al*., 2008; Zheng *et al*., 2011]. At the same time, PIK3CA/p110a is relevant for mammary tumorigenesis and angiogenesis [Renner *et al*., 2008] as well as for resistance to endocrine or anti-HER2 therapies [Eichhorn *et al*., 2008; Miller *et al*., 2010]. In addition, NRAS is a well known oncogene and its silencing in tumor cells leads to increased apoptosis [Eskandarpour *et al*., 2005]. Regarding chemotherapy response, elevated levels and activity of α5β1 have previously been implicated in drug-resistance [Nista *et al*., 1997] and inhibition of α5β1/fibronectin interactions promotes apoptosis in malignant cells and enhances radiation effects [Nam *et al*., 2009]. In addition, perturbations of the actin cytoskeleton integrity via ROCK1 inhibition commit cells to apoptosis [Shi & Wei, 2007]. Remarkably, ITGA5 and its downstream player RHOA, a ROCK activator, have been previously found to be suppressed by miR-31, another small non-coding RNA that suppresses metastasis [Valastyan *et al*., 2009]. In addition, ROCK1 and RHOC are also directly targeted by two other miRs involved in tumor progression, miR-146a/b and miR-10b [Liu *et al*., 2008; Ma *et al*., 2007]. The fact that CSF1 is also a direct target of miR-148b opens up a role for this small RNA in tumor-stroma cell interactions, which will be part of a future study.

In conclusion, our study unravels the association of a group of 16 miRNAs with bad prognosis tumors and identifies miR-148b as a suppressor of tumor progression and modulator of chemotherapy response acting via the integrin.

5. REFERENCES

Abraham, D., Zins, K., Sioud, M., Lucas, T., Schafer, R., Stanley, E. R., and Aharinejad, S. Stromal cell-derived CSF-1 blockade prolongs xenograft survival of CSF-1-negative neuroblastoma. (2010) *Int J Cancer* **126**:1339-1352.

Aharinejad, S., Paulus, P., Sioud, M., Hofmann, M., Zins, K., Schafer, R., Stanley, E. R., and Abraham, D. (2004) Colony-stimulating factor-1 blockade by antisense oligonucleotides and small interfering RNAs suppresses growth of human mammary tumor xenografts in mice. *Cancer Res* **64**:5378-5384.

Alvarez-Garcia, I., Miska, E.A. (2005) MicroRNA functions in animal development and human disease. *Development* **132**(21):4653-62.

Bartel, D.P. (2004). MicroRNAs: genomics, biogenesis, mechanism, and function. *Cell* **116**:281-97.

Bartel, D.P. (2009). MicroRNAs: target recognition and regulatory functions. *Cell* **136**(2):215-33.

Bertucci, F., Birnbaum, D. (2008) Reasons for breast cancer heterogeneity. *J Biol.* **7**(2):6.

Bhayani, M.K., Calin, G.A., Lai, S.Y. (2012) Functional relevance of miRNA* sequences in human disease. *Mutat Res*. **731**:14-19.

Blenkiron, C., Goldstein, L.D., Thorne, N.P., Spiteri, I., Chin, S.F., Dunning, M.J. *et al*. (2007) MicroRNA expression profiling of human breast cancer identifies new markers of tumor subtype. *Genome Biol.* **8**:R214.

Bolstad, B.M., Irizarry, R.A., Astrand, M., Speed, T.P. (2003) A comparison of normalization methods for high density oligonucleotide array data based on variance and bias. *Bioinformatics* **19**:185-93.

Bookout, A.L., Mangelsdorf, D.J. (2003) Quantitative real-time PCR protocol for analysis of nuclear receptor signaling pathways. *Nucl Recept Signal.* **1**:e012.

Braun, S., Vogl, F.D., Naume, B., Janni, W., Osborne, M.P., Coombes, R.C., Schlimok, G., Diel, I.J., Gerber, B., Gebauer, G., *et al*. (2005). A pooled analysis of bone marrow micrometastasis in breast cancer. *N. Engl. J. Med*. **353**:793–802.

Calin, G.A., Cimmino, A., Fabbri, M., Ferracin, M.,Wojcik, S.E., Shimizu, M., *et al*. (2008) miR-15a and miR-16–1 cluster functions in human leukemia. *Proc Natl Acad Sci USA* **105**:5166–71.

Calin, G.A., Dumitru, C.D., Shimizu, M., Bichi, R., Zupo, S., Noch, E., *et al*. (2002) Frequent deletions and down-regulation of micro-RNA genes miR15 and miR16 at 13q14 in chronic lymphocytic leukemia. *Proc Natl Acad Sci U S A* **99**:15524–9.

Calin, G.A., Ferracin, M., Cimmino, A., Di Leva, G., Shimizu, M., Wojcik, S.E., Iorio, M.V., Vison,e R. *et al*. (2005) A microRNA signature associated with prognosis and progression in Chronic Lymphocytic leukemia. *N Engl J Med.* **353**:1793-1801.

Chen, C., Ridzon, D.A., Broomer, A.J., Zhou, Z., Lee, D.H., Nguyen, J.T. *et al*. (2005) Real-time quantification of microRNAs by stem-loop RT-PCR. *Nucleic Acids Res.* **33**:e179.

Cho, W.C. 2007. OncomiRs: the discovery and progress of microRNAs in cancers. *Mol Cancer* **6:**60.

Collins, T.J. (2007) ImageJ for microscopy. *Biotechniques* **43**:25-30.

Colozza, M., Cardoso, F., Sotiriou, C., Larsimont, D., Piccart, M.J. (2005) Bringing molecular prognosis and prediction to the clinic. *Clin Breast Cancer* **6**(1)**:** 61-76.

Damasco, C., Lembo, A., Somma, M. P., Gatti, M., Di Cunto, F., and Provero, P. (2011) A signature inferred from Drosophila mitotic genes predicts survival of breast cancer patients. *PLoS One* **6**:e14737.

Desgrosellier, J. S., and Cheresh, D. A. Integrins in cancer: biological implications and therapeutic opportunities. (2010) *Nat Rev Cancer* **10**:9-22

Dunnwald, L.K., Rossing, M.A., Li, C.I. (2007) Hormone receptor status, tumor characteristics, and prognosis: a prospective cohort of breast cancer patients. *Breast Cancer Res.* **9**(1)**:** R6.

Eichhorn, P.J., Gili, M., Scaltriti, M., Serra, V., Guzman, M., Nijkamp, W. *et al*. (2008) Phosphatidylinositol 3-kinase hyperactivation results in lapatinib resistance that is reversed by the mTOR/phosphatidylinositol 3-kinase inhibitor NVPBEZ235. *Cancer Res*. **68**:9221–9230.

Eifel, P., Axelson, J.A., Costa, J., *et al*. (2000) National Institutes of Health Consensus Development Conference Statement: adjuvant therapy for breast cancer, November 1-3, 2000. *J Natl Cancer Inst.* **93**:979-89.

Enerly, E., Steinfeld, I., Kleivi, K., Leivonen, S.K., Aure, M.R., Russnes, H.G. *et al*. (2011) miRNA-mRNA integrated analysis reveals roles for miRNAs in primary breast tumors. *PLoS One* **6**:e1691529.

Eskandarpour, M., Kiaii, S., Zhu, C., Castro, J., Sakko, A.J., and Hansson, J. (2005) Suppression of oncogenic NRAS by RNA interference induces apoptosis of human melanoma cells. *Int. J. Cancer* **115**:65–73.

Filipowicz, W., Bhattacharyya, S.N., Sonenberg, N. (2008) Mechanisms of post-transcriptional regulation by microRNAs: are the answers in sight? *Nature Reviews Genetics* **9**:102–114.

Finak, G., Bertos, N., Pepin, F., Sadekova, S., Souleimanova, M., Zhao, H. *et al*. (2008). Stromal gene expression predicts clinical outcome in breast cancer. *Nat. Med.* **14**:518–527.

Galea, M.H., Blamey, R.W., Elston, C.E., Ellis, I.O. (1992) The Nottingham Prognostic Index in primary breast cancer. *Breast Cancer Res Treat*. **22**:207-19.

Gill, R. (1982) Understanding Cox's regression model. *Exper. Suppl.* **41**:187–199.

Goldhirsch, A., Ingle, J.N., Gelber, R.D., Coates, A.S., Thurlimann, B., Senn, H.J. (2009) Thresholds for therapies: highlights of the St Gallen International Expert Consensus on the primary therapy of early breast cancer 2009. *Ann Oncol*. **20**:1319-29.

Hammond, S.M. (2007) MicroRNAs as tumor suppressors. *Nat Genet.* **39**:582-3.

Harari, D., Yarden, Y. (2000) Molecular mechanisms underlying ErbB2/HER2 action in breast cancer. *Oncogene* **19**:6102-14.

Harris, L., Fritsche, H., Mennel, R., Norton, L., Ravdin, P., Taube, S., Somerfield, M.R., Hayes, D.F., Bast, R.C. Jr. (2007) American Society of Clinical Oncology 2007 update of recommendations for the use of tumor markers in breast cancer. *J Clin Oncol.* **25**:5287-312.

Holliday, D.L., Speirs, V. (2011) Choosing the right cell line for breast cancer research. *Breast Cancer* **12**;13(4):215.

Hurst, D.R., Edmonds, M.D., Welch, D.R. (2009) MetastamiR: the field of metastasis-regulatory microRNA is spreading. *Cancer Res*. **69**:7495-8.

Iorio, M.V., Casalini, P., Piovan, C., Braccioli, L., Tagliabue, E. (2011) Breast cancer and microRNAs: therapeutic impact. *Breast* **20**(3):S63-70.

Jemal, A., Siegel, R., Xu, J., Ward, E. (2010) Cancer statistics. *CA Cancer J Clin* **60**(5):277-300.

Kim, V.N., Han, J., Siomi, M.C. (2009) Biogenesis of small RNAs in animals. *Nat Rev Mol Cell Biol*. **10**:126–139.

Kim, V.N., Nam, J-W. (2006) Genomics of microRNA. *Trends in Genetics* **22**:165–173.

Korpal, M., Kang, Y. (2008) The emerging role of miR-200 family of microRNAs in epithelial-mesenchymal transition and cancer metastasis. *RNA Biol.* **5**:115–9.

Kueng, W., Silber, E., Eppenberger, U. (1989) Quantification of cells cultured on 96-well plates. *Anal Biochem.* **182**:16-9.

Landgraf, P., Rusu, M., Sheridan, R., Sewer, A., Iovino, N., Aravin, A., Pfeffer, S., Rice, A. *et al*. (2007) A mammalian microRNA expression atlas based on small RNA library sequencing. *Cell* **129**:1401-14.

Lane, J., Martin, T. A., Watkins, G., Mansel, R. E., and Jiang, W.G. (2008) The expression and prognostic value of ROCK I and ROCK II and their role in human breast cancer. *Int J Oncol* **33**:585-593.

Laukaitis, C.M., Webb, D.J., Donais, K., Horwitz, A.F. (2001) Differential dynamics of alpha 5 integrin, paxillin, and alpha-actinin during formation and disassembly of adhesions in migrating cells. *J Cell Biol*. **153**:1427-40.

Leonardo, T.R., Schultheisz, H.L., Loring, J.F., Laurent, L.C. (2012) The functions of microRNAs in pluripotency and reprogramming. *Nat Cell Biol*. **14**(11):1114-21.

Lewis, B.P., Burge, C.B., Bartel, D.P. (2005) Conserved seed pairing, often flanked by adenosines, indicates that thousands of human genes are microRNA targets. *Cell* **120**:15-20.

Liu, S., Goldstein, R. H., Scepansky, E. M., and Rosenblatt, M. (2009) Inhibition of rho-associated kinase signaling prevents breast cancer metastasis to human bone. *Cancer Res* **69**, 8742-8751.

Liu, Y. (2008) Box plots: use and interpretation. *Transfusion* **48**, 2279–2280.

Livak, K.J., Schmittgen, T.D. (2001) Analysis of relative gene expression data using Real-Time Quantitative PCR and the $2^{-\Delta\Delta Ct}$ method. *Methods* **25**:402-408.

Lu, J., Getz, G., Miska, E.A., Alvarez-Saavedra, E., Lamb, J., Peck, D. *et al*. (2005) MicroRNA expression profiles classify human cancers. *Nature* **435**:834–838.

Ma L, Reinhardt F, Pan E, Soutschek J, Bhat B, Marcusson EG, *et al*. (2010) Therapeutic silencing of miR-10b inhibits metastasis in a mouse mammary tumor model. *Nat Biotechnol*. **28**:341–7.

Ma, L., and Weinberg, R. A. (2008) Micromanagers of malignancy: role of microRNAs in regulating metastasis. *Trends Genet* **24**:448-456.

Ma, L., Teruya-Feldstein, J., and Weinberg, R.A. (2007) Tumour invasion and metastasis initiated by microRNA-10b in breast cancer. *Nature* **449**:682–688.

Mah, S.M., Buske, C., Humphries, R.K., Kuchenbauer, F. (2010) miRNA*: a passenger stranded in RNA-induced silencing complex? *Crit Rev Eukaryot Gene Expr*. **20**(2):141-8.

Mantel, N. (1966) Evaluation of survival data and two new rank order statistics arising in its consideration. *Cancer Chemother. Rep.* **50**:163–170.

Martello, G., Rosato, A., Ferrari, F., Manfrin, A., Cordenonsi, M., Dupont, S., *et al*. (2010) A microRNA targeting Dicer for metastasis control. *Cell* **141**:1195–207.

Mattie, M.D., Benz, C.C., Bowers, J., Sensinger, K., Wong, L., Scott, G. K., Fedele, V., Ginzinger, D., Getts, R., and Haqq, C. (2006) Optimized high-throughput microRNA

expression profiling provides novel biomarker assessment of clinical prostate and breast cancer biopsies. *Mol Cancer* **5**:24.

Mierke, C. T., Frey, B., Fellner, M., Herrmann, M., and Fabry, B. Integrin alpha5beta1 facilitates cancer cell invasion through enhanced contractile forces. (2011) *J Cell Sci* **124**:369-383.

Miller, T.W., Hennessy, B.T., Gonzalez-Angulo, A.M., Fox, E.M., Mills, G.B., Chen, H. *et al*. (2010) Hyperactivation of phosphatidylinositol-3 kinase promotes escape from hormone dependence in estrogen receptor-positive human breast cancer. *J. Clin. Invest*. **120**:2406–2413.

Minn, A.J., Kang, Y., Serganova, I., Gupta, G.P., Giri, D.D., Doubrovin, M. *et al*. (2005) Distinct organ-specific metastatic potential of individual breast cancer cells and primary tumors. *J Clin Invest.* **115**:44-55.

Nam, J. M., Chung, Y., Hsu, H. C., and Park, C. C. (2009) beta1 integrin targeting to enhance radiation therapy. *Int J Radiat Biol* **85**:923-928.

Nista, A., Leonetti, C., Bernardini, G., Mattioni, M., and Santoni, A. (1997) Functional role of alpha4beta1 and alpha5beta1 integrin fibronectin receptors expressed on adriamycin-resistant MCF-7 human mammary carcinoma cells. *Int. J. Cancer* **72**:133–141.

Pantel, K., Brakenhoff, R.H., and Brandt, B. (2008). Detection, clinical relevance and specific biological properties of disseminating tumour cells. *Nat. Rev. Cancer* **8**:329–340.

Penna E, Orso F, Cimino D, Tenaglia E, Lembo A, Quaglino E, *et al*. (2011) microRNA-214 contributes to melanoma tumour progression through suppression of TFAP2C. *EMBO J*. **30**:1990–2007.

Png, K.J., Halberg, N., Yoshida, M., Tavazoie, S.F. (2011) A microRNA regulon that mediates endothelial recruitment and metastasis by cancer cells. *Nature* **481**:190–4.

Poy, M.N., Spranger, M., Stoffel, M. (2007) microRNAs and the regulation of glucose and lipid metabolism. *Diabetes Obes Metab* **9**(2):67-73.

Quintana, E., Shackleton, M., Sabel, M.S., Fullen, D.R., Johnson, T.M., Morrison, S.J. (2008) Efficient tumour formation by single human melanoma cells. *Nature* **456**(7222):593-8.

Rasola, A., Geuna, M. (2001) A flow cytometry assay simultaneously detects independent apoptotic parameters. *Cytometry* **45**:151-7.

Renner, O., Blanco-Aparicio, C., Grassow, M., Canamero, M., Leal, J. F., and Carnero, A. (2008) Activation of phosphatidylinositol 3-kinase by membrane localization of p110alpha predisposes mammary glands to neoplastic transformation. *Cancer Res*. **68**: 9643–9653.

Risso, D., Massa, M.S., Chiogna, M., Romualdi, C. (2009) A modified LOESS normalization applied to microRNA arrays: a comparative evaluation. *Bioinformatics* **25**:2685-91.

Saeed, A. I., Bhagabati, N. K., Braisted, J. C., Liang, W., Sharov, V., Howe, E. A., Li, J., Thiagarajan, M., White, J. A., and Quackenbush, J. (2006) TM4 microarray software suite. *Methods Enzymol.* **411**:134–193.

Shi, J., and Wei, L. (2007) Rho kinase in the regulation of cell death and survival. *Arch. Immunol. Ther. Exp. (Warsz.)* **55**:61–75.

Si, M.L., Zhu, S., Wu, H., Lu, Z., Wu, F., Mo, Y.Y. (2007) miR-21-mediated tumor growth. *Oncogene* **26**:2799–803.

Siegel, R., DeSantis, C., Virgo, K., Stein, K., Mariotto, A., Smith, T. *et al*. (2012) Cancer treatment and survivorship statistics, 2012. CA *Cancer J Clin.* **62**(4):220-41.

Simpson, J.F., Gray, R., Dressler, L.G., Cobau, C.D., Falkson, C.I., Gilchrist, K.W., Pandya, K.J., Page, D.L., Robert, N.J. (2000) Prognostic value of histologic grade and proliferative activity in axillary node-positive breast cancer: results from the Eastern Cooperative Oncology Group Companion Study, EST 4189. *J Clin Oncol.* **18**:2059-69.

Song, B.,Wang, C., Liu, J.,Wang, X., Lv, L.,Wei, L., *et al*. (2010) MicroRNA-21 regulates breast cancer invasion partly by targeting tissue inhibitor of metalloproteinase 3 expression. *J Exp Clin Cancer Res*. **29**:29.

Sorlie, T., Perou, C.M., Tibshirani, R., Aas, T., Geisler, S., Johnsen, H. *et al*. (2001) Gene expression patterns of breast carcinomas distinguish tumor subclasses with clinical implications. *Proc. Natl. Acad. Sci. U. S. A.* **98**:10869–10874.

Sotiriou, C., and Piccart, M. J. (2007) Taking gene-expression profiling to the clinic: when will molecular signatures become relevant to patient care? *Nat. Rev. Cancer* **7**:545–553.

Stern-Ginossar, N., Elefant, N., Zimmermann, A., Wolf, D.G., Saleh, N., Biton, M. *et al*. (2007) Host immune system gene targeting by a viral miRNA. *Science* **317**:376-81.

Subramanian, S., Lui, W.O., Lee, C.H., Espinosa, I., Nielsen, T.O., Heinrich, M.C., Corless, C.L., Fire, A.Z., van de Rijn, M. (2008) MicroRNA expression signature of human sarcomas. *Oncogene* **27**(14):2015-26.

Tarone, G., Russo, M. A., Hirsch, E., Odorisio, T., Altruda, F., Silengo, L., and Siracusa, G. (1993) Expression of beta 1 integrin complexes on the surface of unfertilized mouse oocyte. *Development* **117**:369–1375.

Tavazoie, S. F., Alarcon, C., Oskarsson, T., Padua, D., Wang, Q., Bos, P. D., Gerald, W. L., and Massague, J. (2008) Endogenous human microRNAs that suppress breast cancer metastasis. *Nature* **451**:147-152.

Taverna, D., and Hynes, R.O. (2001) Reduced blood vessel formation and tumor growth in alpha5-integrin-negative teratocarcinomas and embryoid bodies. *Cancer Res* **61**:5255-5261

Thiery, J.P., Acloque, H., Huang, R.Y.J., and Nieto, M.A. (2009). Epithelialmesenchymal transitions in development and disease. *Cell* **139**:871–890.

Tibshirani, R., Hastie, T., Narasimhan, B., and Chu, G. (2002) Diagnosis of multiple cancer types by shrunken centroids of gene expression. *Proc. Natl. Acad. Sci. U. S. A.* **99**:6567–6572 11.

Tili, E., Croce, C.M., Michaille, J.J. (2009) miR-155: on the crosstalk between inflammation and cancer. *Int Rev Immunol*. **28**:264–84.

Valastyan, S. (2012) Roles of microRNAs and other non-coding RNAs in breast cancer metastasis. *J Mammary Gland Biol Neoplasia* **17**(1):23-32.

Valastyan, S., Benaich, N., Chang, A., Reinhardt, F., and Weinberg, R. A. (2009) Concomitant suppression of three target genes can explain the impact of a microRNA on metastasis. *Genes Dev* **23**:2592-2597.

Valastyan, S., Chang, A., Benaich, N., Reinhardt, F., and Weinberg, R. A. (2010) Concurrent suppression of integrin alpha5, radixin, and RhoA phenocopies the effects of miR-31 on metastasis. *Cancer Res* **70**, 5147-5154.

Valastyan, S., Reinhardt, F., Benaich, N., Calogrias, D., Sza´ sz, A.M., Wang, Z.C., Brock, J.E., Richardson, A.L., and Weinberg, R.A. (2009). A pleiotropically acting microRNA, miR-31, inhibits breast cancer metastasis. *Cell* **137**:1032–1046.

Valastyan, S., Weinberg, R.A. (2011) Tumor metastasis: molecular insights and evolving paradigms. *Cell* **147**(2):275-92.

Vargo-Gogola, T., Rosen, J.M. (2007) Modelling breast cancer: one size does not fit all. *Nat Rev Cancer*. **7**(9):659-72.

Voorhoeve, P.M., Agami, R. (2006) Classifying microRNAs in cancer: the good, the bad and the ugly. *Biochim Biophys Acta* **1775**:274-82.

Wang, H., Ach, R.A., Curry, B. (2007) Direct and sensitive miRNA profiling from low-input total RNA. *RNA* **13**:151-159.

Wang, Y., Klijn, J. G., Zhang, Y., Sieuwerts, A. M., Look, M. P., Yang, F. *et al*. (2005) Gene-expression profiles to predict distant metastasis of lymph-node-negative primary breast cancer. *Lancet* **365**, 671–679.

Wang, Y., Klijn, J. G., Zhang, Y., Sieuwerts, A. M., Look, M. P., Yang, F. *et al*. (2005) Gene-expression profiles to predict distant metastasis of lymph-node-negative primary breast cancer. *Lancet* **365**, 671-679.

Webster, R.J., Giles, K.M., Price, K.J., Zhang, P.M., Mattick, J.S., Leedman, P.J. (2009) Regulation of epidermal growth factor receptor signaling in human cancer cells by microRNA-7. *J Biol Chem.* **284**:5731–41.

Weidhaas, J.B., Babar, I., Nallur, S.M., Trang, P., Roush, S., Boehm, M., *et al*. (2007) MicroRNAs as potential agents to alter resistance to cytotoxic anticancer therapy. *Cancer Res*. **67**:11111–6.

Wiemer, E.A. (2007) The role of microRNAs in cancer: no small matter. *Eur J Cancer* **43**:1529-44.

Winter, J., Jung, S., Keller, S., Gregory, R.I., Diederichs, S. (2009) Many roads to maturity: microRNA biogenesis pathways and their regulation. *Nature Cell Biology* **11**:228–234.

Zhang, B., Pan, X., Cobb, G.P., Anderson, T.A. (2007) microRNAs as oncogenes and tumor suppressors. *Dev Biol.* **302**:1-12.

Zheng, B., Liang, L., Wang, C., Huang, S., Cao, X., Zha, R. *et al*. (2011) MicroRNA-148a Suppresses Tumor Cell Invasion and Metastasis by Downregulating ROCK1 in Gastric Cancer. *Clin Cancer Res.* **17**(24):7574-83.

Zweig, M. H., and Campbell, G. (1993) Receiver-operating characteristic (ROC) plots: a fundamental evaluation tool in clinical medicine. *Clin. Chem*. **39**:561–577.

6. SUPPLEMENTAL DATA

Figure S1. Differentially expressed miRNAs comparing estrogen receptor positive (ER+) and estrogen receptor negative (ER-) tumor samples. Table shows the levels of expression of the 29 most modulated miRNAs in ER+ (n=53) *versus* ER- (n=24) tumor samples. The averaged level of each miRNA in tumor samples *versus* mammoplastic reductions (controls) is shown as Log2. SAM two classes, False Discovery Rate (FDR): 14%.

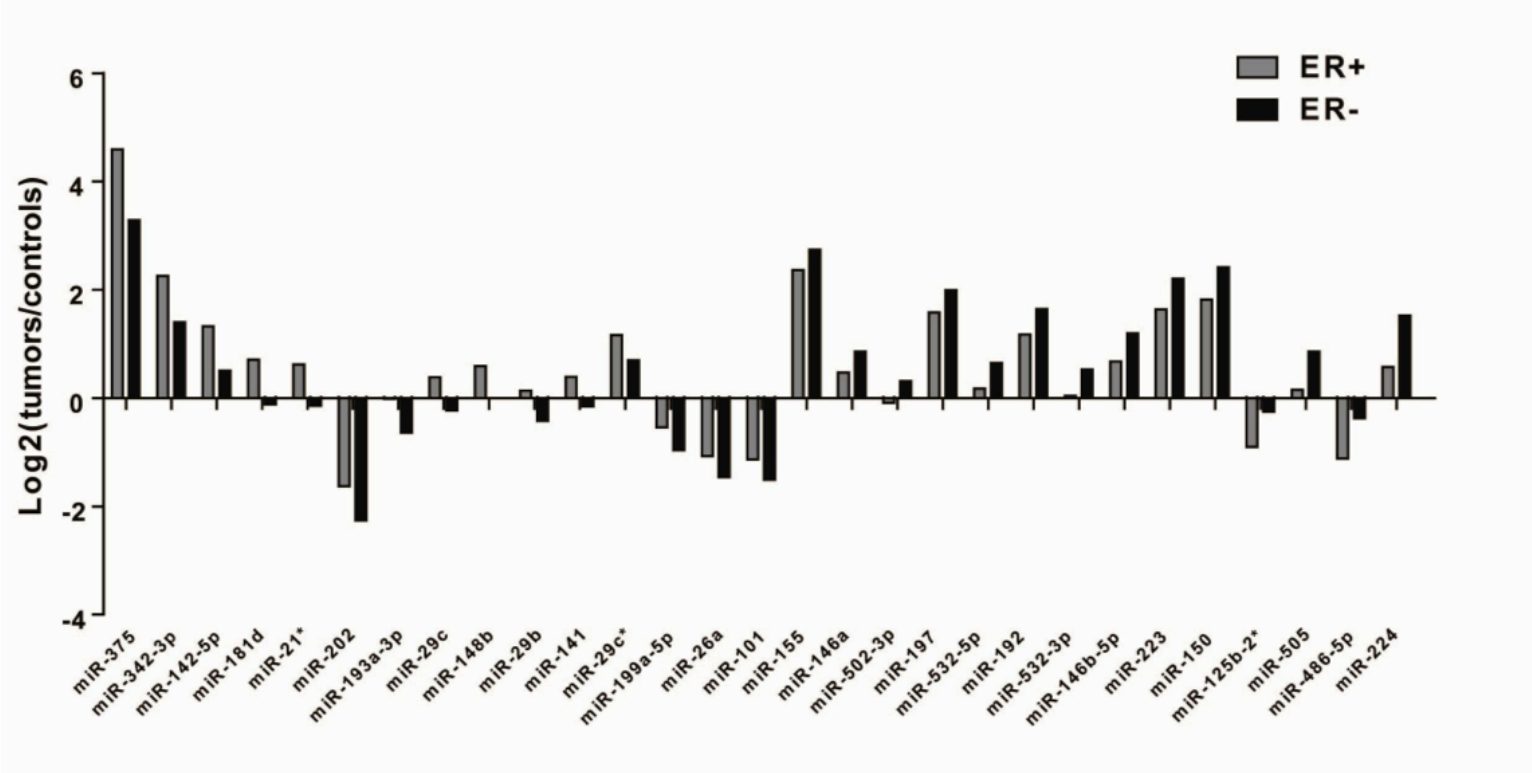

Figure S2 – Differentially expressed miRNAs comparing progesterone receptor positive (PR+) and progesterone receptor negative (PR-) tumor samples.

Table shows the levels of expression of the 56 most modulated miRNAs in PR+ (n=42) *versus* PR- (n=35) tumor samples. The averaged level of each miRNA in tumor samples *versus* mammoplastic reductions (controls) is shown as Log2. SAM two classes, False Discovery Rate (FDR): 9.30%.

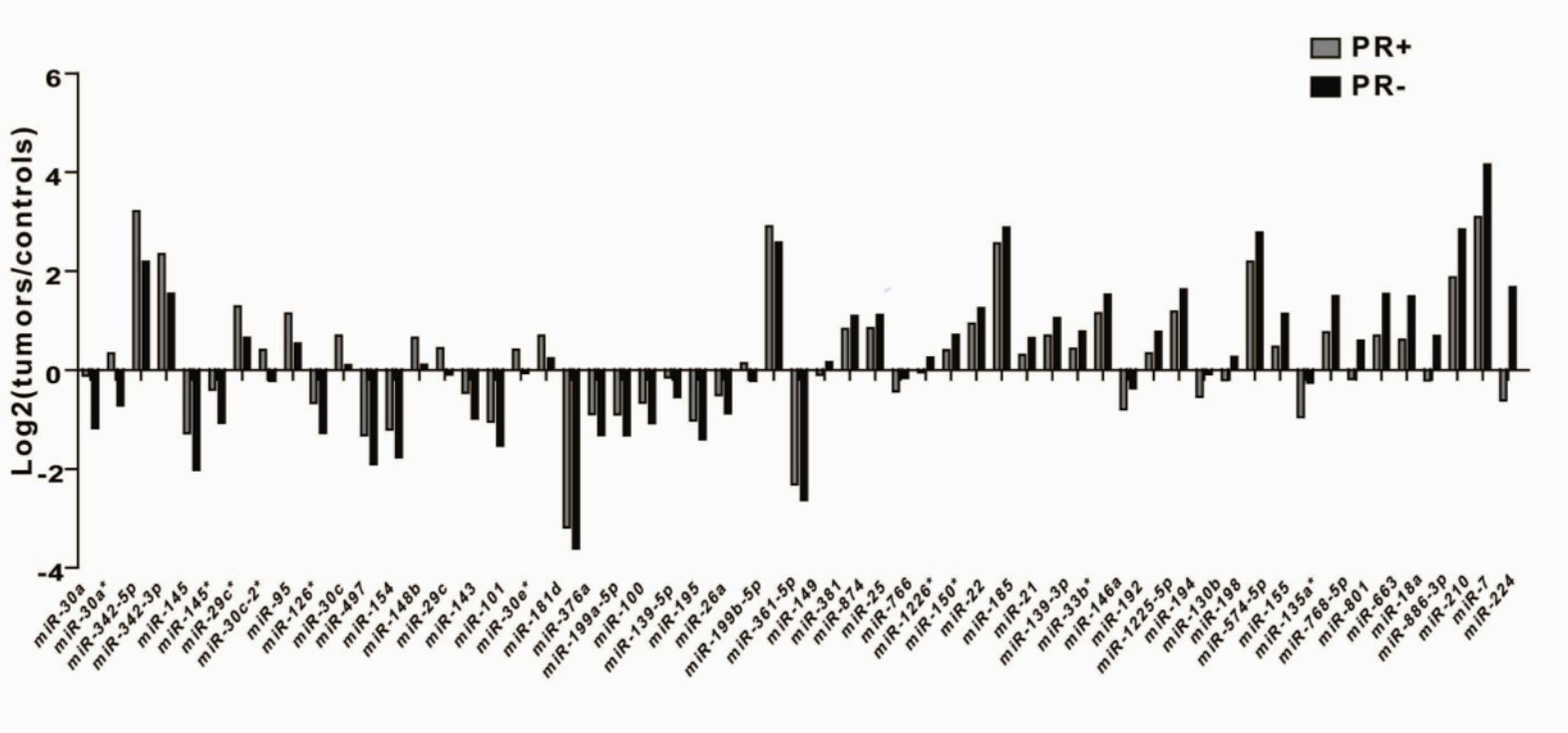

Table S1. Cloning oligonucleotides employed in this study.

Primer ID	Sequence (5'→ 3')
miR-148b_forw (miR-148b overexpression)	TTTCATAGGCACCACTCACTTTAC
miR-148b_rev (miR-148b overexpression)	CCCTTTCCCCTTACTCTCCA
miR-187_forw (miR-187 overexpression)	GTCGAGTCCCTCAGGACAAG
miR-187_rev (miR-187 overexpression)	TTAGGCTGAACGACACGTAG
miR-148b_sensor_forw (luciferase miR-148b sensor)	CTAGTCCACTGCCTGTCTGTGCCTGCTGTCGTAGGATCTACTGCCTGTCTGTGCCTGCTGTTGGACCTGACACTGCCTGTCTGTGCCTGCTGTCCCA
miR-148b_sensor_rev (luciferase miR-148b sensor)	AGCTTGGGACAGCAGGCACAGACAGGCAGTGTCAGGTCCAACAGCAGGCACAGACAGGCAGTAGATCCTACGACAGCAGGCACAGACAGGCAGTGGA
ROCK1-3'UTR_forw (ROCK1 3'UTR cloning)	GCACTAGTGTTCCATCTTCGGACGTTGA
ROCK1-3'UTR_rev (ROCK1 3'UTR cloning)	ATACGCGTCTTCAACAGACCATGCTCCC
ITGA5-3'UTR_forw (ITGA5 3'UTR cloning)	ATACTAGTAGGCTGACCGACGACTACTG
ITGA5-3'UTR_rev (ITGA5 3'UTR cloning)	TAACGCGTTTTTGCATACAAACTGGGAGC
PIK3CA-3'UTR_forw (PIK3CA 3'UTR cloning)	CTCGACTAGTATGATGCTTGGCTCTGGAAT
PIK3CA-3'UTR_rev (PIK3CA 3'UTR cloning)	CTCGACGCGTATGCTGTTCATGGATTGTGC
CSF1-3'UTR_forw (CSF1 3'UTR cloning)	CTCGACTAGTTGGACGCACAGAACAGTCTC
CSF1-3'UTR_rev (CSF1 3'UTR cloning)	CTCGACGCGTTGTTCAGCAGGCAGGTACAG
NRAS-3'UTR_forw (NRAS 3'UTR cloning)	CTCGACTAGTTAAGTTTTGTCAGAAAAGAGCCAC
NRAS-3'UTR_rev (NRAS 3'UTR cloning)	CTCGACGCGTCAAAACAGGCCTCTGGAAAA
ITGA5-3'UTR-mut-site a_forw (ITGA5 3'UTR mutagenesis)	CTGGGGATCCCTCCCCCCCACGTATTATGAAGGACCCTTGTTTA
ITGA5-3'UTR-mut-site a_rev (ITGA5 3'UTR mutagenesis)	TAAACAAGGGTCCTTCATAATACGTGGGGGGGAGGGATCCCCAG
ITGA5-3'UTR-mut-site b_forw (ITGA5 3'UTR mutagenesis)	GGGTTCTGCCTGCCAGCCGTAATTATGCTGCCCCTCATCTC
ITGA5-3'UTR-mut-site b_rev (ITGA5 3'UTR mutagenesis)	GAGATGAGGGGCAGCATAATTACGGCTGGCAGGCAGAACCC
ROCK1-3'UTR-del_forw (ROCK1 3'UTR mutagenesis)	CATTAAGTTAACAAACATATAAGAAATGTATGTTTGAAATGTAAATTATTCTTAGAACACTTTC
ROCK1-3'UTR-del_rev (ROCK1 3'UTR mutagenesis)	GAAAGTGTTCTAAGAATAATTTACATTTCAAACATACATTTCTTATATGTTTGTTAACTTAATG
PIK3CA-3'UTR-mut_forw (PIK3CA 3'UTR mutagenesis)	GCTCACTCTGGATTCCACACGGTACGGTTAATAACTCTCAGCAGGC
PIK3CA-3'UTR-mut_rev (PIK3CA 3'UTR mutagenesis)	GCCTGCTGAGAGTTATTAACCGTACCGTGTGGAATCCAGAGTGAGC
NRAS-3'UTR-del_forw (NRAS 3'UTR mutagenesis)	GCCACTTTCAAGCTGTGACACCCTGGTCCT
NRAS-3'UTR-del_rev (NRAS 3'UTR mutagenesis)	AGGACCAGGGTGTCACAGCTTGAAAGTGGC
CSF1-3'UTR-del-site a_forw (CSF1 3'UTR mutagenesis)	GACCTGCTGGTCTGTGACAGCCTGAAGG
CSF1-3'UTR-del-site a_rev (CSF1 3'UTR mutagenesis)	CCTTCAGGCTGTCACAGACCAGCAGGTC
CSF1-3'UTR-del-site b_forw (CSF1 3'UTR mutagenesis)	CATGAAGGAAGCCATTGTGTGAACACTGTACCTG
CSF1-3'UTR-del-site b_rev (CSF1 3'UTR mutagenesis)	CAGGTACAGTGTTCACACAATGGCTTCCTTCATG

Table S2. miR-148b modulated protein-coding genes

MDAMB231 cells either transfected with miR-148b precursors or negative controls (pre-miR-148b or control) were used to perform a microarray analysis ("Whole Human Genome Oligo Microarray", Agilent). Up- and down-modulated protein-coding genes considering: minimum fold change (FC)=1.5; false discovery rate (FDR)=16%.

Down			Up		
Probe Name	Gene Name	pre-miR-148b vs control*	Probe Name	Gene Name	pre-miR-148b vs control*
A_24_P255114	ENST00000299512	-2.18	A_32_P68148	ZNF738	1.50
A_23_P311912	AHNAK2	-2.12	A_32_P81334	LARP4	1.50
A_24_P74371	CTSA	-2.12	A_23_P204048	DYRK2	1.51
A_24_P74374	CTSA	-2.10	A_24_P551028	LOC339745	1.51
A_23_P103496	GBP4	-2.02	A_23_P352266	BCL2	1.51
A_24_P259276	ZDHHC24	-1.96	A_23_P432034	CCDC117	1.52
A_32_P97798	AU184995	-1.94	A_24_P247044	ENST00000355095	1.54
A_23_P62768	TMEM54	-1.92	A_24_P752362	A_24_P752362	1.54
A_24_P845223	M27126	-1.90	A_24_P22657	AK096415	1.55
A_23_P99883	PDIA3	-1.90	A_23_P400580	KIAA1450	1.55
A_24_P273253	AHNAK2	-1.86	A_24_P760672	KRTHB5	1.56
A_24_P291401	TMEM150	-1.85	A_23_P404606	LOC153222	1.58
A_23_P31006	HLA-DRB5	-1.85	A_24_P295452	ROD1	1.58
A_24_P258277	LOC51035	-1.85	A_24_P5935	Kua-UEV	1.61
A_23_P97700	TXNIP	-1.84	A_23_P167269	FLJ11184	1.62
A_23_P346093	TMC8	-1.81	A_23_P110184	SC4MOL	1.62
A_23_P144622	GNPDA1	-1.81	A_32_P95914	C6orf167	1.62
A_23_P21207	UBE1L	-1.80	A_24_P263776	MST101	1.63
A_23_P66715	PIGS	-1.80	A_32_P194779	ZBTB34	1.63
A_23_P76829	HOMEZ	-1.79	A_23_P144916	GFPT2	1.63
A_24_P57528	SLC39A11	-1.77	A_23_P35376	NHLRC2	1.64
A_23_P49467	C1orf144	-1.77	A_24_P80776	AK129879	1.64
A_23_P15108	YPEL3	-1.75	A_32_P234827	ARMC1	1.65
A_23_P257164	AMT	-1.72	A_24_P943888	GRWD1	1.65
A_23_P407012	CSF1	-1.72	A_23_P133582	ETF1	1.66
A_23_P66117	ITFG3	-1.72	A_23_P145397	CCNC	1.68
A_24_P71700	ZBTB47	-1.71	A_23_P86623	ENTPD7	1.71
A_24_P402222	HLA-DRB3	-1.71	A_24_P372217	ERLIN2	1.72
A_23_P98900	CCDC92	-1.69	A_24_P402836	ZNF141	1.73
A_23_P42306	HLA-DMA	-1.68	A_32_P137604	BC018597	1.74
A_23_P429046	RP11-56A21.1	-1.68	A_23_P104138	MGC15634	1.74
A_24_P172481	TRIM22	-1.67	A_24_P941441	GNA13	1.75
A_23_P36562	ITGA5	-1.66	A_23_P121064	PTX3	1.76
A_32_P217773	SYTL1	-1.66	A_24_P166663	CDK6	1.76
A_32_P422453	FAM21C	-1.66	A_23_P501996	Kua-UEV	1.81
A_23_P150249	CCDC85B	-1.66	A_24_P112447	ENTPD7	1.84
A_23_P85800	CD52	-1.66	A_23_P94095	ANKRD46	1.84
A_32_P122373	MSTP9	-1.64	A_24_P521409	RPS6KB1	1.84
A_24_P928052	NRP1	-1.64	A_24_P118862	ZNF678	1.84
A_23_P50389	NAT14	-1.64	A_24_P358868	LOC388523	1.91
A_24_P50245	HLA-DMA	-1.62	A_32_P207789	BQ017638	1.95
A_23_P98605	LOC51035	-1.62	A_32_P190737	KIAA1450	2.01
A_23_P99186	UBE3B	-1.62	A_24_P778836	RSL1D1	2.02
A_23_P16834	FNDC4	-1.61	A_24_P162319	SCML1	2.06
A_23_P67151	OLFM2	-1.61	A_23_P165239	ZNF208	2.12
A_23_P155057	PSCD4	-1.60	A_32_P158723	AK123861	2.15
A_24_P513764	A_24_P513764	-1.60	A_23_P108437	FZD5	2.16
A_23_P254353	NOXA1	-1.60	A_32_P43826	AL832540	2.18
A_23_P411379	C6orf1	-1.59	A_23_P60210	RLN1	2.37
A_32_P10960	FAM21C	-1.59			
A_24_P455972	BC130416	-1.59			
A_23_P95353	SAPS2	-1.59			
A_24_P68079	LBA1	-1.58			
A_24_P857624	BC041417	-1.58			
A_32_P98136	KIAA1107	-1.58			
A_23_P87500	ORMDL2	-1.58			
A_23_P56933	RTN4	-1.58			
A_23_P21382	LAMB2	-1.57			
A_32_P128391	AL162073	-1.57			
A_24_P148796	MST1	-1.56			
A_23_P24157	C10orf33	-1.56			
A_23_P353478	CIITA	-1.56			
A_24_P396489	C1orf144	-1.56			
A_23_P61823	RAB24	-1.56			
A_24_P278299	ASB13	-1.56			
A_24_P343233	HLA-DRB1	-1.55			
A_23_P203463	TAF10	-1.54			
A_32_P216841	SPATA18	-1.54			
A_24_P116535	MMP15	-1.54			
A_23_P217737	ENST00000341514	-1.54			
A_24_P390055	USP30	-1.53			
A_23_P60977	LAT	-1.53			
A_23_P123454	NUDT18	-1.53			
A_23_P131646	RPIA	-1.52			
A_23_P139912	IGFBP6	-1.52			
A_23_P353097	MEGF8	-1.52			
A_23_P143600	LOC91316	-1.51			
A_23_P148556	ABCD1	-1.51			
A_32_P72611	AK097472	-1.50			
A_24_P329065	BTN3A1	-1.50			

7. ACKNOWLEDGEMENTS

Firstly, I would like to thank Momi that greatly encouraged and supported my scientific growth and, for his constant guidance and discussions, in day-to-day lab life, during the twelve years in his lab.

A special thank to Daniela Taverna that introduced me to cancer biology. A particular thanks to Daniela Cimino and Francesca Orso for all in vivo experiments.

I want to thank all members of the Lanfranchi's lab for their helpful advice and the nice time, in particular Matteo Zampini and Silvia Casara for their help in microarray experiments and 3'-UTR cloning.

PUBLISHED PAPERS

Cimino D*, **De Pittà C***, Orso F, Zampini M, Casara S, Penna E, Quaglino E, Forni M, Damasco C, Pinatel E, Ponzone R, Romualdi C, Brisken C, De Bortoli M, Biglia N, Provero P, Lanfranchi G, Taverna D. miR148b is a major coordinator of breast cancer progression in a relapse-associated microRNA signature by targeting ITGA5, ROCK1, PIK3CA, NRAS, and CSF1. *FASEB J*. 2012 Dec 11. [Epub ahead of print] [*equally contributed to this work].

Girardi C*, **De Pittà C***, Casara S, Sales G, Lanfranchi G, Celotti L, Mognato M. Analysis of miRNA and mRNA expression profiles highlights alterations in ionizing radiation response of human lymphocytes under modeled microgravity. *PLoS One*. 2012; **7**(2):e31293. [*equally contributed to this work].

Tombolan L, Orso F, Guzzardo V, Casara S, Zin A, Bonora M, Romualdi C, Giorgi C, Bisogno G, Alaggio R, Pinton P, **De Pittà C**, Taverna D, Rosolen A, Lanfranchi G. High IGFBP2 expression correlates with tumor severity in pediatric rhabdomyosarcoma. *Am J Pathol*. 2011; **179**(5):2611-24.

Penna E, Orso F, Cimino D, Tenaglia E, Lembo A, Quaglino E, Poliseno L, Haimovic A, Osella-Abate S, **De Pittà C**, Pinatel E, Stadler MB, Provero P, Bernengo MG, Osman I, Taverna D. microRNA-214 contributes to melanoma tumour progression through suppression of TFAP2C. *EMBO J*. 2011; 30(10):1990-2007.

Biscontin A, Casara S, Cagnin S, Tombolan L, Rosolen A, Lanfranchi G, **De Pittà C**. New miRNA labeling method for bead-based quantification. *BMC Mol Biol*. 2010; **11**:44.

The FASEB Journal article fj.12-214692. Published online December 11, 2012.

miR148b is a major coordinator of breast cancer progression in a relapse-associated microRNA signature by targeting ITGA5, ROCK1, PIK3CA, NRAS, and CSF1

Daniela Cimino,[*,†,‡,1] Cristiano De Pittà,[#,1] Francesca Orso,[*,†,‡] Matteo Zampini,[#] Silvia Casara,[#] Elisa Penna,[*,†] Elena Quaglino,[*,§] Marco Forni,[*] Christian Damasco,[*,‖] Eva Pinatel,[*,‖] Riccardo Ponzone,[**] Chiara Romualdi,[#] Cathrin Brisken,[††] Michele De Bortoli,[†,‡] Nicoletta Biglia,[¶] Paolo Provero,[*,‖] Gerolamo Lanfranchi,[#] and Daniela Taverna[*,†,‡,2]

[*]Molecular Biotechnology Center (MBC), [†]Department of Oncological Sciences, [‡]Center for Molecular Systems Biology, [§]Department of Clinical and Biological Sciences, [‖]Department of Genetics, Biology, and Biochemistry, and [¶]Department of Gynecology and Obstetrics, University of Torino, Turin, Italy; [#]Department of Biology and Centro Ricerche Interdepartimentale Biotecnologie Innovative (CRIBI) Biotechnology Center, University of Padova, Padua, Italy; [**]Institute for Cancer Research and Treatment (IRCC), Candiolo, Italy; and [††]National Centers of Competence in Research (NCCR) Molecular Oncology, Institut Suisse de Recherche Expérimentale sur le Cancer (ISREC), School of Life Sciences, École Polytechnique Fédérale de Lausanne (EPFL), Lausanne, Switzerland

ABSTRACT **Breast cancer is often fatal during its metastatic dissemination. To unravel the role of microRNAs (miRs) during malignancy, we analyzed miR expression in 77 primary breast carcinomas and identified 16 relapse-associated miRs that correlate with survival and/or distinguish tumor subtypes in different datasets. Among them, miR-148b, down-regulated in aggressive breast tumors, was found to be a major coordinator of malignancy. In fact, it is able to oppose various steps of tumor progression when overexpressed in cell lines by influencing invasion, survival to anoikis, extravasation, lung metastasis formation, and chemotherapy response. miR-148b controls malignancy by coordinating a novel pathway involving over 130 genes and, in particular, it directly targets players of the integrin signaling, such as ITGA5, ROCK1, PIK3CA/p110α, and NRAS, as well as CSF1, a growth factor for stroma cells. Our findings reveal the importance of the identified 16 miRs for disease outcome predictions and suggest a critical role for miR-148b in the control of breast cancer progression.—Cimino, D., De Pittà, C., Orso, F., Zampini, M., Casara, C., Penna, E., Quaglino, E., Forni, M., Damasco, C., Pinatel, E., Ponzone, R., Romualdi, C., Brisken, C., De Bortoli, M., Biglia, N., Provero, P., Lanfranchi' G., Taverna, D. miR148b is a major coordinator of breast cancer progression in a relapse-associated microRNA signature by targeting ITGA5, ROCK1, PIK3CA, NRAS, and CSF1. *FASEB J.* 27, 000–000 (2013). www.fasebj.org**

Key Words: microRNA profiling · malignancy · mammary tumor · integrin signaling · prognosis

Breast cancer is the most common malignancy in women worldwide, often fatal because of metastasis dissemination (1). Clinical and pathological parameters, including tumor size, lymph node involvement, and histological grade and age (2), as well as molecular tumor markers, such as estrogen receptor (ER) and progesterone receptor (PR) or ERBB2, are routinely employed to stratify patients with breast cancer according to risk, assess prognosis, and define appropriate therapies (3). However, since patients with similar combinations of features may often have different clinical outcomes, it is urgent to identify new ways to classify the disease. More recently, protein-coding gene expression profilings have been used to improve tumor classifications (4) and expression of certain gene sets, defined as "signatures," were shown to have a prognostic and/or predictive role for patients (5).

Abbreviations: 3′-UTR, 3′ untranslated region; DFS, disease-free survival; ER, estrogen receptor; FDR, false discovery rate; H&E, hematoxylin and eosin; IPA, Ingenuity Pathway Analysis; miR, microRNA; PCA, principal component analysis; PR, progesterone receptor; SAM, significance analysis of microarray; TMRM, tetramethylrhodamine methyl ester

[1] These authors contributed equally to this work.

[2] Correspondence: MBC and Department Onc. Sci., University of Torino, Via Nizza, 52, 10126 Torino, Italy. E-mail: daniela.taverna@unito.it

doi: 10.1096/fj.12-214692

This article includes supplemental data. Please visit *http://www.fasebj.org* to obtain this information.

MicroRNAs (miRs) are new players involved in the establishment and progression of human tumors that appear to be critical biomarkers of cancer with strong classification power. miRs are a class of small noncoding RNAs that negatively regulate protein-coding gene expression post-transcriptionally by targeting mRNAs, mostly at the 3′ untranslated region (3′-UTR) and triggering either translation repression or RNA degradation (6). Investigations for miR levels in human tumors showed that miR expression is altered in cancer compared to normal tissues, and these changes can help to classify tumors more accurately than mRNA expression profiles according to developmental lineage and differentiation status (7). Recent studies demonstrated that breast cancers can be classified into specific tumor pathological phenotypes (ER, PR, proliferation, stage, metastasis, ERBB2) as well as subtypes (luminal A or B, basal-like, $ERBB2^+$ and normal-like) based on miR expression profiles (8, 9). Thus, it seems essential to combine miR and protein-coding gene expression analyses to obtain information for prognosis and cancer treatment. miRs such as let-7, miR-9, miR-10b, miR-21, miR-31, miR-34, miR-126, miR-146, miR-155, miR-200, miR-214, miR-221/222, miR-373, and 520c have been proven to control tumor dissemination. In fact, alterations of their expression in breast cancer cells profoundly affect tumor dissemination (10–12). In our work, we investigated the relationship between altered miR expression and breast cancer metastasis by analyzing miR levels in a cohort of patients with breast cancer, grouped based on disease relapse. In particular, we investigated the biological function and molecular mechanism of a relapse-associated small noncoding RNA, miR-148b.

MATERIALS AND METHODS

Cell culture

Human MDAMB231, 4175 TGL (13), MCF7, and T47D cells and mouse 4T1 cells were maintained in standard conditions: Dulbecco's modified Eagle's medium containing 10 mM Glutamax and 4.5 mg/ml glucose(DMEM Glutamax; Gibco; Invitrogen Life Technologies, Carlsbad, CA, USA), supplemented with 10% heat-inactivated FCS (Biochrom AG, Berlin, Germany), 1 mM sodium pyruvate, 25 mM HEPES (pH 7.4), and 100 mg/ml gentamicin (all from Gibco).

Patients and samples

Frozen primary invasive ductal breast cancer specimens (77) from 25- to 82-yr-old patients were selected from the Tumor Bank of the Department of Obstetrics and Gynecology, University of Torino (Turin, Italy; primary surgery: 1988–2001) for a retrospective study. There was no distant metastasis at diagnosis (M0). Complete clinical-pathological data were updated by follow-up for ≥72 mo (up to 100 mo). All patients were treated with radical modified mastectomy or quadrantectomy and axillary dissection plus breast irradiation. High-risk node-negative and node-positive patients received adjuvant treatments (generally 6 cycles of CMF: 600 mg/m^2 cyclophosphamide, 40 mg/m^2 metotrexate, 600 mg/m^2 5-fluorouracil), and/or 20 mg tamoxifen daily for 5 yr in ER^+ cases. Patient stage distribution was assessed as prescribed by the Union for International Cancer Control (UICC) clinical staging guidelines, and tumor grading was performed as described previously (14). As normal breast controls, 17 frozen mammoplastic reductions were included in the screening. Appropriate ethical approval was obtained for this study.

Reagents and antibodies

miR precursors and inhibitors

Pre-miR miRNA Precursor Molecules–Negative Control 1, miRNA precursors hsa-miR-148b (PM10264) (000471), hsa-miR-214 (PM12124), Anti-miR miRNA Inhibitor–Negative Control 1, and miRNA inhibitor hsa-miR-148b (AM10264) were from Ambion (Austin, TX, USA).

miR detection

TaqMan miRNA assays hsa-miR-148b (000471), hsa-miR-187 (000487), hsa-miR-365 (001020), hsa-miR-10a (000387), hsa-miR-19a (000395), hsa-miR-342-3p (002260), hsa-miR-214 (002306), hsa-RNU44 (001094), and U6 snRNA (001973) were from Applied Biosystems (Foster City, CA, USA).

ECM

Collagen IV and fibronectin were from Sigma-Aldrich (St. Louis, MO, USA).

Apoptosis reagents

FITC-conjugated annexin V was provided by Boehringer Mannheim (Indianapolis, IN, USA). PE-conjugated annexin V was provided by BD Biosciences (Bedford, MA, USA). Tetramethylrhodamine methyl ester (TMRM) was provided by Molecular Probes (Invitrogen Life Technologies). Paclitaxel (Onco-Tain brand) was from Mayne Pharma (Melbourne, Australia), cisplatin was from Ebewe Italia Srl. (Rome, Italy), and doxorubicin was from Sigma-Aldrich.

RNAi

si ITGA5 (Hs_ITGA5_5 siRNA) and All Stars Negative Control siRNA were purchased from Qiagen (Stanford, CA, USA).

Primary antibodies

Anti-N-RAS mAb F155, anti-hsp90 mAb F-8, anti-ROCK1 pAb H-85, and anti-actin pAb I-19 were from Santa Cruz Biotechnology (Santa Cruz, CA, USA). Anti-PIK3CA (4255) was from Cell Signaling Technology (Danvers, MA, USA). Anti-ITGA5 pAb RM10 was kindly provided by G. Tarone (University of Torino, Turin, Italy; ref. 15). Anti-CSF1 mAb M01-1A9 was from Abnova (Taipei, Taiwan), and anti-α-tubulin mAb B5-1-2 was from Sigma-Aldrich.

Secondary antibodies

Goat anti-mouse and goat anti-rabbit HRP-conjugated IgG were from Santa Cruz Biotechnology. All antibodies were used at the producer's suggested concentrations. Matrigel used for *in vivo* tumor growth experiments (BD Matrigel Basement Membrane Matrix High Concentration) was from BD Biosciences.

Primers

Cloning oligonucleotides employed in this study are listed in **Table 1**. RT-PCR assays (Qiagen) employed in this study are listed in **Table 2**.

Plasmid construction and lentiviral infections

Luciferase reporter vectors containing the partial 3′-UTR of the indicated miR-148b target genes were generated following PCR amplification of the 3′-UTR from human cDNA and cloned into the firefly luciferase reporter pMIR-Report vector (Ambion). When indicated, the 3′-UTRs were mutagenized at miR-148b recognition sites using the QuickChange Site-Directed Mutagenesis kit (Stratagene, Cedar Creek, TX, USA) according to the manufacturer's instructions. The miR-148b sensor was obtained by annealing, purifying, and cloning short oligonucleotides containing 3 perfect miR-148b binding sites into the *Spe*I and *Hind*III sites of the pMIR-Report vector. The human pre-miR-148b sequence (a 306-bp fragment containing the pre-miR sequence) was amplified from genomic DNA (MDAMB231) and cloned into pLemiR-tRFP (Open Biosystems, Huntsville, AL, USA) vector to obtain pLemiR-148b (still containing tRFP) vector. The human pre-miR-187 sequence (a 251-bp fragment containing the pre-miR sequence) was amplified from genomic DNA (MDAMB231) and cloned into pWPT (Addgene, Cambridge, MA, USA) vector to obtain pWPT-miR-187 vector. Stable cell lines were generated by lentiviral infection. Lentiviruses were produced by calcium phosphate transfection of 293T cells with 20 μg of specific vector together with 15 μg packaging (pCMVdR8.74) and 6 μg envelope (pMD2.G-VSVG) plasmids, according to D. Trono's laboratory protocol (École Polytechnique Fédérale de Lausanne, Lausanne, Switzerland; http://tronolab.epfl.ch). Supernatant was harvested 48 h post-transfection, filtered with 0.45-μm filters, diluted, and used to infect 3.5×10^5 cells in 6-well plates, in presence of 8 μg/ml Polybrene (Sigma-Aldrich). ITGA5 overexepression was obtained by transfecting pEGFP-N3-ITGA5 expression vector (plasmid 15238; Addgene; ref. 16).

RNA isolation from tissues or cells

After surgical removal, tumor samples were macrodissected by pathologists, quickly frozen, and stored at −80°C. Total RNA was isolated with Concert cytoplasmic RNA reagent (Invitrogen Life Technologies) from 20 to 50 mg tumor tissues, according to the manufacturer's guidelines. Frozen tumors were then homogenized using a ball mill (MM200; Retsch, Düsseldorf, Germany). The suspension was centrifuged at 14,000 *g* for 5 min at 4°C, and then lysed with 0.1 ml of 10% SDS, followed by 0.3 ml of 5 M sodium chloride and

TABLE 1. *Cloning oligonucleotides employed in this study*

Primer ID	Sequence, 5′ → 3′
miR-148b_forw (miR-148b overexpression)	TTTCATAGGCACCACTCACTTTAC
miR-148b_rev (miR-148b overexpression)	CCCTTTCCCCTTACTCTCCA
miR-187_forw (miR-187 overexpression)	GTCGAGTCCCTCAGGACAAG
miR-187_rev (miR-187 overexpression)	TTAGGCTGAACGACACGTAG
miR-148b_sensor_forw (luciferase miR-148b sensor)	CTAGTCCACTGCCTGTCTGTGCCTGCTGTCGTAGGATCTACTG CCTGTCTGTGCCTGCTGTTGGACCTGACACTGCCTGTCTGTGCC TGCTGTCCCA
miR-148b_sensor_rev (luciferase miR-148b sensor)	AGCTTGGGACAGCAGGCACAGACAGGCAGTGTCAGGTCCAACA GCAGGCACAGACAGGCAGTAGATCCTACGACAGCAGGCACAGAC AGGCAGTGGA
ROCK1-3′UTR_forw (ROCK1 3′-UTR cloning)	GCACTAGTGTTCCATCTTCGGACGTTGA
ROCK1-3′UTR_rev (ROCK1 3′-UTR cloning)	ATACGCGTCTTCAACAGACCATGCTCCC
ITGA5-3′UTR_forw (ITGA5 3′-UTR cloning)	ATACTAGTAGGCTGACCGACGACTACTG
ITGA5-3′UTR_rev (ITGA5 3′-UTR cloning)	TAACGCGTTTTTGCATACAAACTGGGAGC
PIK3CA-3′UTR_forw (PIK3CA 3′-UTR cloning)	CTCGACTAGTATGATGCTTGGCTCTGGAAT
PIK3CA-3′UTR_rev (PIK3CA 3′-UTR cloning)	CTCGACGCGTATGCTGTTCATGGATTGTGC
CSF1-3′UTR_forw (CSF1 3′-UTR cloning)	CTCGACTAGTTGGACGCACAGAACAGTCTC
CSF1-3′UTR_rev (CSF1 3′-UTR cloning)	CTCGACGCGTTGTTCAGCAGGCAGGTACAG
NRAS-3′UTR_forw (NRAS 3′-UTR cloning)	CTCGACTAGTTAAGTTTTGTCAGAAAAGAGCCAC
NRAS-3′UTR_rev (NRAS 3′-UTR cloning)	CTCGACGCGTCAAAACAGGCCTCTGGAAAA
ITGA5-3′UTR-mut-site a_forw (ITGA5 3′-UTR mutagenesis)	CTGGGGATCCCTCCCCCCCACGTATTATGAAGGACCCTTGTTTA
ITGA5-3′UTR-mut-site a_rev (ITGA5 3′-UTR mutagenesis)	TAAACAAGGGTCCTTCATAATACGTGGGGGGGAGGGATCCCCAG
ITGA5-3′UTR-mut-site b_forw (ITGA5 3′-UTR mutagenesis)	GGGTTCTGCCTGCCAGCCGTAATTATGCTGCCCCTCATCTC
ITGA5-3′UTR-mut-site b_rev (ITGA5 3′-UTR mutagenesis)	GAGATGAGGGGCAGCATAATTACGGCTGGCAGGCAGAACCC
ROCK1-3′UTR-del_forw (ROCK1 3′-UTR mutagenesis)	CATTAAGTTAACAAACATATAAGAAATGTATGTTTGAAATGTA AATTATTCTTAGAACACTTTC
ROCK1-3′UTR-del_rev (ROCK1 3′-UTR mutagenesis)	GAAAGTGTTCTAAGAATAATTTACATTTCAAACATACATTTCT TATATGTTTGTTAACTTAATG
PIK3CA-3′UTR-mut_forw (PIK3CA 3′-UTR mutagenesis)	GCTCACTCTGGATTCCACACGGTACGGTTAATAACTCTCAGCAGGC
PIK3CA-3′UTR-mut_rev (PIK3CA 3′-UTR mutagenesis)	GCCTGCTGAGAGTTATTAACCGTACCGTGTGGAATCCAGAGTGAGC
NRAS-3′UTR-del_forw (NRAS 3′-UTR mutagenesis)	GCCACTTTCAAGCTGTGACACCCTGGTCCT
NRAS-3′UTR-del_rev (NRAS 3′-UTR mutagenesis)	AGGACCAGGGTGTCACAGCTTGAAAGTGGC
CSF1-3′UTR-del-site a_forw (CSF1 3′-UTR mutagenesis)	GACCTGCTGGTCTGTGACAGCCTGAAGG
CSF1-3′UTR-del-site a_rev (CSF1 3′-UTR mutagenesis)	CCTTCAGGCTGTCACAGACCAGCAGGTC
CSF1-3′UTR-del-site b_forw (CSF1 3′-UTR mutagenesis)	CATGAAGGAAGCCATTGTGTGAACACTGTACCTG
CSF1-3′UTR-del-site b_rev (CSF1 3′-UTR mutagenesis)	CAGGTACAGTGTTCACACAATGGCTTCCTTCATG

TABLE 2. *RT-PCR assays employed in this study*

Primer ID	Assay ID
COPZ1	QT00087024
CSF1	QT00035224
CTSA	QT00087381
CXCL5	QT00203686
DYRK2	QT01011073
GRB2	QT00065289
ITGA5	QT00080871
MMP15	QT00014063
NRAS	QT00076874
NRP1	QT00023009
PIK3CA	QT00014861
ROCK1	QT00034972
RRN18S	QT00199367

0.2 ml of chloroform per milliliter of reagent. The lysate was centrifuged at 14,000 *g* for 15 min at 4°C, and the upper aqueous phase was removed and combined with 0.8 vol of isopropyl alcohol for 10 min at room temperature. Total RNA was recovered by centrifugation, washed with 75% ethanol, and finally dissolved in RNase-free water. Total RNA from normal samples or cells in culture was isolated with TRIzol reagent (Invitrogen Life Technologies). Frozen samples were homogenized using an Ultra Turax T50 Basic homogenizer (Bioclass, Pistoia, Italy) and extracted with an acid-phenol: chloroform solution according to the manufacturer's guidelines. RNA quantitation was performed using the NanoDrop 1000 spectrophotometer (Nanodrop, Wilmington, DE, USA). Total RNA integrity and the percentage content of miRs in each sample were assessed by capillary electrophoresis using the Agilent Bioanalyzer 2100 with the RNA 6000 Nano and the Small RNA Nano LabChips, respectively (Agilent Technologies, Palo Alto, CA, USA). Only total RNA samples with an RNA integrity number (RIN) $\geq$ 6 and $<$30% of small RNAs were used for miR microarray analysis.

miR and gene expression profilings

The miR and protein-coding expression profilings were carried out using the Human MicroRNA Microarray kit (V2, 723 miRs) and the Whole Human Genome Oligo Microarray (~41,000, 60-mer oligonucleotide probes), respectively, both from Agilent Technologies. For miR analysis, total RNA (200 ng) was labeled with pCp-Cy3, according to the Agilent protocol (17), and probes were hybridized at 55°C for 22 h. For protein-coding investigations, total RNA (800 ng) was labeled by the Agilent One-Color Microarray-Based Gene Expression protocol, according to the manufacturer's instructions. The synthesized cDNA was transcribed into cRNA and labeled with Cy3. Labeled cRNA (1.65 μg) was used for hybridization at 65°C for 17 h. Slides were scanned on an Agilent microarray scanner. Raw miR and gene expression data are available in the U.S. National Center for Biotechnology Information Gene Expression Omnibus (GEO) database (GSE26666; http:/www.ncbi.nlm.nih.gov/geo/query/acc.cgi?token_jveltssyquiywvo&acc_GSE26666). Interarray normalization was performed with cyclic Lowess for miRs and with quantile for protein-coding expression profilings (18, 19), and the average of replicates was used. To perform differential gene expression analysis, the level of each miR was calculated as $\log_2$ of tumor sample/mammoplastic reduction median. The identification of differential expression for miRs or protein-coding genes was performed using the 2-class significance analysis of microarray (SAM) algorithm (20). SAM uses a permutation-based multiple testing algorithm and associates a variable false discovery rate (FDR) to the significant genes. FDR refers to the percentage of error that can occur in the identification of the statistically significant differentially expressed genes in multiple comparisons; it can be manually adjusted.

Statistical analysis of miR and gene expression data

For miRs, Feature Extraction software (Agilent Technologies) was used to obtain spot quality measures in order to evaluate the quality and the reliability of the hybridization. In particular, the flag glsFound (set to 1 if the spot has an intensity value significantly different from the local background, 0 otherwise) was used to filter out unreliable probes: flag equal to 0 will be noted as not available (NA). So, in order to perform a more robust and unbiased statistical analysis, probes with a high proportion of NA values were removed from the dataset. NA (40%) was used as threshold in the filtering process, obtaining a total of 237 available human miRs. Principal component analysis (PCA), cluster analysis, and profile similarity searches were performed with Multi Experiment Viewer 4.5.1 (TMev) of the TM4 Microarray Software Suite (21). All heath maps were obtained by TMeV software using an unsupervised 2-dimensional hierarchical clustering approach with average linkage method and Pearson correlation.

Statistical analyses of biological samples

Data are presented as means ± SEM or SD, and 2-tailed Student's *t* test was used for comparison analysis, with values of $P < 0.05$ considered to be statistically significant. Box and whisker plots were prepared based on Liu (22). The bottom and top of the box are, respectively, the first (bottom) and third (top) quartile; the line in the middle corresponds to the median, and circles label outliers.

Statistics for survival analysis

Survival association analyses were performed using the SPSS 18.0 statistical software (SPSS Inc., Chicago, IL, USA) and the Bioconductor suite of software tools (http://www.bioconductor.org). The receiver operating characteristic (ROC) method (23) was used to categorize samples according to miR or mRNA expression. Kaplan-Meier survival curves were used to estimate time-to-event models in the presence of censored cases. Risk differences between the two groups were assessed using the Mantel-Haenszel log-rank test (24). Survival analysis was carried out in both univariate and multivariate setting using Cox's proportional hazard model (25). ITGA5 survival association was evaluated in GSE2034 (26); gene expression values were calculated as described previously (27), and results were divided into two categories according to gene expression levels.

Analysis of human breast cancer data sets

Blenkiron *et al.* (8) and Enerly *et al.* (9) miR expression values and sample phenodata were obtained from GSE7842 and GSE19536, respectively, and from the supplemental materials of the publications.

Target prediction and pathway analysis

The TargetScan 5.1 algorithm (28) was used to predict miR targets. The Ingenuity Pathways Knowledge Base (http://www.ingenuity.com) is currently the world's largest database of knowledge on biological networks, with annotations orga-

nized by experts. We exploited this database to look for enrichments in specific pathways among the relapse (or other category)-associated miR putative targets. Enrichment significance in pathways analysis is shown as the negative $\log_{10}$ of the *P* value. The *P* value is calculated with the right-tailed Fisher's exact test. Ingenuity networks are scored based on the number of network eligible molecules they contain. The network score is based on the hypergeometric distribution and is calculated with the right-tailed Fisher's exact test. The score is the negative log of this *P* value.

Additional cell transfections and infections, qRT-PCRs, apoptosis, luciferase assays, protein preparation, immunoblotting, and i*n vitro* and *in vivo* biological studies were all performed as indicated in detail in Penna *et al.* (12).

RESULTS

Sixteen relapse-associated miRs classify breast tumors

In a retrospective study, we analyzed miR expression in 77 primary human breast ductal tumors as well as 17 mammoplastic reductions (**Table 3**), using microarrays (a 723-miR platform) and a 2-class SAM. In particular, when we compared patients with relapse (n=41) or without relapse (n=36), within ≥72 mo from surgery, 16 differentially expressed miRs were identified and expressed as fold changes or levels, relative to the median of the healthy controls, $\log_2$ tumors/controls (**Fig. 1**). Within relapsing/nonrelapsing patients, validation of microarray data was performed by qRT-PCR analysis for miR-148b, miR-365, and miR-10a using n = 10/group (not shown). By using the 16 relapse-associated miRs together as a whole (as a group), we identified two groups of patients with different overall survival (OS; P=0.018) and disease-free survival (DFS; P=0.016), independent of the lymph node status (Cox proportional-hazards regression model; P=0.015) in our study. The same was found when certain individual specific miRs were used, for instance, miR-148b, downregulated in relapsing tumors (OS, P=0.027; DFS, P=0.036). However, a correlation with survival was not found when our 16 relapse-associated miRs were used as a whole for two other available public datasets (8, 9). These studies refer to ~100 patients each; the primary tumors were used to measure mRNA and miR expression with the goal of identifying tumor subtypes. Notably, in these datasets, our group of 16 relapse-associated miRs could identify tumor subtypes and separate more aggressive (ERBB2$^+$ or basal-like) *vs.* less aggressive (luminal A/B) cancers (Fig. 1*C*, compare solid *vs.* shaded symbols), based on the breast cancer classification in Sorlie *et al.* (4). Moreover, our 16-miR signature could also predict survival, in our cohort, when only luminal tumors (n=53) were considered (DFS, P=0.0097). In addition, some of the 16 miRs, such as miR10a, miR-101, miR-142-5p, miR-148b, miR-342-3p, miR-342-5p, miR-365, and miR-551b, could distinguish tumor subtypes individually (8, 9 and data not shown). In summary, we identified 16 relapse-associated miRs that could be used in the clinics to identify tumor subtypes and to predict disease outcome.

TABLE 3. *Clinical characteristics of the patients: summary*

Characteristic	Value	%
Tumor samples		
Patients (n)	77	
Age (yr)		
Median	54	
Range	25–82	
Tumor stage (n)		
1	20	26.0
2	51	66.2
3	3	3.9
4	3	3.9
Tumor grade (n)		
1	4	5.2
2	35	45.4
3	33	42.8
Unknown	5	6.5
LN (n)		
Positive	44	57.1
Negative	33	42.9
ER (n)[a]		
Positive	53	68.8
Negative	24	31.2
PR (n)[a]		
Positive	42	54.5
Negative	35	45.4
Subtype (n)[b]		
Luminal	53	68.0
ERBB2[b]	14	18.0
Basal	10	12.0
Relapse, ≥72 mo (n)		
Yes	41	53.2
ER$^+$	25	61[c]
ER$^-$	16	39[c]
No	36	46.7
ER$^+$	28	78[c]
ER$^-$	8	22[c]
Normal samples		
Patients (n)	17	
Age (yr)	13	
Median	43	
Range	20–67	

n, number; LN, lymph node status; ER, estrogen receptor status; PR, progesterone receptor status. [a]ER and PR are defined positive when tumors contain >10 fmol receptors/mg proteins or <10% positive tumor cells. [b]Samples were classified according to ERBB2 mRNA level combined to ER and PR status. [c]Percentage refers to the total of relapsing or nonrelapsing samples.

miR-148b impairs tumor growth and suppresses metastasis formation by altering extravasation and survival

A detailed bioinformatics analysis was carried out for the putative targets of the 16 relapse-associated miRs, as predicted by TargetScan 5.1, using Ingenuity Pathway Analysis (IPA) in order to identify pathways and functions in which each miR was involved. This analysis, together with literature searches, let us to conclude that miR-148b has the potential to coordinate a very high number of pathways relevant for breast cancer and that its function has still to be elucidated. With this in mind, we investigated the biological role of miR-148b in

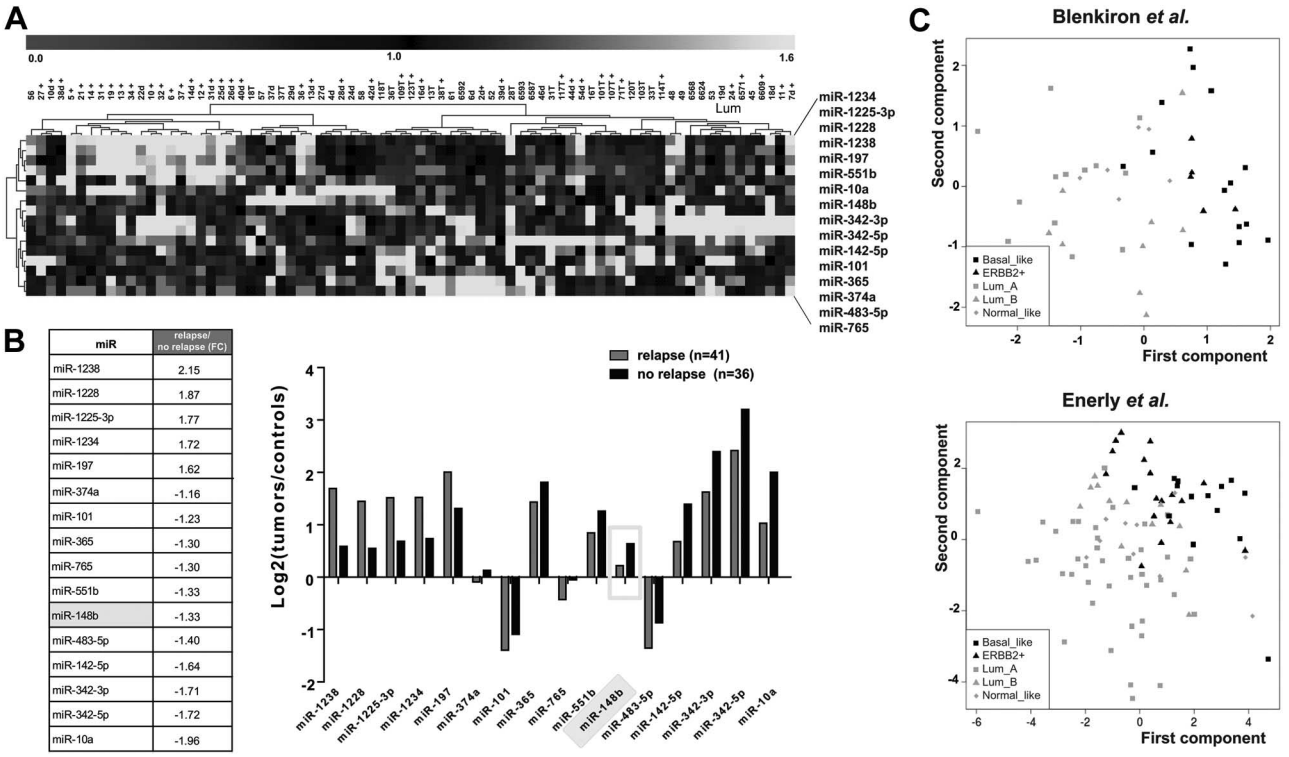

miR	relapse/ no relapse (FC)
miR-1238	2.15
miR-1228	1.87
miR-1225-3p	1.77
miR-1234	1.72
miR-197	1.62
miR-374a	-1.16
miR-101	-1.23
miR-365	-1.30
miR-765	-1.30
miR-551b	-1.33
miR-148b	-1.33
miR-483-5p	-1.40
miR-142-5p	-1.64
miR-342-3p	-1.71
miR-342-5p	-1.72
miR-10a	-1.96

Figure 1. Expression of 16 miRs in relapse-positive (R^+) or relapse-negative (R^-) primary cancers and tumor subtype identification. *A*) Clustering (Pearson correlation, average linkage) for the 16 most modulated miRs considering relapsing (n=41) *vs.* nonrelapsing (n=36) tumors. Heatmap represents relative miR levels with reference to the median expression across all samples; rows: miR; columns: tumors. *B*) Summary (left panel) and graph (right panel) showing the levels of expression of the 16 most modulated miRs, expressed as fold change (FC) of relapsing/nonrelapsing median values (left panel) or averaged levels ($\log_2$) in R^+ or R^- tumor samples *vs.* mammoplastic reductions (controls). Two-class SAM, FDR 16%. *C*) PCA plots for tumor subtypes using all 16 miRs in Blenkiron *et al.* (8) and Enerly *et al.* (9) datasets. Basal_like, basal; $ERBB2^+$, ERBB2 positive; Lum_A, luminal A; Lum_B, luminal B; normal_like, normal-like breast cancer.

neoplasia by modulating (up or down) its expression in MDAMB231, 4175TGL, 4T1, T47D, and MCF7 mammary tumor cell lines with a different level of malignancy (independently of ER, PR, and ERBB2 expression) and of miR-148b, as measured by qRT-PCR (Supplemental Fig. S1*A*). Transient modulations were obtained using miR-148b precursors or inhibitors or negative controls (pre-miR-148b, anti-miR-148b, or precontrol or anticontrol) and evaluated 48 or 72 h post-transfection for expression and biology (Supplemental Fig. S1*B*, *C*). Instead, for stable expression, cells were transduced with pLemiR-empty or pLemiR-148b overexpressing lentivirus vectors and selected with puromycin as pools; expression evaluation is shown in Supplemental Fig. S1*C*.

In vitro proliferation was not affected or only slightly modulated up to 4 d for MDAMB231, 4175TGL, and 4T1 cells in stable or transient conditions (Supplemental Fig. S2A and data not shown). However, tumors derived from transduced pLemiR-148b 4175TGL cells grew significantly less compared to controls (pLemiR-EV) when analyzed up to 12 d following injection in the fat pad of immunocompromised NOD/SCID IL2Rγ^{null} mice (see below). When invasion through fibronectin or Matrigel was evaluated by transwell assays for the same cell lines, reduced cell movement was observed in the presence of miR-148b overexpression compared to controls (Supplemental Fig. S2*B* and data not shown). However, no effect was observed when cells were transduced with pWPT-miR-187 (negative control) lentivirus overexpression vectors compared to controls (pWPT-EV or precontrol; Supplemental Fig. S2*B* and data not shown). Instead, increased cell invasion was observed when miR-214 was overexpressed in these cells (Supplemental Fig. S2*B*, ref. 12, and data not shown). When cell adhesion was investigated, increased adhesion on fibronectin and collagen IV was found for MDAMB231 cells overexpressing miR-148b compared to controls. Conversely, down-modulation of miR-148b in MCF7 and T47D cells led to decreased adhesion (Supplemental Fig. S2*C*).

To study the role of miR-148b in *in vivo* metastasis formation, we injected miR-148b-overexpressing (pre-miR-148b) 4T1 cells into the tail vein of female BALB/c syngeneic mice, and analyzed dissemination in lungs. A significant reduction in the number of lung colonies or area occupied by the lesions was found 5 d postinjection compared with controls, as measured in hematoxylin and eosin (H&E)-stained sections (**Fig. 2*A***). More relevantly, when red fluorescent pLemiR-148b-transduced, 4175TGL cells were injected orthotopically into NOD/SCID/IL2Rγ^{null} mice and primary tumors formed, a striking reduction of malignant cell dissemination from the primary tumors to the lungs was observed com-

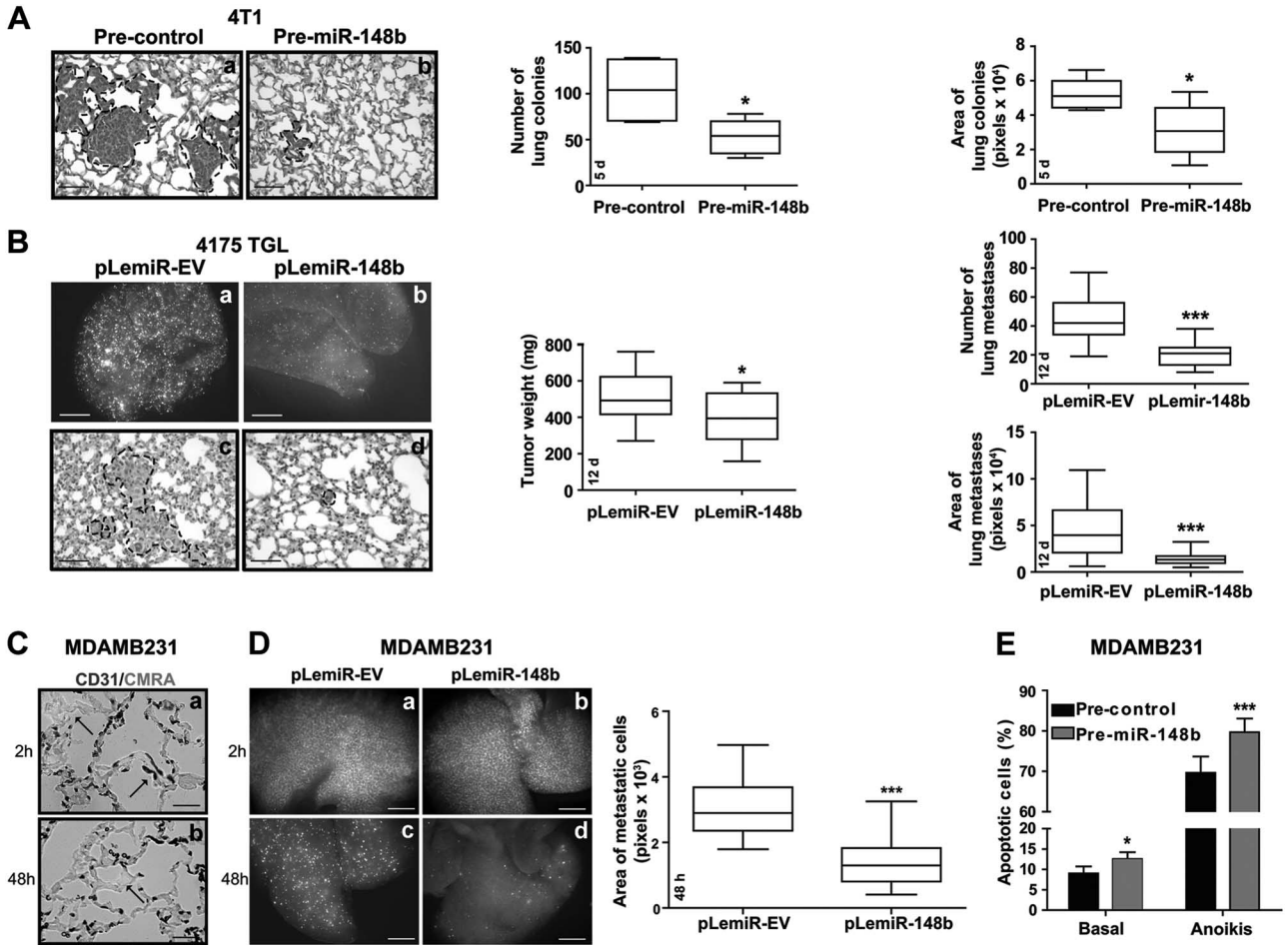

Figure 2. miR-148b impairs metastasis formation in mice by affecting extravasation and survival. *A*) 4T1 cells transiently transfected with negative controls (pre-control; *a*) or miR-148b precursors (pre-miR-148b; *b*) were used to evaluate lung colony formation in BALB/c mice at 5 d after tail vein injection. *B*) Alternatively, 4175TGL cells stably transduced with pLemiR-EV (*a*, *c*) or pLemiR-148b (*b*, *d*) overexpression vectors were injected into the mammary gland fat pad of NOD/SCID/IL2Rγ^{null} mice, and primary tumor growth as well as metastasis formation in the lungs were analyzed at 12 d postinjection. *A*, *B*) Two independent experiments were performed, and results were pooled together (n=10 mice/group) and shown as box and whisker plots for primary tumor weights (*B*) or number (or area) of microscopic colonies (*A*) or metastasis (*B*) in the lungs. Tumor cell dissemination was evaluated in H&E-stained sections at d 5 (*A*) or as fluorescent lesions in the whole lung at d 12 (*B*). Representative H&E stainings are shown. *C*, *D*) *In vivo* seeding/extravasation assays following tail vein injections in nude mice of red fluorescent MDAMB231 cells, stably transduced with pLemiR-EV or pLemiR-148b overexpression vectors. *C*) Representative fields of lung sections at 2 h (*a*) or 48 h (*b*) postinjection, stained for CD31 (black) and containing red fluorescent MDAMB231 cells (here visible in light gray). No cells were found in the vessels at 48 h. *D*) Left panels: red fluorescent cells in the whole lungs at 2 h (*a*, *b*) or 48 h (*c*, *d*) postinjection. Right panel: quantitation of the red fluorescent cells (area) at 48 h for n = 8 mice/group. *E*) MDAMB231 cells transfected with miR-148b precursors or their negative controls (pre-miR-148b or control) were grown in presence or absence (anoikis) of attachment and without serum for 48 h. Percentage of apoptotic cells was evaluated by TMRM and annexinV-FITC staining in a FACS analysis. ^{High}TMRM-^{Low}AnnexinV, healthy cells; ^{Low}TMRM-^{High}AnnexinV, apoptotic cells. Three independent experiments were performed in duplicate; pooled quantitations are shown as means ± SEM. Scale bars = 60 μm (*A*; *Bc*, *d*); 2 mm (*Ba*, *b*; *D*); 120 μm (*C*). *$P < 0.05$; **$P < 0.01$; ***$P < 0.001$.

pared to controls (Fig. 2*B*). Quantitations refer to the red fluorescent metastatic foci (number/area) in the lungs at 12 d postinjection (Fig. 2*B*); H&E sections are shown (Fig. 2*B*). Similar results were obtained with pLemiR-148b-transduced 4T1 cells (not shown). Notably, when similar experiments were previously performed with miR-214-overexpressing 4T1 cells, increased dissemination was observed (12).

Based on this, we assessed the involvement of miR-148b in extravasation and survival in the blood circulation, two essential steps of the metastatic dissemination. To investigate extravasation *in vivo*, red fluorescent pLemiR-148b-transduced MDAMB231 cells were injected into the tail vein of immunocompromised mice, and cell seeding and extravasation in the lung were evaluated at 2 or 48 h postinjection. A high percentage of cells lodged in the lung at 2 h (within the vessels or outside) in the presence or absence of miR-148b. However, extravasation was highly reduced for miR-148b-overexpressing cells compared to controls, as quantitation of the area occupied by metastatic cells showed (Fig. 2*C*, *D*). Vessels were labeled for CD31

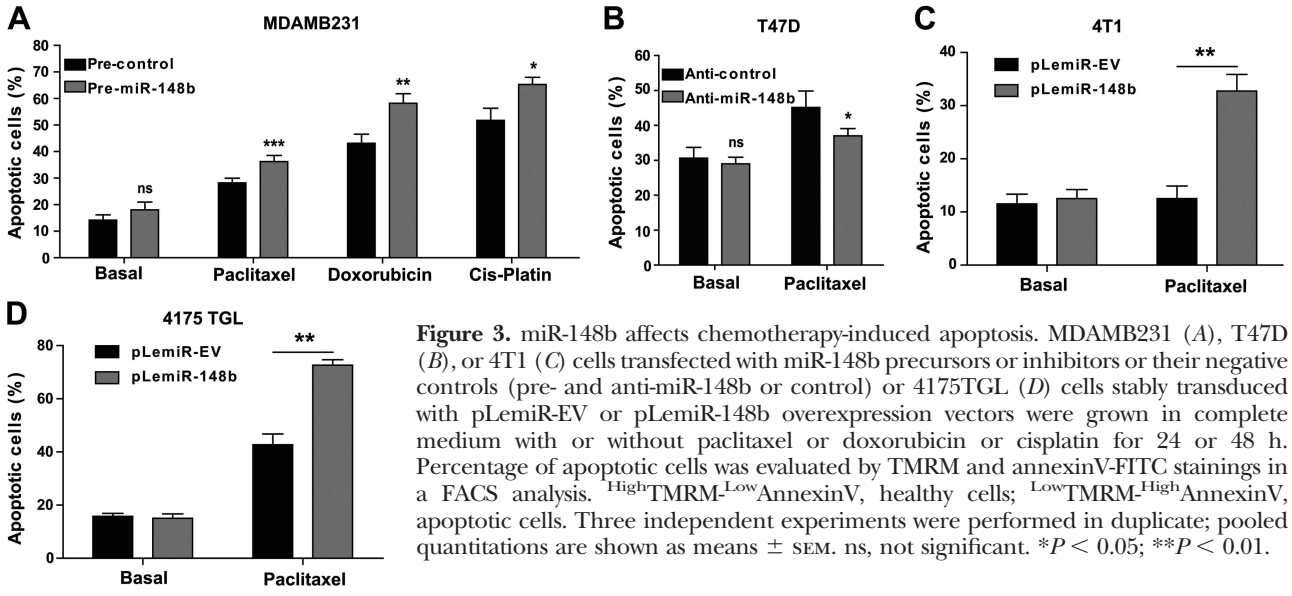

Figure 3. miR-148b affects chemotherapy-induced apoptosis. MDAMB231 (*A*), T47D (*B*), or 4T1 (*C*) cells transfected with miR-148b precursors or inhibitors or their negative controls (pre- and anti-miR-148b or control) or 4175TGL (*D*) cells stably transduced with pLemiR-EV or pLemiR-148b overexpression vectors were grown in complete medium with or without paclitaxel or doxorubicin or cisplatin for 24 or 48 h. Percentage of apoptotic cells was evaluated by TMRM and annexinV-FITC stainings in a FACS analysis. ^{High}TMRM-^{Low}AnnexinV, healthy cells; ^{Low}TMRM-^{High}AnnexinV, apoptotic cells. Three independent experiments were performed in duplicate; pooled quantitations are shown as means ± SEM. ns, not significant. $*P < 0.05$; $**P < 0.01$.

(Fig. 2*C*). To investigate survival in the blood circulation, we evaluated apoptosis in miR-148b-overexpressing MDAMB231 cells kept without serum and with or without (anoikis) adhesion for 48 h by cytofluorimetric analyses, and reduced survival was observed compared to controls (Fig. 2*E*), which suggests a potential role for miR-148b in tumor cell intraluminal viability and initial survival. All these experiments strongly suggest that miR-148b is involved in metastatic cell dissemination by controlling tumor growth and cell survival in anoikis but mostly by inhibiting cell escaping through the endothelial cells of the vessels.

miR-148b expression enhances chemotherapy-induced apoptosis

Considering the relevance of chemotherapy response for tumor progression, we analyzed the response to paclitaxel, doxorubicin, and cisplatin following 24 or 48 h treatment in miR-148b-overexpressing (MDAMB231, 4175TGL, 4T1) or down-modulated (T47D) cells by cytofluorimetric analyses. A significant modulation in cell survival was found for all cell lines and treatments compared to controls (**Fig. 3**), favoring a positive role for miR-148b in chemotherapy response.

miR-148b modulates multiple genes

To identify genes directly or indirectly modulated by miR-148b, miR-148b-overexpressing MDAMB231 cells were first used to perform whole human genome gene expression analysis. A total of 129 differentially expressed genes (49 up-regulated; 80 down-regulated) were found, considering a 1.5-fold change and a 16% FDR (Supplemental Table S1). qRT-PCR analysis was used to validate expression of the nonmodulated NRAS, ROCK1, PI3KCA, COPZ1, GRB2, and CXCL5 and of the differentially expressed DYRK2, CSF1, CTSA, ITGA5, MMP15, and NRP1 (not shown). By crossing these results with putative miR-148b targets (TargetScan 5.1), 20 common genes (19 down-regulated; 1 up-regulated) were found (**Fig. 4*A***), among them ITGA5, known to modulate apoptosis, adhesion, migration, and invasion (29, 30), and CSF1, involved in tumor-stroma interactions (31, 32). Using TargetScan predictions for an IPA, GM-CSF and integrin pathways were identified as statistically significant (Supplemental Fig. S3). Therefore, we investigated the plausible direct regulation of these pathways by miR-148b and their involvement in breast tumor progression. Protein expression was evaluated for ITGA5 and its downstream players ROCK1, PI3KCA/p110α, and NRAS (predicted targets) and for CSF1 in miR-148b-overexpressing MDAMB231 or 4175TGL cells by Western blot analysis. Strong reductions were found compared to controls (Fig. 4*B*). Instead, when miR-148b was down-modulated in MCF7 cells, increased levels of ITGA5 proteins were observed (Fig. 4*B*). Interestingly, ROCK1, PI3KCA/p110α, and NRAS were not modulated at the mRNA level (not shown). Direct modulation of miR-148b on its targets was proven by performing luciferase assays in miR-148b-overexpressing or control MDAMB231 cells transfected with reporter vectors containing wild-type or mutated 3′-UTRs (Fig. 4*C*, *D*). As positive control, a miR-148b-sensor construct was used (Fig. 4*C*). Notably, when we evaluated miR-148b target expression on a subset of relapsing/nonrelapsing human tumors, differential expression was found (**Fig. 5*A***). Relevantly, when the 23 predicted and modulated miR-148b target genes were used in IPA to look for gene connections, cell-to-cell signaling and interaction, tissue development, cellular movement network was identified (Ingenuity score=22; Fig. 5*B*). Given the relevance of the integrin pathway in our investigations, we evaluated the possibility that the upstream player ITGA5 can be used to predict survival in a large microarray dataset of human breast tumors (26). Performing hierarchical clustering and Kaplan-Meier analyses and referring to

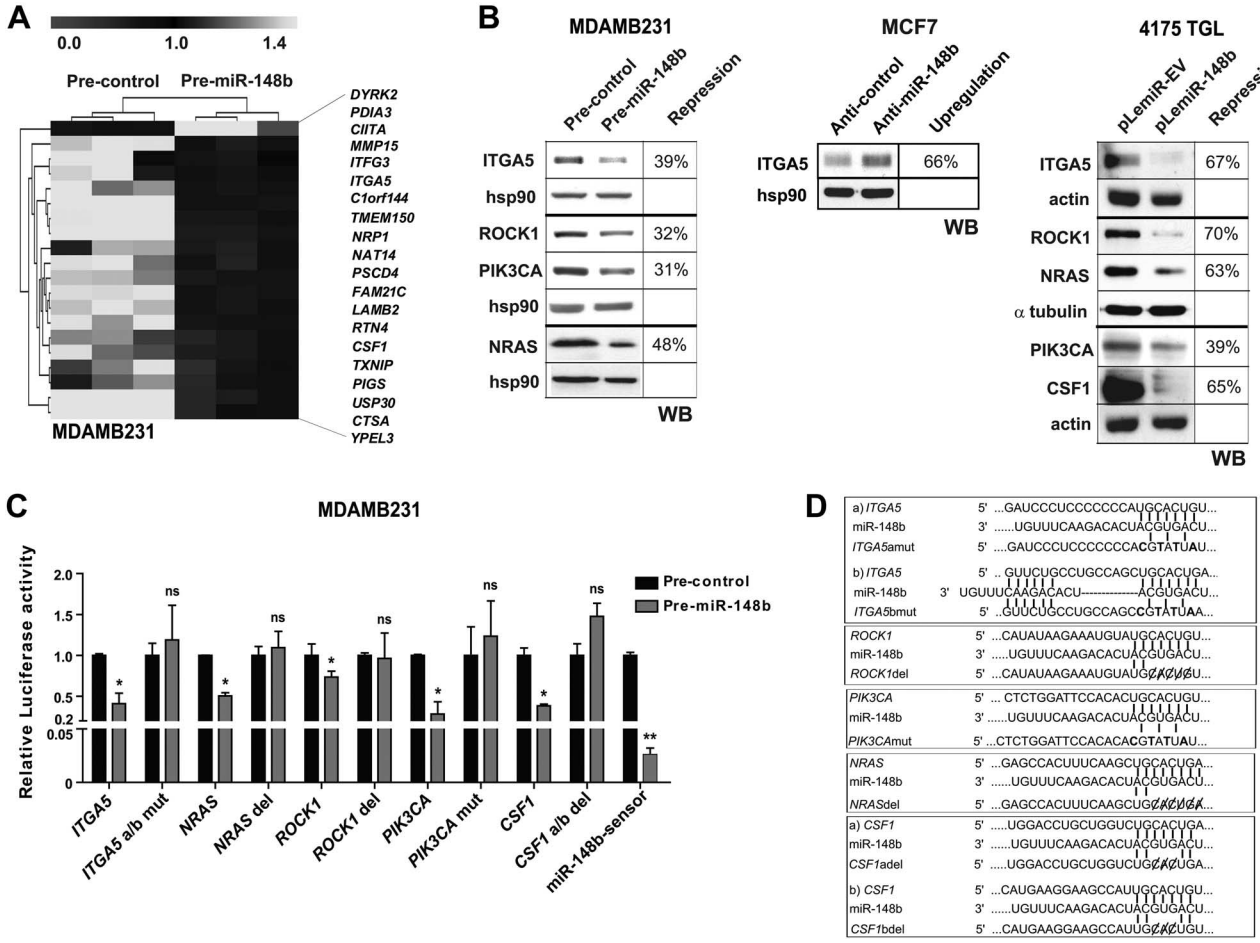

Figure 4. miR-148b modulates multiple genes. MDAMB231 or MCF7 cells transfected with miR-148b precursors or inhibitors or their negative controls (pre- and anti-miR-148b or pre- and anti-control) analyzed at 48 or 72 h post-transfection or 4175TGL cells stably transduced with pLemiR-EV or pLemiR-148b overexpression vectors were used to perform microarray analysis (*A*), Western blots (*B*), or luciferase assays (*C*). *A*) Clustering (Pearson correlation, average linkage) was performed for 20 putative miR-148b targets. Heatmap represents relative gene expression with reference to the median across all samples; row: protein-coding gene; column: cell preparation. *B*) Western blot (WB) analysis was performed for 5 putative miR-148b targets: ITGA5, ROCK1, p110α (PIK3CA), NRAS, and CSF1. Protein expression was calculated relative to controls, following miR-148b overexpression or down-modulation, normalized on the indicated loading controls (hsp90/actin/αtubulin) and expressed as repression percentages. *C*, *D*) Luciferase assays (*C*) in cells transfected with reporter constructs containing wild-type or mutant 3′-UTRs (*D*) for the indicated genes or a synthetic sequence including 3 perfect miR-148b binding sites (sensor). Results are shown as means ± SEM of firefly luciferase activity relative to controls, normalized on *Renilla* luciferase activity. mut, mutation; del, deletion; a/b, a and b binding sites; ns, not significant. Three independent experiments were performed with independent protein (WB and luciferase) or RNA preparations. Representative results are shown in *B*; results are pooled in *C*. $^*P < 0.05$; $^{**}P < 0.01$.

ITGA5 median expression, we predicted DFS (Fig. 5*C*). This, together with similar results reported previously (33), suggests that repression of ITGA5 correlates with better clinical outcome and can be used as a prognostic marker.

Down-modulation of ITGA5 accounts for miR-148b chemotherapy response

The effect of integrin signaling on cell survival and chemotherapy response was evaluated in the absence of serum and adhesion (anoikis) or in presence of paclitaxel. When ITGA5 was silenced with siRNAs in MDAMB231 cells, reduction in cell survival was observed in anoikis conditions and for paclitaxel-treated cells *vs.* controls (**Fig. 6*A***). Instead, when ITGA5 (cDNA lacking its 3′-UTR) was overexpressed (pEGFP-ITGA5), together with pre-miR-148b, in MDAMB231 or MCF7 cells (Fig. 6*B*), and with cells kept in the presence of paclitaxel, the effect of miR-148b on cell death was abolished (Fig. 3). Figure 6*B* considers only the difference (Δ) observed when comparing the presence or absence of miR-148b. ITGA5 and miR-148b levels were evaluated by qRT-PCR analysis (Fig. 6*C–E*). From these results, we can conclude that ITGA5 directly controls, at least partially, miR-148b-driven apoptosis in anoikis conditions and in the presence of paclitaxel.

DISCUSSION

In this work, we identified a group of 16 miRs that are associated with bad prognosis in our breast cancer

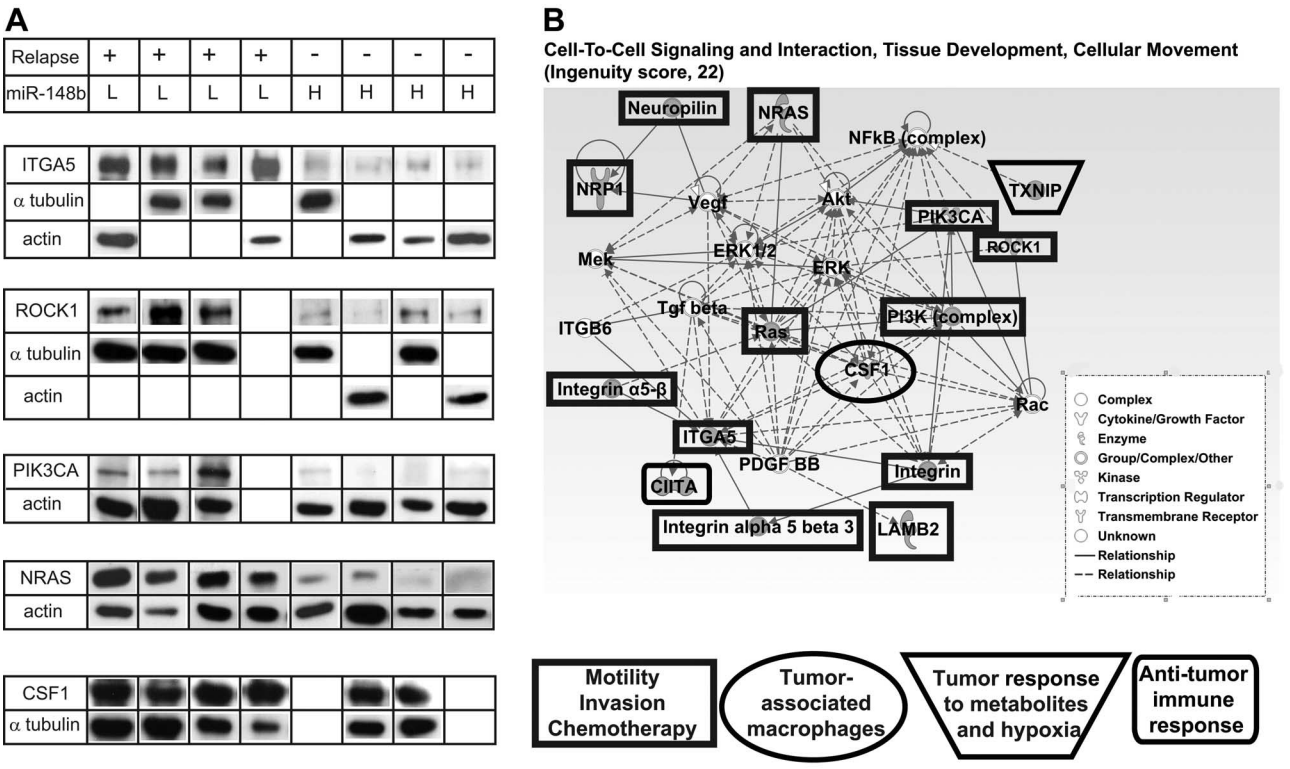

Figure 5. Analysis of miR-148b-modulated genes in human tumors and by IPA. *A*) Proteins were extracted from relapsing or nonrelapsing primary breast tumors, and Western blot (WB) analysis was performed for the direct miR-148b targets, ITGA5, ROCK1, PIK3CA, NRAS, and CSF1. miR-148b expression is indicated as low (L) or high (H), according to previous microarray and/or qRT-PCR analyses. α-Tubulin or actin was used as loading control. *B*) Twenty miR-148b down-modulated genes identified in the microarray analysis (Fig. 4*A*) plus the 3 direct targets, ROCK1, PIK3CA, and NRAS, were used to perform an IPA searching for gene connections; the cell-to-cell signaling and interaction, tissue development, cellular movement functional network was generated. Ingenuity score: $-\log_{10} P = 22$. Gene products are represented as nodes and biological relationships between two nodes as a line. Continuous lines indicate direct interactions; dashed lines represent indirect connections. Shapes of nodes symbolize functional classes of gene products (see legend in panel). Gray symbols indicate down-regulation; white symbols indicate genes absent in the input but related with the dataset used. *C*) Kaplan-Meier analyses of the probability of DFS of breast cancer patients based on ITGA5 expression (median) in Wang *et al.* (26) dataset for 286 breast tumor samples. *P* value was calculated using the log-rank test.

patient cohort, and we revealed the function of miR-148b as a metastasis suppressor in mice, as well as its molecular mechanism of action. The identification of a group of miRs that could identify primary tumor subtypes is highly relevant for the clinics. In fact, it represents a potent molecular tool that clinicians can use at the time of surgery to attempt the most appropriate therapy for every patient. The strength of this tool is further marked by the fact that single components of the signature, for instance miR-148b, can predict tumor outcome individually. Relevantly, low levels of miR-148b were observed previously in basal-like (9) and $ERBB2^+/ER^-/PR^-$ (34) breast tumors, which suggests its involvement in malignancy.

Our functional experiments with metastatic cells strongly suggest that miR-148b exerts its metastasis-suppressing role mostly by controlling cell movement. In fact, while it is true that ectopic expression of miR-148b in malignant tumor cells leads to decreased tumor growth, this effect is modest and not sufficient to justify the much more pronounced control of metastasis dissemination. On this line, increased miR-148b levels lead to stronger adhesion and anoikis and reduce invasion *in vitro*. Moreover, *in vivo*, miR-148b strongly reduces extravasation and lung colonization shortly after injection of the cells in the blood circulation, when proliferation has no time to play a major role. Overall, it is well accepted that miRs have pleiotropic functions and therefore can act in independent events, such as tumor formation and progression, *via* the activation/repression of a selective and rate-limiting cascade of specific genes (8, 35–37).

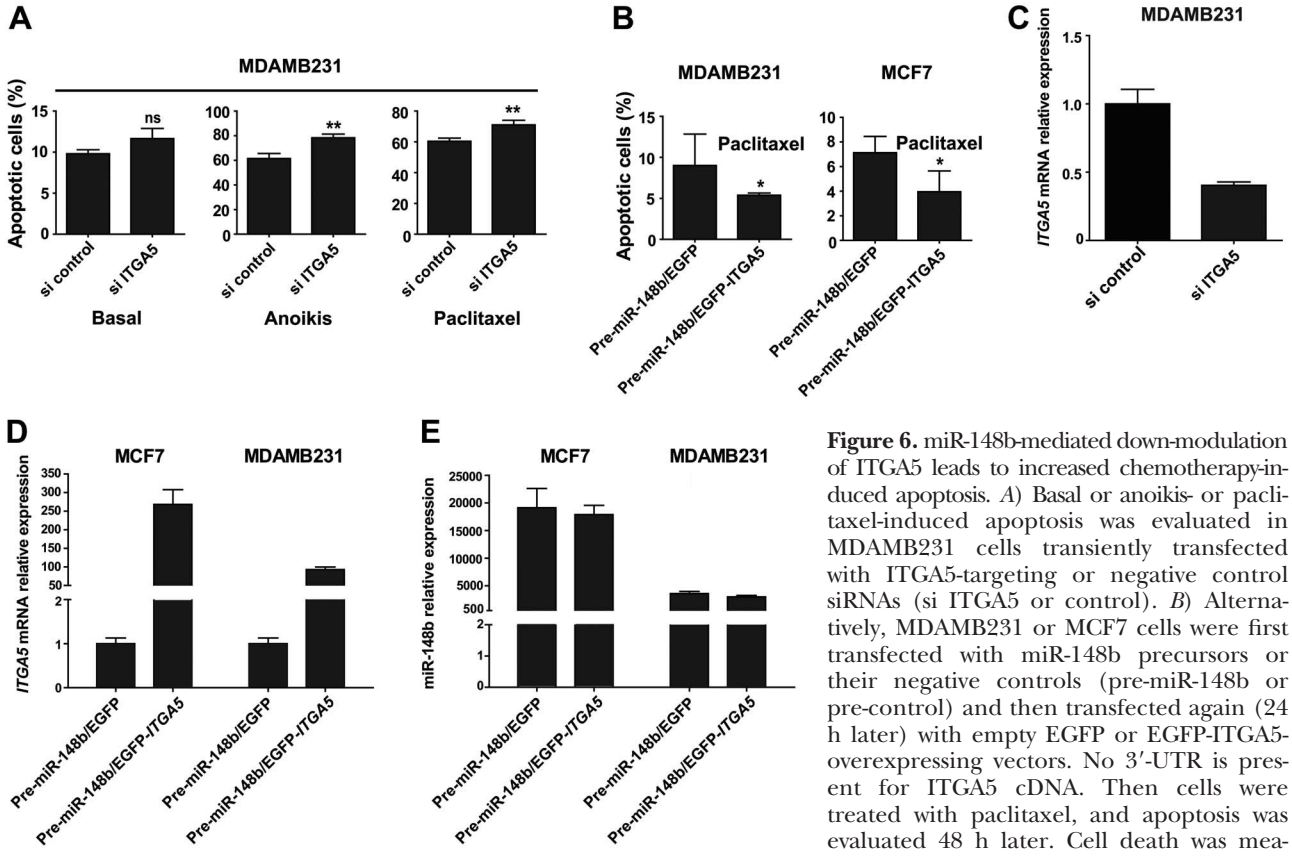

Figure 6. miR-148b-mediated down-modulation of ITGA5 leads to increased chemotherapy-induced apoptosis. *A*) Basal or anoikis- or paclitaxel-induced apoptosis was evaluated in MDAMB231 cells transiently transfected with ITGA5-targeting or negative control siRNAs (si ITGA5 or control). *B*) Alternatively, MDAMB231 or MCF7 cells were first transfected with miR-148b precursors or their negative controls (pre-miR-148b or pre-control) and then transfected again (24 h later) with empty EGFP or EGFP-ITGA5-overexpressing vectors. No 3′-UTR is present for ITGA5 cDNA. Then cells were treated with paclitaxel, and apoptosis was evaluated 48 h later. Cell death was measured by TMRM and annexinV-FITC (*A*) or AnnexinV-PE stainings (*B*) by FACS analysis. *A*) ^{High}TMRM-^{Low}AnnexinV, healthy cells; ^{Low}TMRM-^{High}AnnexinV, apoptotic cells. *B*) ^{Low}AnnexinV, healthy cells; ^{High}AnnexinV, apoptotic cells. Two or 3 independent experiments were performed in duplicate; pooled quantitations are shown as means ± SD. *C–E*) qRT-PCR analyses were performed to evaluate ITGA5 mRNA or miR-148b expression for the cells shown in *A* and *B*. Two independent experiments were performed in triplicate, and a representative one is shown. ns, not significant. $*P < 0.05$; $**P < 0.01$.

Among all the miR-148b-modulated genes identified in this study, many are known to be relevant in tumor progression, among them, CTSA, NRP1, CSF1, MMP15, and ITGA5, all suppressed by miR-148b. By focusing on the ITGA5 signaling, we found that not only ITGA5 but also ROCK1, PIK3CA/p110α, and NRAS are directly down-regulated by miR-148b, which suggests a specific control for this miR on a pathway known to be involved in metastasis dissemination and chemotherapy response. In fact, ITGA5 and ROCK1 were found previously to be highly expressed in malignant breast tumors and are known to increase tumor growth or progression (33, 38–42). At the same time, PIK3CA/p110α is relevant for mammary tumorigenesis and angiogenesis (43), as well as for resistance to endocrine or anti-HER2 therapies (44, 45). In addition, NRAS is a well-known oncogene, and its silencing in tumor cells leads to increased apoptosis (46). Regarding chemotherapy response, elevated levels and activity of α5β1 have previously been implicated in drug resistance (47), and inhibition of α5β1/fibronectin interactions promotes apoptosis in malignant cells and enhances radiation effects (33). In addition, perturbations of the actin cytoskeleton integrity *via* ROCK1 inhibition commit cells to apoptosis (48). Remarkably, ITGA5 and its downstream player RHOA, a ROCK activator, have been previously found to be suppressed by miR-31, another small noncoding RNA that suppresses metastasis (36). In addition, ROCK1 and RHOC are also directly targeted by two other miRs involved in tumor progression, miR-146a/b and miR-10b (49, 50). The fact that CSF1 is also a direct target of miR-148b opens up a role for this small RNA in tumor-stroma cell interactions, which will be part of a future study. In summary, our study unravels the association of a group of 16 miRs with bad prognosis tumors and identifies miR-148b as a suppressor of tumor progression and modulator of chemotherapy response acting *via* the integrin. FJ

This work was supported by grants from the University of Torino (Local Research Funding, 2007 and 2008; D.T.), Compagnia-San-Paolo (2008.1054; D.T.), Programma di Ricerca di Rilevante Interesse Nazionale (PRIN; 2008; D.T. and PRIN 2009; M.D.B.), Associazione Italiana Ricerca Cancro (AIRC; 2008-IG-6014, G.L.; 2009-IG-9408, P.P.; 2010-IG-10104; D.T.), and Fondo per gli Investimenti della Ricerca di Base (FIRB-giovani2008, RBFR08F2FS-002; F.O.). F.O. and D.C. were fellows of the Regione Piemonte. The authors thank P.P. Pandolfi for helpful discussions; V. Poli and E. Hirsch for critical reading of the manuscript; J. Massaguè (Memorial Sloan-Kettering Cancer Center, New York, NY, USA) and L. Primo and P. Circosta (University of Torino, Turin, Italy) for providing cell lines; A. R. Elia for the FACS analysis; A. Mana for performing

some experiments; L. Fuso, G. M. Milano, F. Maggiorotto, and C. Robba for the patient datasets; and A. F. Horwitz (University of Illinois, Urbana-Champaign, IL, USA, *via* Addgene, Cambridge, MA, USA) for the 15238 plasmid. The authors declare no conflicts of interest.

REFERENCES

1. Liu, S., Clouthier, S. G., and Wicha, M. S. Role of microRNAs in the regulation of breast cancer stem cells. *J. Mammary Gland Biol. Neoplasia* **17,** 15–21
2. Dunnwald, L. K., Rossing, M. A., and Li, C. I. (2007) Hormone receptor status, tumor characteristics, and prognosis: a prospective cohort of breast cancer patients. *Breast Cancer Res.* **9,** R6
3. Colozza, M., Cardoso, F., Sotiriou, C., Larsimont, D., and Piccart, M. J. (2005) Bringing molecular prognosis and prediction to the clinic. *Clin. Breast Cancer* **6,** 61–76
4. Sorlie, T., Perou, C. M., Tibshirani, R., Aas, T., Geisler, S., Johnsen, H., Hastie, T., Eisen, M. B., van de Rijn, M., Jeffrey, S. S., Thorsen, T., Quist, H., Matese, J. C., Brown, P. O., Botstein, D., Eystein Lonning, P., and Borresen-Dale, A. L. (2001) Gene expression patterns of breast carcinomas distinguish tumor subclasses with clinical implications. *Proc. Natl. Acad. Sci. U. S. A.* **98,** 10869–10874
5. Sotiriou, C., and Piccart, M. J. (2007) Taking gene-expression profiling to the clinic: when will molecular signatures become relevant to patient care? *Nat. Rev. Cancer* **7,** 545–553
6. Bartel, D. P. (2009) MicroRNAs: target recognition and regulatory functions. *Cell* **136,** 215–233
7. Lu, J., Getz, G., Miska, E. A., Alvarez-Saavedra, E., Lamb, J., Peck, D., Sweet-Cordero, A., Ebert, B. L., Mak, R. H., Ferrando, A. A., Downing, J. R., Jacks, T., Horvitz, H. R., and Golub, T. R. (2005) MicroRNA expression profiles classify human cancers. *Nature* **435,** 834–838
8. Blenkiron, C., Goldstein, L. D., Thorne, N. P., Spiteri, I., Chin, S. F., Dunning, M. J., Barbosa-Morais, N. L., Teschendorff, A. E., Green, A. R., Ellis, I. O., Tavare, S., Caldas, C., and Miska, E. A. (2007) MicroRNA expression profiling of human breast cancer identifies new markers of tumor subtype. *Genome Biol.* **8,** R214
9. Enerly, E., Steinfeld, I., Kleivi, K., Leivonen, S. K., Aure, M. R., Russnes, H. G., Ronneberg, J. A., Johnsen, H., Navon, R., Rodland, E., Makela, R., Naume, B., Perala, M., Kallioniemi, O., Kristensen, V. N., Yakhini, Z., and Borresen-Dale, A. L. miRNA-mRNA integrated analysis reveals roles for miRNAs in primary breast tumors. *PLoS One* **6,** e16915
10. Shi, M., Liu, D., Duan, H., Shen, B., and Guo, N. Metastasis-related miRNAs, active players in breast cancer invasion, and metastasis. *Cancer Metastasis Rev.* **29,** 785–799
11. Le, X. F., Merchant, O., Bast, R. C., and Calin, G. A. The roles of MicroRNAs in the cancer invasion-metastasis cascade. *Cancer Microenviron.* **3,** 137–147
12. Penna, E., Orso, F., Cimino, D., Tenaglia, E., Lembo, A., Quaglino, E., Poliseno, L., Haimovic, A., Osella-Abate, S., De Pitta, C., Pinatel, E., Stadler, M. B., Provero, P., Bernengo, M. G., Osman, I., and Taverna, D. microRNA-214 contributes to melanoma tumour progression through suppression of TFAP2C. *EMBO J.* **30,** 1990–2007
13. Minn, A. J., Kang, Y., Serganova, I., Gupta, G. P., Giri, D. D., Doubrovin, M., Ponomarev, V., Gerald, W. L., Blasberg, R., and Massague, J. (2005) Distinct organ-specific metastatic potential of individual breast cancer cells and primary tumors. *J. Clin. Invest.* **115,** 44–55
14. Simpson, J. F., Gray, R., Dressler, L. G., Cobau, C. D., Falkson, C. I., Gilchrist, K. W., Pandya, K. J., Page, D. L., and Robert, N. J. (2000) Prognostic value of histologic grade and proliferative activity in axillary node-positive breast cancer: results from the Eastern Cooperative Oncology Group Companion Study, EST 4189. *J. Clin. Oncol.* **18,** 2059–2069
15. Tarone, G., Russo, M. A., Hirsch, E., Odorisio, T., Altruda, F., Silengo, L., and Siracusa, G. (1993) Expression of beta 1 integrin complexes on the surface of unfertilized mouse oocyte. *Development* **117,** 1369–1375
16. Laukaitis, C. M., Webb, D. J., Donais, K., and Horwitz, A. F. (2001) Differential dynamics of alpha 5 integrin, paxillin, and alpha-actinin during formation and disassembly of adhesions in migrating cells. *J. Cell Biol.* **153,** 1427–1440
17. Wang, X., Tian, W., and Li, Y. (2008) Development of an efficient protocol of RNA isolation from recalcitrant tree tissues. *Mol. Biotechnol.* **38,** 57–64
18. Bolstad, B. M., Irizarry, R. A., Astrand, M., and Speed, T. P. (2003) A comparison of normalization methods for high density oligonucleotide array data based on variance and bias. *Bioinformatics* **19,** 185–193
19. Risso, D., Massa, M. S., Chiogna, M., and Romualdi, C. (2009) A modified LOESS normalization applied to microRNA arrays: a comparative evaluation. *Bioinformatics* **25,** 2685–2691
20. Tibshirani, R., Hastie, T., Narasimhan, B., and Chu, G. (2002) Diagnosis of multiple cancer types by shrunken centroids of gene expression. *Proc. Natl. Acad. Sci. U. S. A.* **99,** 6567–6572
21. Saeed, A. I., Bhagabati, N. K., Braisted, J. C., Liang, W., Sharov, V., Howe, E. A., Li, J., Thiagarajan, M., White, J. A., and Quackenbush, J. (2006) TM4 microarray software suite. *Methods Enzymol.* **411,** 134–193
22. Liu, Y. (2008) Box plots: use and interpretation. *Transfusion* **48,** 2279–2280
23. Zweig, M. H., and Campbell, G. (1993) Receiver-operating characteristic (ROC) plots: a fundamental evaluation tool in clinical medicine. *Clin. Chem.* **39,** 561–577
24. Mantel, N. (1966) Evaluation of survival data and two new rank order statistics arising in its consideration. *Cancer Chemother. Rep.* **50,** 163–170
25. Gill, R. (1982) Understanding Cox's regression model. *Exper. Suppl.* **41,** 187–199
26. Wang, Y., Klijn, J. G., Zhang, Y., Sieuwerts, A. M., Look, M. P., Yang, F., Talantov, D., Timmermans, M., Meijer-van Gelder, M. E., Yu, J., Jatkoe, T., Berns, E. M., Atkins, D., and Foekens, J. A. (2005) Gene-expression profiles to predict distant metastasis of lymph-node-negative primary breast cancer. *Lancet* **365,** 671–679
27. Damasco, C., Lembo, A., Somma, M. P., Gatti, M., Di Cunto, F., and Provero, P. A signature inferred from Drosophila mitotic genes predicts survival of breast cancer patients. *PLoS One* **6,** e14737
28. Lewis, B. P., Burge, C. B., and Bartel, D. P. (2005) Conserved seed pairing, often flanked by adenosines, indicates that thousands of human genes are microRNA targets. *Cell* **120,** 15–20
29. Mierke, C. T., Frey, B., Fellner, M., Herrmann, M., and Fabry, B. Integrin alpha5beta1 facilitates cancer cell invasion through enhanced contractile forces. *J. Cell Sci.* **124,** 369–383
30. Desgrosellier, J. S., and Cheresh, D. A. Integrins in cancer: biological implications and therapeutic opportunities. *Nat. Rev. Cancer* **10,** 9–22
31. Abraham, D., Zins, K., Sioud, M., Lucas, T., Schafer, R., Stanley, E. R., and Aharinejad, S. Stromal cell-derived CSF-1 blockade prolongs xenograft survival of CSF-1-negative neuroblastoma. *Int. J. Cancer* **126,** 1339–1352
32. Aharinejad, S., Paulus, P., Sioud, M., Hofmann, M., Zins, K., Schafer, R., Stanley, E. R., and Abraham, D. (2004) Colony-stimulating factor-1 blockade by antisense oligonucleotides and small interfering RNAs suppresses growth of human mammary tumor xenografts in mice. *Cancer Res.* **64,** 5378–5384
33. Nam, J. M., Chung, Y., Hsu, H. C., and Park, C. C. (2009) beta1 integrin targeting to enhance radiation therapy. *Int. J. Radiat. Biol.* **85,** 923–928
34. Mattie, M. D., Benz, C. C., Bowers, J., Sensinger, K., Wong, L., Scott, G. K., Fedele, V., Ginzinger, D., Getts, R., and Haqq, C. (2006) Optimized high-throughput microRNA expression profiling provides novel biomarker assessment of clinical prostate and breast cancer biopsies. *Mol. Cancer* **5,** 24
35. Ma, L., and Weinberg, R. A. (2008) Micromanagers of malignancy: role of microRNAs in regulating metastasis. *Trends Genet.* **24,** 448–456
36. Valastyan, S., Chang, A., Benaich, N., Reinhardt, F., and Weinberg, R. A. Concurrent suppression of integrin alpha5, radixin, and RhoA phenocopies the effects of miR-31 on metastasis. *Cancer Res.* **70,** 5147–5154
37. Tavazoie, S. F., Alarcon, C., Oskarsson, T., Padua, D., Wang, Q., Bos, P. D., Gerald, W. L., and Massague, J. (2008) Endogenous human microRNAs that suppress breast cancer metastasis. *Nature* **451,** 147–152

38. Valastyan, S., Benaich, N., Chang, A., Reinhardt, F., and Weinberg, R. A. (2009) Concomitant suppression of three target genes can explain the impact of a microRNA on metastasis. *Genes Dev.* **23,** 2592–2597
39. Taverna, D., and Hynes, R. O. (2001) Reduced blood vessel formation and tumor growth in alpha5-integrin-negative teratocarcinomas and embryoid bodies. *Cancer Res.* **61,** 5255–5261
40. Liu, S., Goldstein, R. H., Scepansky, E. M., and Rosenblatt, M. (2009) Inhibition of rho-associated kinase signaling prevents breast cancer metastasis to human bone. *Cancer Res.* **69,** 8742–8751
41. Lane, J., Martin, T. A., Watkins, G., Mansel, R. E., and Jiang, W. G. (2008) The expression and prognostic value of ROCK I and ROCK II and their role in human breast cancer. *Int. J. Oncol.* **33,** 585–593
42. Zheng, B., Liang, L., Wang, C., Huang, S., Cao, X., Zha, R., Liu, L., Jia, D., Tian, Q., Wu, J., Ye, Y. W., Wang, Q., Long, Z., Zhou, Y., Du, C., He, X., and Shi, Y. MicroRNA-148a suppresses tumor cell invasion and metastasis by downregulating ROCK1 in gastric cancer. *Clin. Cancer Res.* **17,** 7574–7583
43. Renner, O., Blanco-Aparicio, C., Grassow, M., Canamero, M., Leal, J. F., and Carnero, A. (2008) Activation of phosphatidylinositol 3-kinase by membrane localization of p110alpha predisposes mammary glands to neoplastic transformation. *Cancer Res.* **68,** 9643–9653
44. Eichhorn, P. J., Gili, M., Scaltriti, M., Serra, V., Guzman, M., Nijkamp, W., Beijersbergen, R. L., Valero, V., Seoane, J., Bernards, R., and Baselga, J. (2008) Phosphatidylinositol 3-kinase hyperactivation results in lapatinib resistance that is reversed by the mTOR/phosphatidylinositol 3-kinase inhibitor NVP-BEZ235. *Cancer Res.* **68,** 9221–9230
45. Miller, T. W., Hennessy, B. T., Gonzalez-Angulo, A. M., Fox, E. M., Mills, G. B., Chen, H., Higham, C., Garcia-Echeverriav C., Shyr, Y., and Arteaga, C. L. Hyperactivation of phosphatidylinositol-3 kinase promotes escape from hormone dependence in estrogen receptor-positive human breast cancer. *J. Clin. Invest.* **120,** 2406–2413
46. Eskandarpour, M., Kiaii, S., Zhu, C., Castro, J., Sakko, A. J., and Hansson, J. (2005) Suppression of oncogenic NRAS by RNA interference induces apoptosis of human melanoma cells. *Int. J. Cancer* **115,** 65–73
47. Nista, A., Leonetti, C., Bernardini, G., Mattioni, M., and Santoni, A. (1997) Functional role of alpha4beta1 and alpha5beta1 integrin fibronectin receptors expressed on adriamycin-resistant MCF-7 human mammary carcinoma cells. *Int. J. Cancer* **72,** 133–141
48. Shi, J., and Wei, L. (2007) Rho kinase in the regulation of cell death and survival. *Arch. Immunol. Ther. Exp. (Warsz.)* **55,** 61–75
49. Lin, S. L., Chiang, A., Chang, D., and Ying, S. Y. (2008) Loss of mir-146a function in hormone-refractory prostate cancer. *RNA* **14,** 417–424
50. Ma, L., Teruya-Feldstein, J., and Weinberg, R. A. (2007) Tumour invasion and metastasis initiated by microRNA-10b in breast cancer. *Nature* **449,** 682–688

Received for publication July 25, 2012.
Accepted for publication November 13, 2012.

OPEN ACCESS Freely available online

PLoS one

Analysis of miRNA and mRNA Expression Profiles Highlights Alterations in Ionizing Radiation Response of Human Lymphocytes under Modeled Microgravity

Cristina Girardi[1☯], Cristiano De Pittà[1☯], Silvia Casara[1], Gabriele Sales[1], Gerolamo Lanfranchi[1], Lucia Celotti[1,2], Maddalena Mognato[1]*

1 Dipartimento di Biologia, Università degli Studi di Padova, Padova, Italy, **2** Laboratori Nazionali di Legnaro, INFN, Padova, Italy

Abstract

Background: Ionizing radiation (IR) can be extremely harmful for human cells since an improper DNA-damage response (DDR) to IR can contribute to carcinogenesis initiation. Perturbations in DDR pathway can originate from alteration in the functionality of the microRNA-mediated gene regulation, being microRNAs (miRNAs) small noncoding RNA that act as post-transcriptional regulators of gene expression. In this study we gained insight into the role of miRNAs in the regulation of DDR to IR under microgravity, a condition of weightlessness experienced by astronauts during space missions, which could have a synergistic action on cells, increasing the risk of radiation exposure.

Methodology/Principal Findings: We analyzed miRNA expression profile of human peripheral blood lymphocytes (PBL) incubated for 4 and 24 h in normal gravity (1 g) and in modeled microgravity (MMG) during the repair time after irradiation with 0.2 and 2Gy of γ-rays. Our results show that MMG alters miRNA expression signature of irradiated PBL by decreasing the number of radio-responsive miRNAs. Moreover, let-7i*, miR-7, miR-7-1*, miR-27a, miR-144, miR-200a, miR-598, miR-650 are deregulated by the combined action of radiation and MMG. Integrated analyses of miRNA and mRNA expression profiles, carried out on PBL of the same donors, identified significant miRNA-mRNA anti-correlations of DDR pathway. Gene Ontology analysis reports that the biological category of "Response to DNA damage" is enriched when PBL are incubated in 1 g but not in MMG. Moreover, some anti-correlated genes of p53-pathway show a different expression level between 1 g and MMG. Functional validation assays using luciferase reporter constructs confirmed miRNA-mRNA interactions derived from target prediction analyses.

Conclusions/Significance: On the whole, by integrating the transcriptome and microRNome, we provide evidence that modeled microgravity can affects the DNA-damage response to IR in human PBL.

Citation: Girardi C, De Pittà C, Casara S, Sales G, Lanfranchi G, et al. (2012) Analysis of miRNA and mRNA Expression Profiles Highlights Alterations in Ionizing Radiation Response of Human Lymphocytes under Modeled Microgravity. PLoS ONE 7(2): e31293. doi:10.1371/journal.pone.0031293

Editor: John R. Battista, Louisiana State University and A & M College, United States of America

Received September 15, 2011; **Accepted** January 5, 2012; **Published** February 9, 2012

Funding: This work was supported by grants from the Italian Space Agency (ASI, XMAB-from Molecules to Man, 1/014/06/0) to L.C., from the Associazione Italiana per la Ricerca sul Cancro-AIRC (2008/6014) to G.L. and from the University of Padova (CPDA061783) to M.M. The funders had no role in study design, data collection and analysis, decision to publish, or preparation of the manuscript.

Competing Interests: The authors have declared that no competing interests exist.

* E-mail: maddalena.mognato@unipd.it

☯ These authors contributed equally to this work.

Introduction

Eukaryotic cells have evolved efficient DNA-damage response to genotoxic agents in order to eliminate any detrimental effect of DNA lesions. Ionizing radiation (IR) in out-of Earth represents an environmental mutagen to which humans are daily exposed on Earth. Crewmembers of space mission are even more exposed to IR because the cosmic radiation field is rather different from that experienced on Earth, and fragmentation with spacecraft shielding modifies the radiation quality spectrum, hence modifying the biological effectiveness of IR in a manner that is still undetermined. The cell response to the space environment, which is characterized by a condition of weightlessness (i.e. microgravity, 10^{-4}–10^{-6} g), includes immune cell function suppression [1,2], skeletal muscle atrophy [3–5], cardiovascular disorders [6], loss of bone [7,8], changes of gene expression [9,10], increase in chromosomal aberrations and apoptosis [11,12]. Studies carried out with systems simulating on Earth some aspects of microgravity, such clinostats and Rotating Wall Vessel bioreactors, reported similar results, indicating that the experiments performed with modeled microgravity can be used as surrogate of space conditions [13–20]. Despite the abundance of data about the biological effects of space and simulated microgravity, it is still unclear whether microgravity can affects the DNA-damage response (DDR) to IR. DDR is a complex pathway addressed to maintain genome integrity through the activation of proteins involved in sensing, signaling, and transducing the DNA damage signal to effector proteins of cell cycle progression/arrest, DNA repair and apoptosis [21]. While several studies reported additive/synergistic interactions of radiation and microgravity in different biological

systems [22–26], other studies did not report such interactions [27–29]. In particular, the repair of radiation-induced DNA damage seems to be unaffected by microgravity in bacteria and human fibroblasts [30,31] and in yeast [32]. On the contrary, in our previous work we detected a significant delay in the rejoining of DNA double-strand breaks induced by IR in human peripheral blood lymphocytes incubated in microgravity conditions [33]. Recent findings show the tendency of radioadaptation to DNA damage when space flown cells recovered on Earth are exposed to subsequent irradiation [34]. By considering the complexity of DDR and the controversial impact of reduced gravity on radiosensitivity, we expected that the analysis of microRNA (miRNA) profiles could contribute to increase our knowledge on the features of space environment.

MiRNAs are endogenous small noncoding RNAs (18–24 nt), acting as post-transcriptional modulators of gene expression, by pairing to target mRNAs and leading to decreased translational efficiency and/or decreased mRNA levels [35]. A single miRNA can influence the expression of up to thousand genes, thus the function of a miRNA is ultimately defined by the genes it targets. Besides a physiological role of miRNAs in a variety of important biological processes including differentiation, apoptosis [36], fat metabolism [37], viral infection [38] and pathological processes, such as tumorigenesis [39–43], the miRNA-mediated gene regulation operates also in response to cellular stress. Ionizing radiation induces changes in miRNA expression both *in vitro* and *in vivo*, according to cell type, radiation dose and post-irradiation time [44–49]. Several studies suggested that miRNA expression is regulated in the DDR at the transcriptional level, in a p53-dependent manner [50], and through modulation of miRNAs processing and maturation steps [51]. Whilst miRNA-mediated DDR has been studied after ionizing radiation, UV radiation and hypoxic stress [52,53], the response to IR combined with microgravity has not been studied yet, and should give important information about the risk of the exposure to space environment.

In our previous studies carried out with peripheral blood lymphocytes (PBL) incubated in modeled microgravity (MMG) during the repair time after IR, we reported significant decrease of cell survival, delay of double strand break repair, increase of mutant frequency and apoptosis [33,54]. In the present study we analyzed miRNA expression profile of human PBL irradiated *in vitro* with 0.2 and 2Gy of γ-rays and incubated for a short (4 h) and medium-long (24 h) period in MMG and in parallel ground conditions (1 g). The results obtained from this study show differences in miRNA expression profile as a function of the dose and the time after irradiation in both gravity conditions. Interestingly, under MMG many miRNAs were not responsive to radiation compared with 1 g-condition. Analysis of mRNA expression profiles and further miRNA-mRNA anti-correlation analyses allowed the identification of DDR genes differently modulated in the two gravity conditions.

Methods

Ethics Statement

Human peripheral blood lymphocytes (PBL) were obtained from freshly collected "buffy coats" of healthy donors at the Blood Centre of the City Hospital of Padova (Italy). This study obtained ethics approval from the Transfusion Medicine (TM) ethics committee of Blood Centre of the City Hospital of Padova. The informed consent from donors was not required by the TM/ethics committee because PBL samples were analyzed anonymously.

Cells, irradiation and microgravity simulation

PBL were isolated by separation on Biocoll (Biochrom KG, Seromed) density gradient from freshly collected buffy coats from 12 healthy donors. After overnight incubation, PBL, consisting of peripheral mononuclear cells depleted of monocytes, were irradiated with γ-rays (0.2 and 2Gy) at the Department of Oncological and Surgical Sciences of Padova's University with a ^{137}Cs source (dose-rate: 2.8Gy/min). PBL from six donors (named D, E, F, I, L, M) were irradiated with 0.2Gy whereas PBL from other six donors (named A, B, C, G, H, P) were irradiated with 2Gy, for a total of 12 independent experiments. For each experiment, irradiated and non-irradiated PBL of the same donor were incubated in 1 g and MMG conditions for 4 and 24 h. MMG was simulated by the Rotating Wall Vessel (RWV) bioreactor (Synthecon, Cellon), as previously described [14,20]. PBL incubated in 1 g, irradiated and non, were kept in 75 cm^2 flasks at the same density (Figure 1). In all experiments were used unstimulated quiescent (G_0) PBL.

Total RNA isolation

At the end of incubation time (4 and 24 h) in 1 g and MMG, total RNA was isolated from 10^7 irradiated and non-irradiated PBL, by using Trizol® Reagent (Invitrogen, CA), according to the manufacturer's protocol. Total RNA quantification was performed using the ND-1000 spectrophotometer (Nanodrop, Wilmington, DE); RNA integrity and the content of miRNAs were assessed by capillary electrophoresis using the Agilent Bioanalyzer 2100, with the RNA 6000 Nano and the small RNA Nano chips, respectively (Agilent Technologies, Palo Alto, CA). Only total RNA samples

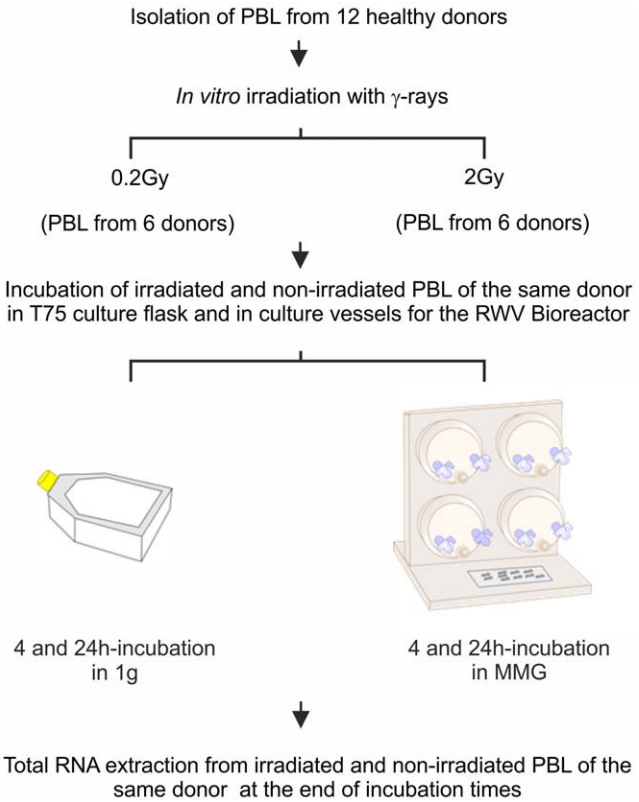

Figure 1. Experimental procedure of irradiation and microgravity simulation.
doi:10.1371/journal.pone.0031293.g001

with RNA Integrity Number (RIN) values ≥6 and with miRNA <20% were used for microarray analysis.

MiRNA and gene expression profiling

MiRNA expression profiles were carried out in irradiated (0.2, 2Gy) vs. non-irradiated PBL, incubated for 4 and 24 h in 1 g and MMG. Analyses were performed by using the "Human miRNA Microarray kit (V2)" (Agilent Technologies), that allows the detection of 723 known human (miRBase v.10.1) and 76 human viral miRNAs. Total RNA (200 ng) was labeled with pCp Cy3, according to the Agilent protocol and unincorporated dyes were removed with MicroBioSpin6 columns (BioRad) [55]. Probes were hybridized at 55°C for 22 hours using the Agilent's Hybridization Oven that is suited for bubble-mixing and microarray hybridization processes. Then, the slides were washed by Agilent Gene expression wash buffer 1 and 2 and scanned using an Agilent microarray scanner (model G2565CA) at 100% and 5% sensitivity settings. Agilent Feature Extraction software version 10.5.1.1 was used for image analysis.

Gene expression profiling was carried out in 2Gy-irradiated vs. non-irradiated PBL, incubated for 24 h in 1 g or MMG, previously analyzed for miRNA profiling. We used the "Whole Human Genome Oligo Microarray" (Agilent), consisting of ~41.000 (60-mer) oligonucleotide probes, which span conserved exons across the transcripts of the targeted full-length genes. 800 ng of total RNA were labeled with "Agilent One-Color Microarray-Based Gene Expression protocol" according to the manufacturer's instructions. 1.65 μg of labeled cRNA were used to prepare the hybridization samples and the hybridization was carried out at 65°C for 17 hours in a hybridization oven rotator (Agilent). The arrays were washed by Agilent Gene expression wash buffers and Stabilization and Drying Solution as suggest by the supplier. Slides were scanned on an Agilent microarray scanner (model G2565CA) and Agilent Feature Extraction software version 10.5.1.1 was used for image analysis. Raw data are available on the Gene Expression Omnibus (GEO) website (*http://www.ncbi.nlm.nih.gov/geo/*) using accession number GSE20120 for miRNA expression profiling (72 experiments) and accession number GSE20173 for mRNA expression profiling (20 experiments).

Statistical analysis of miRNA and gene expression data

Inter-array normalization of expression levels was performed with cyclic Lowess for miRNA experiments and with quantile for gene expression profiling [56] to correct possible experimental distortions. Normalization function was applied to expression data of all experiments and then values of spot replicates within arrays were averaged. Furthermore, Feature Extraction Software provides spot quality measures in order to evaluate the goodness and the reliability of hybridization. In particular flag "glsFound" (set to 1 if the spot has an intensity value significantly different from the local background, 0 otherwise) was used to filter out unreliable probes: flag equal to 0 will be noted as "not available (NA)". So, in order to make more robust and unbiased statistical analysis, probes with a high proportion of "NA" values were removed from the dataset. We decided to use the 40% of NA as threshold in the filtering process obtaining a total of 270 available human miRNAs. Principal component analysis, cluster analysis and profile similarity searching were performed with tMev that is part of the TM4 Microarray Software Suite [57]. The identification of differentially expressed genes and miRNAs was performed with one and two class Significance Analysis of Microarray (SAM) program [58] with default settings. The expression level of each miRNA and mRNA was calculated as the log 2 (irradiated/non-irradiated) PBL of the same donor.

Identification of miRNA target genes and anti-correlation analysis of miRNA and mRNA expression data

To predict miRNA targets we have performed a computational analyses using PITA algorithm based on thermodynamic stability of the RNA-RNA duplex, considering free energy minimization [59]. PITA algorithm was applied over up-to-date version 38 of RefSeq transcript sequences and it used miRNAs sequences downloaded from mirBase version 14. To identify the most likely targets, we have integrated mRNA and miRNA expression data, obtained on the same biological samples, using MAGIA web tool [60]. We used a non-parametric index (Spearman correlation coefficient), the most indicated statistical coefficient for a small number of measures, to estimate the degree of anti-correlation (e.g. up-regulated miRNA and corresponding down-regulated mRNA target) between any putative pairs of miRNA and mRNA [61,62] and we have selected as functional only those anti-correlated less than −0.775. To identify biological processes most involved in the biological phenomena under study we have performed a Gene Ontology (GO) analysis, using DAVID tool [63], on significant anti-correlated target genes identifying biological pathways significantly enriched ($P<0.05$). Pathway enrichment analysis was carried out by KEGG web tool [63] whereas miRNA-mRNA anti-correlations were visualized by Cytoscape software package [64].

Validation of miRNA and mRNA expression levels with qRT-PCR

The data of miRNA expression analysis were validated by using the TaqMan® MicroRNA Assay kit (Applied Biosystems, Foster City, CA), that incorporate a target-specific stem-loop reverse transcription primer to provide specificity for the mature miRNA target. In brief, each RT reaction (15 μl) contained 10 ng of total purified RNA, 5× stem-loop RT primer, 1× RT buffer, 0.25 mM each of dNTPs, 50 U MultiScribe™ reverse transcriptase and 3.8 U RNase inhibitor. The reactions were incubated in a Mastercycler EP gradient S (Eppendorf) in 0.2 ml PCR tubes for 30 min at 16°C, 30 min at 42°C, followed by 5 min at 85°C, and then held at 4°C. The resulting cDNA was quantitatively amplified in 40 cycles on an ABI 7500 Real-Time PCR System, using TaqMan Universal PCR Master Mix and Taqman MicroRNA Assays for miR-34a, miR-424*, miR-181a-2*, miR-144, miR-598, miR-27a, and for U48 small nuclear (RNU48) as endogenous control.

For mRNA detection, 1 μg of total RNA was retrotranscribed with ImProm-II Reverse Transcription System (Promega). qRT-PCR was performed with the GoTaq qPCR Master Mix (Promega) and gene-specific primers for ATM, BAX, FANCF, STAT5A, TNFRSF10B genes and for GADPH as reference. qRT-PCR reactions were always performed in quadruplicates, in PBL samples from 4–6 donors. The relative expression levels of miRNAs and mRNAs between samples were calculated using the comparative delta *C*T (threshold cycle number) method ($2^{-\Delta\Delta CT}$) implemented in the 7500 Real Time PCR System software [65].

Luciferase reporter assays

Luciferase reporter vectors containing the 3′-UTR of miR-27a, miR-144 and miR-424* target genes ATM, FANCF, STAT5A, TNFRSF10B, BAX, were generated following PCR amplification from human cDNA and cloned into the pmirGLO Dual-Luciferase miRNA Target Expression Vector (Promega, Madison,

WI), immediately downstream from the stop codon of the luciferase gene. The sequence of each insert was confirmed by sequencing. MiR-27a-sensor, miR-144-sensor and miR-424*-sensor, were obtained by annealing, purifying and cloning short oligonucleotides containing the perfect miRNA binding site into the *Sac*I and *Xba*I sites of the pmirGLO vector. A549 cells were plated in 24-well plates (14×10^5 cells/well) and 24 h later co-transfected with 50 ng of the pmirGLO dual-luciferase constructs, containing the indicated 3′UTRs of target genes, and with 32 nM pre-miR^{TM} miRNA Precursor Molecules-Negative Control or pre-miR^{TM} miRNA Precursor hsa-miR-27a (PM10939), hsa-miR-424*(PM12641), and hsa-miR-144 (PM11051) (all from Ambion, Austin, TX), using Lipofectamine2000 (Invitrogen Life Technologies). Lysates were collected 24 h after transfection and Firefly and Renilla Luciferase activities were consecutively measured by using Dual-Luciferase Reporter Assay (Promega) according to manufacturer's instructions. Relative luciferase activity was calculated by normalizing the ratio of Firefly/Renilla luciferase to that of negative control-transfected cells. Transfections were performed in triplicate and repeated 3–4 times.

Results

Radio-responsive miRNAs in static condition (1 g)

Human PBL were irradiated *in vitro* with γ-rays (0.2Gy; 2Gy) and incubated in normal gravity (1 g) and in MMG during the post-irradiation time. Twelve total donors were analyzed, six for each dose, by performing independent experiments, in which irradiated and non-irradiated PBL of the same donor were incubated in 1 g and in MMG for 4 and 24 h. MicroRNA expression profiling was performed on total RNA extracted at the end of incubation times (Figure 1), by comparing the expression profile of irradiated vs. non-irradiated PBL of the same donor. Data obtained from PBL incubated in 1 g allowed to identify 26 (0.2Gy) and 20 (2Gy) radio-responsive miRNAs at 4 h after irradiation; miRNAs differentially expressed at 24 h after irradiation were 17 (0.2Gy) and 52 (2Gy), (Figure 2A and Table 1). Raw data and means of miRNA expression values are available on Table S1. Besides a fraction of radio-responsive miRNAs common between 0.2 and 2Gy (28% and 19% at 4 and 24 h after IR, respectively), most of miRNA species was activated in a dose-related manner (Figure 2B). Our results showed that, early after irradiation, both doses induced consistent changes in miRNA expression, whereas late after irradiation, the effect of the higher dose was predominant. Furthermore, most of radio-responsive miRNAs showed a time-related expression pattern, with a substantial down-regulation at 4 h and up-regulation at 24 h after IR (Figure 2C).

Radio-responsive miRNAs in modeled microgravity (MMG)

To check whether the expression of radio-responsive miRNAs was altered under modeled microgravity condition, we characterized the miRNA profile of PBL irradiated with 0.2 and 2Gy and incubated in MMG. After 4 h of incubation in MMG we identified 16 miRNAs responsive to 0.2Gy (vs. 26 in 1 g) and 22 miRNAs responsive to 2Gy (vs. 20 in 1 g). After 24 h of incubation in MMG we identified only 4 miRNAs responsive to 0.2Gy (vs. 17 in 1 g) and 32 miRNAs responsive to 2Gy (vs. 52 in 1 g) (Figure 3 and Table S2). The dose- and time-effect of IR on miRNA profile persisted in MMG, in spite of the decreased radio-responsiveness. In Figure S1 we report miRNAs which changed their expression level in a time-related pattern, showing the down-regulation at 4 h and the up-regulation at 24 h after irradiation, in common with 1 g.

The Venn diagram in Figure 4A shows the number of shared and exclusively modulated miRNAs as a consequence of radiation alone (i.e. in 1 g) and radiation associated with MMG. Radio-responsive miRNAs specific to 1 g condition were 15 (0.2Gy) and 29 (2Gy), whereas those specific to MMG condition were 2 in 0.2Gy PBL and 9 in 2Gy PBL. Except for miR-371-5p and miR-886-3p, which were differently altered in 1 g at 24 h after irradiation (Table 1), miR-99b, let-7i*, miR-144, miR-200a, miR-27a, miR-598, miR-650, miR-7, miR-7-1* were activated by the combined exposure to IR and MMG (Figure 4B).

Target prediction and integration analysis of miRNA and mRNA expression profiles

To predict the target genes of differentially expressed miRNAs we first performed a computational analyses using PITA algorithm available on line [46,59]. However, all available softwares for target prediction are characterized by a large fraction of false positive, thus, the integration of target predictions with miRNA and gene target expression profiles has been proposed to refine functional miRNA-mRNA relationships. For this purpose, we defined the gene expression signature on the same PBL samples used to assess miRNA expression profile, and then we compared miRNA and mRNA expression levels (Figure 5). Gene expression profiles were carried out only in 2Gy PBL incubated for 24 h in 1 g or in MMG, since for this dose and this time point, several IR-responsive genes involved in DDR pathway were previously identified in human quiescent PBL [66] and in human peripheral blood [67]. In addition, our previous results demonstrated that cell survival, double-strand break (DSB) repair, mutant frequency and apoptosis, were significantly altered when 2Gy PBL were incubated for 24 h in MMG [33,54]. We did not perform gene expression profiling in 0.2Gy PBL incubated 24 h in 1 g or in MMG, since the number of miRNAs differentially expressed in MMG was too small (n = 4, Figure 3) to obtain informative data from the anti-correlation analysis. The 52 (in 1 g) and 32 (in MMG) differentially expressed miRNAs in 2Gy PBL resulted anti-correlated to a total of 379 and 391 transcripts, respectively. These transcripts were then classified according to DAVID [63], to determine which Gene Ontology (GO) terms were significantly enriched in our set of genes, in relation to the different gravity conditions. Biological categories common to 1 g and MMG were those of "Immune response", "Leukocyte activation", "Cell activation", "Regulation of cell proliferation", "Regulation of cell cycle", "Positive regulation of apoptosis" (Figure 6). Biological categories of "Response to DNA damage stimulus", "DNA damage response, signal transduction by p53 class mediator", "Apoptotic mitochondrial changes" and "DNA metabolic process" were enriched only when PBL were incubated in 1 g. In MMG, instead were enriched categories of "Hemopoiesis", "Regulation of cytokine production", "Immune system development" and "Lymphocyte differentiation", all characterized by a general gene down-regulation of gene expression (not-shown). By pathway enrichment analysis using the KEGG web tool [63] we found that the p53-pathway was enriched in both gravity conditions, but with some differences between 1 g and MMG (Figure S2). Table 2 provides the identity and associated functions of each altered gene belonging to p53 pathway, together with additional DDR genes found deregulated from miRNA-mRNA integrated analyses. Genes in italic are included in the GO category "Response to DNA damage stimulus", which was enriched in 1 g but not in MMG.

Table 1. Differentially expressed miRNAs in γ-irradiated versus non-irradiated human PBL.

4 h after irradiation			24 h after irradiation		
miRNA name	**0.2Gy**	**2Gy**	**miRNA name**	**0.2Gy**	**2Gy**
hsa-miR-21*	−0.84	−0.72	hsa-miR-1225-5p	0.44	0.60
hsa-miR-34b*	−0.89	−0.85	hsa-miR-135a*	0.48	0.67
hsa-miR-210	0.53	0.46	hsa-miR-152	−0.43	−0.41
hsa-miR-630	−1.75	−1.41	hsa-miR-181a-2*	−0.57	−0.99
hsa-miR-886-3p	−0.59	−0.91	hsa-miR-188-5p [46]	0.60	0.73
hsa-miR-199b-5p	0.58	0.39	hsa-miR-34a [44,48,52,70,71]	1.53	1.76
hsa-miR-582-5p	0.48	0.39	hsa-miR-34b* [68]	1.02	1.66
hsa-miR-378	−0.71	−0.46	hsa-miR-424*	1.00	2.08
hsa-miR-513b	−0.96	−0.65	hsa-miR-638 [49,70]	0.57	0.59
hsa-miR-923	−0.99	−0.53	hsa-miR-663 [46,49,68,70]	0.46	0.99
hsa-let-7e [45,47,49]	−0.31		hsa-miR-765	0.63	0.71
hsa-miR-16 [52]	0.30		hsa-miR-1226*	0.76	
hsa-miR-23a*	0.17		hsa-miR-150*	0.38	
hsa-miR-34a	−0.64		hsa-miR-202	0.43	
hsa-miR-145	0.75		hsa-miR-601	0.78	
hsa-miR-181b	0.30		hsa-miR-760	0.42	
hsa-miR-196b	0.55		hsa-miR-886-3p	−0.60	
hsa-miR-202	0.49		hsa-miR-100 [72]		−0.50
hsa-miR-221 [52,69]	0.51		hsa-miR-101*		−0.37
hsa-miR-339-3p	−0.34		hsa-miR-10a		−0.57
hsa-miR-345	−0.62		hsa-miR-141		−0.38
hsa-miR-425*	0.43		hsa-miR-151-3p		−0.32
hsa-miR-450a	0.52		hsa-miR-16-2*		−0.66
hsa-miR-494	−0.76		hsa-miR-17 [69,73]		−0.22
hsa-miR-629*	0.71		hsa-miR-181a [44,69]		−0.31
hsa-miR-801	−0.85		hsa-miR-18b [52]		−0.35
hsa-miR-223		0.47	hsa-miR-196a		−0.91
hsa-miR-301a		0.45	hsa-miR-196b [70]		−0.51
hsa-miR-513a-5p		−1.19	hsa-miR-19b		−0.25
hsa-miR-940		0.53	hsa-miR-200b [70]		−0.24
hsa-miR-768-5p		−0.38	hsa-miR-210 [44,53]		−0.31
hsa-miR-146a		−0.41	hsa-miR-221*		−0.36
hsa-miR-575		−0.47	hsa-miR-29b-1*		−0.47
hsa-miR-378*		−0.47	hsa-miR-30d [69]		−0.18
hsa-miR-188-5p		−0.59	hsa-miR-30e*		−0.24
hsa-miR-126* [69]		−0.60	hsa-miR-330-3p		−0.34
			hsa-miR-335		−0.35
			hsa-miR-345 [44,53,71]		1.16
			hsa-miR-363		0.99
			hsa-miR-371-5p		0.55
			hsa-miR-421		0.50
			hsa-miR-483-5p		1.33
			hsa-miR-494		0.87
			hsa-miR-505*		−0.40
			hsa-miR-513a-5p		1.06
			hsa-miR-513b		1.19
			hsa-miR-513c		1.22
			hsa-miR-551b		−0.40
			hsa-miR-574-5p		0.97

Table 1. Cont.

4 h after irradiation			24 h after irradiation		
miRNA name	**0.2Gy**	**2Gy**	**miRNA name**	**0.2Gy**	**2Gy**
			hsa-miR-630 [68,73]		0.96
			hsa-miR-769-5p		−0.34
			hsa-miR-801		0.66
			hsa-miR-873		−0.64
			hsa-miR-877*		0.72
			hsa-miR-923		0.89
			hsa-miR-940		0.49
			hsa-miR-95		−0.44
			hsa-miR-99a		−0.64

Irradiated and non-irradiated PBL of the same donors were incubated in static gravity (1 g) for 4 and 24 h, and miRNA expression profile was analyzed at the end of each incubation time. The expression value of each radio-responsive miRNA is the mean of expression levels calculated as the log2 (irradiated/non-irradiated) PBL from six donors/dose (see Table S1). References of miRNAs differentially expressed in other cell types following the exposure to different stressors are given in parentheses.
doi:10.1371/journal.pone.0031293.t001

By using Cytoscape [64] we were able to visualize miRNA-mRNA interactions of DDR pathway in the two gravity conditions (Figure 7). Our results show that the same transcript deregulated in both 1 g and MMG (i.e. PCNA, XPC, CDKN1C, BAX, BIRC5, PHLDA3, TNFRSF10B, TRIAP1) was, in most cases, anti-correlated to different miRNA species, according to the condition of gravity.

The microarray data from miRNA and mRNA expression profiling were validated by real time-qPCR experiments for six miRNAs and four mRNAs, whose expression level was significantly altered in response to radiation (Figure 8). MiR-27a, miR-144, miR-598, together with ATM and STAT5A transcripts, were down-regulated in 2Gy MMG samples. MiR-34a, miR-424*, miR-181a-2*, together with BAX and TNFRSF10B transcripts, were deregulated in 2Gy PBL incubated in both gravity conditions.

Functional correlation between miRNAs and some of their potential target mRNAs

The modulation of miRNAs involved in the DNA-damage response to radiation showed some differences between samples incubated in normal gravity and microgravity. To validate some of the predicted miRNA-mRNA anti-correlations identified in 2Gy-PBL incubated in 1 g and MMG, we selected three miRNAs (miR-27a, miR-424*, miR-144) and at least 2 of their potential targets, for functional testing *in vitro* with the luciferase reporter assay. While miR-424* was up-regulated in response to radiation in both gravity conditions, miR-27a and miR-144 were respectively up-regulated and down-regulated, in 2Gy-PBL incubated in MMG. A549 cells were co-transfected with the synthetic miRNA precursors (pre-miRNA) of interest or miRNA precursor-negative control (pre-control), and expression vectors containing the 3′UTR of the target gene, cloned downstream of the luciferase gene. The results show that pre-miR-27a reduced significantly the luciferase activity from constructs containing the ATM 3′UTR, but not the FANCF and STAT5A 3′UTR. Pre-miR-424* reduced significantly the luciferase activity of both FANCF and STAT5A 3′UTR containing vectors, whereas pre-miR-144 reduced significantly that from constructs containing the BAX 3′UTR (Figure 9). As positive controls were used miR-27a-sensor, miR-144-sensor, and mR-424*-sensor constructs, containing the perfect binding site for each miRNA.

Discussion

With the present study, carried out on human PBL, we evaluated whether the expression of miRNAs involved in the DNA-damage response to γ-radiation was affected by modeled microgravity incubation during the repair time, enhancing the biological effects of ionizing radiation. In ground gravity the exposure to γ-radiation alters miRNA expression profile as a function of the dose and the time after IR. These results are in accordance with data from normal human fibroblasts [46,53] and lymphoblastic IM9 cells [68], but not with those from lymphoblastoid TK6 cells [44], and from human endothelial cells [69], strengthening the existence of cell-specific miRNA radio-response. Several of the radio-responsive miRNAs here identified have been found deregulated in other cells types exposed to different kind of stressors (Table 1), [44–49,52,53,68–73].

Also modeled microgravity alters miRNA expression profile of irradiated PBL in a dose- and time-manner, but with a decreased radio-responsiveness compared with in 1 g. Indeed, 15 and 29 miRNAs were not responsive to 0.2 and 2Gy, respectively, when incubation occurred in MMG. Due to the decrease of radio-responsiveness of miRNA expression, we believe that the DNA-damage response to radiation might be affected by MMG incubation during the repair time. From our analyses we individuated common and distinct miRNAs differentially expressed in response to radiation alone (in 1 g) or associated with MMG. Eight miRNAs (let-7i*, miR-7, miR-7-1*, miR-27a, miR-144, miR-200a, miR-598, miR-650), were differentially expressed only when PBL were incubated in MMG. Probably, they not respond to the direct insult of γ-radiation, but are instead altered by the combined action of ionizing radiation and microgravity.

To improve the detection of functional miRNA-mRNA relationships, we analyzed the gene expression profiles on the same PBL samples used to assess miRNA expression levels. Then, we integrated the transcriptome and microRNome and we performed the anti-correlation analysis. Gene Ontology (GO) analysis was conducted on significant anti-correlated target genes to identify common and distinct biological categories significantly over-represented in our set of anti-correlated transcripts. Our results show that most genes were gravity-specific. While in PBL incubated in 1 g a great number of hits were achieved by the categories of DDR pathway, in PBL incubated in MMG these

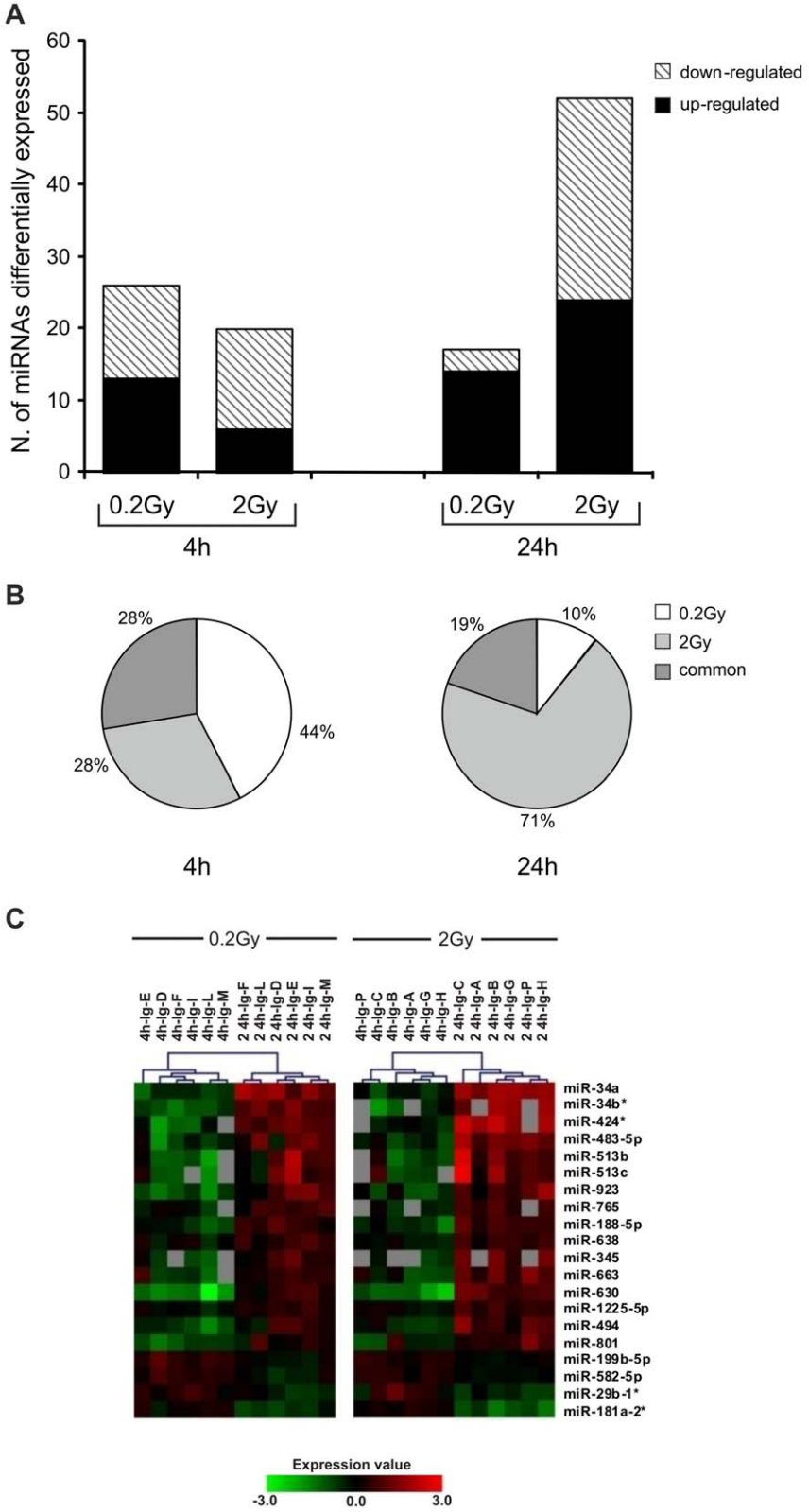

Figure 2. Differentially expressed miRNAs in irradiated PBL incubated in 1 g condition. (A) Number of radio-responsive miRNAs at 4 and 24 h after irradiation with 0.2 and 2Gy of γ-rays. (B) Percentage of dose-responsive miRNAs at the same time points. The expression level of each radio-responsive miRNA is the mean of expression values from six different donors/dose determined by the log2 (irradiated/non-irradiated) PBL. (C) Dendrogram showing radio-responsive miRNAs common to 0.2 and 2Gy of γ-rays, whose expression changed between 4 and 24 h after irradiation. Six different donors were analyzed for each dose, as indicated by the capital letters. The range of expression value is from -3.0 (green, down-regulation) to 3.0 (red, up-regulation). Grey boxes correspond to not available (N/A) fluorescent signal from the microarray platform.
doi:10.1371/journal.pone.0031293.g002

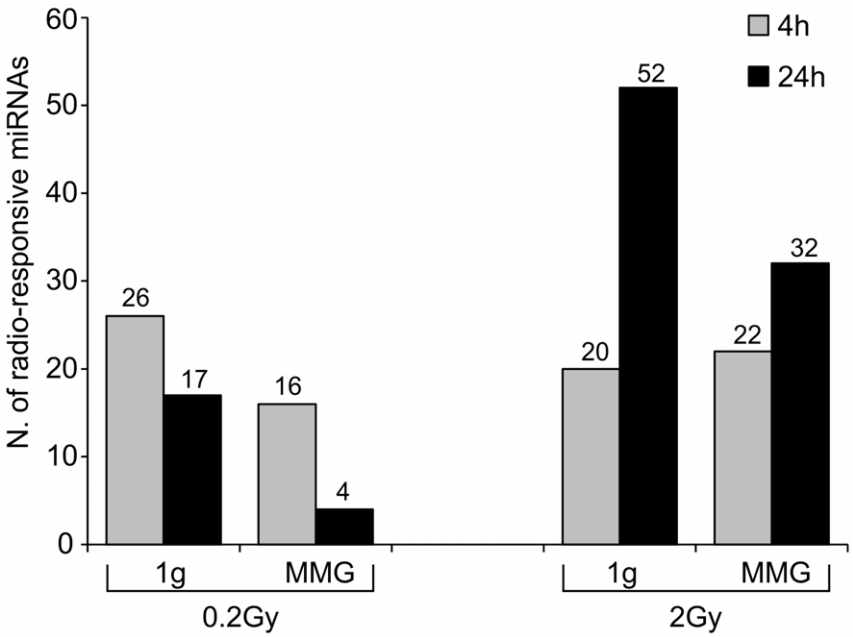

Figure 3. Effect of modeled microgravity on miRNA expression of irradiated PBL. Number of differentially expressed miRNAs in PBL irradiated with 0.2 and 2Gy and incubated for 4 and 24 h in MMG and in 1 g condition.
doi:10.1371/journal.pone.0031293.g003

categories were not enriched. We instead found enriched processes involved in hemopoiesis, regulation of cytokine production, immune system development and lymphocyte differentiation.

To investigate on the differences of DDR pathway between 1 g and MMG conditions, we focused on p53-pathway, which is pivotal in eliciting a complex DDR in response to genotoxic and non-genotoxic stresses [74–77]. The ATM transcript resulted down-regulated in MMG and anti-correlated to miR-27a, as confirmed by functional validation with the luciferase reporter assay. Mir-27a, which is activated by the combined action of IR and MMG, is abnormally up-regulated in several types of cancers and has been identified to play an oncogenic role in the progression of cancers [78–81]. Moreover, miR-27a is a member of the miR-24 cluster, whose over-expression enhances TNF-a induced apoptosis in human embryonic kidney cells [82] and affects DSB repair in terminally differentiated blood cells by deregulating H2AX expression [83].

The results of anti-correlation analyses reported the down-regulation of p53 transcript (TP53) and alterations in the expression levels of several p53-related transcripts (BBC3, CCNG1, CDKN1A, CDKN2A, DDB2, GADD45A, PPM1D, RRM2B,SESN1,THBS1, TP53I3, ZMAT3), when 2Gy PBL were incubated in MMG. PPM1D transcript encodes for the p53-induced protein phosphatase 1 (WIP1), which modulates the expression of H2AX, the histone with a key role in DNA damage signaling and DSB repairing [84]. Since overexpression of WIP1 facilitates the clearance of IR-induced γ-H2AX foci after DNA repair is completed [85], the up-regulation of WIP1 transcript observed in 1 g but not in MMG, is consistent with our previous results, showing s slower disappearance of γ-H2AX foci in irradiated PBL incubated in MMG [33]. From our results the extrinsic pathway of apoptosis appeared more targeted in MMG than in 1 g. Indeed, miR-7, miR-7-1*, miR-144 and miR-650, which were anti-correlated to pro-apoptotic TNFRSF10B, were exclusively radio-responsive in MMG. The expression level of the gene, which encodes the receptor for the cytotoxic ligand TNFSF10/TRAIL, was 3.65-fold induced in MMG vs. 2.6-fold in 1 g. Also PHLDA3, which contributes to p53/TP53-dependent apoptosis by repressing AKT1 activity, showed a higher expression level in MMG. This gene was anti-correlated to miR-200a, itself activated by the associated action of IR and MMG. On the contrary, the intrinsic apoptotic pathway appeared more targeted in 1 g, with four up-regulated genes (BBC3, TP53I3, ZMAT3, FDXR). Notably, pro-apoptotic BAX was anti-correlated to four miRNAs (miR-144, miR-200a, miR-598,miR-650) deregulated in only 2Gy MMG PBL. The luciferase assay confirmed the functional interaction between miR-144 and BAX, suggesting that this miRNA may contribute to, or amplify, IR-induced apoptosis in MMG. Instead, the interaction between miR-144 and miR-27a with their putative target genes involved in apoptosis (respectively TNFRSF10B and STAT5A), diminished the luciferase activity, but not significantly. It should be noted that such transcripts are anti-correlated to 4–6 different miRNAs that can act together on individual mRNA to produce additive or synergistic effects [86,87].

On the whole our results evidence that 1) many transcripts are targeted by multiple miRNAs; 2) the same transcript can be targeted by different miRNA species according to the gravity condition; 3) miRNAs responsive to IR in both gravities not always target the same transcript. The possibility that a single mRNA can be targeted by multiple miRNAs has been reported [88,89] and recently demonstrated by Wu et al. [86]. The reason why the same mRNA could be anti-correlated to different miRNA species in relation to the gravity condition, is not clear. We hypothesize that the reduced number of radio-responsive miRNAs in MMG can operate an unscheduled regulation of transcripts. Moreover, the dysregulation of mRNAs caused by microgravity-mediated gene expression changes, could impact on miRNAs recruitment. This idea is consistent with the recent findings of Poliseno and co-authors [90] which demonstrated that mRNAs introduced into a cell can potentially perturb the interaction between miRNAs and their multiple targets, thus having a biological activity independent of the

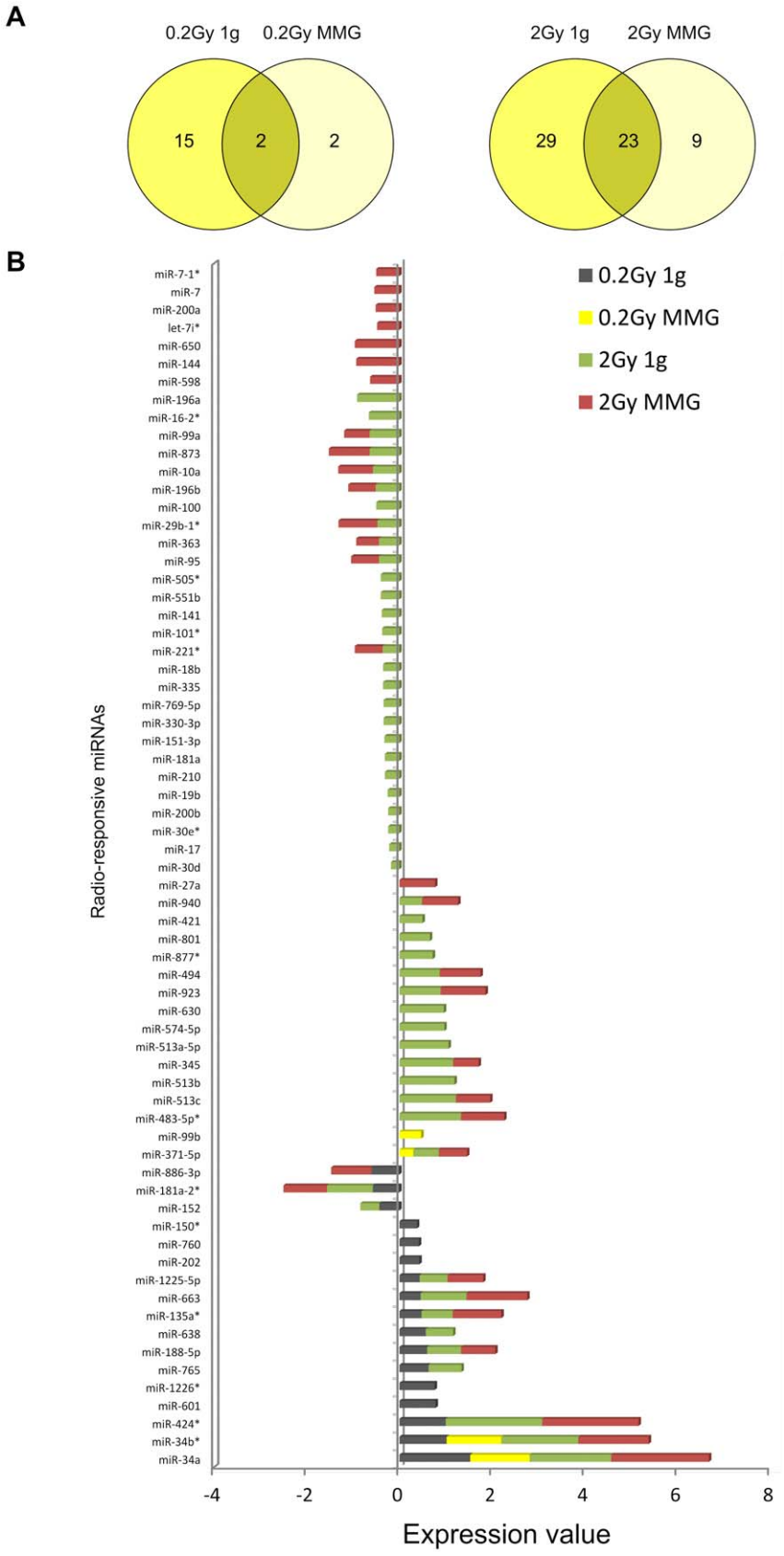

Figure 4. miRNA changes in human irradiated PBL incubated 24 h in 1 g and in MMG. A) The Venn Diagram shows the number of common and exclusively expressed miRNAs as a consequence of only radiation (0.2Gy 1 g, 2Gy 1 g) and radiation with microgravity (0.2Gy MMG, 2Gy MMG). B) miRNAs differentially expressed in PBL incubated 24 h in 1 g or MMG after irradiation with 0.2 and 2Gy. The expression level is given as log 2 (irradiated/non-irradiated) PBL incubated in the indicated gravity condition.
doi:10.1371/journal.pone.0031293.g004

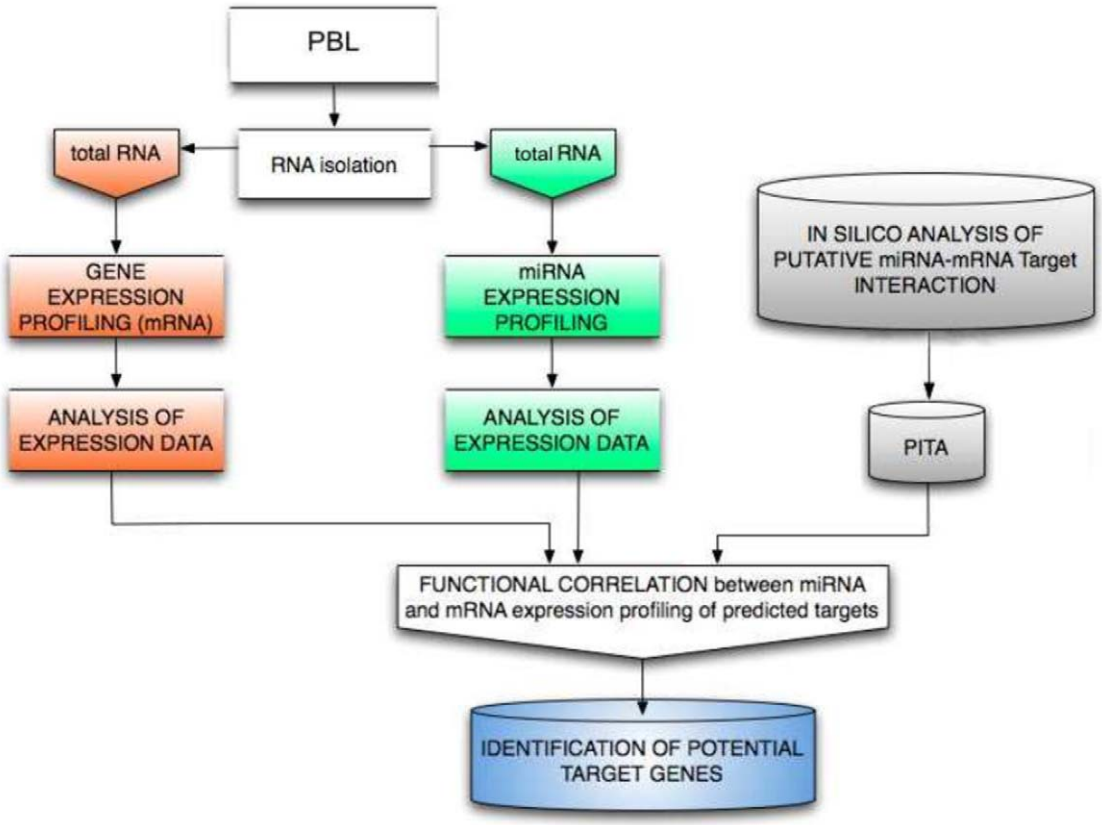

Figure 5. The procedure of computational prediction of miRNA targets. miRNA and gene expression profiles were defined in PBL irradiated with 2Gy versus non-irradiated PBL of the same donors, at the end of 24 h-incubation in 1 g and in MMG. Target prediction was first performed by PITA algorithm, then expression data were integrated to improve the detection of functional correlation between miRNA and mRNA expression profiling.
doi:10.1371/journal.pone.0031293.g005

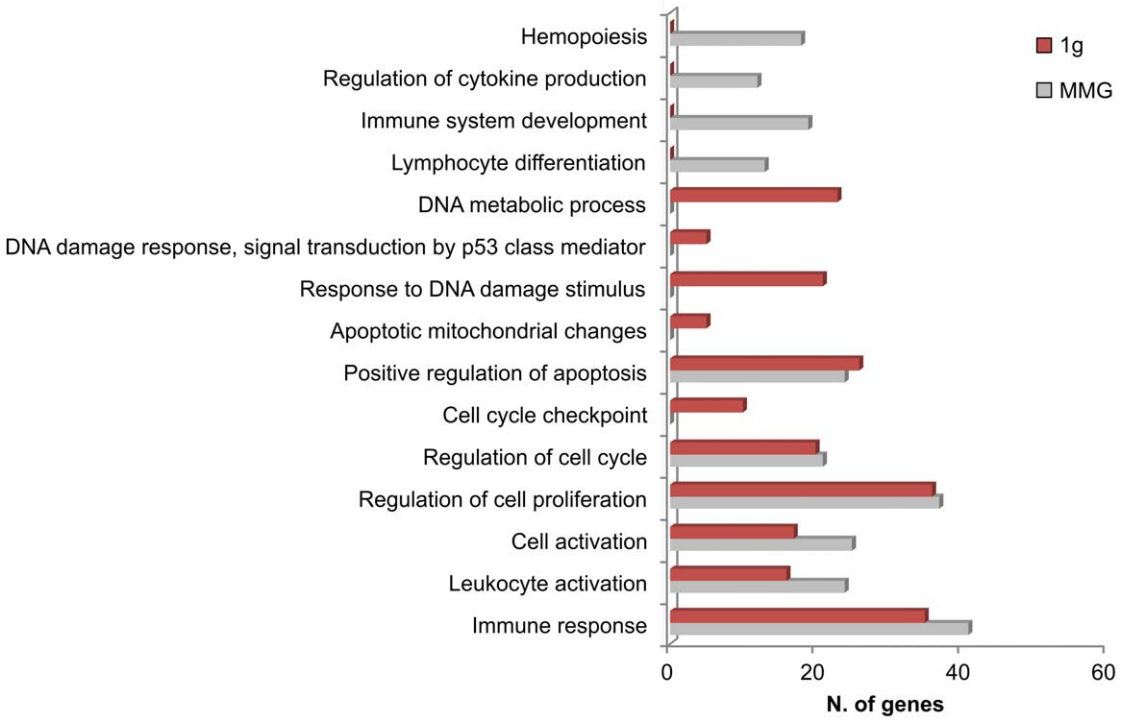

Figure 6. Gene Ontology (GO) analysis of anti-correlated target genes in 2Gy-irradiated PBL incubated 24 h in 1 g or MMG. Biological processes found enriched from GO analysis are shown. For each functional category is shown the number of genes differentially expressed in the two gravity condition.
doi:10.1371/journal.pone.0031293.g006

Table 2. Significantly anti-correlated genes involved in the DNA-damage response to IR of human PBL.

Gene symbol	Gene name	Function	2Gy 1 g	2Gy MMG
			F.C.	F.C.
ATM	Ataxia Telangiectasia Mutated	DNA damage signal transduction; cell cycle checkpoint	- -	−1.42
BAX	BCL2-associated X protein	Apoptosis	3.40	3.22
BBC3	BCL2-binding component 3 (PUMA)	Apoptosis	5.94	- -
CCND2	Cyclin D2	Cell cycle progression	−1.81	−1.59
CCNG1	Cyclin G1	Cell cycle progression/arrest	2.83	- -
CDC2	Cell division cycle 2 (CDK1)	Cell cycle progression	−1.94	−2.48
CDKN1A	Cyclin-dependent kinase inhibitor 1A (p21)	Cell cycle arrest	3.89	- -
CDKN2A	Cyclin-dependent kinase inhibitor 2A (p14ARF)	DNA damage sensor; cell cycle arrest; apoptosis	−1.61	- -
DDB2	Damage-specific DNA binding protein 2 (p48)	DNA repair	4.89	- -
EI24	Tumor protein p53 inducible protein 8 (PIGs)	Apoptosis p53-dependent	1.46	1.40
GADD45A	Growth arrest and DNA-damage-inducible, alpha	Growth arrest; DNA repair; apoptosis	6.23	- -
GADD45B	Growth arrest and DNA-damage-inducible, beta	Growth arrest; apoptosis	- -	−2.54
MDM2	Mdm2 p53 binding protein homolog	Inactivation of tumour protein p53	3.75	2.86
PPM1D	Protein phosphatase 1D magnesium-dependent (Wild type p53-induced phosphatase,Wip1)	DNA damage sensor (phosphorylates H2AX)	1.49	- -
RRM2B	p53-inducible ribonucleotide reductase small subunit (p53R2)	DNA repair	- -	1.76
SESN1	Sestrin 1 (Sestrins)	Cell cycle arrest	2.56	- -
THBS1	Thrombospondin 1 (TSP1)	Cell growth	2.44	- -
TNFRSF10B	Tumor necrosis factor receptor superfamily, member 10b (DR5)	Apoptosis	2.60	3.65
TP53	Tumor protein p53	Cell cycle arrest; DNA repair; apoptosis	- -	−1.73
TP53I3	Tumor protein p53 inducible protein 3 (PIGs)	Apoptosis p53-dependent	1.72	- -
ZMAT3	Zinc finger, matrin type 3 (PAG608)	Cell growth; apoptosis p53-dependent	4.60	- -
AEN	Apoptosis Enhancing Nuclease	Apoptosis	5.42	4.44
BIRC5	Baculoviral IAP repeat-containing 5	Apoptosis	−2.90	−3.43
CDKN1C	Cyclin-dependent kinase inhibitor 1C (p57)	Cell cycle	2.11	4.22
FANCA	Fanconi anemia, complementation group A	DNA repair	−1.56	- -
FANCF	Fanconi anemia, complementation group F	DNA repair	- -	−1.47
FDXR	Ferrodoxin reductase	DNA damage, apoptosis	10.20	- -
IER5	Immediate early response 5	Apoptosis	1.86	- -
LIG1	Ligase I	DNA Repair	0.79	- -
MYC	v-myc myelocytomatosis viral oncogene homolog	Cell growth; apoptosis	−2.48	−2.88
PCNA	Proliferating cell nuclear antigen	DNA repair	2.41	2.60
PHLDA3	Pleckstrin homology-like domain, family A, member 3	Apoptosis	7.57	9.98
STAT5A	Signal transducer and activator of transcription 5A	Apoptosis	- -	−1.52
TNFRSF10D	Tumor necrosis factor receptor superfamily, member 10d	Apoptosis	1.75	- -
TRIAP1	TP53 regulated inhibitor of apoptosis 1	Apoptosis	2.34	2.88
XPC	Xeroderma pigmentosum, complementation group C	DNA repair	2.36	2.08

Significantly anti-correlated genes of DDR pathway in 2Gy PBL incubated for 24 h in 1 g or in MMG. Fold change (F.C.) is the mean of the expression values obtained from the transformed log2 (irradiated/non-irradiated) PBL (see Table S5 and Table S6). Genes in bold belong to p53-pathway; genes in italic belong to the GO category ''Response to DNA damage stimulus''.

doi:10.1371/journal.pone.0031293.t002

translation of the protein they encode. These authors propose that mRNAs could possess a regulatory role that relies on their ability to compete for miRNA binding, independently of their protein-coding function. Furthermore, it has been shown that miRNAs themselves are subjected to post-transcriptional regulation. Various proteins induce processing of specific pri-miRNAs into mature miRNAs by influencing the Drosha-dgcr8 complex, while other proteins block miRNAs maturation by binding to the pre-miRNA [91–93]. Thus, microgravity could affect post-transcriptional regulation of miRNAs. In addition, since miRNA biogenesis is globally induced upon DNA damage in an ATM-dependent manner and the loss of ATM abolishes miRNA induction after DNA damage [94], we suggest that ATM down-regulation in MMG could affect miRNA biogenesis in response to radio-induced DNA damage.

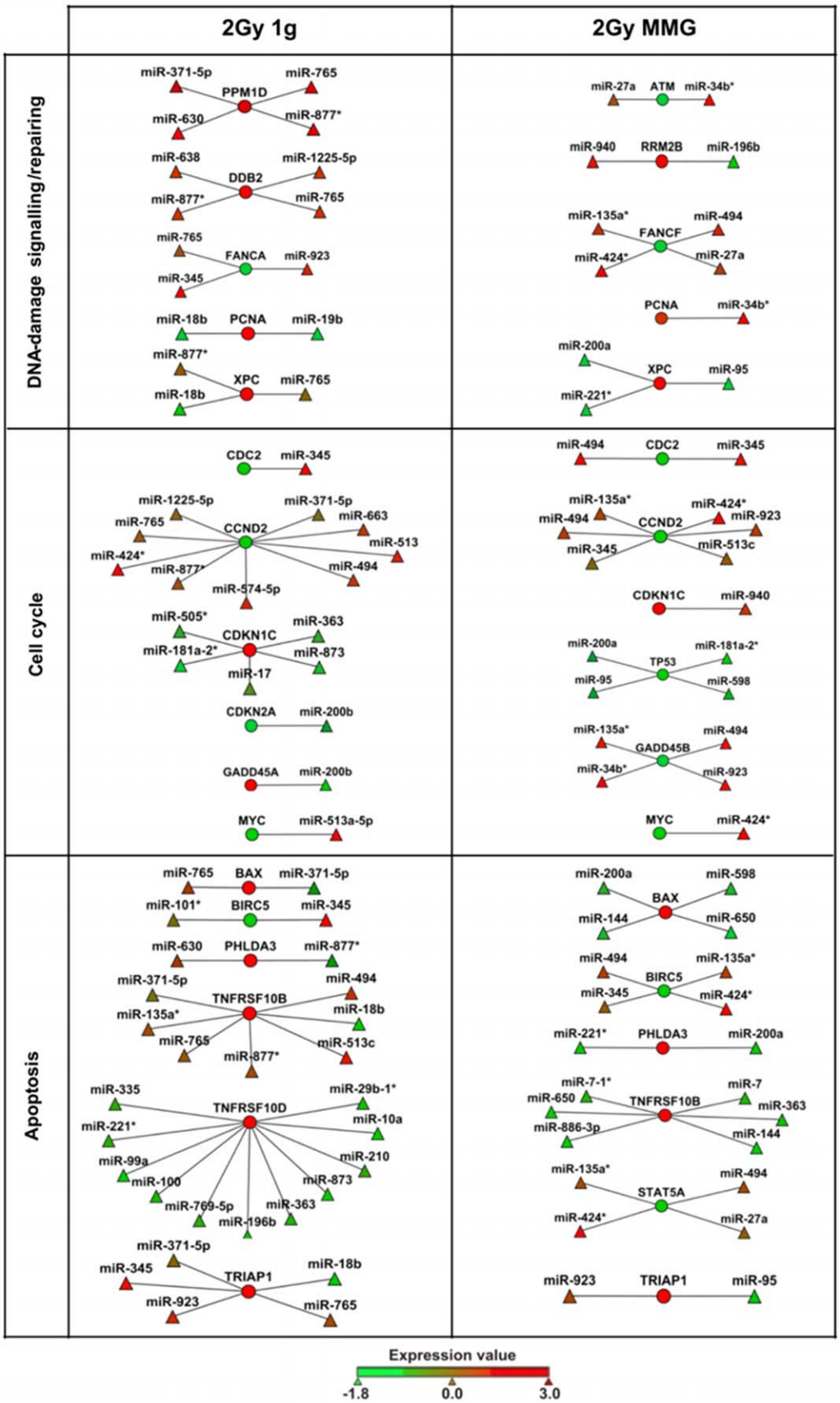

Figure 7. Visualization of functional miRNA-mRNA anti-correlation in the main pathways of DNA-damage response. Analyses were carried out in 2Gy-irradiated PBL incubated for 24 hours in gravity 1 g or in MMG. Circles represent transcripts and triangles miRNAs; the expression levels of each features are represented as color scale. The lists of significantly miRNA-mRNA anti-correlations are reported in Table S3 and Table S4.
doi:10.1371/journal.pone.0031293.g007

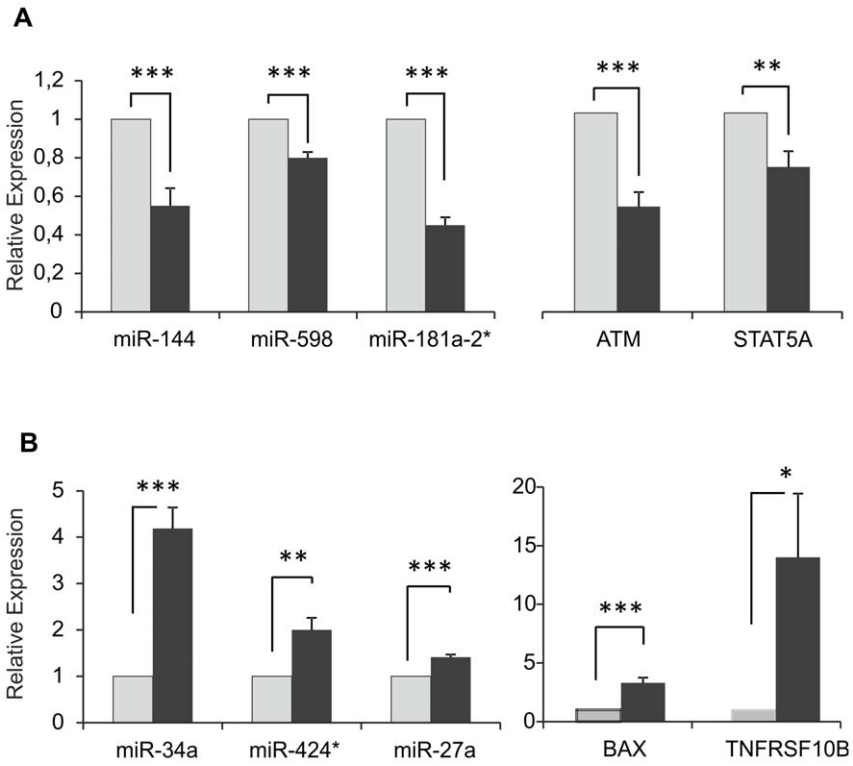

Figure 8. Microarray data validation by quantitative real-time PCR (qRT-PCR). Validation of microarray data by qRT-PCR in irradiated (2Gy) vs. non-irradiated PBL. A) Down-regulated miRNAs (miR-144, miR-598, miR-181a-2*) and mRNAs (ATM, STAT5A); B) Up-regulated miRNAs (miR-34a, miR-424*, miR-27a) and mRNAs (BAX, TNFRSF10B). Values (fold change, dark grey bars) are means ± S.E. of independent experiments performed in quadruplicate on PBL samples from 4–6 different donors. The value ''1'' of control PBL (light grey bars) is arbitrarly given when no change is observed (***$P<0.001$; **$P<0.01$, *$P<0.05$, *t*-test).
doi:10.1371/journal.pone.0031293.g008

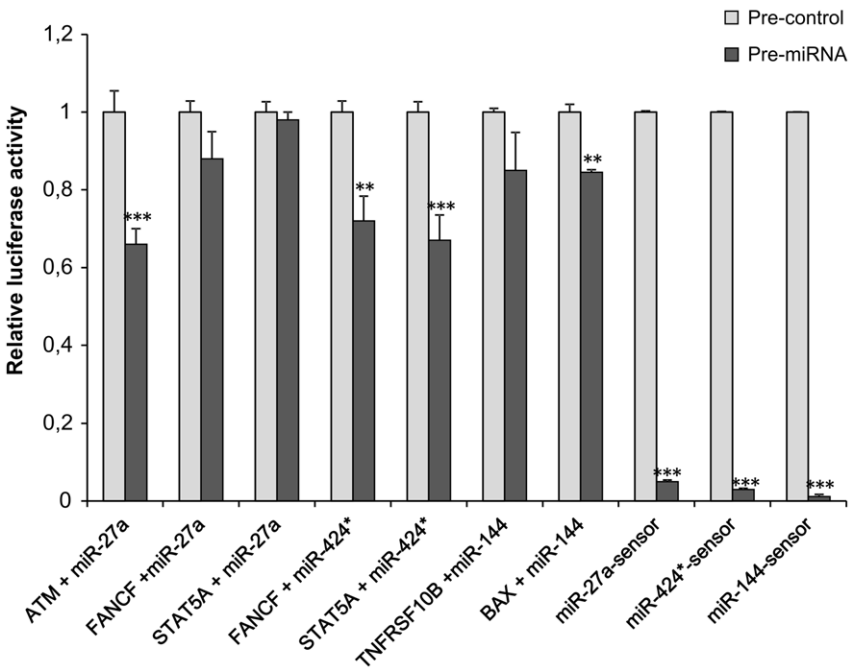

Figure 9. Luciferase reporter assay. Transient transfection analysis for luciferase expression in A549 cells co-transfected with pre-miRNA precursors (pre-miRNAs) miR-27a, miR-144, miR-424*, or pre-miRNA precursor-Negative Control (pre-control), and reporter constructs containing the 3′UTR of the indicated target genes or synthetic sequence including the perfect miR-27a, miR-144 and miR-424* binding site (sensors). Results are shown as mean ± S.D. of Firefly luciferase activity relative to controls, normalized on Renilla luciferase activity, from 3–4 independent experiments (***$P<0.001$, **$P<0.01$, *t*-test).
doi:10.1371/journal.pone.0031293.g009

In conclusion, the miRNA-mRNA changes observed in 2Gy PBL incubated in MMG conditions may translate into alterations of DDR pathway, at the DNA level and/or in the processing of IR-induced DNA damage, that could affect cell survival, mutation rate and apoptosis induction.

Supporting Information

Figure S1 Radio-responsive miRNAs common to 1 g and MMG, changed as a function of the time after irradiation. Heatmap of differentially expressed miRNAs at 4 and 24 h after irradiation with 0.2Gy (A) and 2Gy (B), common to 1 g- and MMG-incubated PBL. Range of expression value expressed as log2 (irradiated/non-irradiated) PBL is from −2.0 (green, down-regulation) to 2.0 (red, up-regulation).
(TIFF)

Figure S2 p53 regulatory pathway. Network diagram of KEGG p53 signaling pathway in human PBL incubated 24 h in 1 g (A) or in MMG (B) after irradiation with 2Gy. Over-expressed (red), under-expressed (dark green) and not significantly changed (light green) transcripts are shown. The identity and associated functions of each altered gene are given in Table 2 of the text.
(TIFF)

Table S1 miRNAs differentially expressed in 1 g-incubated PBL. This table lists differentially expressed miRNAs in human PBL at 4 and 24 h after irradiation with 0.2 and 2Gy and incubation in ground condition (1 g). The table includes miRNA ID and the expression value of each sample expressed as log2 (irradiated/non-irradiated) PBL.
(XLS)

Table S2 miRNAs differentially expressed in MMG-incubated PBL. This table lists differentially expressed miRNAs in human PBL at 4 and 24 h after irradiation with 0.2 and 2Gy and incubation in modeled microgravity (MMG). The table includes miRNA ID and the expression value of each sample expressed as log2 (irradiated/non-irradiated) PBL.
(XLS)

Table S3 Functional anti-correlations in 1 g. List of the most significant miRNA-mRNA relationships (Spearman index <-0.775) performed by MAGIA, in human PBL at 24 h after irradiation with 2Gy and incubation in 1 g. The table includes RefSeq ID, gene symbol, mRNA description, anti-correlated miRNA, Spearman correlation index, gene and miRNA expression levels of each putative anti-correlated pairs of miRNA and mRNA in the same sample.
(XLS)

Table S4 Functional anti-correlations in MMG. List of the most significant miRNA-mRNA relationships (Spearman index <-0.775) performed by MAGIA, in human PBL at 24 h after irradiation with 2Gy and incubation in modeled microgravity. The table includes RefSeq ID, gene symbol, mRNA description, anti-correlated miRNA, Spearman correlation index, gene and miRNA expression levels of each putative anti-correlated pairs of miRNA and mRNA in the same sample.
(XLS)

Acknowledgments

We gratefully acknowledge Dr. Vito Barbieri of the Department of Oncological and Surgical Sciences of Padova's University for cell irradiation and Dr. Chiara Romualdi for statistical assistance.

Author Contributions

Conceived and designed the experiments: MM CDP. Performed the experiments: CG CDP SC. Analyzed the data: CDP GS. Contributed reagents/materials/analysis tools: CDP GL LC MM. Wrote the paper: MM LC.

References

1. Ullrich O, Huber K, Lang K (2008) Signal transduction in cells of the immune system in microgravity. Cell Commun Signal 6: 9.
2. Crucian BE, Stowe RP, Pierson DL, Sams CF (2008) Immune system dysregulation following short- vs long-duration spaceflight. Aviat Space Environ Med 79: 835–43.
3. Fitts RH, Riley DR, Widrick JJ (2001) Functional and structural adaptations of skeletal muscle to microgravity. J Exp Biol 204: 3201–8.
4. Narici M, Kayser B, Barattini P, Cerretelli P (2003) Effects of 17-day spaceflight on electrically evoked torque and cross-sectional area of the human triceps surae. Eur J Appl Physiol 90: 275–82.
5. Trappe S, Costill D, Gallagher P, Creer A, Peters JR, et al. (2009) Exercise in space: human skeletal muscle after 6 months aboard the International Space Station. J Appl Physiol 106: 1159–68.
6. Baevsky RM, Baranov VM, Funtova II, Diedrich A, Pashenko AV, et al. (2007) Autonomic cardiovascular and respiratory control during prolonged spaceflights aboard the International Space Station. J Appl Physiol 103: 156–61.
7. Sibonga JD, Evans HJ, Sung HG, Spector ER, Lang TF, et al. (2007) Recovery of spaceflight-induced bone loss: bone mineral density after long-duration missions as fitted with an exponential function. Bone 41: 973–8.
8. Keyak JH, Koyama AK, LeBlanc A, Lu Y, Lang TF (2009) Reduction in proximal femoral strength due to long-duration spaceflight. Bone 44: 449–53.
9. Hammond TG, Benes E, O'Reilly KC, Wolf DA, Linnehan RM, et al. (2000) Mechanical culture conditions effect gene expression: gravity induced changes on the space shuttle. Physiol Genom 3(3): 163–173.
10. Lewis ML, Reynolds JL, Cubano LA, Hatton JP, Lawless BD, et al. (2001) cDNA microarray reveals altered cytoskeletal gene expression in space-flown leukemic T lymphocytes (Jurkat). FASEB J 18: 1783–1785.
11. George K, Wu H, Willingham V, Cucinotta FA (2001) The effect of space radiation on the induction of chromosome damage. Phys Med 17: 222–225.
12. Lewis ML, Reynolds JL, Cubano LA, Hatton JP, Lawless BD, et al. (1998) Spaceflight alters microtubules and increases apoptosis in human lymphocytes (Jurkat). The FASEB J 12: 1007–1018.
13. Grimm D, Bauer J, Kossmehl P, Shakibaei M, Schonberger J, et al. (2002) Simulated microgravity alters differentiation and increases apoptosis in human follicular thyroid carcinoma cells. The FASEB J 16: 604–606.
14. Maccarone M, Battista N, Meloni M, Bari M, Galleri G, et al. (2003) Creating conditions similar to those that occur during exposure of cells to microgravity induces apoptosis in human lymphocytes by 5-lipoxygenase-mediated mitochondrial uncoupling and cytochrome c release. Journal of Leukocyte Biology 73: 472–481.
15. Kang CY, Zou L, Yuan M, Wang Y, Li TZ, et al. (2011) Impact of simulated microgravity on microvascular endothelial cell apoptosis. Eur J Appl Physiol 111: 2131–8.
16. Kumari R, Singh KP, DuMond Jr. JW (2009) Simulated microgravity decreases DNA repair capacity and induces DNA damage in human lymphocytes. Journal of Cell Biochem 107: 723–731.
17. Crawford-Young SJ (2006) Effect of microgravity on cytoskeleton and embryogenesis. Int J Dev Biol 50: 183–91.
18. Infanger M, Kossmehl P, Shakibaei M, Baatout S, Witzing A, et al. (2006) Induction of three-dimensional assembly and increase in apoptosis of human endothelial cells by simulated microgravity: impact of vascular endothelial growth factor. Apoptosis 11: 749–64.
19. Clement JQ, Lacy SM, Wilson BL (2008) Gene expression profiling of human epidermal keratinocytes in simulated microgravity and recovery cultures. Genomics Proteomics Bioinformatics 6: 8–28.
20. Simons DM, Gardner EM, Lelkes PI (2010) Intact T cell receptor signaling by CD4(+) T cells cultured in the rotating wall-vessel bioreactor. J Cell Biochem 109: 1201–9.
21. Harper JW, Elledge SJ (2007) The DNA damage response: ten years after. Mol Cell 28(5): 739–45.
22. Bucker H, Facius R, Horneck G, Reitz G, Graul EH, et al. (1986) Embryogenesis and organogenesis of Carausius morosus under spaceflight conditions. Adv Space Res 6(12): 115–24.
23. Horneck G (1992) Radiobiological experiments in space: a review. Nucl Tracks Radiat Meas 20: 185–205.
24. Horneck G (1999) Impact of microgravity on radiobiological processes and efficiency of DNA repair. Mutation research 430: 221–228.
25. Mosesso P, Schuber M, Seibt D, Schmitz C, Fiore M, et al. (2001) X-ray-induced chromosome aberrations in human lymphocytes in vitro are potentiated under simulated microgravity conditions (Clinostat). Phys Med 17(1): 264–6.

26. Canova S, Fiorasi F, Mognato M, Grifalconi M, Reddi E, et al. (2005) Modeled microgravity affects cell response to ionizing radiation and increases genomic damage. Radiat Res 163(2): 191–9.
27. Pross HD, Casares A, Kiefer J (2000) Induction and repair of DNA double-strand breaks under irradiation and microgravity. Radiat Res 153(5 Pt 1): 521–5.
28. Manti L, Durante M, Cirrone GA, Grossi G, Lattuada M, et al. (2005) Modelled microgravity does not modify the yield of chromosome aberrations induced by high-energy protons in human lymphocytes. Int J Radiat Biol 81(2): 147–55.
29. Manti L (2006) Does reduced gravity alter cellular response to ionizing radiation? Radiat Environ Biophys 45(1): 1–8.
30. Horneck G, Rettberg P, Baumstark-Khan C, Rink H, Kozubek S, et al. (1996) Biotechnol 47(2–3): 99–112. DNA repair in microgravity: studies on bacteria and mammalian cells in the experiments REPAIR and KINETICS.
31. Horneck G, Rettberg P, Kozubek S, Baumstark-Khan C, Rink H, et al. (1997) The influence of microgravity on repair of radiation-induced DNA damage in bacteria and human fibroblasts. Radiat Res 147(3): 376–84.
32. Kiefer J, Pross HD (1999) Space radiation effects and microgravity. Mutation Research 430: 299–305.
33. Mognato M, Girardi C, Fabris S, Celotti L (2009) DNA repair in modeled microgravity: double strand break rejoining activity in human lymphocytes irradiated with gamma-rays. Mutat Res 663: 32–9.
34. Yatagai F, Honma M, Takahashi A, Omori K, Suzuki H, et al. (2011) Frozen human cells can record radiation damage accumulated during space flight: mutation induction and radioadaptation. Radiat Environ Biophys 50(1): 125–34.
35. Bartel DP (2009) MicroRNAs: target recognition and regulatory functions. Cell 136: 215–233.
36. Frankel LB, Christoffersen NR, Jacobsen A, Lindow M, Krogh A, et al. (2008) Programmed cell death 4 (PDCD4) is an important functional target of the microRNA miR-21 in breast cancer cells. J Biol Chem 283: 1026–33.
37. Poy MN, Spranger M, Stoffel M (2007) microRNAs and the regulation of glucose and lipid metabolism. Diabetes Obes Metab 9(Suppl 2): 67–73.
38. Stern-Ginossar N, Elefant N, Zimmermann A, Wolf DG, Saleh N, et al. (2007) Host immune system gene targeting by a viral miRNA. Science 317: 376–81.
39. Voorhoeve PM, le Sage C, Schrier M, Gillis AJ, Stoop H, et al. (2006) A genetic screen implicates miRNA-372 and miRNA-373 as oncogenes in testicular germ cell tumors. Cell 124: 1169–81.
40. Wiemer EA (2007) The role of microRNAs in cancer: no small matter. Eur J Cancer 43: 1529–44.
41. Cho WC (2007) OncomiRs: the discovery and progress of microRNAs in cancers. Eur J Cancer 43: 1529–44.
42. Mi S, Lu J, Sun M, Li Z, Zhang H, et al. (2007) MicroRNA expression signatures accurately discriminate acute lymphoblastic leukemia from acute myeloid leukemia. Proc Natl Acad Sci U S A 104: 19971–6.
43. Hammond SM (2007) microRNAs as tumor suppressors. Nat Genet 39: 582–3.
44. Marsit CJ, Eddy K, Kelsey KT (2006) MicroRNA responses to cellular stress. Cancer Res 66: 10843–8.
45. Weidhaas JB, Babar I, Nallur SM, Trang P, Roush S, et al. (2007) MicroRNAs as potential agents to alter resistance to cytotoxic anticancer therapy. Cancer Res 67: 11111–6.
46. Maes OC, An J, Sarojini H, Wu H, Wang E (2008) Changes in MicroRNA expression patterns in human fibroblasts after low-LET radiation. J Cell Biochem 105: 824–34.
47. Chaudhry MA (2009) Real-time PCR analysis of micro-RNA expression in ionizing radiation-treated cells. Cancer Biother Radiopharm 24: 49–56.
48. Kato M, Paranjape T, Müller RU, Nallur S, Gillespie E, et al. (2009) The mir-34 microRNA is required for the DNA damage response in vivo in C. elegans and in vitro in human breast cancer cells. Oncogene 28: 2419–2424.
49. Simone NL, Soule BP, Ly D, Saleh AD, Savage JE, et al. (2009) Ionizing radiation-induced oxidative stress alters miRNA expression. PLoS One 4: e6377.
50. He L, He X, Lowe SW, Hannon GJ (2007) microRNAs join the p53 network–another piece in the tumour-suppression puzzle. Nat Rev Cancer 7(11): 819–22.
51. Suzuki HI, Yamagata K, Sugimoto K, Iwamoto T, Kato S, et al. (2009) Modulation of microRNA processing by p53. Nature 460: 529–33.
52. Pothof J, Verkaik NS, van IJcken W, Wiemer EA, Ta VT, et al. (2009) MicroRNA-mediated gene silencing modulates the UV-induced DNA-damage response. EMBO J 28: 2090–9.
53. Crosby ME, Kulshreshtha R, Ivan M, Glazer PM (2009) MicroRNA regulation of DNA repair gene expression in hypoxic stress. Cancer Research 69: 1221–1229.
54. Mognato M, Celotti L (2005) Modeled microgravity affects cell survival and HPRT mutant frequency, but not the expression of DNA repair genes in human lymphocytes irradiated with ionising radiation. Mutat Res 578: 417–29.
55. Wang H, Ach RA, Curry B (2007) Direct and sensitive miRNA profiling from low-input total RNA. RNA 13: 151–159.
56. Bolstad BM, Irizarry RA, Astrand M, Speed TP (2003) A comparison of normalization methods for high density oligonucleotide array data based on variance and bias. Bioinformatics 19: 185–93.
57. Saeed AI, Bhagabati NK, Braisted JC, Liang W, Sharov V, et al. (2006) TM4 Microarray Software Suite. Methods Enzymol 411: 134–93.
58. Tusher VG, Tibshirani R, Chu G (2001) Diagnosis of multiple cancer types by shrunken centroids of gene expression. Proc Natl Acad Sci U S A 98: 5116–121.
59. Kertesz M, Iovino N, Unnerstall U, Gaul U, Segal E (2007) The role of site accessibility in microRNA target recognition. Nat Genet 39: 1278–84.
60. Sales G, Coppe A, Bisognin A, Biasiolo M, Bortoluzzi S, et al. (2010) MAGIA, a web-based tool for MiRNA and Genes Integrated Analysis. Nucleic Acid Research 38 Suppl: W352–9.
61. Xin F, Li M, Balch C, Thomson M, Fan M, et al. (2009) Computational analysis of microRNA profiles and their target genes suggests significant involvement in breast cancer antiestrogen resistance. Bioinformatics 25: 430–434.
62. Wang H, Li WH (2009) Increasing MicroRNA target prediction confidence by the relative R(2) method. J Theor Biol 259: 793–8.
63. Huang DW, Sherman BT, Lempicki R (2009) Systematic and integrative analysis of large gene lists using DAVID bioinformatics resources. Nature Protocols 4: 44–57.
64. Cline MS, Smoot M, Cerami E, Kuchinsky A, Landys N, et al. (2007) Integration of biological networks and gene expression data using Cytoscape. Nat Protoc 2: 2366–82.
65. Livak KJ, Schmittgen TD (2001) Analysis of relative gene expression data using real-time quantitative PCR and the 2(-Delta Delta C(T)). Method Methods 25: 402–8.
66. Amundson SA, Do KT, Shahab S, Bittner M, Meltzer P, et al. (2000) Identification of potential mRNA biomarkers in peripheral blood lymphocytes for human exposure to ionizing radiation. Radiat Res 154(3): 342–6.
67. Paul S, Amundson SA (2008) Development of gene expression signatures for practical radiation biodosimetry. Int J Radiat Biol Phys 71(4): 1236–1244.
68. Cha HJ, Shin S, Yoo H, Lee EM, Bae S, et al. (2009) Identification of ionizing radiation-responsive microRNAs in the IM9 human B lymphoblastic cell line. Int J Oncol 34: 1661–8.
69. Vincenti S, Brillante N, Lanza V, Bozzoni I, Presutti C, et al. (2011) HUVEC respond to radiation by inducing the expression of pro-angiogenic microRNAs. Radiat Res 175(5): 535–546.
70. Maes OC, Sarojini H, Wang E (2009) Stepwise up-regulation of microRNA expression levels from replicating to reversible and irreversible growth arrest states in WI-38 human fibroblasts. J Cell Physiol 221: 109–19.
71. Shin S, Cha HJ, Lee EM, Lee SJ, Seo SK, et al. (2009) Alteration of miRNA profiles by ionizing radiation in A549 human non-small cell lung cancer cells. Int J Oncol 35: 81–6.
72. Josson S, Sung SY, Lao K, Chung LW, Johnstone PA (2008) Radiation modulation of microRNA in prostate cancer cell lines. Prostate 68: 1599–606.
73. Galluzzi L, Morselli E, Vitale I, Kepp O, Senovilla L, et al. (2010) miR-181a and miR-630 regulate cisplatin-induced cancer cell death. Cancer Res 70: 1793–803.
74. Vogelstein B, Lane D, Levine AJ (2000) Surfing the p53 network. Nature 408: 307–10.
75. Vousden KH, Lu X (2002) Live or let die: the cell's response to p53. Nat Rev Cancer 2: 594–604.
76. Sengupta S, Harris CC (2005) p53: traffic cop at the crossroads of DNA repair and recombination. Nat Rev Mol Cell Biol 6: 44–55.
77. Chipuk JE, Kuwana T, Bouchier-Hayes L, Droin NM, Newmeyer DD, et al. (2004) Direct activation of Bax by p53 mediates mitochondrial membrane permeabilization and apoptosis. Science 303: 1010–4.
78. Guttilla IK, White BA (2009) Coordinate regulation of FOXO1 by miR-27a, miR-96, and miR-182 in breast cancer cells. J Biol Chem 284: 23204–23216.
79. Chintharlapalli S, Papineni S, Abdelrahim M, Abudayyeh A, Jutooru I, et al. (2009) Oncogenic microRNA-27a is a target for anticancer agent methyl 2-cyano-3,11-dioxo-18beta-olean-1,12-dien-30-oate in colon cancer cells. Int J Cancer 125(8): 1965–74.
80. Liu R, Zhang C, Hu Z, Li G, Wang C, et al. (2011) A five-microRNA signature identified from genome-wide serum microRNA expression profiling serves as a fingerprint for gastric cancer diagnosis. Eur J Cancer 47(5): 784–91.
81. Ma Y, Yu S, Zhao W, Lu Z, Chen J (2010) miR-27a regulates the growth, colony formation and migration of pancreatic cancer cells by targeting Sprouty2. Cancer Lett 298(2): 150–8.
82. Chhabra R, Adlakha YK, Hariharan M, Scaria V, Saini N (2009) Upregulation of miR-23a-27a-24–2 cluster induces caspase-dependent and -independent apoptosis in human embryonic kidney cells. PLoS One 4: e5848.
83. Lal A, Pan Y, Navarro F, Dykxhoorn DM, Moreau L, et al. (2009) miR-24-mediated downregulation of H2AX suppresses DNA repair in terminally differentiated blood cells. Nat Struct Mol Biol 16: 492–8.
84. Fernandez-Capetillo O, Lee A, Nussenzweig M, Nussenzweig A (2004) H2AX: the histone guardian of the genome. DNA Repair 3: 959–67.
85. Moon SH, Lin L, Zhang X, Nguyen TA, Darlington Y, et al. (2010) Wild-type p53-induced phosphatase 1 dephosphorylates histone variant gamma-H2AX and suppresses DNA double strand break repair. J Biol Chem 285: 12935–47.
86. Wu S, Huang S, Ding J, Zhao Y, Liang L, et al. (2010) Multiple microRNAs modulate p21Cip1/Waf1 expression by directly targeting its 3′ untranslated region. Oncogene 29: 2302–8.
87. Vo NK, Dalton RP, Liu N, Olson EN, Goodman RH (2010) Affinity purification of microRNA-133a with the cardiac transcription factor, Hand2. Proc Natl Acad Sci USA 107: 19231–19236.
88. Krek A, Grün D, Poy MN, Wolf R, Rosenberg L, et al. (2005) Combinatorial microRNA target predictions. Nat Genet 37: 495–500.
89. Lewis BP, Burge CB, Bartel DP (2005) Conserved seed pairing, often flanked by adenosines, indicates that thousands of human genes are microRNA targets. Cell 120: 15–20.
90. Poliseno L, Salmena L, Zhang J, Carver B, Haveman WJ, et al. (2010) A coding-independent function of gene and pseudogene mRNAs regulates tumour biology. Nature 465(7301): 1033–8.

91. Trabucchi M, Briata P, Filipowicz W, Rosenfeld MG, Ramos A, et al. (2009) How to control miRNA maturation? RNA Biol 6(5): 536–40.
92. Katoh T, Sakaguchi Y, Miyauchi K, Suzuki T, Kashiwabara S, et al. (2009) Selective stabilization of mammalian microRNAs by 3′ adenylation mediated by the cytoplasmic poly(A) polymerase GLD-2. Genes Dev 23(4): 433–8.
93. Heo I, Joo C, Cho J, Ha M, Han J, et al. (2008) Lin28 mediates the terminal uridylation of let-7 precursor MicroRNA. Mol Cell 32(2): 276–84.
94. Zhang X, Wan G, Berger FG, He X, Lu X (2011) The ATM kinase induces microRNA biogenesis in the DNA damage response. Mol Cell 41(4): 371–83.

The American Journal of Pathology, Vol. 179, No. 5, November 2011

DOI: 10.1016/j.ajpath.2011.07.018

Tumorigenesis and Neoplastic Progression

High IGFBP2 Expression Correlates with Tumor Severity in Pediatric Rhabdomyosarcoma

Lucia Tombolan,* Francesca Orso,[†‡§] Vincenza Guzzardo,[¶] Silvia Casara,* Angelica Zin,[‖] Massimo Bonora,** Chiara Romualdi,* Carlotta Giorgi,** Gianni Bisogno,[‖] Rita Alaggio,[¶] Paolo Pinton,** Cristiano De Pittà,* Daniela Taverna,[†‡§] Angelo Rosolen,[‖] and Gerolamo Lanfranchi*

From the Department of Biology and the Interdepartmental Research Center in Innovative Biotechnology (CRIBI), and the Departments of Medical and Diagnostic Sciences and Special Therapies,[¶] and Paediatric Hematology and Oncology,[‖] Padova Hospital, University of Padova, Padova; the Department of Oncological Sciences,[†] the Molecular Biotechnology Center,[‡] and the Center for Complex Systems in Molecular Biology and Medicine,[§] University of Torino, Torino; and the Department of Experimental and Diagnostic Medicine,** the Section of General Pathology, Interdisciplinary Center for the Study of Inflammation, Laboratory for Technologies of Advanced Therapies, University of Ferrara, Ferrara, Italy*

Rhabdomyosarcoma (RMS) is the most common childhood sarcoma and is identified as either the embryonal or alveolar (ARMS) subtype. In approximately 75% of cases, ARMSs are characterized by specific chromosomal translocations that involve *PAX* and *FKHR* genes. ARMS gene expression signatures vary, depending on the presence or absence of the translocations. Insulin-like growth factor–binding protein 2 (IGFBP2) is strongly overexpressed in translocation-negative RMS. Because IGFBP2 is associated with tumorigenesis, we investigated its functional role in RMS. An analysis of IGFBP2 distribution in RMS cell lines revealed a strong accumulation in the Golgi complex, in which morphological characteristics appeared peculiarly modified. After silencing IGFBP2 expression, our microarray analysis revealed mostly cell cycle and actin cytoskeleton gene modulations. In parallel, IGFBP2-silenced cells showed reduced cell cycle and rates of invasion and decreased seeding in the lungs after tail vein injections in immunodeficient mice. An analysis of IGFBP2 mRNA and protein localization in human tumors showed abnormal protein accumulation in the Golgi complex, mostly in *PAX/FKHR*-negative RMS. Moreover, an analysis of patients with RMS revealed the presence of conspicuous circulating levels of IGFBP2 proteins in children with highly aggressive RMS tumors. Taken together, our data provide evidence that IGFBP2 contributes to tumor progression and that it could be used as a marker to better classify clinical and biological risks in RMS. ***(Am J Pathol 2011, 179:2611–2624; DOI: 10.1016/j.ajpath.2011.07.018)***

Insulin-like growth factor–binding proteins (IGFBPs) are a family of six serum proteins that bind IGFs, thus modulating the availability and interactions of these growth factors with their receptors. The 36-kDa IGFBP2 is the second most abundant IGF-binding protein, being highly expressed in the fetus and in several tissues and biological fluids of the adult.[1] Both stimulatory and inhibitory effects of IGFBP2 on IGF signaling have been reported, but its biological pathways and mechanisms have not been fully elucidated. IGFBP2 binds extracellular matrix proteins, most likely via its heparin-binding domain or its distinctive integrin-interaction arg-gly-asp motif.[2] The association of IGFBP2 with cell surface probably modulates cell function in two ways: by affecting the bioavailability of IGFs in the pericellular space, thereby regulating receptor targeting of IGFs, and by a direct IGF-independent action on cell signaling pathways.[3,4]

Supported by grants from the Italian Association for Cancer Research (AIRC) (2008/6014; 2010-IG 10476 to P.P.; 2010-IG 10104 to D.T.); Fondazione Città della Speranza ONLUS, Padova, Italy; a grant from Fondazione Telethon (GGP09128); Compagnia di San Paolo (D.T.); and a grant from FIRB giovani 2008 (RBFR08F2FS-002 to F.O.). Lucia Tombolan is a PostDoc Fellow of the University of Padova.

Accepted for publication July 26, 2011.

Supplemental material for this article can be found at *http://ajp.amjpathol.org* or at doi: 10.1016/j.ajpath.2011.07.018.

Address reprint requests to Gerolamo Lanfranchi, M.S., Department of Biology and Interdepartmental Research Center in Innovative Biotechnology (CRIBI), University of Padova, Via Ugo Bassi 58/b, 35151 Padova, Italy; or Angelo Rosolen, M.D., Department of Paediatric Hematology and Oncology, Padova Hospital, University of Padova, Via Giustiniani 3, 35128 Padua, Italy. E-mail: gerolamo.lanfranchi@unipd.it or angelo.rosolen@unipd.it.

Although the effects of IGFBP2 vary depending on cell model, this protein is involved in several important cellular processes, such as proliferation, cell migration, and adhesion, all of which play key roles in cancer establishment and progression.

Overexpression of IGFBP2 in neuroblastoma cells and its interaction with components of the pericellular and extracellular matrices result in local sequestration of IGF1 and then in a dramatic enhancement of cell proliferation.[5] In contrast, the interaction of IGFBP2 with integrin $\alpha5\beta1$ produces an antiproliferative effect.[4] Pereira et al[6] proposed that the interaction between $\alpha v\beta3$ integrin and IGFBP2 negatively modulates IGF-mediated cellular migration responses.

The involvement of IGFBP2 in cell migration and adhesion has been extensively studied in human gliomas because consistent IGFBP2 overexpression was discovered in this malignancy.[7] Signatures of glioma cell lines stably expressing *IGFBP2* were compared with parental cells revealing an increased expression of several invasion-related genes, including matrix metalloproteinase (MMP) 2.[8,9] An independent study[10] by which the *IGFBP2* gene was inactivated in two glioma cell lines indicated that the surface glycoprotein CD24 acted as a candidate downstream target of IGFBP2, promoting invasiveness. Furthermore, IGFBP2 directly interacts with IIp45, an intracellular molecule that appears to antagonize the IGFBP2-induced invasiveness of glioblastoma cells.[11] Recent studies[12,13] also suggested an inverse correlation between *IGFBP2* and tumor suppressor genes, such as *PTEN* and *p16/INK4*, whose loss of function is frequently observed in human cancer. *PTEN* induces the decrease of IGFBP2 expression, and this effect is mediated by phosphorylation of Akt.[14]

Overall, elevated expression of IGFBP2 has been reported in a variety of tumors, such as glioma,[15] prostate cancer,[16] ovarian cancer,[17] breast cancer,[18–20] and sarcoma.[21,22] In many instances, its expression correlates with grade of malignancy. Taken together, these findings suggest that IGFBP2 may participate in the regulation of tumor growth and invasion.

Rhabdomyosarcoma (RMS) is the most common soft tissue sarcoma of childhood, divided into two major histological subtypes: alveolar RMS (ARMS) and embryonal RMS (ERMS). ARMS shows a dismal prognosis, significantly worse than ERMS.[23] However, it is not known why ARMSs have a greater aggressiveness and metastatic potential than ERMSs. Cytogenetic and molecular analyses have demonstrated that ARMSs frequently harbor the reciprocal chromosomal translocation t(2;13) in which *PAX3* and *FKHR* genes are juxtaposed and, albeit less commonly, the variant translocation t(1;13).[24] There is also some evidence that *PAX3/FKHR*-positive ARMSs have a worse prognosis than the *PAX3/FKHR*-negative counterpart.[25,26]

Knock-in mouse experiments demonstrated that the expression of PAX3/FKHR fusion protein was not able to generate histologically and immunohistochemically (IHC) genuine ARMS at a high frequency, suggesting that PAX3/FKHR protein is necessary, but not sufficient, for tumor initiation.[27] Moreover, expression profiling studies[28,29] have shown that the *PAX/FKHR* gene confers to ARMS an expression signature that is distinct from translocation-negative ARMS and from ERMS. In whole, these findings would suggest that ARMS differs from ERMS and, despite the almost identical morphological appearance, that ARMS is not a single biological, and possibly clinical, entity.

We performed an expression study[29] on RMS, identifying a series of genes that were differentially expressed in *PAX3/FKHR*-positive versus *PAX3/FKHR*-negative ARMS. From a detailed analysis of these genes, *IGFBP2* emerged as one of the most interesting overexpressed genes in *PAX/FKHR*-negative ARMS compared with *PAX/FKHR*-positive ARMS. Most RMS studies[30] have focused on the consequences of the PAX/FKHR fusion protein in the activation of a myogenic program, transformation, or cellular growth, but it is unclear which signaling pathways are altered in *PAX/FKHR*-negative RMS. In the present study, we focused on the role of *IGFBP2* as a distinctive overexpressed gene in ARMS and *PAX/FKHR*-negative ERMS. From *in vitro* and *in vivo* experiments using RMS cell lines, we demonstrated the positive role of IGFBP2 in cell cycle progression and invasiveness. A study on a cohort of patients with RMS suggests that IGFBP2 could be used as an IHC marker to distinguish between *PAX/FKHR*-positive and *PAX/FKHR*-negative RMS and as a plasma marker with potential prognostic impact in patients with RMS.

Materials and Methods

Cell Culture

Human ARMS cells (RH4, RH28, RH30, and RH18), human ERMS cells (RD, RH36, and SMS-CTR), and mouse C2C12 myoblast cells were maintained in Dulbecco's modified Eagle's medium containing 10% fetal calf serum, penicillin (100 U/mL), and streptomycin (100 μg/mL) (Invitrogen Life Technologies, Carlsbad, CA) at 37°C in 5% CO_2 in a humidified incubator.

The human RMS cell lines RH30 and RD and C2C12 control cells were obtained from American Type Culture Collection (Manassas, VA); RH4 and RH18 were a gift from Dr. Peter J. Houghton (St Jude Children's Hospital, Memphis, TN); and SMS-CTR, RH36, CCA were obtained from Dr. Maria Tsokos (National Cancer Institute, Bethesda, MD).

Tumor Samples

Selected clinical parameters of patients with RMS used for this analysis are available (see Supplemental Tables S1 and S2 at *http://ajp.amjpathol.org*).

RNA Interference

RH36 cells at 50% to 70% confluence were transfected with SMARTpool small-interfering RNA (siRNA) for target gene *IGFBP2* (siIGFBP2) or with nontargeting siRNA pool (siCONTROL) using Dharmafect 3 transfection reagent

(Dharmacon; Thermo Scientific, Lafayette, CO). We performed preliminary experiments to achieve the highest efficiency and reproducibility. The efficacy of gene knockdown was evaluated at the mRNA or protein level by using RT-PCR and Western blot analysis after 48 hours.

Real-Time RT-qPCR

Total RNA was isolated using the TRIzol reagent (Invitrogen Life Technologies) and reverse transcribed using Super-Script II (Invitrogen Life Technologies), according to the manufacturer's instructions. Each total RNA sample was analyzed for quality control by capillary electrophoresis using the RNA 6000 Nano LabChip and the Agilent Bioanalyzer 2100 (Agilent Technologies, Palo Alto, CA). An aliquot of first-strand cDNA was PCR amplified using SYBR Green chemistry (Finnzymes, Espoo, Finland). Quantitative RT-PCR (RT-qPCR) was performed in the Applied Biosystems SDS-7500 thermal cycler (Applied Biosystems, Life Technologies, Foster City, CA). Gene-specific primers were designed using Primer3 software (*http://frodo.wi.mit.edu/primer3*, last accessed July 20, 2008) or Application Design Tools (Roche Applied Science, Monza, Italy). The sequences used are as follows: IGFBP2, 5′-ACTCCCTGCCAACAGGAAC-3′ (forward) and 5′-GTTGGGGTTCACACACCAG-3′ (reverse); glyceraldehyde-3-phosphate dehydrogenase (GADH), 5′-TCCTCTGACTTCAACAGCGA-3′ (forward) and 5′-GGGTCTTACTCCTTGGAGGC-3′ (reverse); and guanine nucleotidebinding protein, beta-peptide 2-like 1 (GNB2L1), 5′-GGGTCTTACTCCTTGGAGGC 3′ (forward) and 5′-GCTTGCAGTTAGCCAGGTTC-3′ (reverse).

By using SYBR Green chemistry, we performed the dissociation curve to confirm the specificity of the amplicon. Cycling parameters consisted of an initial denaturation step at 95°C for 15 minutes; followed by 40 cycles of denaturation at 95°C for 25 seconds, annealing, and elongation steps at 59°C for 1 minute; and a final elongation step at 72°C for 3 minutes. To evaluate differences in gene expression, we chose a relative quantification method in which the expression of target gene is standardized by one or two nonregulated reference genes (ie, *GADPH* or *GNB2L1*). The mathematical method presented by Pfaffl,[31] which calculates the efficiency of each PCR using a standard curve, was applied. To calculate the relative expression ratio, we used the $\Delta\Delta C_T$ method implemented in the software of the Applied Biosystems thermal cycler.[32]

Gene Expression Experiments

Control RNA pool and RNA samples obtained from three different silencing experiments were linearly amplified with the MessageAmp amplified RNA (aRNA) amplification kit (Ambion, Austin, TX), labeled with Cy3 and Cy5 dye (Amersham Biosciences, Chandler, AZ) and competitively hybridized to oligonucleotide microarray platforms (GeneExpression Omnibus ID: GPL2136). For each sample, we performed at least two microarray experiments. Array fluorescence was quantified with ScanArray Express software (PerkinElmer Inc, Wellesley, MA), and data were normalized with MIDAS tool.[33] All experiments were analyzed by the SAM program,[34] implemented in tMEV software.[35] The list of differentially expressed genes was functionally classified using Gene Ontology (GO) criteria, as implemented in DAVID.[36] The data discussed in this publication have been deposited in the National Center for Biotechnology Information's GeneExpression Omnibus[37] database (*http://www.ncbi.nlm.nih.gov/geo*, last accessed July 27, 2010) and are accessible through accession number GSE23196.

Western Blot Analysis

Cells cultured under desired conditions were lysed in buffer (50 mmol/L Tris-HCl, pH 7.5; 150 mmol/L sodium chloride; 2 mmol/L EDTA; 1% Triton; 0.5% sodium deoxycholate; and 0.1% SDS) containing protease inhibitors (Sigma-Aldrich, St Louis, MO). Lysates were incubated on ice and centrifuged for 30 minutes at 13,000 $\times$ *g*, and supernatants were removed and stored at 20°C until use. Conditioned medium for analysis of secreted proteins was concentrated using a Centricon filter (Millipore, Billerica, MA). Equal amounts of secreted or whole-lysate proteins (30 μg of protein per lane) were separated by 4% to 12% SDS-PAGE (Invitrogen Life Technologies) and transferred to nitrocellulose membranes (Amersham Biosciences). Membranes were blocked for 1 hour at room temperature with 3% nonfat milk in PBS and then incubated with diluted goat polyclonal anti-IGFBP2 (1:1000, C-18; Santa Cruz Biotechnology, Santa Cruz, CA) or with anti-β-actin (1:3000; Sigma-Aldrich) in PBS containing 0.1% (v/v) Tween 20 overnight at 4°C. After washing three times for 5 minutes each with PBS containing 0.1% (v/v) Tween 20 at room temperature, membranes were incubated at room temperature for 1 hour with a diluted peroxidase-labeled secondary antibody. The membranes were then washed three times for 5 minutes with PBS containing 0.1% (v/v) Tween 20 at room temperature, and immunopositive signals were visualized using an enhanced chemiluminescence detection kit (Cyanagen, Bologna, Italy). The protein levels were quantified using Quantity One software (ChemiDoc-Bio-Rad, Hercules, CA). The control sample was set to one, and all RMS cell results were related to this value. β-Actin was used as an internal reference for data normalization.

Immunofluorescence Assays

Cells cultured on glass coverslips in six-well dishes were washed in PBS, fixed with 4% paraformaldehyde, and permeabilized in 50 mmol/L NH_4Cl and 0.2% Triton X-100 in PBS. After fixation, the cells were blocked with 1% bovine serum albumin in PBS for 30 minutes at room temperature. Cells were incubated with primary antibodies (IGFBP2, 1:50, and GM130, 1:500; BD Biosciences, San Jose, CA), diluted in 1% bovine serum albumin in PBS for 1 hour in a humidified incubator at 37°C. After washing with PBS, cells were incubated for 30 minutes in a dark chamber with the corresponding secondary goat fluorochrome-conjugated antibodies. Alexa Fluor 488 (green) or 568 (red) secondary antibodies were obtained

from Invitrogen (Life Technologies). Subsequently, the slides were washed three times with PBS, and cell nuclei were counterstained with DAPI mounted with gel Mount Aqueous Mounting medium (Sigma-Aldrich) and examined using an ×40 or ×63 objective of a Leica 5000B microscope (Leica Microsystems, Newcastle upon Tyne, UK). Controls with no or only one primary antibody or both secondary antibodies alone or in combination were used to exclude nonspecific background staining. In case of treatment with brefeldin A (BFA) before fixation for staining, the culture medium was replaced with serum-free medium containing BFA (Sigma-Aldrich) to a final concentration of 10 μg/mL, and the cells were cultured for 1 hour.

Aequorin Measurements

All measurements were performed as previously described.[38] Briefly, for reconstituting with high efficiency the aequorin chimera targeted to the Golgi apparatus (GoAEQ), the luminal Ca^{2+} concentration of this compartment must be reduced first. This was achieved by incubating cells for 1 hour at 4°C in Krebs-Ringer buffer (125 mmol/L NaCl, 5 mmol/L KCl, 1 mmol/L Na_3PO_4, 1 mmol/L $MgSO_4$, 5.5 mmol/L glucose, 20 mmol/L HEPES, pH 7.4, at 37°C) supplemented with 5 μmol/L coelenterazine, 5 μmol/L Ca^{2+} ionophore ionomycin, and 600 μmol/L EGTA. After this incubation, cells were extensively washed with Krebs-Ringer buffer supplemented with 2% bovine serum albumin and then a 13-mm round coverslip with the transfected cells was placed in a perfused thermostatic chamber placed in close proximity to a low-noise photomultiplier, with a built-in amplifier-discriminator. The output of the discriminator was captured by a Thorn-EMI photon counting board (Torn-EMI Ltd, Hayes, Middlesex, UK) and stored in a computer for further analyses. When the EGTA of the perfusion buffer was replaced with 1 mmol/L $CaCl_2$, Ca^{2+} concentration Golgi rapidly increased. Then, the addition of ATP, an agonist coupled to inositol 1,4,5-trisphosphate production, caused a rapid and extensive decrease in the Golgi Ca^{2+} concentration.

The aequorin luminescence data were calibrated off-line into Ca^{2+} concentration values, using a computer algorithm based on the Ca^{2+} response curve of wild-type and mutant aequorins, as previously described.[39]

VSVG Imaging

C2C12, RH30, and RH36 cells were seeded on 25-mm coverslips previously coated with 0.01% poly-D-lysine (for 1 hour at 37°C). At 48 hours after plating, cells were transfected with the temperature-sensitive variant of the G protein of vesicular stomatitis virus (VSVG), tagged with green fluorescent protein (GFP; provided from Dr. Jennifer Lippincott-Schwartz, NIH, Bethesda, MD) using Lipofectamine 2000 (Invitrogen Life Technologies). In detail, a Lipofectamine-DNA mix was prepared in Optimem (Invitrogen Life Technologies) with a ratio of 8 μL/1 μg. After 30 minutes, the mixture was placed on cells growing in Dulbecco's modified Eagle's medium plus 10% fetal bovine serum. At 48 hours after transfection, the cells were shifted to 15°C for 3 hours to accumulate cargoes in the intermediate compartments. Then, cargoes were released to proceed into the Golgi complex by shifting the temperature back to 37°C. Cells were then imaged with Nikon Swept Field Confocal equipped with CFI Plan Apo VC60XH objective (numerical aperture, 1.4) (Nikon Instruments, Melville, NY) and an Andor DU885 electron multiplying charge-coupled device (EM-CCD) camera (Andor Technology Ltd, Belfast, Northern Ireland). Coverslips were placed in an incubated chamber with a controlled temperature, CO_2, and humidity; then, z-stacks were acquired by 21 planes with a 0.6-μm distance, to allow acquisition of the whole cell. Intensity measurements and three-dimensional rendering were obtained by using open source software Fiji (*http://fiji.sc/wiki/index.php/Fiji*, last accessed June 20, 2011). In detail, membrane regions were obtained by generating a threshold-based mask of the whole cell; then, with the edge detection and dilated functions, a region for measuring the membrane signal was obtained. A higher threshold was used to detect Golgi aggregates (because of the distribution of the signal) and vesicles with VSVG-GFP localization. Golgi aggregates were then filtered from vesicles using the analyzed particle function; objects <100 pixels^2 were excluded.

Electron Microscopy

C2C12 and RMS cells were grown to 70% confluence. After washing with PBS, cells were fixed with 4% paraformaldehyde in PBS for 1 hour, embedded in 12% gelatin, infiltrated with 2.3 mol/L sucrose, and then frozen in liquid nitrogen. Ultrathin cryosections were obtained with Leica Ultracut UCT microtome, with a Leica EM FCS cryoattachment and collected on copper-formavar carbon-coated grids (Leica Microsystems). Double-immunogold labeling was performed as previously described.[40] Briefly, the sections were incubated with goat anti-IGFBP2 antibody. Rabbit anti-goat 10-nm gold-conjugated protein A was used to reveal the primary antibody staining. Then, sections were incubated with rabbit anti-giantin, followed by 15-nm gold-conjugated protein A as the secondary antibody. The samples were examined using an FEI CM10 and Tecnai G12 electron microscope (FEI company, Eindhoven, The Netherlands).

Flow Cytometric Analysis of the Cell Cycle

After transfection, IGFBP2-silenced (siIGFBP2) and control (siCONTROL) cells were harvested. For each sample, 1×10^6 cells were fixed with 70% cold ethanol, washed with PBS, and incubated with propidium iodide (50 μg/mL) and RNase (100 μg/mL) for 60 minutes at 37°C. Samples were run in a BD FACScan (Becton Dickinson, Labware, Bedford, MA), and data were analyzed with ModFitLT V3.0 software (Verity Software House, Topsham, ME). Two independent samples were analyzed for each cell type.

Migration and Invasion Transwell Assay

Migration was tested using cell culture inserts (Transwell) with an 8-μm pore size membrane (24-well format; Becton Dickinson). Chemoinvasion was measured using 24-well BioCoat Matrigel invasion chambers (Becton Dickinson) with an 8-μm pore polycarbonate filter coated with Matrigel. The lower compartment contained 0.5 mL of 1% serum medium conditioned by the NIH3T3 cell line as a chemoattractant or serum-free Dulbecco's modified Eagle's medium as a control. In the upper compartment, 10^5 RH36 cells per well were placed in triplicate wells and incubated for 18 hours at 37°C in a humidified incubator with a 5% CO_2 atmosphere. After incubation, the cells on the upper surface of the filter were wiped off with a cotton swab, whereas the cells on the lower surface were fixed in 2.5% glutaraldehyde, stained with 0.2% crystal violet in 20% methanol, and then photographed using a stereomicroscope (model MZ16; Leica Microsystems) equipped with a CCD camera. Images were elaborated with CorelDraw software (Corel, Ottawa, Canada), and the area occupied by the migrated cells was measured by using ImageJ software (*http://rsbweb.nih.gov/ij*, last accessed September 4, 2009).

Lentiviral Infections and Gene Silencing with shRNAs

The lentiviral expression vectors were obtained from Sigma-Aldrich, and cells were infected as previously described.[41]

Seeding Assay

All animal experiments were conducted in compliance with national legislation on ethical animal care. Female CD1 nude mice, aged 7 weeks (Charles River Laboratories, Wilmington, MA), were injected in the tail vein with 1.6×10^6 RH36 IGFBP2-silenced or control RH36 cells, previously labeled with CellTracker Orange CMRA (Molecular Probes, Invitrogen Life Technologies), and resuspended in PBS. After 48 hours, mice were sacrificed and 4% paraformaldehyde was injected into the trachea. Lungs were dissected and photographed using a Leica MZ16F fluorescence stereomicroscope (Leica Microsystems), and the mean of the total red fluorescent (CMRA) tumor cells present in three representative pictures per lungs per animal was evaluated using ImageJ software. Twelve mice per group were used.

IHC Analysis

Sections (4-μm thick) from paraffin-embedded tissues were dewaxed in xylene, rinsed in graded ethanol, and rehydrated in distilled water. For antigen retrieval, slides were pretreated by steaming in EDTA citrate buffer (pH 9.0) for 15 minutes at 100°C. Then, the sections were treated with 3% H_2O_2 for 5 minutes at room temperature to block endogenous peroxidase activity. After washing with PBS, the sections were manually immunostained with anti-IGFBP2 antibody at 1:100 dilution. For mouse monoclonal anti-58k antibody (GeneTex, Irvine, CA), the IHC stain was performed using a Bond MaX automated immunostainer (Leica Microsystems). The 58k primary antibody was used at 1:1000 dilution for 15 minutes. IGFBP2 was detected using the ABC Elite method (Vector Laboratories, Burlingame, CA), whereas mouse monoclonal anti-58K was detected using the polymer Refine detection kit (Leica Microsystems), according to the manufacturer's instructions. Hematoxylin was used for counterstaining. Specimens were then dehydrated with alcohol. The sections were analyzed with a Leica DM4000B-M microscope at either $\times$20 or $\times$40 amplification (Leica Microsystems). A human placenta tissue section was used as the positive control.

ELISA Assays

IGFBP2 plasma levels were determined by using the IGFBP2 enzyme-linked immunosorbent assay (ELISA) kit (RayBiotech, Inc., Norcross, GA), according to the manufacturer's instructions. Each assay was repeated three times, and the mean concentration of IGFBP2 was used for further statistical analysis.

Statistical Analysis

Microarray

All microarray experiments were analyzed by the SAM program implemented in tMEV software. SAM uses a permutation-based multiple testing algorithm and identifies significant genes with variable false-discovery rates. The list of differentially expressed genes presenting a false-discovery rate of 0 was classified in terms of biological functions using DAVID, a functional annotation tool. This type of analysis was aimed at identifying functional categories from the GO and public gene annotation databases that are present in the IGFBP2-silenced expression signature more frequently than expected by chance alone. The Group Enrichment Score is used to rank their biological significance. Thus, the top ranked annotation groups most likely have consistent lower P values for their annotation members.

Seeding

Data are calculated as mean $\pm$ SEM number of seeded cells 48 hours after injections for 12 mice per group, and the two-tailed Student's t-test was used for comparisons, with $P < 0.05$ considered a statistically significant value.

ELISA Data

Two or three independent experiments were performed in triplicate for each sample. Significance was evaluated using the Student's t-test or an F test that does not assume equal variances, and $P < 0.05$ was considered statistically significant. We performed the nonparametric U-test and the Wilcoxon signed rank test. An analysis of variance multiway analysis was used to correlate

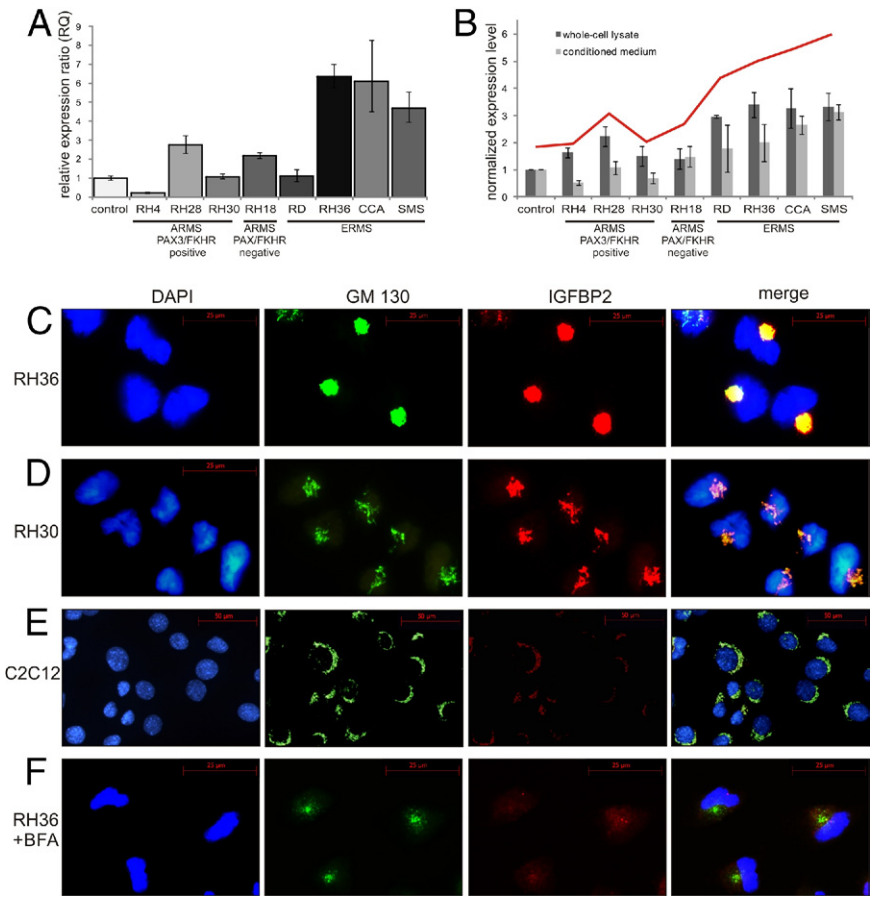

Figure 1. IGFBP2 accumulates in the Golgi of RMS cell lines. **A:** RT-qPCR evaluation of IGFBP2 expression in different RMS cell lines classified as indicated. Results are shown as relative expression ratio obtained with the $\Delta\Delta C_T$ method. *GADH* and *G2BNL1* were used as reference genes. Vertical bars indicate 95% confidence interval. **B:** IGFBP2 protein content was measured in whole-cell lysate (dark gray bars) and in medium (light gray bars) of the same RMS cell lines as in **A** by using Western blot analysis. Quantity One software was used for quantitation. Values are calculated as fold changes relative to C2C12 control cells and normalized to β-actin level. Vertical bars indicate 95% confidence interval. The trend line (red) was calculated by adding the lysate and medium protein values. **C–F:** Immunostaining of ERMS cell line RH36 (**C**), *PAX3/FKHR*-positive ARMS cell line RH30 (**D**), and control cell line C2C12 (**E**) with DAPI for nuclei (blue), anti-GM130 antibody for Golgi (green), and anti-IGFBP2 antibody (red). The pictures of the last column are obtained by merging the GM130 and IGFBP2 antibody signals. **F:** Immunostaining of RH36 cells after BFA treatment shows the simultaneous releasing of GM130 antigen and IGFBP2 from Golgi into the cytoplasm. The image is restricted to few cells to highlight the distribution of Golgi marker protein, but all of the cells show the same staining pattern.

the IGFBP2 level with other clinical parameters, and $P < 0.05$ was considered statistically significant.

Results

Analysis of IGFBP2 in RMS Cell Lines

The presence or absence of the *PAX/FKHR* fusion gene identifies two different gene expression signatures in RMS.[28,29] Because *IGFBP2* emerged as one of highly overexpressed genes in *PAX/FKHR*-negative RMS, we hypothesized that it may play a role in growth and differentiation of this tumor. To test this, we first studied the expression of IGFBP2 in eight RMS cell lines and in the myoblast C2C12 cell line as a control. We found that IGFBP2 expression in cell lines mirrors the expression pattern of the histologically related RMS samples analyzed in our previous microarray study.[29] In fact, IGFBP2 mRNA (Figure 1A) and both the intracellular and secreted protein fractions (Figure 1B) were significantly more abundant in most *PAX/FKHR* fusion-negative cell lines. The higher concentration of secreted IGFBP2 in culture medium of fusion-negative cells was also confirmed by ELISA (see Supplemental Figure S1 at *http://ajp.amjpathol.org*).

An analysis of the intracellular localization of IGFBP2 revealed that the protein was concentrated in a perinuclear region of RMS cells (Figure 1C). IGFBP2 was more abundant in the embryonal RH36 cell line compared with the alveolar *PAX3/FKHR*-positive RH30 cell line (Figure 1D). The differential expression of IGFBP2 between ARMS and ERMS was confirmed in other RMS cell lines (data not shown). In the cytoplasm of the control cell line C2C12, the IGFBP2 signal was low (Figure 1E). Co-immunostaining with an antibody directed against the *cis*-Golgi matrix protein GM130 demonstrated the concentration of IGFBP2 in the Golgi apparatus. This finding was confirmed by treatment of RMS cells with BFA, a fungal metabolite that inhibits protein secretion in eukaryotic cells by interfering with the function of the Golgi apparatus.[42] On BFA treatment, we observed a redistribution of IGFBP2 in the cytoplasm of RMS cells (Figure 1F). Interestingly, IGFBP2-expressing RMS cells showed an unusual modification of the Golgi morphological features that appeared condensed in a juxtanuclear position and without their typical stack organization. This peculiar organization appears to depend on the level of accumulated protein, as shown in the different cell lines analyzed (Figure 1, C and D).

RMS Cells Show Morphological and Functional Alterations of Golgi Apparatus

We analyzed whether the conspicuous morphological changes in the Golgi apparatus complex, seen in RMS cells by immunofluorescence experiments, were accompanied by functional alterations of this organelle. The

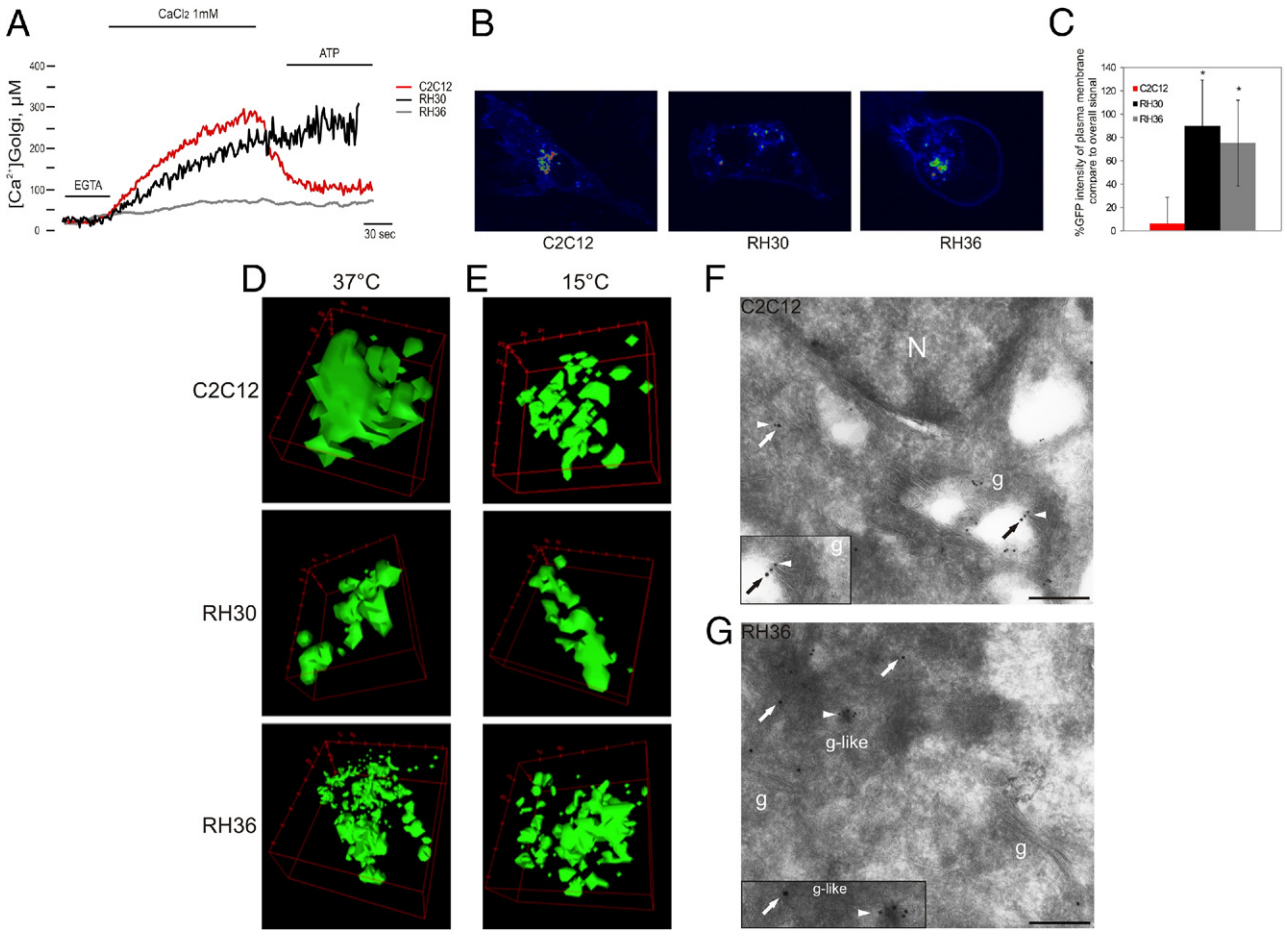

Figure 2. Morphological and functional alterations of Golgi apparatus in RMS cells. **A:** Golgi Ca^{2+} homeostasis measurements with aequorins in C2C12 and RMS cells. Where indicated, cells were treated with $CaCl_2$ to assess the filling of the Golgi compartments and with ATP, as agonist, to analyze the release of Ca^{2+} from the organelle. RMS cells showed a deregulation of Golgi Ca^{2+} homeostasis, in particular RH36 (gray line), in which the Golgi apparatus apparently failed to both accumulate and release Ca^{2+} after agonist stimulation. **B:** Analysis of VSVG-GFP distribution in C2C12 and RMS cell lines at 37°C. **C:** Percentage of VSVG-GFP intensity at plasma membrane compared with overall signal. A significant ($^*P < 0.05$) increase in VSVG-GFP at the cell surface of RMS cells was observed compared with control cells. Vertical bars represent the confidence interval of single-cell signals of three independent experiments. **D** and **E:** VSVG-GFP signal from the Golgi compartment at 37°C (**D**) and at 15°C (**E**) revealed a more fragmented Golgi apparatus with clear morphological changes in RMS cells compared with C2C12 cells. **F** and **G:** Ultrathin cryosections of C2C12 (**F**) and RMS (**G**) cells were double labeled with antibodies against giantin (15-nm gold, **arrows**), a Golgi marker, and IGFBP2 (10-nm gold, **arrowhead**). IGFBP2 colocalizes in giantin-labeled enlarged vesicles at the edge of Golgi cisterns in RH36 cells. Scale bars: 192 nm (**F** and **G**). g, Golgi; N, nuclei.

Golgi apparatus acts as Ca^{2+} store, and changes in calcium concentration within the Golgi lumen regulate Golgi function, controlling some of the key processes of cell biology, such as protein trafficking and sorting.[38] Therefore, we assayed the dynamic variations of Ca^{2+} concentration homeostasis within the Golgi apparatus using the recombinant Ca^{2+}-sensitive bioluminescent protein aequorin, modified with a specific tag for localization in this organelle (Golgi aequorin protein [GoAEQ]).[38] To obtain reliable quantitative estimates of Ca^{2+} concentration in the lumen of the Golgi apparatus, its Ca^{2+} concentration needs to be decreased during both the reconstitution of aequorin with coelenterazine and the subsequent initial phase of perfusion with Krebs-Ringer buffer–EGTA in the luminometer (see *Materials and Methods*). After Ca^{2+} depletion of the organelle, we investigated the characteristics of the Ca^{2+} uptake and release after agonist stimulation. When the EGTA in the perfusion buffer was replaced with 1 mmol/L $CaCl_2$, Golgi Ca^{2+} rapidly increased up to a concentration of approximately 300 μmol/L (Figure 2A) in C2C12 cells. Production of inositol 1,4,5-trisphosphate activates channels on the Golgi membrane, resulting in Ca^{2+} release from the apparatus. Indeed, when C2C12 cells were stimulated with ATP (an agonist of inositol 1,4,5-trisphosphate production), a release of Ca^{2+} from the Golgi membrane was observed (Figure 2A). On the contrary, a deregulation of Golgi Ca^{2+} homeostasis was detected in two different RMS cell lines. The Golgi apparatus of RH30 cells showed a normal Ca^{2+} uptake, reaching the same steady state observed in C2C12 but a completely compromised Ca^{2+} release after ATP treatment (Figure 2A). The alteration is more evident in RH36 cells, in which the Golgi apparatus apparently failed to both accumulate and, in turn, release Ca^{2+} after agonist stimulation (Figure 2A). These data suggest that RMS cells have a defective Ca^{2+} homeostasis in the Golgi apparatus.

To investigate whether the deregulation of Ca^{2+} can affect protein sorting and trafficking from Golgi to the plasma membrane, we used the viral glycoprotein VSVG,

tagged with GFP (VSVG-GFP).[43] Protein transport analysis in control C2C12 cells showed that, at 37°C, VSVG-GFP moves from the Golgi to the plasma membrane (Figure 2B). An analysis of VSVG-GFP protein distribution in RMS cells at 37°C revealed significant accumulation of protein at the cell surface compared with control cells ($P < 0.05$, Figure 2C). These data suggest an active production of secreted proteins in RMS cells, probably linked to the deregulation of protein transport. A colocalization experiment, using GM130 as a specific Golgi marker, confirmed that VSVG-GFP transits through Golgi in control and RMS cells during its secretory process (see Supplemental Figure S2 at *http://ajp.amjpathol.org*). Therefore, by focusing on the VSVG-GFP signal from the Golgi compartment, in C2C12 cells, we observed normal morphological features of the Golgi apparatus that appeared with its stacking organization (Figure 2D). In contrast, in RMS cells, the distribution of VSVG-GFP protein revealed a more fragmented Golgi, with clear morphological changes (see Supplemental Videos S1, S2, and S3 at *http://ajp.amjpathol.org*).

The use of a mutant gene encoding a temperature-sensitive VSVG-GFP allowed us to localize the protein in different cellular compartments. At temperatures as low as 15°C, mutant VSVG-GFP accumulates in intermediate structures called pre-Golgi apparatus that appeared markedly enlarged and accumulate secretory products.[44] Indeed, at 15°C, we observed an altered distribution of VSVG-GFP in C2C12 cells with accumulation of the protein in Golgi structures that appear more fragmented, similar to RMS cells (Figure 2E). However, VSVG-GFP protein localization in RH30 and RH36 cells was not affected by temperature, indicating that, in these cells, there is a continuous accumulation of secretory products in an altered Golgi compartment.

This hypothesis was confirmed by electron microscopy analysis. Cryosections of C2C12 control cells and IGFBP2-overexpressing RH36 cells were immunolabeled with specific antibodies against IGFBP2 and giantin, a Golgi apparatus marker. In C2C12 cells, the distribution of IGFBP2 in the Golgi apparatus was as expected for a typical secreted protein (Figure 2F). In ERMS cell RH36, some normal Golgi apparatus stacks were found, but the IGFBP2 pattern was peculiar because the protein accumulated at the edge of membrane-bound cisterns, reactive with Golgi-specific marker, that appeared less defined than normal Golgi apparatus cisterns (Figure 2G). Taken together, these data suggest that, in RMS cells, the morphological alterations are likely involving only a selected portion of the Golgi apparatus that appears to be made up of structures resembling altered and enlarged vesicles, possibly because of abnormal accumulation of secreted proteins.

Gene Expression Modification in RMS Cells after Silencing IGFBP2

We used siRNA to examine the effects of IGFBP2 suppression in the IGFBP2-overexpressing ERMS cell line RH36. As a result, IGFBP2 abundance was dramatically reduced at both the mRNA and protein levels after 48 hours of siRNA treatment (Figure 3, A and B). Moreover, a low level of IGFBP2 protein positively correlated with a change of Golgi shape that appears less condensed, probably because of a decrease of secretory vesicles (Figure 3C).

To identify the networks of genes whose expression was influenced by and functionally related to IGFBP2 reduction, we obtained the profiles of RMS cells from three independent experiments of IGFBP2 silencing and compared them with RMS cells treated with a pool of nontargeted siRNAs, used as controls. A total of 603 genes were differentially expressed in silenced RMS cells, equally distributed between up- and down-regulated genes (see Supplemental Table S3 at *http://ajp.amjpathol.org*). A functional annotation web tool (DAVID) was used to analyze the biological meaning of the differentially expressed genes. This type of analysis was aimed at identifying functional categories from the GO and public gene annotation databases that are present in the IGFBP2-silenced expression signature more frequently than expected by chance. The Group Enrichment Score was used to rank their biological significance. Thus, the top-ranked annotation groups most likely have consistently lower *P* values for their annotation members. As a result, we observed that GO functional categories overrepresented in the up-regulated component of the expression signature included protein transport and Golgi-vesicle transport; in contrast, the down-regulated component showed an overrepresentation of GO categories (ie, regulation of the cell cycle, cell adhesion, and cell motility or migration) (Figure 3, D and E). Among the deregulated genes, cyclin D1 (CCND1), MMP2, and minichromosome maintenance protein (MCM) family expression levels were remarkable. Cyclin D1 and the MCMs are implicated in tumorigenesis because of their involvement in the regulation of cell cycle progression. Moreover, correlation of IGFBP2 expression and MMP2 expression was reported. Metalloproteinase proteins act in the modeling of extracellular matrix and are implicated in the acquisition of invasive potential and in tumor progression. Microarray results were validated by RT-qPCR for a sample of 12 genes belonging to different annotation clusters (see Supplemental Figure S3 at *http://ajp.amjpathol.org*).

IGFBP2 Silencing Reduces Cell Cycle Progression, Migration, and Invasiveness of RMS Cells in Vitro

The signatures of IGFBP2-silenced cells showed the involvement of IGFBP2 in cellular pathways generally associated with cancer growth and progression. To validate this observation, cell cycle progression of the IGFBP2-silenced cell line (siIGFBP2) was compared with control cells (siCONTROL) by flow cytometry. Cells with reduced levels of IGFBP2 showed a decreased proliferation rate and G_0/G_1 phase arrest ($P < 0.05$, Figure 4A). Moreover, we tested whether IGFBP2 suppression affected RMS cell migration and invasion *in vitro*. Both assays revealed

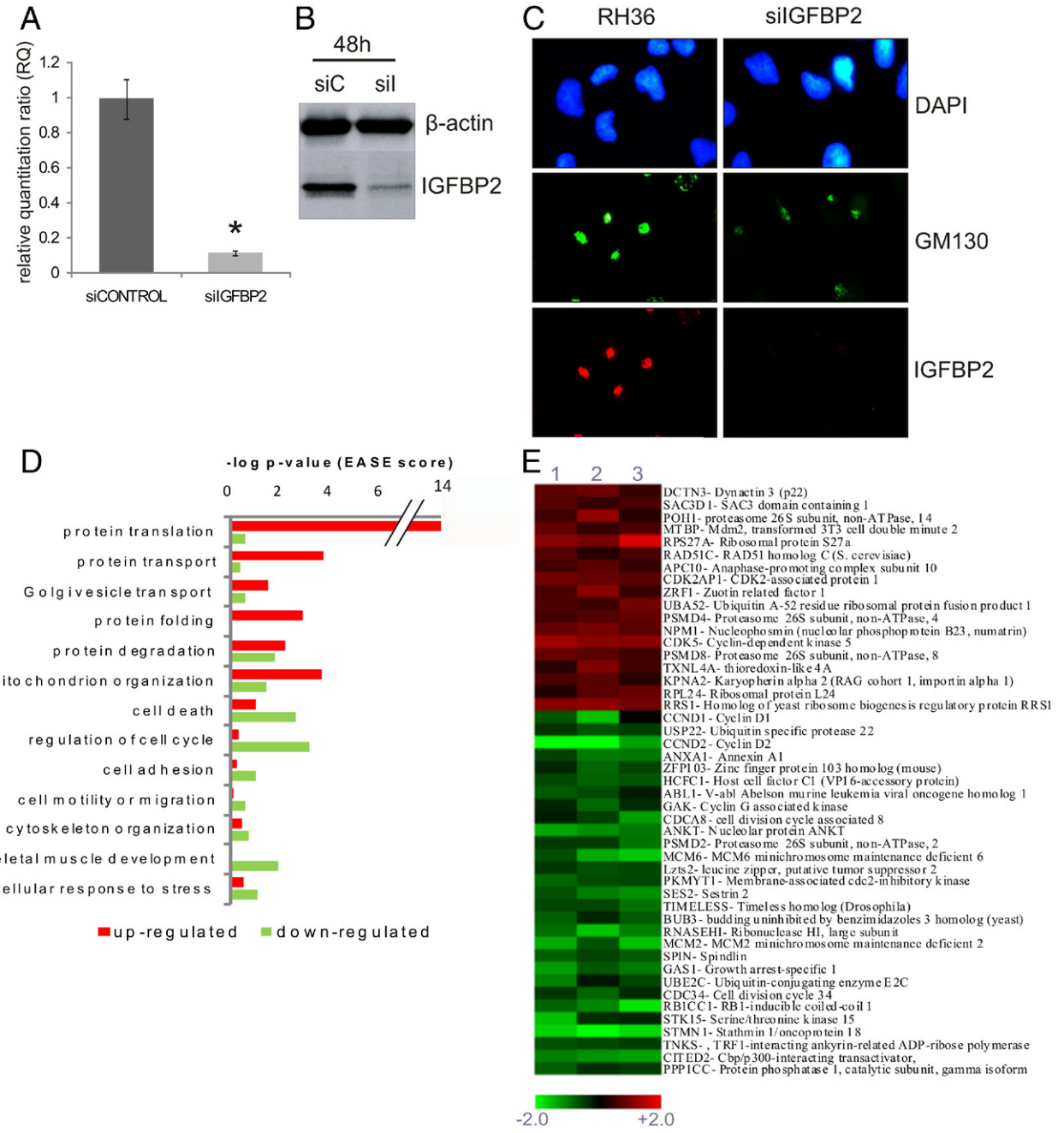

Figure 3. Altered gene pathways in IGFBP2-silenced RMS cells. **A:** IGFBP2 mRNA level (RQ) measured by RT-qPCR in RH36 cells transfected with the siRNA pool for IGFBP2 (siIGFBP2) or with the nontargeted siRNA pool (siCONTROL). A significant (*$P < 0.05$) decrease of IGFBP2 mRNA level was observed after silencing. **B:** IGFBP2 protein content measured by immunoblotting of whole cell lysate of RH36 cells treated as in **A**. Both assays indicate a significant reduction of IGFBP2 mRNA and protein after 48 hours of silencing (siC, siCONTROL; siI, siIGFBP2). **C:** Immunostaining of RMS cell line RH36 after IGFBP2 silencing (siIGFBP2). Treatment shows that low levels of IGFBP2 correlate with change of Golgi shape that appears less condensed, possibly because of a decrease of secretory vesicles. DAPI for nuclei (blue), anti-GM130 antibody for Golgi (green), and anti-IGFBP2 antibody (red) were used. **D:** GO functional categories were enriched in up-regulated (red) or down-regulated (green) genes in IGFBP2-silenced RH36 cells. Data were obtained by DAVID and are plotted by the negative log of *P* value (Group Enrichment Score). **E:** Heat map representing a selection of deregulated transcripts involved in cell cycle regulation, common to three different IGFBP2-silenced RH36-infected cells. Globally, the microarray data analyzed with the tMEV tool and the SAM algorithm have identified 603 differentially expressed genes. A color-coded scale for the normalized expression values was used, where red represents up-regulation and green represents down-regulation relative to RH36 cells transfected with the siRNA pool (siCONTROL).

a significant reduction of migration and invasion capability of IGFBP2-silenced cells compared with parental cells ($P < 0.05$, Figure 4B). Altogether, these results suggest that a high level of IGFBP2 facilitates RMS tumor cell invasion and cell cycle progression *in vitro*.

IGFBP2 Silencing Reduces Seeding of RMS Cells in Vivo

To assess whether IGFBP2 influenced tumor progression *in vivo*, we measured the lung seeding ability of

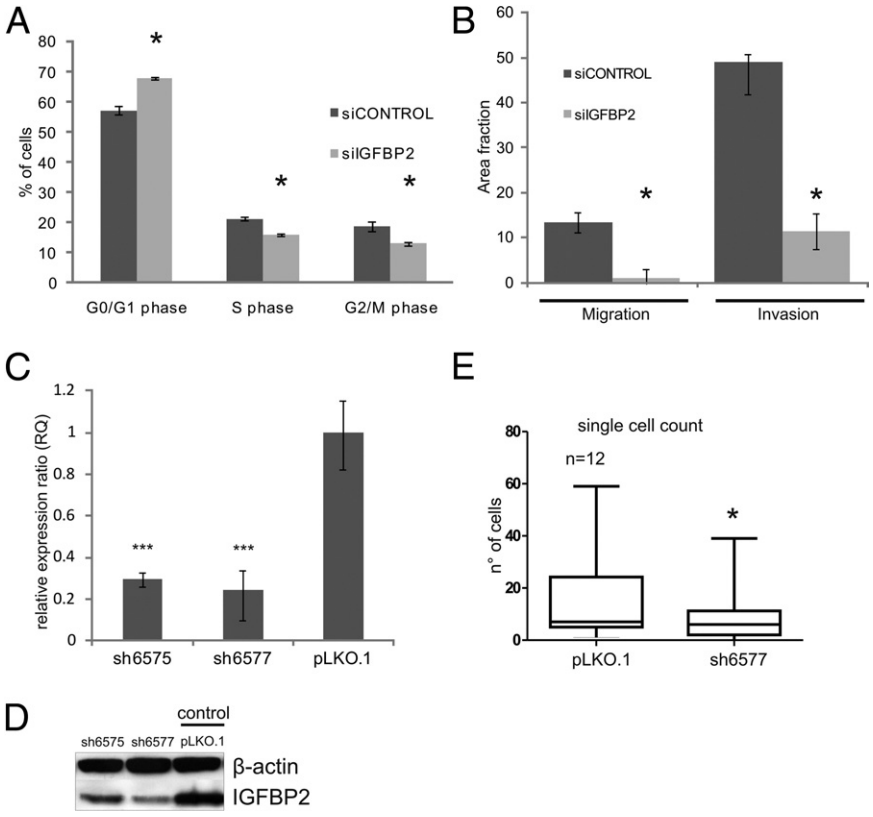

Figure 4. IGFBP2 silencing reduces proliferation, cell migration, and invasion of RMS cells *in vitro* and lung seeding ability *in vivo*. **A:** Mean percentages of cells in different cycle phases in RH36 cells silenced with siRNA for IGFBP2 (siIGFBP2, light gray boxes) or with nontargeted siRNA (siCONTROL, dark gray boxes), as measured by flow cytometry. Vertical bars represent the confidence interval among two independent experiments, each performed in triplicate. A significant ($^*P < 0.05$) increase in G_0/G_1 cells is seen in IGFBP2-silenced cells, accompanied by a decrease in S and G_2/M cells. **B:** Mean area fractions covered by siIGFBP2 (light gray boxes) and siCONTROL-transfected RH36 cells (dark gray boxes) after Transwell migration (Migration) and Matrigel invasion (Invasion) assays. Vertical bars represent the confidence interval among three independent experiments, each performed in triplicate. Significant ($^*P < 0.05$) declines in both parameters are evident after IGFBP2 silencing. **C:** RT-qPCR measurements of IGFBP2 mRNA (RQ) in RH36 cells stably transduced with lentiviral vectors expressing different IGFBP2-silencing shRNAs (ie, sh6575 and sh6577) or with empty vector controls (pLKO.1). Expression values are calculated as relative expression ratio obtained with the $\Delta\Delta C_T$ method. Vertical bars represent the confidence interval of at least three experiments. The data demonstrate a significant ($^{***}P < 0.01$) stable down-regulation of the *IGFBP2* gene in the two different IGFBP2-silenced RMS cells. **D:** IGFBP2 protein content of the same transfected RH36 cells described in **A**, measured by immunoblotting of whole cell lysate with anti-IGFBP2 antibody. IGFBP2 is reduced in both stably silenced cells. **E:** *In vivo* seeding analysis after tail vein injections in nude mice of CMRA-labeled RH36 cells, infected as in **C** and **D**. Data are presented as the mean ± SEM of the number of cells seeding the lungs, 48 hours after injections for 12 mice per group (see also *Materials and Methods*). The two-tailed Student's *t*-test was used for statistics. $^*P < 0.05$.

IGFBP2-silenced RMS and control cells. The RH36 cell line was transduced with five lentiviral vectors containing different IGFBP2 short hairpin RNA (shRNA) sequences. Control cells were transduced with empty pLKO.1 lentiviral vectors or with the same vectors expressing IGFBP2-mutated shRNAs. Specific, strong, and stable IGFBP2 gene silencing was obtained with two shRNA sequences (ie, sh6575 and sh6577), as demonstrated by using RT-qPCR and Western blot assays (Figure 4, C and D). Cells expressing either the sh6575 or the sh6577 sequence showed defects in migration, invasion, and cell cycle compared with control (pLKO.1) cells (see Supplemental Figure S4 at *http://ajp.amjpathol.org*), as also observed for cells transiently transfected with siIGFBP2 (Figure 4B). CMRA-labeled (red) control (pLKO.1) or IGFBP2 sh6577-expressing RH36 cells were tail vein injected in nude mice, and their ability to seed in the lung parenchyma was evaluated 2 and 48 hours later. Two hours after injection, many cells were still associated with the lung blood vessels, although some cells already crossed the endothelial barrier and were already visible in the lung parenchyma (data not shown). No difference in lodging was observed between IGFBP2 sh6577 and control cells. When cells were counted 48 hours after injection, a reduced seeding ability was observed for IGFBP2 sh6577 cells compared with controls (Figure 4E). These results indicate a positive role for IGFBP2 in early lung colonization events of tumor cells that could depend on intraluminal viability or extravasation or early growth capabilities.

IGFBP2 Expression and Distribution in Patients with RMS Resemble Those of RMS Cell Lines

The data obtained from both *in vitro* and *in vivo* experiments using RMS cell lines indicate IGFPB2 as a protein that plays an important role in RMS tumor progression, proliferation, and invasiveness. Thus, we determined whether these findings could be extended to patients with RMS. Our previous gene expression profiling study,[29] using patient samples, showed that IGFBP2 is an important discriminating transcript between *PAX3*/*FKHR*-positive ARMS and *PAX3*/*FKHR*-negative RMS. To confirm and extend these observations, we tested IGFBP2 mRNA expression in tumor specimens of a novel cohort of patients with RMS using RT-qPCR and demonstrated that *PAX*/*FKHR*-positive ARMS expressed significantly less IGFBP2 than *PAX*/*FKHR*-negative RMS (Figure 5A).

Subsequently, we assessed the pattern of cellular IGFBP2 distribution in tumor specimens. Thus, we studied paraffin-embedded biopsy specimens of patients with RMS by IHC using anti-IGFBP2 and anti-58k Golgi marker antibodies. Of 13 RMS samples studied (seven ERMS, four *PAX3*/*FKHR* positive, and two ARMS negative), all *PAX*/*FHKR*-positive ARMS samples showed absent or low IGFBP2 expression (Figure 5B). Six of seven ERMS specimens and all *PAX*/*FHKR* fusion-negative ARMSs analyzed were positive for IGFBP2. In the IGFBP2-positive RMSs, we observed a specific staining pattern ranging from diffuse cytoplasmic staining to a more intense signal in the perinuclear region (Figure 5, C

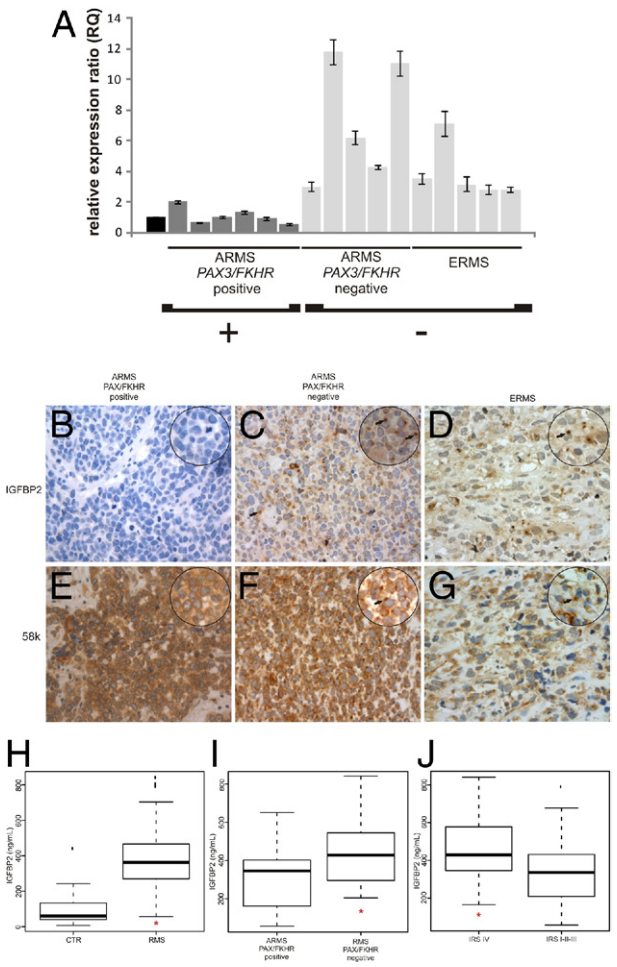

Figure 5. Evaluation of IGFBP2 status in patients with RMS. **A:** RT-qPCR quantitation of IGFBP2 mRNA in tumor biopsy specimens from 16 patients affected by different subtypes of RMS (ARMS translocation positive and negative and ERMS). Values are calculated as the ratio to the IGFBP2 mRNA content of fetal skeletal muscle (black box) with the $\Delta\Delta C_T$ method using glyceraldehyde-3-phosphate dehydrogenase (GAPDH) as the reference transcript. Vertical bars are the 95% confidence interval among at least three measurements. **B–G:** Immunodetection of IGFBP2 (**B–D**) and a 58K *cis*-Golgi protein marker (**E–G**) in paraffin-embedded sections of tumor samples from the three RMS subtypes described in **A**. *PAX/FKHR*-positive ARMS shows a negative signal for IGFBP2 (**B**) and positive staining for 58K protein (**E**). Original magnification, ×20. Instead, *PAX/FKHR*-negative ARMS shows positive IGFBP2 staining that resembles that of *cis*-Golgi marker (**F**). ERMS sections show similar results as *PAX/FKHR*-negative ARMS for both IGFBP2 (**D**) and 58K *cis*-Golgi (**F**) proteins, even though the number of stained cells appears to be reduced. Original magnification: ×40; ×63 (zoomed images). **Arrows**, peculiar perinuclear accumulation of IGFBP2 and condensed Golgi apparatus (in IGFBP2- and 58k-stained sections, respectively), already seen in RMS cell lines (see Figure 1, C and D). Hematoxylin was used as a counterstain. **H:** Plasma levels of IGFBP2 evaluated by ELISA assay are significantly higher in patients with RMS (*$P < 0.001$) versus healthy controls (CTRs). **I:** Plasma levels of IGFBP2 in translocation-negative RMS are significantly higher than in translocation-positive RMS. **J:** The plasma level of IGFBP2 is markedly higher ($P = 0.05$) in the group of patients with RMS who have advanced stage tumors (IRS stage IV). Box, interquartile range; center bar, median; whiskers, data range; and lines, outliers.

and D). This pattern mimics what we observed in RMS cell lines. Moreover, the staining of the 58k Golgi marker was superimposable to the signals of IGFBP2 antibody, confirming that IGFBP2 localized and accumulated in the Golgi apparatus of RMS cells *in vivo* (Figure 5, E–G). Overall, the expression and staining patterns of IGFBP2 differed between *PAX/FKHR*-positive and *PAX/FKHR*-negative patients with ARMS (Figure 5, B–D).

Elevated IGFBP2 in Plasma Correlates to RMS Severity

To test whether IGFBP2 protein was present in the plasma of patients with RMS and to assess whether its concentration was associated with aggressiveness, we used ELISA assays to detect plasma IGFBP2 in 41 patients with RMS before any therapy and in 15 healthy subjects as controls. Plasma levels of IGFBP2 were significantly higher in patients with RMS than in controls: median levels of 362.42 ng/mL in RMS patient samples and 60.11 ng/mL in controls ($P < 0.001$, Figure 5H). Moreover, we found that the IGFBP2 plasma level varies significantly between *PAX/FKHR* fusion-positive and *PAX/FKHR* fusion-negative patients ($P = 0.030$, Figure 5I).

To assess whether IGFBP2 correlated with RMS severity, we compared IGFBP2 plasma levels of nonmetastatic with metastatic RMS based on the Intergroup Rhabdomyosarcoma Study (IRS) grouping. Comparing nonmetastatic (IRS I-II-II) with metastatic (IRS IV) patients with RMS, we found that IGFBP2 levels were significantly higher in group IV patients with advanced-stage tumors ($P = 0.05$), demonstrating a positive correlation between IGFBP2 and tumor invasiveness (Figure 5J). Moreover, an analysis of variance multiway analysis was performed to evaluate if the combination of IRS group and the presence of the *PAX/FKHR* fusion gene were related to IGFBP2 plasma level. This analysis confirmed and validated that an elevated plasma concentration of IGFBP2 positively correlated with higher aggressiveness of tumor ($P = 0.024$) and with *PAX/FKHR*-negative subtype ($P = 0.001$).

Discussion

Our previous studies[29,45] on the human RMS transcriptome indicated that *IGFPB2* was one of the genes that may play an important role in the biological characteristics of this pediatric cancer because it is differentially expressed in different RMS subtypes. To analyze the IGFBP2-induced signaling pathway in RMS, we studied gene expression profiling of RMS cells undergoing forced inhibition of IGFBP2 expression. In the signature of these cells, we observed a significant deregulation of transcripts belonging to protein transport and Golgi vesicle-mediated transport. At the same time, RMS cells showed packaging of IGFBP2 in the Golgi apparatus that appeared morphologically altered.

These results were confirmed by immunogold labeling of ultrathin cryosections showing that, in RMS cells, IGFBP2 associates with unusual perinuclear Golgi structures that resemble enlarged vesicles. The Golgi luminal Ca^{2+} concentration and variations may be key controllers of the function of this organelle.[38] By using a Ca^{2+}-sensitive photoprotein to investigate the Ca^{2+} homeostasis in RMS cells, we showed a marked deregulation of the Golgi Ca^{2+} cycle, suggesting a functional alteration. Because depletion of Ca^{2+} from the Golgi organelle has

several effects on the secretory pathway,[43] we used the VSVG-GFP mutant protein to study protein transport. We found that the characteristic rearrangement of Golgi complex was associated with increased VSVG transport to the cell surface in RMS cells. Babiá et al[46] observed that transformation of a murine cell line with the oncogenic N-Ras caused a rearrangement of the Golgi complex into collapsed morphological features, similar to that caused by IGFBP2. Furthermore, in agreement with our findings, they reported an increase in protein transport from the *trans*-Golgi network to the cell surface, suggesting an alteration in membrane trafficking.

Our hypothesis is that IGFBP2 is produced in abnormal amounts and accumulates in atypical Golgi structures. Subsequently, the unusually high quantity of IGFBP2 moves from the Golgi apparatus to the cell surface, entering in a defective secretory pathway, as suggested by VSVG-GFP results. In cell tumor ultrathin sections, we observed that the organelle was rearranged only in part. RMS cells showed normal Golgi stacks, and this is expected given that the cells have an active secretion of proteins. However, cells also showed atypical Golgi structures that probably function as storage of an abnormal amount of secreted proteins and that could be responsible for the strong signal observed in immunofluorescence experiments.

Gene expression profiling of IGFBP2-silenced cells also revealed an alteration of transcripts involved in the regulation of the cell cycle and in cell migration and adhesion, such as MCMs and cyclin D1. The MCMs are a family of highly conserved proteins, playing an essential role in the early stages of eukaryotic genome replication. The requirement for MCM proteins in cycling cells and their absence in quiescent cells have led to their potential clinical application as proliferation markers, useful in cancer diagnosis. Microarray analyses and IHC studies[47,48] have shown increased mRNA and protein levels of MCMs in many different tumor cells and in carcinomas with a clinically aggressive phenotype. Typically, cyclin D1 acts together with their CDK partners to control G_1-S–phase progression through the inactivation of retinoblastoma protein and the release of the E2F transcription factor. The protein is frequently overexpressed in a large spectrum of human cancers, such as breast, lung, and bladder cancers, in which it may contribute to tumorigenesis.[49] We found that IGFBP2-silenced cells showed a significant, but not dramatic, decrease of the proliferation rate, paralleled by an enrichment of cells in the G_1 phase, probably because of weak involvement of IGFBP2 in this specific cellular process. Literature data[15,17] are conflicting regarding the role of IGFBP2 on cell cycle progression. Moreover, recent studies[50] revealed a role of cyclin D1 in cell migration, correlating its overexpression with cellular metastasis. Cell migration is essential for the invasion of tumor cells into the surrounding tissues. This coordinated migration process leads to tumor metastasis. An important contribution to cell motility depends on several changes in actin cytoskeletal structures.[51] Our microarray results confirmed that many transcripts involved in cytoskeleton remodeling are correlated to IGFBP2 expression.

Another interesting finding that supports a key role of IGFBP2 in the invasiveness of RMS cells is the deregulation of MMP2 as a consequence of IGFBP2 silencing. Several studies[52] have shown that an increased level of MMP2 expression is associated with an aggressive phenotype and poor prognosis in various human cancers, indicating MMP2 as a biomarker useful for stratifying patients with cancer into different risk groups. Moreover, a gene expression analysis in gliomas revealed a consistent induction of MMP2 by IGFBP2.[8] In our study, we demonstrated that IGFBP2 silencing in RMS cells affects migration and invasion.

Taken together, our results show that the strong silencing of IGFBP2 results in a complex phenotype and, therefore, we suggest that IGFBP2 may modulate an integrated network of genes involved in proliferation, cytoskeleton rearrangement, and tumor progression. This conclusion is further supported by our *in vivo* experiments demonstrating that stably IGFBP2-silenced cells showed reduced seeding ability in the lungs. Although we do not have sufficient experimental data to discuss a direct link between the accumulation of IGFBP2 in the Golgi apparatus, increase of IGFBP2 at the cell surface, and its prometastatic roles, we can speculate that the proinvasive effect is amplified by an alteration of Golgi protein trafficking.

To define the possible role of IGFBP2 in RMS *in vivo*, we determined IGFBP2 expression in tumor specimens. Only RMS fusion-negative patients were positive for IGFBP2 staining. Thus, IGFBP2 could reliably distinguish *PAX*/*FKHR*-positive from *PAX*/*FKHR*-negative tumors and, consequently, may represent a useful marker in clinical practice. Furthermore, we confirmed a perinuclear IGFBP2 staining pattern in *PAX*/*FKHR*-negative tumor biopsy specimens that overlapped a Golgi marker distribution. Thus, IGFBP2 accumulation appears to also correlate with a morphological modification of the Golgi apparatus *in vivo*. The immunostaining pattern of IGFBP2 has been studied by Makawita et al,[53] who assayed the level of all IGF pathway proteins in an RMS group of 29 patients belonging to different subtypes. They found an IGFBP2 expression pattern similar to our results but that focused on differences between ARMS and ERMS independently of the *PAX3*/*FKHR* fusion gene status. They reported that IGFBP2 did not differ significantly ($P = 0.052$) between the two major subgroups of RMS, although a study of a larger cohort of patients was warranted to draw definitive conclusions.

Finally, we tested IGFBP2 plasma levels in patients with RMS. The IGFBP2 plasma level was significantly higher than in healthy subjects, and IGFBP2 plasma levels discriminated between *PAX*/*FKHR*-positive and *PAX*/*FKHR*-negative patients, similar to IHC findings. Interestingly, when the levels of IGFBP2 were considered in relation to the aggressiveness of the tumor, we found that higher IGFBP2 levels were present in patients belonging to the high-risk group with metastatic disease at diagnosis. Further studies are needed to correlate the levels of IGFBP2 with different clinical characteristics of patients with RMS and with response to treatment. High plasma levels of IGFBP2 were associated with tumor progression

and metastasis in a wide spectrum of tumors.[14,17,54,55] A recent study[56] revealed that plasma concentrations of IGFBP2 were elevated in patients with high-grade glioma. Moreover, plasma levels of IGFBP2 and low levels of IGFBP3 at diagnosis correlated with a high risk of relapse or a lack of remission in childhood acute lymphoblastic leukemia.[57] These studies disclose the involvement of IGFBP2 in tumorigenesis and may lead to the discovery of new and specific treatments. In fact, the heat shock protein-90 inhibitors, including the geldanamycin derivative 17-AAG, decrease plasma IGFBP2 in patients with cancer.[19] It would be interesting to determine whether treatments of RMS-overexpressing IGFBP2 with such drugs would influence growth and differentiation of RMS cells. In conclusion, our results provide evidence that IGFBP2 is overexpressed in *PAX/FKHR* fusion-negative RMS and could promote cancer progression by augmenting cell invasiveness and cell proliferation. Moreover, we have identified IGFBP2 as a marker that may contribute to refine a clinical and biological classification of patients with RMS.

Acknowledgments

We thank Beniamina Pacchioni, Caterina Millino, and Barbara Celegato (University of Padova, Interdepartmental Research Center in Innovative Biotechnology, CRIBI Microarray Service MicroCribi) for microarray fabrication; and Prof. Carlo Tacchetti and MariaCristina Gagliani for electron microscopy studies performed at the Telethon Facility for electron microscopy, the MicroSCoBiO Research Center, and the Institute of Molecular Oncology Foundation (IFOM) and Ultrastructure, Genova, Italy.

References

1. Wheatcroft SB, Kearney MT: IGF-dependent and IGF-independent actions of IGF-binding protein-1 and -2: implications for metabolic homeostasis. Trends Endocrinol Metab 2009, 20:153–162
2. Firth SM, Baxter RC: Cellular actions of the insulin-like growth factor binding proteins. Endocr Rev 2002, 23:824–854
3. Frommer KW, Reichenmiller K, Schutt BS, Hoeflich A, Ranke MB, Dodt G, Elmlinger MW: IGF-independent effects of IGFBP-2 on the human breast cancer cell line Hs578T. J Mol Endocrinol 2006, 37: 13–23
4. Schutt BS, Langkamp M, Rauschnabel U, Ranke MB, Elmlinger MW: Integrin-mediated action of insulin-like growth factor binding protein-2 in tumor cells. J Mol Endocrinol 2004, 32:859–868
5. Russo VC, Schutt BS, Andaloro E, Ymer SI, Hoeflich A, Ranke MB, Bach LA, Werther GA: Insulin-like growth factor binding protein-2 binding to extracellular matrix plays a critical role in neuroblastoma cell proliferation, migration, and invasion. Endocrinology 2005, 146: 4445–4455
6. Pereira JJ, Meyer T, Docherty SE, Reid HH, Marshall J, Thompson EW, Rossjohn J, Price JT: Bimolecular interaction of insulin-like growth factor (IGF) binding protein-2 with alphavbeta3 negatively modulates IGF-I-mediated migration and tumor growth. Cancer Res 2004, 64:977–984
7. Fuller GN, Rhee CH, Hess KR, Caskey LS, Wang R, Bruner JM, Yung WK, Zhang W: Reactivation of insulin-like growth factor binding protein 2 expression in glioblastoma multiforme: a revelation by parallel gene expression profiling. Cancer Res 1999, 59:4228–4232
8. Wang H, Shen W, Huang H, Hu L, Ramdas L, Zhou YH, Liao WS, Fuller GN, Zhang W: Insulin-like growth factor binding protein 2 enhances glioblastoma invasion by activating invasion-enhancing genes. Cancer Res 2003, 63:4315–4321
9. Wang GK, Hu L, Fuller GN, Zhang W: An interaction between insulin-like growth factor-binding protein 2 (IGFBP2) and integrin alpha5 is essential for IGFBP2-induced cell mobility. J Biol Chem 2006, 281: 14085–14091
10. Fukushima T, Tezuka T, Shimomura T, Nakano S, Kataoka H: Silencing of insulin-like growth factor-binding protein-2 in human glioblastoma cells reduces both invasiveness and expression of progression-associated gene CD24. J Biol Chem 2007, 282:18634–18644
11. Song SW, Fuller GN, Khan A, Kong S, Shen W, Taylor E, Ramdas L, Lang FF, Zhang W: IIp45, an insulin-like growth factor binding protein 2 (IGFBP-2) binding protein, antagonizes IGFBP-2 stimulation of glioma cell invasion. Proc Natl Acad Sci U S A 2003, 100:13970–13975
12. Moore LM, Holmes KM, Smith SM, Wu Y, Tchougounova E, Uhrbom L, Sawaya R, Bruner JM, Fuller GN, Zhang W: IGFBP2 is a candidate biomarker for Ink4a-Arf status and a therapeutic target for high-grade gliomas. Proc Natl Acad Sci U S A 2009, 106:16675–16679
13. Perks CM, Vernon EG, Rosendahl AH, Tonge D, Holly JM: IGF-II and IGFBP-2 differentially regulate PTEN in human breast cancer cells. Oncogene 2007, 26:5966–5972
14. Mehrian-Shai R, Chen CD, Shi T, Horvath S, Nelson SF, Reichardt JK, Sawyers CL: Insulin growth factor-binding protein 2 is a candidate biomarker for PTEN status and PI3K/Akt pathway activation in glioblastoma and prostate cancer. Proc Natl Acad Sci U S A 2007, 104:5563–5568
15. Dunlap SM, Celestino J, Wang H, Jiang R, Holland EC, Fuller GN, Zhang W: Insulin-like growth factor binding protein 2 promotes glioma development and progression. Proc Natl Acad Sci U S A 2007, 104:11736–11741
16. Degraff DJ, Aguiar AA, Sikes RA: Disease evidence for IGFBP-2 as a key player in prostate cancer progression and development of osteosclerotic lesions. Am J Transl Res 2009, 1:115–130
17. Lee EJ, Mircean C, Shmulevich I, Wang H, Liu J, Niemistö A, Kavanagh JJ, Lee JH, Zhang W: Insulin-like growth factor binding protein 2 promotes ovarian cancer cell invasion. Mol Cancer 2005, 4:7
18. Martin JL, Baxter RC: Expression of insulin-like growth factor binding protein-2 by MCF-7 breast cancer cells is regulated through the phosphatidylinositol 3-kinase/AKT/mammalian target of rapamycin pathway. Endocrinology 2007, 148:2532–2541
19. Eiseman JL, Guo J, Ramanathan RK, Belani CP, Solit DB, Scher HI, Ivy SP, Zuhowski EG, Egorin MJ: Evaluation of plasma insulin-like growth factor binding protein 2 and Her-2 extracellular domain as biomarkers for 17-allylamino-17-demethoxygeldanamycin treatment of adult patients with advanced solid tumors. Clin Cancer Res 2007, 13:2121–2127
20. So AI, Levitt RJ, Eigl B, Fazli L, Muramaki M, Leung S, Cheang MC, Nielsen TO, Gleave M, Pollak M: Insulin-like growth factor binding protein-2 is a novel therapeutic target associated with breast cancer. Clin Cancer Res 2008, 14:6944–6954
21. Allander SV, Illei PB, Chen Y, Antonescu CR, Bittner M, Ladanyi M, Meltzer PS: Expression profiling of synovial sarcoma by cDNA microarrays: association of ERBB2, IGFBP2, and ELF3 with epithelial differentiation. Am J Pathol 2002, 161:1587–1595
22. Tschoep K, Kohlmann A, Schlemmer M, Haferlach T, Issels RD: Gene expression profiling in sarcomas. Crit Rev Oncol Hematol 2007, 63: 111–124
23. Dagher R, Helman L: Rhabdomyosarcoma: an overview. Oncologist 1999, 4:34–44
24. Barr FG: Molecular genetics and pathogenesis of rhabdomyosarcoma. J Pediatr Hematol Oncol 1997, 19:483–491
25. Anderson J, Ramsay A, Gould S, Pritchard-Jones K: PAX3-FKHR induces morphological change and enhances cellular proliferation and invasion in rhabdomyosarcoma. Am J Pathol 2001, 159:1089–1096
26. Sorensen PH, Lynch JC, Qualman SJ, Tirabosco R, Lim JF, Maurer HM, Bridge JA, Crist WM, Triche TJ, Barr FG: PAX3-FKHR and PAX7-FKHR gene fusions are prognostic indicators in alveolar rhabdomyosarcoma: a report from the children's oncology group. J Clin Oncol 2002, 20:2672–2679
27. Keller C, Capecchi MR: New genetic tactics to model alveolar rhabdomyosarcoma in the mouse. Cancer Res 2005, 65:7530–7532
28. Davicioni E, Finckenstein FG, Shahbazian V, Buckley JD, Triche TJ, Anderson MJ: Identification of a PAX-FKHR gene expression signa-

ture that defines molecular classes and determines the prognosis of alveolar rhabdomyosarcomas. Cancer Res 2006, 66:6936–6946
29. De Pitta C, Tombolan L, Albiero G, Sartori F, Romualdi C, Jurman G, Carli M, Furlanello C, Lanfranchi G, Rosolen A: Gene expression profiling identifies potential relevant genes in alveolar rhabdomyosarcoma pathogenesis and discriminates PAX3-FKHR positive and negative tumors. Int J Cancer 2006, 118:2772–2781
30. Charytonowicz E, Cordon-Cardo C, Matushansky I, Ziman M: Alveolar rhabdomyosarcoma: is the cell of origin a mesenchymal stem cell? Cancer Lett 2009, 279:126–136
31. Pfaffl MW: A new mathematical model for relative quantification in real-time RT-PCR. Nucleic Acids Res 2001, 29:e45
32. Livak KJ, Schmittgen TD: Analysis of relative gene expression data using real-time quantitative PCR and the $2^{-\Delta\Delta C}$T Method. Methods 2001, 25:402–408
33. Saeed AI, Sharov V, White J, Li J, Liang W, Bhagabati N, Braisted J, Klapa M, Currier T, Thiagarajan M, Sturn A, Snuffin M, Rezantsev A, Popov D, Ryltsov A, Kostukovich E, Borisovsky I, Liu Z, Vinsavich A, Trush V, Quackenbush J: TM4: a free, open-source system for microarray data management and analysis. Biotechniques 2003, 34: 374–378
34. Tusher VG, Tibshirani R, Chu G: Significance analysis of microarrays applied to the ionizing radiation response. Proc Natl Acad Sci U S A 2001, 98:5116–5121
35. Saeed AI, Bhagabati NK, Braisted JC, Liang W, Sharov V, Howe EA, Li J, Thiagarajan M, White JA, Quackenbush J: TM4 microarray software suite. Methods Enzymol 2006, 411:134–193
36. Huang da W, Sherman BT, Stephens R, Baseler MW, Lane HC, Lempicki RA: DAVID gene ID conversion tool. Bioinformation 2008, 2:428–430
37. Edgar R, Domrachev M, Lash AE: Gene Expression Omnibus: NCBI gene expression and hybridization array data repository. Nucleic Acids Res 2002, 30:207–210
38. Pinton P, Pozzan T, Rizzuto R: The Golgi apparatus is an inositol 1,4,5-trisphosphate-sensitive Ca2+ store, with functional properties distinct from those of the endoplasmic reticulum. EMBO J 1998, 17:5298–5308
39. Pinton P, Rimessi A, Romagnoli A, Prandini A, Rizzuto R: Biosensors for the detection of calcium and pH. Methods Cell Biol 2007, 80:297–325
40. Schiaffino MV, Tacchetti C: The ocular albinism type 1 (OA1) protein and the evidence for an intracellular signal transduction system involved in melanosome biogenesis. Pigment Cell Res 2005, 18:227–233
41. Dull T, Zufferey R, Kelly M, Mandel RJ, Nguyen M, Trono D, Naldini L: A third-generation lentivirus vector with a conditional packaging system. J Virol 1998, 72:8463–8471
42. Misumi Y, Miki K, Takatsuki A, Tamura G, Ikehara Y: Novel blockade by brefeldin A of intracellular transport of secretory proteins in cultured rat hepatocytes. J Biol Chem 1986, 261:11398–11403
43. Presley JF, Cole NB, Schroer TA, Hirschberg K, Zaal KJ, Lippincott-Schwartz J: ER-to-Golgi transport visualized in living cells. Nature 1997, 389:81–85
44. Kuismanen E, Saraste J: Low temperature-induced transport blocks as tools to manipulate membrane traffic. Methods Cell Biol 1989, 32:257–274
45. Romualdi C, De Pittà C, Tombolan L, Bortoluzzi S, Sartori F, Rosolen A, Lanfranchi G: Defining the gene expression signature of rhabdomyosarcoma by meta-analysis. BMC Genomics 2006, 7:287
46. Babiá T, Ayala I, Valderrama F, Mato E, Bosch M, Santarén JF, Renau-Piqueras J, Kok JW, Thomson TM, Egea G: N-Ras induces alterations in Golgi complex architecture and in constitutive protein transport. J Cell Sci 1999, 112(Pt 4):477–489
47. Forsburg SL: Eukaryotic MCM proteins: beyond replication initiation. Microbiol Mol Biol Rev 2004, 68:109–131
48. Tachibana KE, Gonzalez MA, Coleman N: Cell-cycle-dependent regulation of DNA replication and its relevance to cancer pathology. J Pathol 2005, 205:123–129
49. Kim JK, Diehl JA: Nuclear cyclin D1: an oncogenic driver in human cancer. J Cell Physiol 2009, 220:292–296
50. Li Z, Wang C, Prendergast GC, Pestell RG: Cyclin D1 functions in cell migration. Cell Cycle 2006, 5:2440–2442
51. Oser M, Condeelis J: The cofilin activity cycle in lamellipodia and invadopodia. J Cell Biochem 2009, 108:1252–1262
52. Guo CB, Wang S, Deng C, Zhang DL, Wang FL, Jin XQ: Relationship between matrix metalloproteinase 2 and lung cancer progression. Mol Diagn Ther 2007, 11:183–192
53. Makawita S, Ho M, Durbin AD, Thorner PS, Malkin D, Somers GR: Expression of insulin-like growth factor pathway proteins in rhabdomyosarcoma: IGF-2 expression is associated with translocation-negative tumors. Pediatr Dev Pathol 2009, 12:127–135
54. Brady G, O'Regan E, Miller I, Ogungbowale A, Kapas S, Crean SJ: Serum levels of insulin-like growth factors (IGFs) and their binding proteins (IGFBPs), -1, -2, -3, in oral cancer. Int J Oral Maxillofac Surg 2007, 36:259–262
55. Shariat SF, Lamb DJ, Kattan MW, Nguyen C, Kim J, Beck J, Wheeler TM, Slawin KM: Association of preoperative plasma levels of insulin-like growth factor I and insulin-like growth factor binding proteins-2 and -3 with prostate cancer invasion, progression, and metastasis. J Clin Oncol 2002, 20:833–841
56. Lin Y, Jiang T, Zhou K, Xu L, Chen B, Li G, Qiu X, Jiang T, Zhang W, Song SW: Plasma IGFBP-2 levels predict clinical outcomes of patients with high-grade gliomas. Neuro Oncol 2009, 11:468–476
57. Vorwerk P, Mohnike K, Wex H, Rohl FW, Zimmermann M, Blum WF, Mittler U: Insulin-like growth factor binding protein-2 at diagnosis of childhood acute lymphoblastic leukemia and the prediction of relapse risk. J Clin Endocrinol Metab 2005, 90:3022–3027

The EMBO Journal (2011), 1–18 | © 2011 European Molecular Biology Organization | All Rights Reserved 0261-4189/11
www.embojournal.org

THE EMBO JOURNAL

microRNA-214 contributes to melanoma tumour progression through suppression of TFAP2C

Elisa Penna[1,2,10], Francesca Orso[1,2,3,10], Daniela Cimino[1,2,3], Enrico Tenaglia[1,2], Antonio Lembo[1,4], Elena Quaglino[1,5], Laura Poliseno[6], Adele Haimovic[6], Simona Osella-Abate[7], Cristiano De Pittà[8], Eva Pinatel[1,4], Michael B Stadler[9], Paolo Provero[1,4], Maria Grazia Bernengo[7], Iman Osman[6] and Daniela Taverna[1,2,3,*]

[1]Molecular Biotechnology Center (MBC), University of Torino, Torino, Italy, [2]Department of Oncological Sciences, University of Torino, Torino, Italy, [3]Center for Complex Systems in Molecular Biology and Medicine, University of Torino, Torino, Italy, [4]Department of Genetics, Biology and Biochemistry, University of Torino, Torino, Italy, [5]Department of Clinical and Biological Sciences, University of Torino, Torino, Italy, [6]Department of Dermatology, New York University Medical Center, New York, NY, USA, [7]Department of Biomedical Science and Human Oncology, Ist. Dermatologic Clinic, University of Torino, Torino, Italy, [8]Department of Biology and C.R.I.B.I.-Biotechnology Center, University of Padova, Padova, Italy and [9]Friederich Miescher Institute, Basel, Switzerland

Malignant melanoma is fatal in its metastatic stage. It is therefore essential to unravel the molecular mechanisms that govern disease progression to metastasis. MicroRNAs (miRs) are endogenous non-coding RNAs involved in tumourigenesis. Using a melanoma progression model, we identified a novel pathway controlled by miR-214 that coordinates metastatic capability. Pathway components include TFAP2C, homologue of a well-established melanoma tumour suppressor, the adhesion receptor ITGA3 and multiple surface molecules. Modulation of miR-214 influences *in vitro* tumour cell movement and survival to *anoikis* as well as extravasation from blood vessels and lung metastasis formation *in vivo*. Considering that miR-214 is known to be highly expressed in human melanomas, our data suggest a critical role for this miRNA in disease progression and the establishment of distant metastases.

The EMBO Journal advance online publication, 5 April 2011; doi:10.1038/emboj.2011.102
Subject Categories: RNA; molecular biology of disease
Keywords: extravasation; melanoma; miR-214; TFAP2C; tumour progression

Introduction

The ability of tumours to acquire malignancy and spread in their host organism is one of the main issues in cancer treatment, as metastasis formation accounts for >90% of human cancer deaths. Nevertheless, the understanding of the molecular mechanisms that regulate metastatic dissemination remains fragmentary. The cascade of events that lead to metastasis is a complex multi-step process by which primary tumour cells acquire the ability to detach and invade adjacent tissues, intravasate, survive in the systemic circulation and translocate through the vasculature, adhere to the walls of capillaries of distant organs, extravasate in the parenchyma and finally proliferate in secondary tumours (Gupta and Massague, 2006). It is urgent to identify and characterize the genetic and epigenetic changes occurring during tumour progression. Several protein-coding genes involved in malignancy have been identified and characterized (Steeg, 2006; Nguyen *et al*, 2009). More recently, abnormalities in non-coding genes, such as microRNAs (miRs), have also been found to contribute to tumourigenesis (Croce, 2009; Valastyan and Weinberg, 2009). miRs are small endogenous non-coding RNAs able to post-transcriptionally downregulate expression of specific target genes by binding to the 3′UTRs of their mRNAs causing destabilization, degradation or translation inhibition (Filipowicz *et al*, 2008; Bartel, 2009). The ability of miRs to achieve simultaneous fine tuning of numerous different target genes makes them fundamental regulators of cellular signalling and implicates them in tumour progression (Inui *et al*, 2010). Several miRs, such as miR-21, miR-10b, miR-373 and 520c, miR-126, miR-335, miR-31, miR-200, miR-151 and miR-9, have already been reported to regulate tumour progression and metastasis (Valastyan and Weinberg, 2009; Ma *et al*, 2010).

Malignant melanoma is one of the most aggressive human cancers (Parkin *et al*, 2005) which progresses very rapidly *via* specific steps characterized by defined molecular alterations. Melanomas arise when the melanocytes of the epidermis become transformed and start to proliferate abnormally, leading to radial and vertical growth phases and subsequent spreading all over the body (Melnikova and Bar-Eli, 2008). The transition from the non-invasive to the invasive and metastatic stage is accompanied by gain of function of a number of transcription factors such as CREB/ATF-1, ATF-2, NFκB, SNAIL and STATs, while the loss of the AP-2 transcription factors (TFAP2) positively correlates with malignancy. At the same time, alterations in the repertoire of adhesion molecules, including MCAM-MUC18, E-cadherin, N-cadherin and several integrins, as well as changes in genes involved in angiogenesis, invasion and survival, such as VEGF, bFGF, IL-8, c-KIT, EGFR, MMP2 and PAR-1, are linked to the acquirement of higher metastatic potential (Melnikova and Bar-Eli, 2008). Several miRs, including miR-137, miR-221/222, miR-182 and miR-34a, have already been found to be involved in melanoma progression by regulating key genes such as c-KIT, MITF, FOXO3, ITGB3, CCND1 and $p27^{Kip1}$ (Mueller and Bosserhoff, 2009). It now becomes fundamental to unravel how miRs control melanoma aggressiveness.

We identified a new pathway, coordinated by miR-214 and including TFAP2C, ITGA3 as well as multiple surface

*Corresponding author. Department of Oncological Sciences, Molecular Biotechnology Center (MBC), University of Torino, Via Nizza, 52, 10126 Torino, Italy. Tel.: +39 011 670 6497; Fax: +39 011 670 6432;
E-mail: daniela.taverna@unito.it
[10]These authors contributed equally to this work

Received: 17 September 2010; accepted: 9 March 2011

molecules, which controls melanoma metastasis dissemination by increasing migration, invasion, extravasation and survival of melanoma cells.

Results

miR-214 is upregulated in a metastatic melanoma model

To assess a potential correlation between deregulation of miRs and melanoma malignancy, a miR profiling, which will be presented elsewhere (Cimino *et al*, unpublished), was performed in a melanoma progression model (Xu *et al*, 2008). The model consisted of a poorly metastatic A375 parental cell line (A375P) and its four highly metastatic variants, MA-1, MA-2, MC-1 and MC-2 derived by repeated passages in mice. Among the modulated miRs, miR-214 was found to be differentially expressed comparing metastatic (high) versus parental (low) cells in culture, as shown by qRT–PCR (Figure 1A and B). miR-214 showed a very strong enhancement of expression in samples derived from *in vivo* lung metastases following tail vein injections of MA-2 cells in immunodeficient mice (Figure 1B), suggesting an influence of the microenvironment for high expression. Induction of miR-214 expression *in vivo* was also observed in subcutaneous tumours derived from different melanoma cell lines expressing low miR-214 in culture (WK-Mel, GR4-Mel, 1300-Mel, Dett-Mel, SK-Mel-173, SK-Mel-197) (Supplementary Figure S1A). Other miRs, previously found to be involved in melanoma, such as miR-34a, miR-221, miR-222 and miR-137, also showed some differential expression in this system, however, not as pronounced as miR-214 changes (Figure 1A). When we extended expression analysis for miR-137 to other melanoma malignant cell lines it resulted to be overexpressed in some of them, such as WK-Mel, GR4-Mel, SK-Mel-173 and SK-Mel-197 compared with A375P. Instead no expression was detected in 1300-Mel, Dett-Mel and SK-Mel-187 cells (Supplementary Figure S1B). Some miRs were poorly expressed or did not show differential expression in our A375P isogenic model, including miR-210, which we used as a control (Figure 1C). miR-210 was expressed to some extent in most of the melanoma cells analysed although often at a low level (Supplementary Figure S1C). Importantly, miR-214 copy number gain was found in the genome of A375P, its MA-2 and MC-1 variants and in other melanoma cells, such as GR4-Mel,

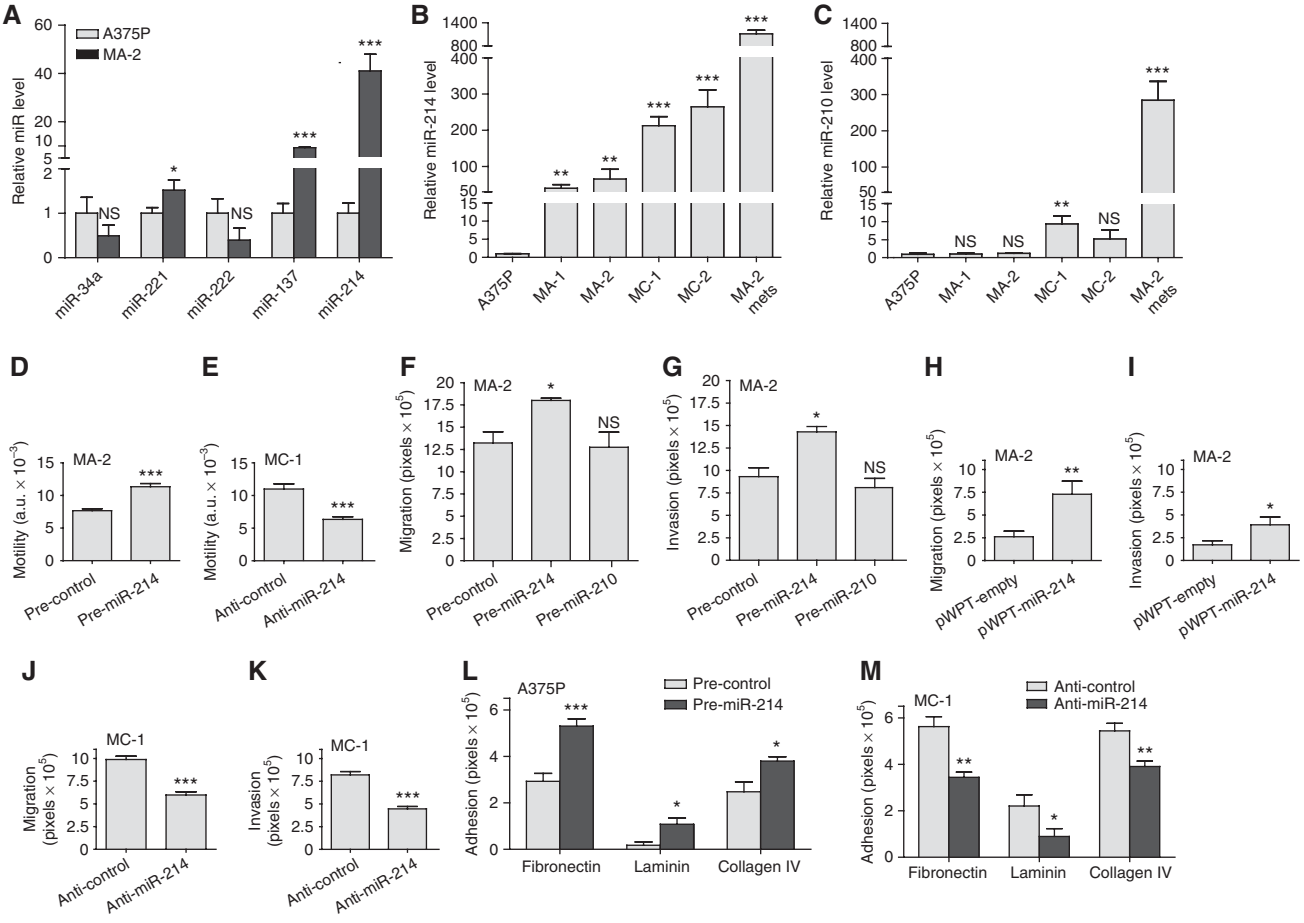

Figure 1 miR-214 modulates cell migration and invasion. (**A**–**C**) Expression levels of the indicated miRs were evaluated in A375P cells or in its metastatic variants MA-1, MA-2, MC-1, MC-2 or in a pool of MA-2-derived lung metastases (MA-2 mets) by qRT–PCR. Results are shown as fold changes (mean ± s.e.m.) relative to A375P cells, normalized on U44 RNA level. (**D**–**M**) Wound healing motility (**D**, **E**) or transwell migration or matrigel invasion (**F**–**K**) or adhesion on fibronectin, laminin or collagen (**L**, **M**) assays for cells either transfected with the indicated miR precursors or inhibitors or their negative controls (pre- and anti-miR or control) or stably transduced with pWPT-empty or miR-214 overexpression vectors. Results are shown as mean ± s.e.m. of the reciprocal of the wound size (motility assay) or of the area covered by migrated or adherent cells (migration, invasion and adhesion assays). Two or three independent experiments were performed in triplicate and results were either shown as representative ones (**A**–**C**) or pooled together (**D**–**M**). $^{*}P<0.05$; $^{**}P<0.01$; $^{***}P<0.001$.

Dett-Mel, SK-Mel-103 and SK-Mel-187, as measured by genomic qRT–PCR (Supplementary Figure S1D) and SNP (not shown) analyses.

miR-214 expression enhances cell movement

The more pronounced expression of miR-214 in metastatic cells prompted us to investigate the potential pro-metastatic role of miR-214 by analysing cell movement following miR-214 expression modulations.

We stably or transiently overexpressed miR-214 in the miR-214-empty, poorly motile A375P cells and in the MA-2 metastatic variant, expressing an intermediate endogenous level of miR-214 (see Figure 1B), as well as in other melanoma cells, such as 1300-Mel, SK-Mel-187, WK-Mel and GR4-Mel, expressing low to undetectable miR-214 in culture (see Supplementary Figure S1A), by lentiviral infections with miR-214 expression or empty vectors (pWPT-miR-214 or pLemiR-214 or empty) or by transfections with miR-214 precursors or negative controls (pre-miR-214 or control). Conversely, we silenced miR-214 in the highly motile and invasive MC-1 and MC-2 variants following transfection with specific miR-214 antisense inhibitors or negative controls (anti-miR-214 or control). The efficacy of miR-214 modulations was tested by qRT–PCRs; miR-214 expression was increased up to 200 000- or 500-fold, respectively, in pre-miR-214 transiently transfected cells and stable infected cells (Supplementary Figure S2A–C) and almost completely silenced following miR-214 inhibition (Supplementary Figure S2D).

Significantly, miR-214 overexpression by pre-miR-214 transfection in MA-2 cells enhanced cell motility, migration and invasion as evaluated by wound healing assays (Figure 1D) or transwell assays in presence or absence of matrigel (Figure 1F and G) compared with negative controls. Migration and invasion were also increased 2–3-fold in stable miR-214-overexpressing MA-2 cells compared with cells containing the empty vector (Figure 1H and I). Moreover, miR-214 overexpression was sufficient to promote a significant increase in migration and/or invasion in poorly motile A375P cells (pWPT-miR-214, Supplementary Figure S3A) and in other unrelated melanoma cell lines, such as 1300-Mel, SK-Mel-187, WK-Mel and GR4-Mel (pre-miR-214, Supplementary Figure S3E–J). The effects observed on cell movement in the A375P isogenic model were specific for miR-214, since no significant variation in migration or invasion was observed following transient miR-210 overexpression (Figure 1F and G). In line with these results, transient miR-214 downregulation in MC-1 or MC-2 cells, following transfection with anti-miR-214, led to a 50% reduction in motility in a wound healing assay (Figure 1E, MC-1) and a 40–80% decrease in migration and matrigel invasion in transwell assays (Figures 1J and K, MC-1; Supplementary Figure S3B and C, MC-2). miR-214 functions were also evaluated by stable silencing in MC-1 cells using miR-214-specific sponges cloned in the 3′UTR of the green fluorescent protein (GFP) gene (see Materials and methods). MC-1 cells were transduced with pLenti-CMV-GFP-Puro-sponge1 (pLenti-sponge1) or pLenti-CMV-GFP-Puro-sponge3 (pLenti-sponge3) or pLenti-CMV-GFP-Puro (pLenti-empty) vectors and the efficacy of each sponge was evaluated by measuring the expression of the GFP in a western blot (WB) analysis (Supplementary Figure S2E). In presence of pLenti-sponge1 or pLenti-sponge3 GFP expression was highly decreased, indicating the efficient binding of miR-214 on the complementary sequences in the 3′UTR of the GFP. As shown in Supplementary Figure S3D, stable miR-214 silencing by sponge1 or sponge3 resulted in impairment of MC-1 cell migration *in vitro* (transwell assays), compared with control cells. Interestingly, miR-214 overexpression (pre-miR-214) was also able to significantly increase cell migration and matrigel invasion in other tumour cells, including human MDA-MB-231 or murine 4T1 mammary epithelial cancer cell lines (Supplementary Figures S2A and S3K–N). When we looked for the involvement of miR-214 in cell adhesion we observed significant adhesion alterations on different extracellular matrices (ECMs). In particular, transient miR-214 overexpression in A375P cells improved adhesion on fibronectin, laminin and collagen (1.5–3-fold increase), while miR-214 silencing in MC-1 cells consistently resulted in comparable adhesion defects on these matrices (Figure 1L and M).

Taken together, these results show that miR-214 significantly enhances *in vitro* cell movement and modulates adhesion, suggesting that it might facilitate metastasis formation by favouring tumour cell invasion and adhesion to the surrounding ECM.

miR-214 expression enhances metastasis formation in vivo

Because of its ability to induce motility and invasion *in vitro*, we asked whether miR-214 could influence cell movement and metastasis formation *in vivo*. Thus, miR-214-overexpressing MA-2 cells or miR-214-silenced MC-1 cells were injected into the tail vein of immunodeficient SCID mice and the number of lung metastases was evaluated 7 weeks later. A significantly higher number of macroscopic lung metastases could be observed for miR-214-overexpressing (pWPT-miR-214) MA-2 cells when compared with control (pWPT-empty) cells (Figure 2A). To investigate whether miR-214 was able to promote or regulate metastasis formation in the poorly metastatic parental cells, miR-214-overexpressing (pWPT-miR-214) or control (pWPT-empty) A375P cells were injected into SCID mice. Metastasis formation was analysed 9 weeks later and no macroscopic metastases were found on the lung surface for the two groups of mice. However, histological analyses revealed that 3 out of 10 mice injected with miR-214-overexpressing cells contained small metastatic formations in their lungs, while no micrometastases were found in control mice (Supplementary Figure S4). In contrast, miR-214-silenced MC-1 cells (by anti-miR-214 transfection) were significantly impaired in their ability to seed lung metastases and formed fewer lesions than the control (anti-control) cells (Figure 2B). High miR-214 expression levels were also able to enhance lung metastasis formation from a primary tumour. In fact, when the 4T1 mammary epithelial cancer cells, transduced with a lentiviral vector encoding for the turbo red-fluorescent protein (tRFP) alone (pLemiR-empty) or for miR-214 plus tRFP (pLemiR-214), were injected in mammary fat pad of female BALB/c mice, a significantly higher distribution of red-fluorescent micrometastasis in the lungs was observed for miR-214-overexpressing cells compared with controls, 20 days after injection (Supplementary Figure S2C; Figure 2C). However, miR-214-overexpressing cells gave rise to similar sized primary tumours as control cells (not shown). miR-214 enhancement effects on *in vitro* cell movement and *in vivo* metastasis formation are directly ascribed to the

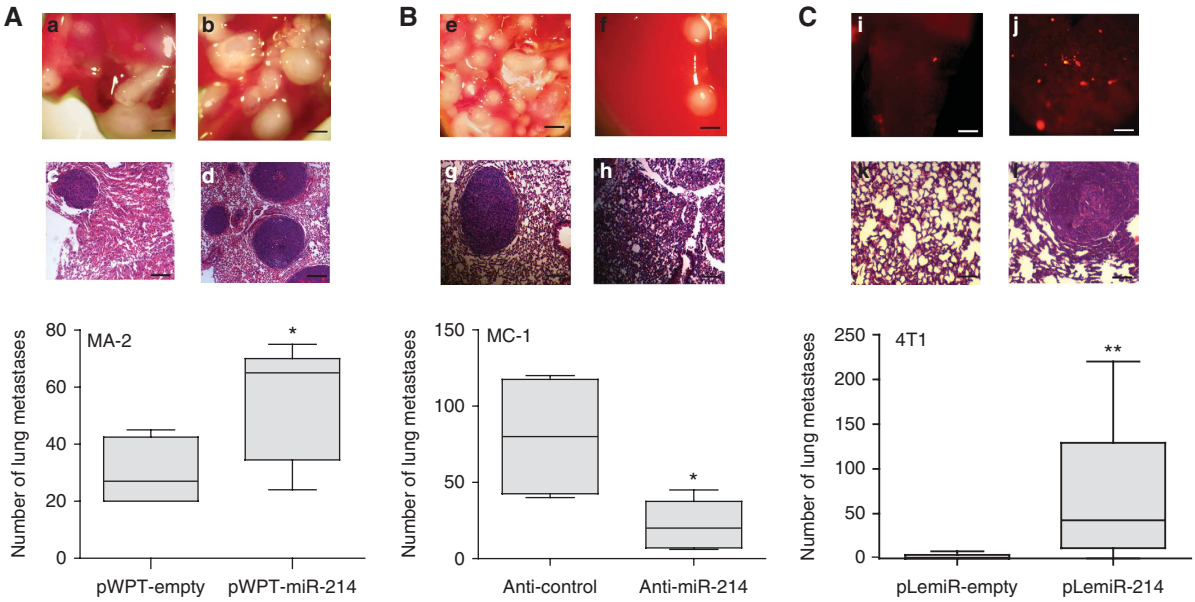

Figure 2 miR-214 enhances metastasis formation *in vivo*. (**A**, **B**) Metastasis formation in the lungs of SCID mice, 7 weeks after tail vein injection of MA-2 or MC-1 cells, stably transduced with pWPT-empty or miR-214 overexpression vectors (**A**) or transfected with miR-214 inhibitors or negative controls (anti-miR-214 or control) (**B**). Total number of macroscopic metastases per lung is shown as box and whiskers plots with median and minimum/maximum ($n = 5$ mice per group). (**C**) Lung metastasis formation 3 weeks after injection of 4T1 cells stably transduced with pLemiR-tRFP (pLemiR-empty) or pLemiR-miR-214 overexpression (pLemiR-214) vectors in the mammary fat pad of BALB/c mice. Number of red-fluorescent micrometastasis per lung is shown as mean ± s.e.m. for $n = 10$ mice per group. Representative whole lung (a, b, e, f, i and j) and H&E staining (c, d, g, h, k and l) pictures are shown; bar = 1 mm and 100 μm, respectively. Two independent experiments were performed and representative ones are shown (**A**, **B**) or results were pooled together (**C**). $^*P<0.05$; $^{**}P<0.01$.

metastatic ability of the cells and not to proliferation effects. In fact, miR-214 overexpression (pre-miR-214) in A375P and MA-2 cells or miR-214 silencing (anti-miR-214) in MC-1 cells did not influence *in vitro* proliferation compared with controls (Figure 3A and B). Moreover, anchorage-independent growth in soft agar was not affected, since the number and the size of colonies for stable miR-214-overexpressing (pWPT-miR-214) A375P and MA-2 cells were comparable with controls (pWPT-empty) (Figure 3C and D). Furthermore, miR-214 did not influence primary tumour growth. In fact, when miR-214-overexpressing (pWPT-miR-214) or control (pWPT-empty) A375P or MA-2 cells were subcutaneously injected in the flanks of nude mice, the final tumour weight was similar for the different samples (Figure 3E and F).

miR-214 modulates extravasation and survival

To assess the involvement of miR-214 in extravasation and survival, we combined *in vitro* and *in vivo* experiments. We first simulated transendothelial migration *in vitro* by seeding CMRA-labelled (red) miR-214-overexpressing (pre-miR-214) or control (pre-control) A375P or MA-2 cells in the upper chambers of fibronectin-coated transwells, covered by a confluent GFP-transduced human umbilical vein endothelial cell (HUVEC) monolayer. The remodelling of the endothelium and the consequent migration of melanoma cells in the lower chamber of the transwell were then evaluated (Figure 4A). The interaction of melanoma and endothelial cells induced the formation of fenestrations in the HUVEC monolayer. In the absence of melanoma cells (panel a) or in the presence of melanoma cell-conditioned medium (not shown), the HUVEC monolayer remains intact, suggesting the requirement of a direct cell–cell contact. Interestingly, the spaces formed in the endothelium were larger in the presence of miR-214-overexpressing A375P or MA-2 cells, compared with those formed with control cells (panels b, c, f and g) and, consequently, an increased number of cells migrated through the endothelial cells (panels d, e, h and i). In conclusion, miR-214 overexpression in A375P and MA-2 cells resulted in a 2–3-fold more efficient transendothelial migration. To evaluate the ability of miR-214 to influence extravasation *in vivo*, we first demonstrated that cell extravasation in the mouse lungs occurs within 48 h following injection of any metastatic variant in the blood circulation. For this, CMRA-labelled (red) negative control-transfected MC-1 (Figure 4B) or MA-2 (not shown) cells were injected in the tail vein of nude mice and their localization in the lungs was evaluated at different times. Two hours after injection, a high percentage of cells was located inside or associated with the lung blood vessels (Figure 4B, panel a), although some cells were already visible in the parenchyma (not shown). Forty-eight hours after injection, most of the cells present in the lungs appeared to be dispersed in the parenchyma (Figure 4B, panel b). To evaluate the role of miR-214 in the regulation of extravasation, CMRA-labelled miR-214-overexpressing A375P or MA-2 cells (pLemiR-214 or pre-miR-214, respectively) or silenced (anti-miR-214) MC-1 cells were injected *via* tail vein in nude mice and their ability to persist in the lungs was quantitated 48 h later. Two- or four-fold increased extravasation was observed, respectively, for miR-214-overexpressing A375P and MA-2 cells (Figure 4C, panels c, d, g and h), while about a 50% reduction in extravasation ability was observed for miR-214-silenced MC-1 cells (Figure 4C, panels k and l), compared with controls. This was not the consequence of a different lodging in the lung microvasculature, evaluated 2 h post-injection, since no difference was observed between

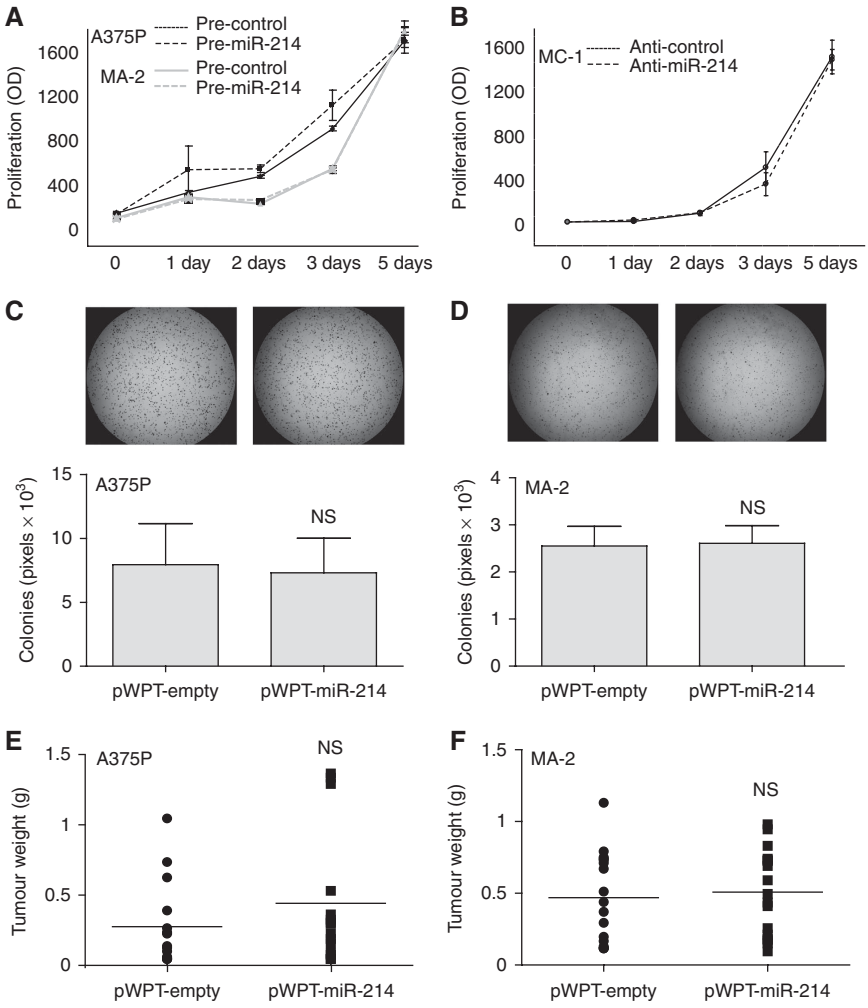

Figure 3 miR-214 does not affect cell and tumour growth. Proliferation (**A**, **B**) or anchorage-independent growth (**C**, **D**) or primary tumour growth 4 weeks after subcutaneous injection in the two flanks of nude mice (**E**, **F**) of cells transfected with miR-214 precursors or inhibitors or their negative controls (pre- and anti-miR-214 or control) or stably transduced with pWPT-empty or miR-214 overexpression vectors. Results are shown as mean ± s.e.m. of the optical density (OD) (**A**, **B**) or of the area covered by colonies (**C**, **D**) or as tumour weight (dots or squares) and mean for $n = 15$ (**E**) or 17 (**F**) mice per group. Two to four independent experiments were performed (in triplicate for **A**–**D**) and results were either shown as representative ones (**A**–**D**) or pooled together (**E**, **F**).

miR-214-modulated cells and negative controls (Figure 4C, panels a, b, e, f, i and j). *In vivo* extravasation experiments were also performed with CMRA-labelled MC-1 cells stably transduced with specific miR-214 sponge (pLenti-sponge3) or empty (pLenti-empty) vectors as in Supplementary Figure S2E. In line with transient anti-miR-214 experiments, MC-1 cells expressing pLenti-sponge3 showed a highly reduced (80–90%) ability to extravasate compared with control cells, 48 h post-injection, as measured in the red (CMRA) or green (GFP) channel (Supplementary Figure S5A and B). No difference in lodging was observed at 2 h. In addition to transendothelial migration and extravasation ability, resistance to apoptosis was evaluated following miR-214 expression modulation in cells kept in the absence of adhesion (*anoikis*) and serum for 72 h, by AnnexinV–FITC and TMRM staining and cytofluorimetric analyses. miR-214-overexpressing (pre-miR-214) A375P cells showed a 20–30% reduction in cell death versus controls (Figure 4D, left); consistently, miR-214 silencing (anti-miR-214) in MC-1 cells led to 20–30% increased cell death (Figure 4D, right) compared with controls, suggesting a miR-214-driven cooperative role between extravasation ability and resistance to *anoikis*.

miR-214 regulates the expression of a panel of target genes

miR-214's ability to coordinate the various steps of metastasis formation can be attributed to multiple direct and indirect regulation of target genes. To identify direct targets of miR-214, we first used different algorithms such as miRecords (Xiao *et al*, 2009), miRanda (John *et al*, 2004) and TargetScan 5.1 (Friedman *et al*, 2009) and obtained >2000 predicted genes containing one or more putative binding sites for this miR. Then, genes were functionally classified using the Ingenuity Systems Analysis software and a large number of genes involved in *Cancer* (557 genes; *P* from 5.96E-13 to 9.7E-04) and *Cellular Movement* (302 genes; *P* from 7.82E-11 to 1.05E-03) were identified. A panel of 11 putative targets predicted by at least one algorithm and present in one or both of the functional categories were selected for experimental validation. For this purpose, the 3′UTRs of these 11 genes were cloned into a reporter vector and luciferase assays

performed in MA-2 and/or MC-1 cells transfected with miR-214 precursors or negative controls (pre-miR-214 or control). As shown in Figure 5A, luciferase expression driven by the 3′UTRs of integrin α3 (ITGA3) or transcription factor AP-2γ (TFAP2C) was significantly repressed. No effect was revealed in the presence of the 3′UTRs of integrin β8 (ITGB8),

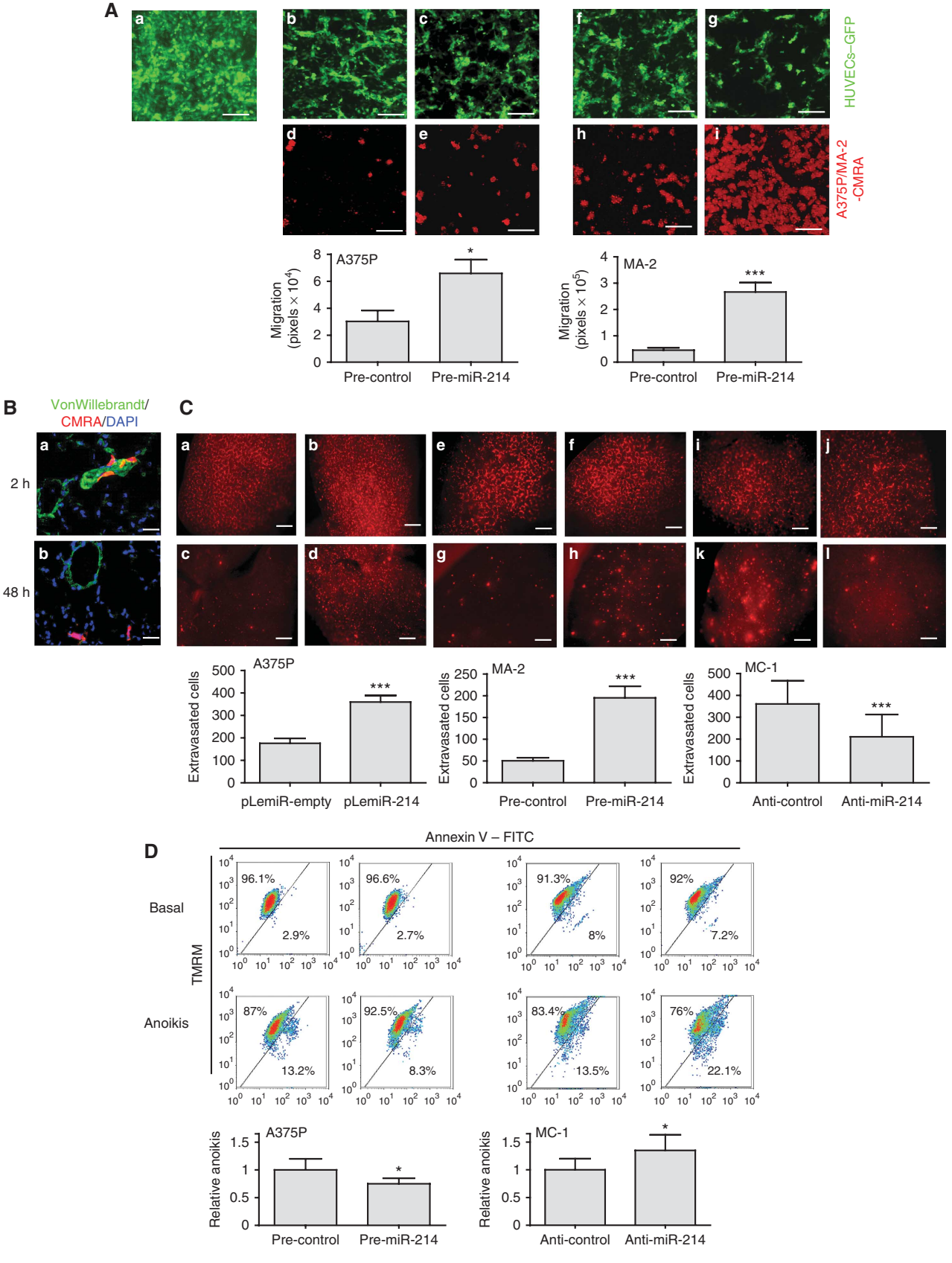

microphthalmia-associated transcription factor (MITF), neuropilin 1 (NRP1), plexinA1 (PLXNA1), phosphatase and tensin homologue (PTEN) and transcription factor AP-2α (TFAP2A) (Figure 5A). A slight luciferase repression was also observed in the presence of the p21 protein (Cdc42/Rac)-activated kinase 2 (PAK2) 3′UTR while, surprisingly, a strong induction of luciferase activity occurred in the presence of met proto-oncogene (MET) and Rho GTPase activating protein 12 (ARHGAP12) 3′UTRs (Supplementary Figure S6A). To assess if the ITGA3 and TFAP2C luciferase expression regulation depended on the binding between miR-214 seed and the complementary sequence present on the 3′UTRs of ITGA3 or TFAP2C, a four nucleotide deletion or three point mutations were inserted in the ITGA3 or TFAP2C 3′UTRs, respectively, as indicated in Figure 5B, left. Both 3′UTR alterations completely abrogated the effect of miR-214 overexpression on luciferase expression in MC-1 (Figure 5B, right), A375P and MA-2 cells (not shown) indicating the specific and direct regulation of miR-214 on ITGA3 and TFAP2C 3′UTR binding sites in our A375P isogenic model. Similar results were obtained also in unrelated melanoma cell lines such as WK-Mel (Supplementary Figure S7A) or GR4-Mel (not shown) transfected with miR-214 precursors or negative controls. As a positive control, a miR-214-sensor construct, containing three perfect bindings for miR-214, was used for each experiment (Figure 5A and B; Supplementary Figures S6A and S7A). ITGA3 and TFAP2C modulations in luciferase activity corresponded to fluctuations of endogenous protein levels following transient miR-214 overexpression (pre-miR-214) in MA-2, WK-Mel, GR4-Mel (Figure 5C; Supplementary Figure S7C and D) or A375P and 1300-Mel (not shown) cells or miR-214 inhibition (anti-miR-214) in MC-1 cells (Figure 5C), as measured by WB analyses 48 h (not shown) or 72 h post-transfection. miR-214 overexpression led to a 30–90% and 40–80% protein decrease in ITGA3 and TFAP2C, respectively (Figure 5C; Supplementary Figure S7C and D). Reduction of protein expression was also observed in stable miR-214-overexpressing (pWPT-miR-214) MA-2 cells (10 and 15% decrease) compared with controls (Supplementary Figure S7B). Consistently, ITGA3 a nd TFAP2C proteins were upregulated (20 and 40%, respectively) in miR-214-silenced MC-1 cells (Figure 5C). Additionally, following transient miR-214 overexpression (pre-miR-214) in MA-2 cells, TFAP2C mRNA was significantly reduced, while ITGA3 mRNA showed a non-statistically significant decrease, as measured by qRT–PCR analyses 48 h post-transfection (Figure 5D).

Consistent with the luciferase results, MET protein levels showed a 60 or 10% induction, respectively, following transient or stable miR-214 overexpression (Supplementary Figure S6B and D), which corresponded to mRNA fluctuations (Supplementary Figure S6E) and a 60% reduction following miR-214 silencing (Supplementary Figure S6C). Slight changes were also detected for PAK2 or PTEN protein expression following miR-214 overexpression or downmodulation, but no mRNA modulations were observed (Supplementary Figure S6B, C and E). Similarly, no mRNA changes were observed for ARHGAP12, ITGB8, MITF and NRP1, while a slight PLXNA1 mRNA decrease was found (Supplementary Figure S6E). On the contrary, TFAP2A was well modulated both at the protein and at the mRNA level (Supplementary Figure S6B and E); however, considering that TFAP2A is only slightly expressed in these melanoma cells.

In parallel, we used a proteomic approach to identify miR-214-modulated surface proteins. The expression profile for 119 surface molecules involved in cell adhesion and movement was evaluated in MA-2 cells 72 h after transfection with miR-214 or control precursors; 65 differentially expressed molecules were found, 36 upregulated and 29 downregulated, following miR-214 overexpression (Table I; Figure 5E). Twenty-five modulated genes were predicted targets of miR-214 (Table I) and 17 genes, miR-214 predicted targets or not, were previously proven to be transcriptionally regulated by members of the AP-2 transcription factor family (TFAP2) or to contain TFAP2 binding sites in their promoters (Table I), suggesting a possible TFAP2-driven modulation in our melanoma model. Since it is well established that TFAP2 proteins contribute to melanoma progression *via* transcriptional regulation of key genes, we evaluated the expression of known TFAP2-activated or -repressed transcriptional targets by qRT–PCR, following miR-214 overexpression in MA-2 cells (pre-miR-214) compared with negative controls (pre-control). As shown in Figure 6A, the TFAP2-activated genes, ERBB2, IGFBP5 and TGFB, were found to be downregulated in the presence of miR-214, while the TFAP2-repressed genes, MCAM-MUC18 and VEGFA, but not MMP2, were upregulated (eight-fold and two-fold, respectively). Taken together, the direct or indirect TFAP2-dependent protein or mRNA modulations suggest that TFAP2 family members could have a relevant role in miR-214-dependent enhancement of melanoma malignancy.

Connections between 70 protein-coding genes found to be modulated in a direct or indirect manner by miR-214 (65 surface molecules in addition to ITGA3, MET, PAK2, TFAP2A and TFAP2C; Figure 5; Supplementary Figure S6; Table I) were searched using the Ingenuity Systems Analysis. Two main networks were identified, such as *Tissue Development*, *Cellular Movement*, *Cell Cycle* (Supplementary Figure S8A)

Figure 4 miR-214 promotes extravasation and cell survival. (**A**) Transendothelial migration assays of CMRA-labelled (red) cells, through a fibronectin-coated transwell membrane covered by a confluent monolayer of HUVECs–GFP. Upper panels: HUVECs–GFP monolayer on the upper side of the transwell at time 0 h (a) or 18 h following the seeding of A375P (b, c) or MA-2 (f, g) cells transfected with miR-214 precursors or negative controls (pre-miR-214 or control). Lower panels: transmigrated A375P (d, e) or MA-2 (h, i) cells transfected as indicated, on the lower side of the transwell. (**B**, **C**) *In vivo* extravasation assays following tail vein injections in nude mice of CMRA-labelled (red) A375P cells stably transduced with pLemiR-empty or pLemiR-214 vectors, or MA-2 cells transfected as in (**A**) or MC-1 cells transfected with miR-214 inhibitors or negative controls (anti-miR-214 or control). (**B**) Representative fields of murine lung sections 2 h (a) or 48 h (b) post-injections, stained for VonWillebrandt factor (green) and counterstained with DAPI (blue). (**C**) CMRA-labelled cells in whole lungs 2 h (a, b, e, f, i and j) or 48 h (c, d, g, h, k and l) post-injections. Results are shown as mean ± s.e.m. of the area covered by migrated cells (**A**) or of the number of extravasated cells at 48 h for $n = 10$ (A375P), 7 (MA-2) or 5 (MC-1) mice per group (**C**). Two independent experiments were performed (in triplicate for (**A**)) and representative ones are shown. Bar = 30 μm (**A**), 10 μm (**B**) or 500 μm (**C**). (**D**) *Anoikis* assays for A375P or MC-1 cells transfected as in (**C**). Cell death percentage was evaluated by TMRM and AnnexinV–FITC stainings, displayed in bidimensional plots. ^{High}TMRM–^{Low}AnnexinV gate: healthy population; ^{Low}TMRM–^{High}AnnexinV gate: apoptotic population. Four independent experiments were performed in duplicate and pooled quantitations refer to fold increased or decreased cell death versus controls, shown as mean ± s.e.m. $^{*}P<0.05$; $^{***}P<0.001$.

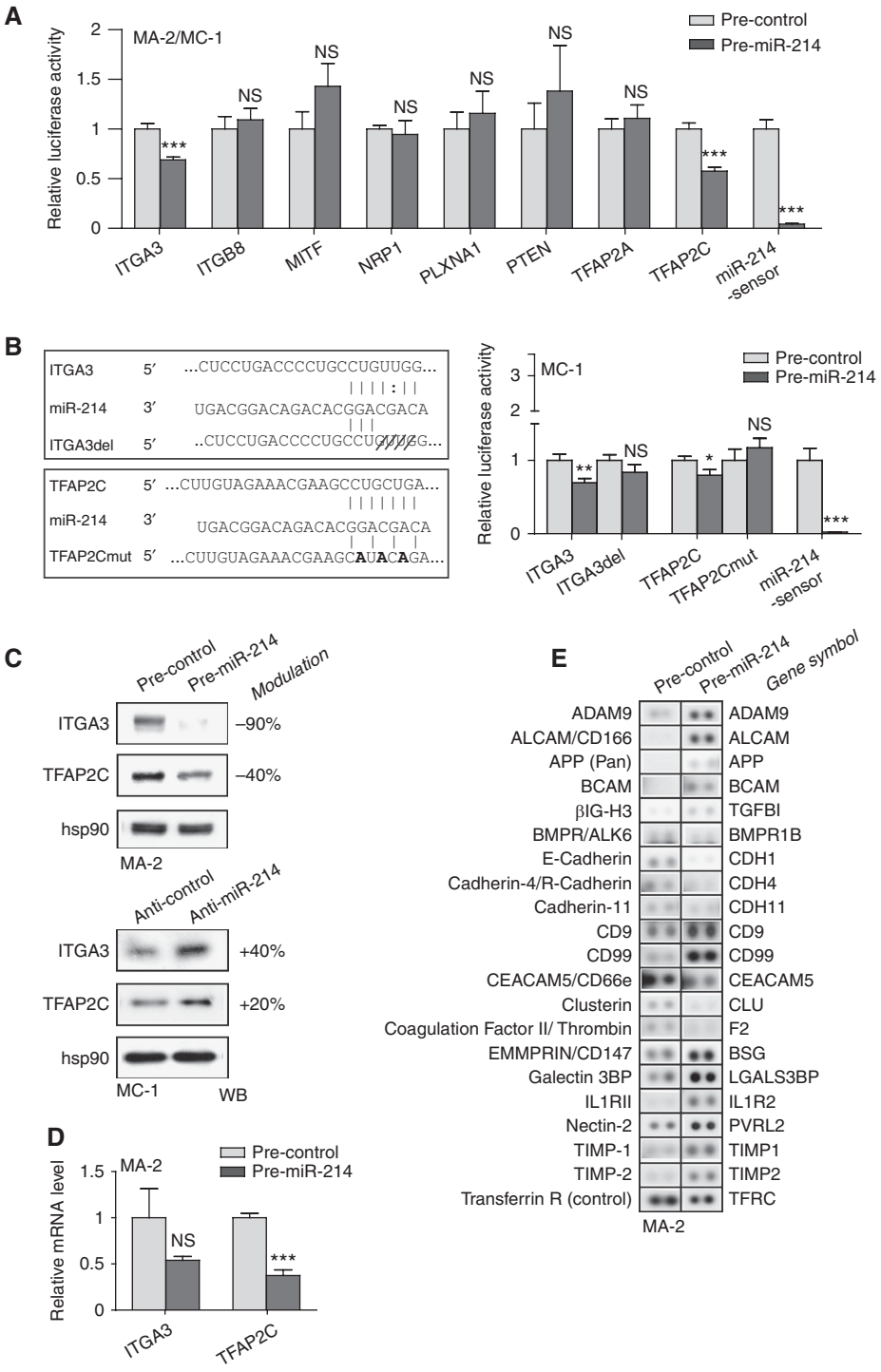

Figure 5 miR-214 downregulates TFAP2C and ITGA3 target genes and modulates multiple surface proteins. (**A**) Luciferase assays in MA-2 or MC-1 cells cotransfected with reporter constructs containing the 3′UTR of the indicated genes or a synthetic sequence including three perfect miR-214 binding sites (miR-214-sensor), cloned downstream of the luciferase coding sequence, together with miR-214 precursors or negative controls (pre-miR-214 or control). (**B**) Left panel: wild-type and miR-214 binding site mutant or deletant (ITGA3del, TFAP2Cmut) ITGA3 or TFAP2C 3′UTRs paired with miR-214 seed (respectively at positions 624 and 1071 of their 3′UTRs). Right panel: luciferase assays in cells cotransfected with wild-type or mutant 3′UTR reporter constructs, together with miR-214 precursors or negative controls (pre-miR-214 or control). Results are shown as mean ± s.e.m. of Firefly luciferase activity relative to controls, normalized on Renilla luciferase activity. (**C**) Western blot (WB) analysis of ITGA3 and TFAP2C protein levels in MA-2 or MC-1 cells 72 h after transfections with miR-214 precursors or inhibitors or their negative controls (pre- and anti-miR-214 or control). Protein modulations were calculated relative to controls, normalized on the hsp90 loading control and expressed as percentages. (**D**) ITGA3 and TFAP2C mRNA levels measured by qRT–PCR in MA-2 cells 48 h after transfection as in (**C**, top). Results were calculated as fold changes (mean ± s.e.m.) relative to controls, normalized on GAPDH. Three independent experiments were performed (in triplicate for (**A**, **B**); with independent protein or RNA preparations for (**C**, **D**)) and representative ones are shown. (**E**) Representative protein expression obtained for MA-2 cells 72 h after transfection with miR-214 precursors or negative controls (pre-miR-214 or control) by Proteome Profiler Human Soluble Receptor Antibody Arrays. Transferrin R was used as loading control. Doublets are shown. Two independent experiments were performed, a representative one is shown. Refer to Table I. $*P<0.05$; $**P<0.01$; $***P<0.001$.

Table I miR-214 modulates multiple surface molecules involved in cell movement and adhesion

Protein	Gene symbol	Pre-miR-214/control FC	Up/down	miR-214 target	TFAP2-dependent modulations
ADAM15	ADAM15	1.6	Up		
ADAM8	ADAM8	1.6	Up	Y	
ADAM9	ADAM9	2.5	Up		
ALCAM/CD166	ALCAM	6.0	Up		
APP (pan)	APP	1.8	Up		Provenzano *et al* (2007)
BCAM	BCAM	1.9	Up	Y	
βIG-H3	TGFBI	2.3	Up		Orso *et al* (2008)
BMPR-IB/ALK-6	BMPR1B	−1.8	Down	Y	
Cadherin-11	CDH11	−1.2	Down	Y	Borchers *et al* (2001)
Cadherin-4/R-Cadherin	CDH4	−1.8	Down	Y	
Cathepsin D	CTSD	−1.2	Down	Y	Redecker *et al* (1991)
CD155/PVR	PVR	1.4	Up		Solecki *et al* (1999)
CD23/FcRII	FCER2	3.1	Up		
CD36/SR-B3	CD36	1.7	Up		
CD40 Ligand/TNFSF5	CD40LG	1.3	Up		
CD40/TNFRSF5	CD40	−1.5	Down		
CD44H	CD44	1.7	Up		
CD9	CD9	2.4	Up		
CD90/Thy1	THY1	1.6	Up		
CD99	CD99	1.8	Up		
CEACAM-1/CD66a	CEACAM1	1.4	Up		
CEACAM-5/CD66e	CEACAM5	−2.0	Down		
Clusterin	CLU	−2.0	Down		Bayon *et al* (2004)
Coagulation factor II/Thrombin	F2	−2.1	Down		
CX3CL1/Fractalkine	CX3CL1	1.7	Up	Y	
CXCL8/IL-8	IL8	1.4	Up	Y	
E-Cadherin	CDH1	−1.7	Down	Y	Schwartz *et al* (2007)
EGF R/ErbB1	EGFR	−1.6	Down	Y	Wang *et al* (2006)
EMMPRIN/CD147	BSG	1.8	Up	Y	
Endoglin/CD105	ENG	1.6	Up	Y	Rìus *et al* (1998)
Endoglycan	PODXL2	−1.4	Down		
EpCAM/TROP-1	EPCAM	−1.5	Down		
Epiregulin	EREG	1.2	Up		Orso *et al* (2008)
ErbB2/HER2	ERBB2	−1.4	Down	Y	Bosher *et al* (1996)
ErbB3/HER3	ERBB3	−1.7	Down		
E-Selectin/CD62e	SELE	−1.9	Down		
Galectin-3BP/MAC-2BP	LGALS3BP	2.7	Up		
HB-EGF	HBEGF	1.7	Up		
HPRG	HRG	1.2	Up		
ICAM-2/CD102	ICAM2	1.6	Up		Grether-Beck *et al* (1996)
IL-1 RII	IL1R2	2.2	Up		
Integrin α6/CD49f	ITGA6	−1.5	Down		
Integrin αV/CD51	ITGAV	−1.4	Down		Kambe *et al* (1998)
Integrin β1/CD29	ITGB1	1.7	Up		
Integrin β3/CD61	ITGB3	1.6	Up		
JAM-A	JAM1	−1.6	Down	Y	
JAM-B	JAM2	−1.5	Down		
JAM-C	JAM3	−1.4	Down	Y	
Jagged 1	JAG1	−1.2	Down	Y	
Lipocalin-2/NGAL	LCN2	1.5	Up		
LRP-6	LRP6	−1.5	Down	Y	
MMP-2 (total)	MMP2	1.5	Up	Y	Nyormoi *et al* (2003)
MUCDHL	CDHR5	1.4	Up		
N-Cadherin	CDH2	−1.5	Down	Y	
NCAM-1/CD56	NCAM1	1.6	Up	Y	
Nectin-2/CD112	PVRL2	2.1	Up	Y	Lui *et al* (2007)
Periostin/OSF-2	POSTN	−1.3	Down		
Podocalyxin	PODXL	−1.5	Down	Y	
Semaphorin 3A	SEMA3A	−1.6	Down		
TIMP-1	TIMP1	2.0	Up		Clark *et al* (1997)
TIMP-2	TIMP2	2.2	Up	Y	Hammani *et al* (1996)
TIMP-3	TIMP3	1.4	Up	Y	
VCAM-1	VCAM1	−1.2	Down		
VEGF R1/Flt1	FLT1	−1.3	Down		
VEGF R2/KDR2/Flk-1	KDR	−1.5	Down	Y	

Expression modulation of 65 out of 119 surface proteins in MA-2 cells 72 h after transfection with miR-214 precursors or negative controls (pre-miR-214 or control), obtained by Proteome Profiler Human Soluble Receptor Antibody Arrays (see also Figure 5E). Modulations are expressed as fold change (FC) referring to miR-214-overexpressing cells versus controls, normalized on Transferrin R expression levels. Y, predicted miR-214 target. Literature references indicate previously demonstrated TFAP2 family members-mediated gene regulation (see references in Supplementary data).

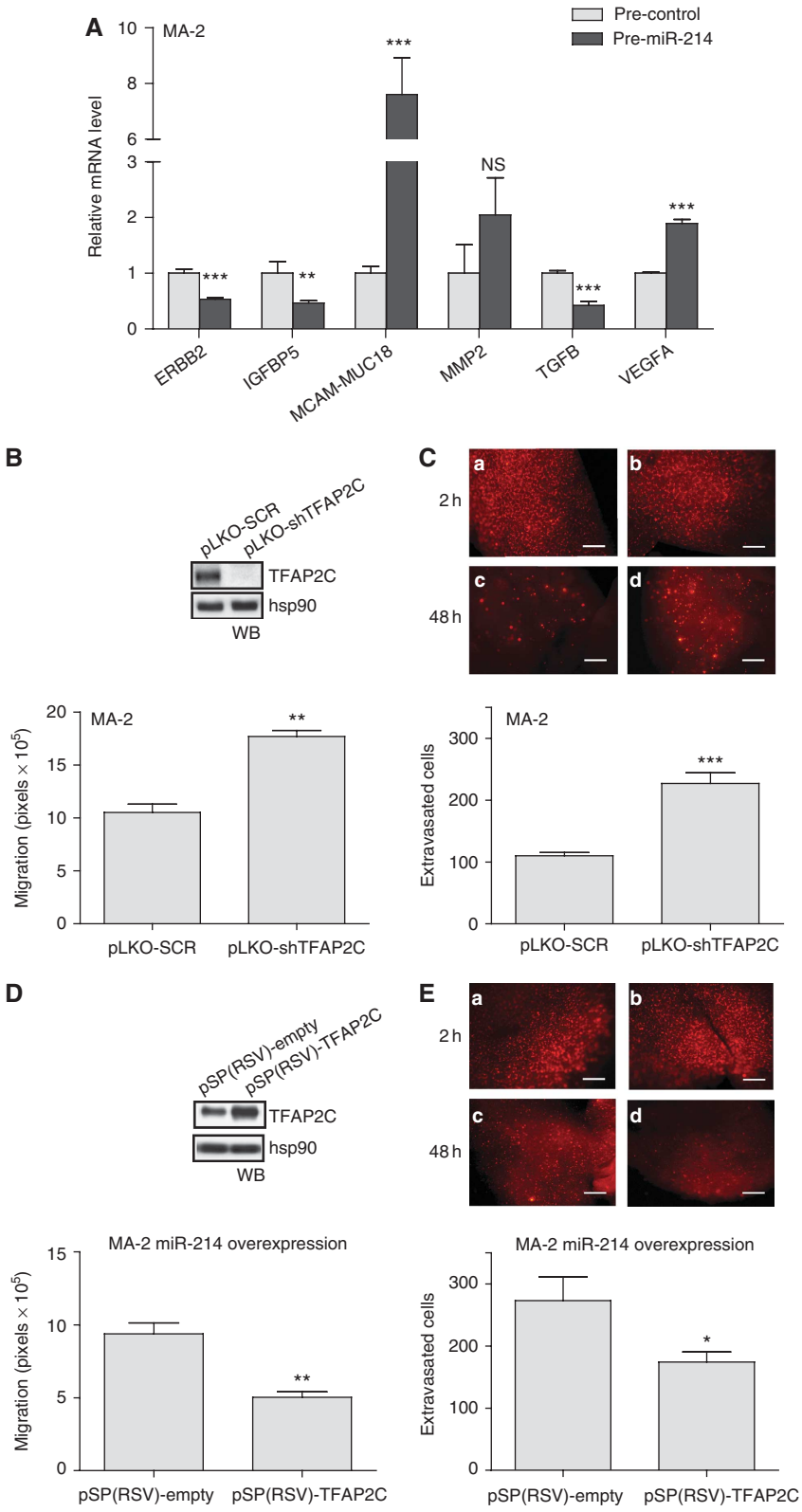

Figure 6 miR-214-mediated downmodulation of TFAP2C accounts for miR-214 functions. (**A**) mRNA levels for the indicated genes measured by qRT–PCR in MA-2 cells 48 h after transfection of miR-214 precursors or negative controls (pre-miR-214 or control). Results were calculated as fold changes (mean ± s.e.m.) relative to controls, normalized on GAPDH. (**B**, **D**) Transwell migration assays for cells stably transduced with TFAP2C-targeting or negative control scramble shRNA vectors (pLKO-shTFAP2C or SCR) (**B**) or first transduced with pLemiR-214 and then transfected with either pSP(RSV)-empty or TFAP2C expression vectors (**D**). In the boxes: western blot (WB) showing TFAP2C protein levels. (**C**, **E**) *In vivo* extravasation assays 2 h (a, b) or 48 h (c, d) following tail vein injection in nude mice of the cells described in (**B**, **D**), previously labelled with CMRA (red). Representative pictures of the lungs are shown; bar = 500 μm. Results are presented as mean ± s.e.m. of the area covered by migrated cells (**B**, **D**) or of the number of extravasated cells at 48 h for $n = 10$ (**C**) or 5 (**E**) mice per group. Two to three independent experiments were performed (in triplicate for (**A**, **B**, **D**)) and results were either shown as representative ones or pooled together (**C**). $^{*}P < 0.05$; $^{**}P < 0.01$; $^{***}P < 0.001$.

and *Cell-To-Cell Signalling and Interaction*, *Tissue Development*, *Embryonic Development* (Supplementary Figure S8B). A top pathway was also identified, *Leukocyte Extravasation Signalling* (not shown), including CD44, CD99, ITGB1, MMP2, JAM2, JAM3, VCAM1 and TIMPs, genes potentially involved in tumour cell movement and blood vessel extravasation.

miR-214-mediated downmodulation of TFAP2C and ITGA3 controls miR-214 functions

As presented above, miR-214 is able to modulate TFAP2C and genes known to be transcriptionally regulated by the TFAP2 family members. To investigate if the metastatic effects of miR-214 in this melanoma model could be explained, in part, *via* its TFAP2C target we first analysed how TFAP2C silencing affected *in vitro* and *in vivo* cell movement. MA-2 cells were transduced with either specific TFAP2C or scramble negative control (pLKO-shTFAP2C or SCR) shRNA lentiviral vectors, leading to almost complete silencing of TFAP2C expression as measured by WB analysis (Figure 6B, top). TFAP2C-silenced cells were used for *in vitro* cell migration and *in vivo* extravasation experiments leading to results that phenocopied miR-214 overexpression. Indeed, >1.5-fold increased *in vitro* cell migration (Figure 6B) and extravasation in the lungs 48 h following tail vein injections (Figure 6C, panels c and d) were observed. No effect on the initial lodging of silenced cells in the lung vasculature 2 h post-injection was observed (Figure 6C, panels a and b). Hence, we asked whether the pro-metastatic phenotype associated with miR-214 overexpression could be rescued by TFAP2C overexpression in miR-214-overexpressing cells. For this purpose, a TFAP2C expression construct lacking its 3′UTR (pSP(RSV)-TFAP2C) was transiently transfected in stable miR-214-overexpressing MA-2 cells (Supplementary Figure S2C), as shown by WB in Figure 6D, top. Remarkably, a 40% decrease in *in vitro* cell migration (Figure 6D) and a significant impairment of *in vivo* lung extravasation at 48 h (Figure 6E) were observed compared with pSP(RSV)-empty controls. In conclusion, these experiments proved that TFAP2C is a major functional player downstream of miR-214, in fact, its direct repression by miR-214 contributes to increased melanoma pro-metastatic traits.

The functional impact of ITGA3 modulation *via* miR-214 was evaluated with similar approaches, by *in vitro* migration and *in vivo* extravasation assays. For this purpose, ITGA3 was silenced in MA-2 cells following transfections with specific siRNAs (si-ITGA3), leading to strong protein downregulation compared with negative control cells (si-control), as evaluated by WB (Supplementary Figure S9A, top). In parallel, ITGA3 overexpression was obtained in miR-214-overexpressing MA-2 cells following transfection with a 3′UTR-deprived ITGA3 expression construct (pCMVzeo-ITGA3), compared with control (pCMVzeo-empty) cells (Supplementary Figure S9C, top). A significant increase in cell migration (Supplementary Figure S9A) was found in ITGA3-silenced cells, compared with controls, while decreased cell migration (Supplementary Figure S9C) was found for miR-214/ITGA3-overexpressing cells compared with controls. In contrast, lung extravasation of CMRA-labelled cells, 48 h post-injection as well as the lodging in the lung vasculature 2 h post-injection were not affected by ITGA3 silencing or overexpression (Supplementary Figures S9B and D). This observation is reinforced by the fact that long-term metastasis formation, 7 weeks following tail vein injection, was also not affected by ITGA3 overexpression in miR-214-overexpressing MA-2 cells (not shown).

Finally, the effect of TFAP2C on ITGA3 and MET protein expression was evaluated in MA-2 cells following TFAP2C silencing or overexpression. As shown in Supplementary Figure S10, only a slight protein modulation was observed for ITGA3 following TFAP2C silencing (10% reduction, left) or overexpression (10% increase, right). In contrast, MET protein expression strongly increased (over 100%) following stable TFAP2C silencing and decreased (20% reduction) when TFAP2C was transiently overexpressed (Supplementary Figure S10). These data suggest that the miR-214-dependent regulation of MET and ITGA3 is at least in part mediated by TFAP2C.

Expression of miR-214 and its modulated genes in human melanoma tumours

qRT–PCR analysis was used to assess miR-214 expression in human primary melanocytes (two preparations), *in situ* melanomas, confined into the basal membrane ($n=13$), primary invasive melanomas ($n=57$) and cutaneous metastases ($n=18$). As shown in Figure 7A, miR-214 was highly expressed in primary and metastatic melanomas, compared with *in situ* tumours and normal melanocytes. Instead, miR-210 expression, which we used as control, did not vary significantly among tumour samples; however, low miR-210 levels were found in primary melanocytes (Figure 7B). Considering the elevated levels of miR-214 in invasive melanomas and in metastases, we investigated the expression of over 70 miR-214-modulated genes (Figures 5 and 7C; Supplementary Figure S6; Table I) in a human protein-coding gene expression data set available in GEO, referring to mRNA expression in normal skin, nevi and primary melanomas (Talantov *et al*, 2005). Differential expression was observed for several of these genes relative to the three groups of samples analysed (Supplementary Figure S11), underlying the relevance of this gene group for melanoma progression. In agreement with our findings, TFAP2C mRNA was downregulated in melanoma but expressed in skin as well as nevus samples; in contrast, ITGA3 mRNA was upregulated in this cohort of melanomas, suggesting different or additional regulations.

Discussion

Our work led to the identification of a novel functional pathway (Figure 7C), controlled by miR-214 and including its direct targets TFAP2C and ITGA3 as well as multiple surface proteins, that coordinates metastasis formation in a melanoma progression model, represented by the A375P poorly metastatic parental cell line and its derived metastatic variants. This pathway can be considered of general relevance for melanoma progression since it was also studied and validated in a panel of unrelated human melanoma cell lines. Importantly, overexpression of miR-214 or silencing of TFAP2C in melanoma cells enables them to acquire or increase invasive and metastatic behaviour. On the other hand, miR-214 silencing or concomitant miR-214 and TFAP2C (lacking its 3′UTR) overexpression impairs the establishment of a metastatic phenotype, suggesting a major role for miR-214 and TFAP2C in controlling melanoma tumour progression.

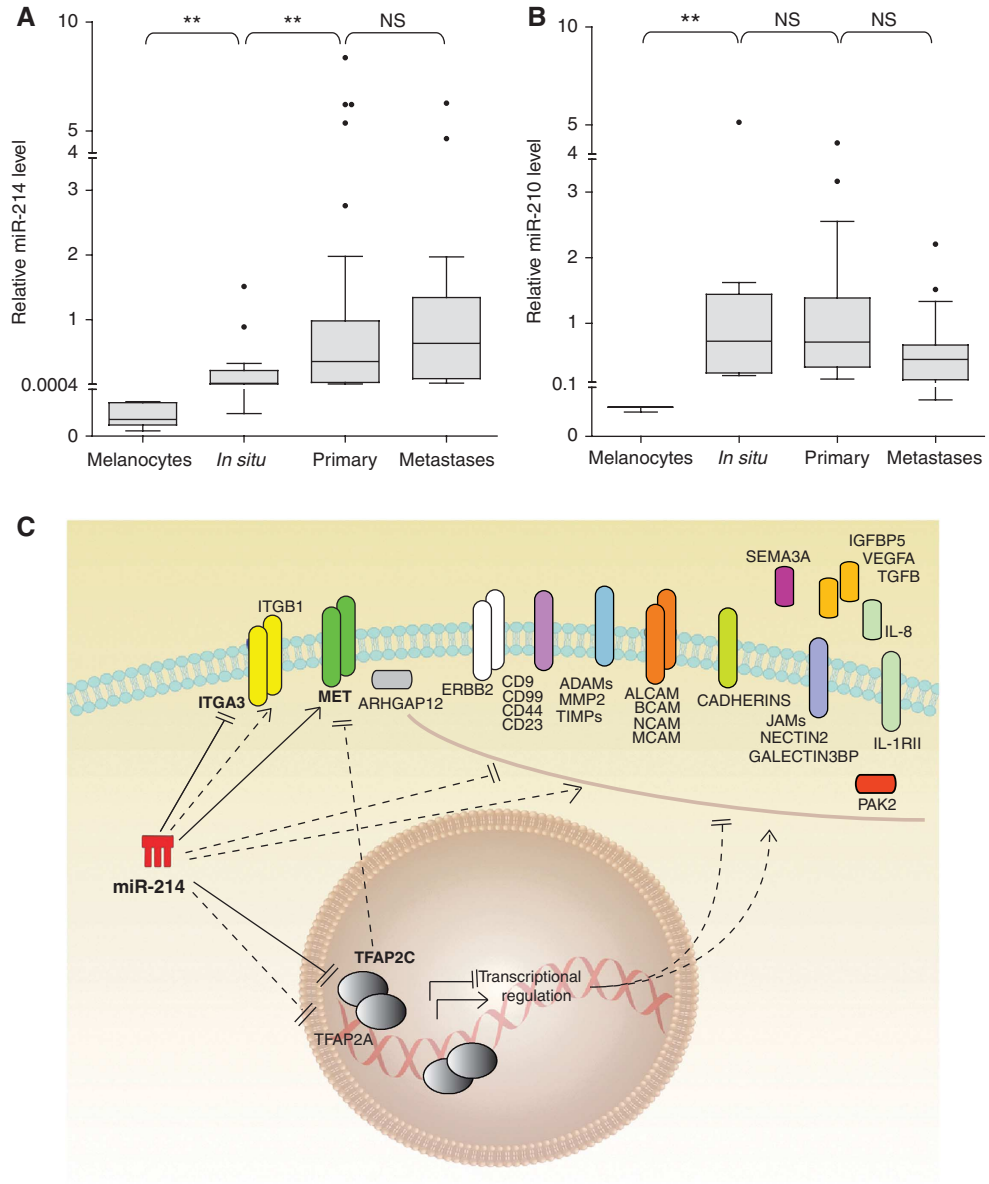

Figure 7 miR-214 is expressed in human melanomas and modulates multiple genes. (**A**, **B**) miR-214 (**A**) and miR-210 (**B**) expression levels were evaluated by qRT–PCR in human primary melanocytes (two independent preparations), *in situ* melanomas ($n=13$), primary melanomas ($n=57$) and cutaneous metastases ($n=18$). miR levels are shown as box and whisker plots; the bottom and the top indicate the 25th and 75th percentile (the lower and upper quartile, respectively), the band inside the box is the 50th percentile and the dots represent the outliers. Relative expression was calculated using the healthy skin miR median expression as reference and normalized on U44 RNA level. Statistical analysis was performed with the Mann–Whitney non-parametric statistical test. (**C**) Drawing summarizing the miR-214-modulated genes identified in this study and their connections. Continuous lines: miR-214 direct (luciferase proven) regulations; dashed lines: indirect regulations. $^{*}P<0.05$; $^{**}P<0.01$.

In agreement with our findings, also high-throughput screenings showed that miR-214 is strongly expressed in malignant cutaneous and ocular melanomas (Worley *et al*, 2008; Segura *et al*, 2010) as well as in various solid tumours, such as pancreas, prostate, gastric, breast and ovary cancers (Volinia *et al*, 2006; Blenkiron *et al*, 2007; Sempere *et al*, 2007; Yang *et al*, 2008; Ueda *et al*, 2010); thus, it will be fundamental to understand the mechanism of miR-214 overexpression in tumours. We showed that gene amplification for miR-214 locus occurs in A375P, MA-2 and MC-1 variants as well as in other melanoma cells. In addition, a main study of Comparative genomic hybridization demonstrated copy number gain in miR-214 locus for various melanomas, ovarian and breast cancer samples (Zhang *et al*, 2006). However, it was previously demonstrated that miR-214 is transcriptionally regulated by Twist-1 (Lee *et al*, 2009; Yin *et al*, 2010) and by Polycomb protein complex (Juan *et al*, 2009), suggesting important transcriptional controls for miR-214. The fact that miR-214 expression is generally low or undetectable in culture while it increases dramatically when cells are injected *in vivo*, i.e., tumours or lung metastases, suggests an essential regulation by the microenvironment, possibly involving secreted growth factors or cytokines or cell-to-cell contacts, currently under investigation.

So far, miR-214 was proposed to be mostly involved during differentiation and morphogenesis of tissues and organs

(Flynt *et al*, 2007; Decembrini *et al*, 2009) and disruption of the mouse genomic locus including miR-214, *Dnm3os*, determined death within 1 month of birth with skeletal abnormalities (Watanabe *et al*, 2008). Considering that genetic programs controlling embryonic development are often reactivated during tumour progression, a role for miR-214 in tumourigenesis is expected. High levels of miR-214 in human tumours suggest an oncogene-like function, but we and others (Fei *et al*, 2008) did not find any positive regulation of cell growth for miR-214. Instead, increased levels of miR-214 could induce chemotherapy resistance in ovarian tumours *via* the direct downregulation of PTEN and consequent upregulation of the Akt pathway (Yang *et al*, 2008); however, we were not able to see any strong miR-214-dependent downmodulation of PTEN, suggesting a cell context role in PTEN targeting by miR-214.

The spread of melanoma cells from the primary lesion to the sites of metastasis formation involves multiple steps (Melnikova and Bar-Eli, 2008) that are coordinated by miR-214. Other miRs were previously found to be involved in some aspects of melanoma tumourigenesis: miR-221/222 and let7b mostly control proliferation and survival, while miR-182, miR-137, let7a and miR-34a affect migration and invasion as well as cell growth (Mueller and Bosserhoff, 2009). miR-214 exerts pleiotropic roles in our melanoma model due to its ability to directly or indirectly modulate the expression of many genes. We were able to identify over 70 miR-214-modulated genes that were previously found to be involved in cell movement and metastasis formation, some specifically in melanoma. Examples are integrins (Desgrosellier and Cheresh, 2010), cadherins (Jeanes *et al*, 2008), cell adhesion molecules (Kobayashi *et al*, 2007), the tyrosine kinase receptor MET (Benvenuti and Comoglio, 2007), MMP2 (Hornebeck *et al*, 2002), ADAMs (Duffy *et al*, 2009), TIMPs (Cruz-Munoz and Khokha, 2008), Semaphorin3A (Neufeld and Kessler, 2008) and PAK2 (Gadea *et al*, 2008). In addition to cell migration and invasion, we showed, for the first time, that a miR promotes transendothelial migration and extravasation of melanoma cells *via* direct tumour-endothelial cell interactions, as proven by the fact that melanoma cells but not conditioned medium are able to induce endothelial cell reorganization. Based on the extravasation experiments, we suggest that miR-214 pro-metastatic effect is mainly due to the earlier steps of the metastatic process, such as the passage through the endothelial barrier, more then post-colonization events. In fact, we observed a significant reduction in both extravasation (48 h) and long-term metastasis formation following transient silencing of miR-214 in cells, a condition in which we expected miR-214 levels to remain low only in the first 48 h post-transfection, as observed in *in vitro* experiments (not shown). Considering that extravasation data were confirmed by permanent knockdown of miR-214 via specific sponges and that miR-214 did not influence tumour cell growth, we can conclude that high levels of miR-214 favour extravasation and survival in the blood circulation but do not control later tumourigenesis steps. Heterotypic interactions are known to occur between endothelial and melanoma cells during extravasation involving, for instance, the CAM family molecules, such as ALCAM (Swart *et al*, 2005) and MCAM-MUC18 (Xie *et al*, 1997), or tetraspanin CD9 and ITGB1 complexes at the melanoma-endothelial cell contact regions (Longo *et al*, 2001), or IL-8 secretion, ICAM-1 expression and E-selectin reduction, as a consequence of B-Raf mutation in melanoma cells (Liang *et al*, 2007). Interestingly, these molecules are modulated by miR-214 in our cells (see Table I). Given that B-Raf is mutated in our melanoma model (Eskandarpour *et al*, 2005), a possible cooperation between B-Raf and miR-214 could occur during extravasation. Moreover, functional classification of miR-214-modulated molecules revealed an enrichment of genes involved in the leukocyte extravasation pathway, suggesting a common mechanism of migration through the endothelial walls for melanoma cells and leukocytes. Since miR-214 reduces *anoikis* in cell culture, we speculate that miR-214 also helps the tumour cells to survive in the blood circulation. Similar functions were shown for miR-31 in breast cancer (Valastyan *et al*, 2009). We found that miR-214 was able to confer various pro-metastatic traits also to the A375P parental cells; however, we observed only a slight effect on lung colonization in our experimental conditions. No macrometastases were found when miR-214-overexpressing or control A375P cells were injected. Nevertheless, micrometastases were detected exclusively for miR-214-overexpressing cells. These results suggest that miR-214 facilitates metastasis formation but it is not a strong metastasis inducer *per se* and that its role depends on the cellular context in which it operates. In any case, we cannot exclude that different experimental settings were needed for these investigations.

Based on bioinformatic predictions we looked for direct miR-214 targets and among various genes tested, we were able to prove that TFAP2C and ITGA3 are directly and specifically repressed *via* miR-214 binding on their 3′UTRs in melanoma cells. At the same time, we observed that miR-214 was able to induce MET overexpression. TFAP2C is a member of the AP-2 transcription factor family involved, together with TFAP2A, in the activation or repression of various genes implicated in tumourigenesis (Hilger-Eversheim *et al*, 2000; Eckert *et al*, 2005). Melanoma progression is clearly associated with loss of expression of total or nuclear TFAP2 proteins and this correlates with poor prognosis and advanced stages of the disease (Bar-Eli, 2001; Berger *et al*, 2005). Loss or deletions of the TFAP2 family member genomic loci were found in some, but not all, melanomas, suggesting other mechanisms for control of gene expression (Karjalainen *et al*, 2000). We were able to demonstrate that miR-214 downregulates expression of TFAP2C directly and TFAP2A indirectly in melanoma cells. We need to underline that only low TFAP2A protein expression was detected in the melanoma progression model we used, consistent with the fact that A375P cells were derived from a metastatic melanoma with low TFAP2A amount (Huang *et al*, 1998). Instead, TFAP2C is well expressed in our system, although at reduced levels in the most invasive variant MC-1 compared with the parental A375P cells due to miR-214 higher expression. Reduction of TFAP2A is, at least in part, due to direct control by TFAP2C, since TFAP2C silencing reduces TFAP2A protein levels partially (Orso *et al*, unpublished), which is in line with the fact that TFAP2 family members are able to regulate each other transcriptionally (Bauer *et al*, 1994). It is known that elimination of TFAP2A from non-metastatic primary melanoma cells increases malignancy (Gershenwald *et al*, 2001), while re-expression abrogates it (Huang *et al*, 1998), by controlling

transcription of genes such as MCAM-MUC18, MMP2, PAR-1, VEGF, BCL2, CDKN1A/p21, E-cadherin and c-KIT (Melnikova and Bar-Eli, 2008). We were able to demonstrate that miR-214 overexpression increases the transcription of MCAM-MUC18 and VEGFA, two well-known TFAP2-repressed genes. In addition, it decreases expression of genes transcriptionally activated by TFAP2 family members, such as ERBB2 and IGFBP5, as well as TGFB. c-KIT, another well-known TFAP2-modulated gene, is expressed at very low levels in our system, consistently with the literature (Huang *et al*, 1998), so we were not able to evaluate its modulation. Other TFAP2-regulated genes including E-Cadherin/CDH1, CTSD, EREG, TGFBI, CDH11, CLU, PVR, EGRF, ERBB2, ICAM2, ITGAV, MMP2, PVRL2, TIMP1, TIMP2, all somehow connected with cell movement and/or malignancy, were found to be differentially expressed following miR-214 modulations. Considering that TFAP2C silencing in MA-2 cells phenocopied miR-214 overexpression biology, while its forced expression in miR-214-overexpressing cells rescued the migration and extravasation phenotypes, we conclude that TFAP2C is one of the main players through which miR-214 controls malignancy in melanoma. TFAP2C modulations were also proven to interfere, at least in part, with the expression of two other miR-214-modulated genes highly involved in cell movement and tumour progression, ITGA3 and MET, thus suggesting an additional relevance for TFAP2C in gene expression regulation in melanomas. The relevancy of TFAP2C is also underlined by its decreased expression in human melanoma samples from a public data set. On the contrary, we found that ITGA3 modulates cell migration *in vitro*, but it is not sufficient *per se* to control the extravasation process or metastasis formation *in vivo*, suggesting that the contribution of ITGA3 on miR-214-mediated functions is only partial and restricted to cell movement in culture. In line with our *in vivo* results, we did not find reduced expression of ITGA3 in the human melanoma public data set we analysed. Considering that ITGA3 is thought to promote invasion and metastasis in various human tumours (Mitchell *et al*, 2010), it is possible that, even if ITGA3 is a *bona fide* target of miR-214, a feedback loop that re-establishes high levels of this adhesion molecule occurs during melanoma progression. Unfortunately, only mRNA (no protein) data were available for the human data set we analysed. Since miR-214 was able to downregulate ITGA3 protein expression without affecting mRNA levels in cells, ITGA3 protein expression needs to be verified in a high number of human melanoma samples, before drawing any conclusions.

Considering that miR-214 is highly expressed in human melanomas and that the pool of miR-214-modulated genes correctly separates melanomas versus nevi or normal skin, we can conclude that the pathway including miR-214 and its modulated genes is able to coordinate melanoma progression and could be considered for therapeutic intervention.

Materials and methods

Cell culture

293T, MDA-MB-231 and 4T1 cells were from American Type Culture Collection and maintained in standard conditions. A375P and derived variants were provided by RO Hynes (Xu *et al*, 2008) and maintained in Dulbecco's Modified Eagle's Medium containing 10 mM Glutamax and 4.5 g/ml glucose (DMEM Glutamax™, GIBCO Invitrogen Life Technologies, Carlsbad, CA), supplemented with 10% heat-inactivated FCS (Seromed, GmbH), 1 mM sodium pyruvate, 25 mM HEPES pH 7.4, 1 × MEM vitamin solution, 1 × MEM non-essential amino acids and 100 μg/ml gentamicin (all from GIBCO Invitrogen Life Technologies). 1300-Mel, GR4-Mel, WK-Mel and Dett-Mel were provided by P Circosta and cultured according to Circosta *et al* (2009) in RPMI medium supplemented with 10% heat-inactivated FCS (Seromed, GmbH), 1 mM sodium pyruvate, 25 mM HEPES pH 7.4, 1 × MEM non-essential amino acids and 100 μg/ml gentamicin. HUVECs–GFP were provided by L Primo and grown as described (Primo *et al*, 2007). Human melanocytes were purchased from Lonza (Basel, CH). SK-MEL-103, -173, -187 and -197 melanoma cell lines were obtained and cultured as described in Segura *et al* (2009). Human epidermal melanocytes, derived from adult, lightly pigmented donor (HEMa-LP), were from Invitrogen Life Technologies (Cascade Biologics brand) and were maintained in Medium 254, supplemented with Human Melanocyte Growth Supplement-2, PMA-Free (Invitrogen Life Technologies, Carlsbad, CA), as indicated by manufacturer's guidelines.

Reagents and antibodies

pLKO.1-SCR (scramble) or pLKO.1-shTFAP2C lentiviral expression vectors were purchased from Open Biosystems (Huntsville, AL, cat. no. RHS3979-19745). pSP(RSV)-TFAP2C and pSP(RSV)-empty expression vectors were a gift from H Hurst (Bosher *et al*, 1995, 1996). siITGA3 (Hs_ITGA3_7 HP Validated siRNA) was purchased from Qiagen (Stanford, CA). pCMVzeo-ITGA3 and pCMVzeo-empty were a gift from M DiPersio (Iyer *et al*, 2005). miR precursors and inhibitors were pre-miR™ miRNA Precursor Molecules-Negative Control #1, pre-miR™ miRNA Precursor Hsa-miR-214 (PM12124), Hsa-miR-210 (PM10516), anti-miR™ miRNA Inhibitors-Negative Control #1, anti-miR™ miRNA Inhibitors Hsa-miR-214 (AM12124) (all from Ambion, Austin, TX). miRNA detection was TaqMan® MicroRNA Assays Hsa-miR-214 assay ID 000517 or Hsa-miR-214 assay ID 002306, Hsa-miR-210 assay ID 000512, Hsa-miR-221 assay ID 000524, Hsa-miR-222 assay ID 002276, Hsa-miR-137 assay ID 001129, Hsa-miR-34a assay ID 000426, Hsa-RNU44 assay ID 001094, U6 snRNA assay ID001973 (all from Applied Biosystems, Foster City, CA). Primary antibodies were anti-TFAP2A mAb 3B5, anti-TFAP2C mAb 6E4/4, anti-GAPDH pAb V-18, anti-hsp90 mAb F-8, anti-MET pAb C-12 (all from Santa Cruz Biotechnology, Santa Cruz, CA), anti-ITGA3 pAb 8-4 B7 gently provided by M DiPersio (DiPersio *et al*, 1995), anti-PAK2 pAb #2608, anti-PTEN pAb #9552 (Cell Signaling Technology, Danvers, MA), anti-Von Willebrand Factor pAb A0082 (DAKO Cytomation, Glostrup, Denmark), anti-GFP Ab (ab290, Abcam, Cambridge, UK). Secondary antibodies were goat anti-mouse IgG HRP conjugated, goat anti-rabbit IgG HRP conjugated, donkey anti-goat IgG HRP conjugated (all from Santa Cruz Biotechnology) and goat anti-rabbit IgG Alexa-Fluor-488 (Molecular Probes, Invitrogen Life Technologies). All antibodies were used at the producer's suggested concentrations.

Primers

Oligonucleotides employed in this study were cloning miR-214, TTTCATAGGCACCACTCACTTTAC and CCCTTTCCCCTTACTCTCCA; miR-214 synthetic binding site CTAGTCCACTGCCTGTCTGTGCCTGC TGTCGTAGGATCTACTGCCTGTCTGTGCCTGCTGTTGGACCTGACACTG CCTGTCTGTGCCTGCTGTCCCA and AGCTTGGGACAGCAGGCACAGA CAGGCAGTGTCAGGTCCAACAGCAGGCACAGACAGGCAGTAGATCCTA CGACAGCAGGCACAGACAGGCAGTGGA; cloning ARHGAP12 3′UTR, GCACTAGTGTTCCATCTTCGGACGTTGA and ATACGCGTCTTCAACAG ACCATGCTCCC; cloning ITGA3 3′UTR, ATACTAGTAGGCTGACCGACG ACTACTG and TAACGCGTTTTTGCATACAAACTGGGAGC; cloning ITGB8 3′UTR, ATGCCGGCGCTCACGGTCATGCCAGTTGCT and TAGTT TAAACCAGGGCTCATGGCCCGTGTA; cloning MET 3′UTR, ATACTAG TCCTCCTTCTGGGAGACATCA and TAACGCGTACAAGATGTTGCATCA CTTTACTTT; cloning MITF 3′UTR, ATACTAGTCCTCCCTGCACTGCA TTCGC and TAACGCGTCAGTGCTATGGACCATACAG; cloning NRP1 3′UTR, TAACTAGTGAGTACTTATTCGGAGGCATGAA and TAACGCGT AATTCAACTGTTTCTTTGGAATG, cloning PAK2 3′UTR, ATACTAGTC CTGTGCCTCTAACAAGCGATTC and TAACGCGTAAGTTTAGGAAAGG GAAAAATGCACA; cloning PLXNA1 3′UTR, ATACTAGTCCCCAGCTGT GATCATCC and TAACGCGTTGTTTAATCTCTCCTTAATGTGTGTG; cloning TFAP2A 3′UTR, ATACTAGTGCGGGTGACAGCTCCGGGAT and TA ACGCGTTGATACCCTGCTCTGAACTCCAAGT; cloning TFAP2C 3′UTR, ATGAGCTCCTGGAGACCAGAGTCCAGCTGAT and TAACGCGTAGGGTT CAGCCCAACAGGAA; TFAP2C 3′UTR mutagenesis, TTCTGGTTTTAGG

AAACTTGTAGAAACGAAGCATACAGATTGATTTTTTTCTCCTTTTTTT TTTTTTTT and AAAAAAAAAAAAAAAAGGAGAAAAAAATCAATCTGT ATGCTTCGTTTCTACAAGTTTCCTAAAACCAGAA; ITGA3 3′UTR deletions, CTCCTGACCCCTGCCTGCAGGCCCA and TGGGCCTGCAGGCA GGGGTCAGGAG, ARHGAP12 RT–PCR, TCAAAACCCTGCTTTCCT GA and CCATATTTCTCTTGATCCTTTGG and probe #7; IGFBP5, CTACCGCGAGCAAGTCAAG and GTCTCCTCGGCCATCTCA and probe #77; ITGA3 RT–PCR, GAGGACATGTGGCTTGGAGT and GTAGCGG TGGGCACAGAC and probe #13, MET RT–PCR AAATGTGCATGAAGC AGGAA and TCTCTGAATTAGAGCGATGTTGA and probe #59; NRP1 RT–PCR CACATTTCACAAGAAGATTGTGC and CATCAATTTTAATTTC TGGGTTCTTT and probe #85; PLXNA1 RT–PCR CAGTGATGTGGCTG TGTCG and CTCACGGGAGTTCCTCCA and probe #68 (all probes from Universal Probe Library, Roche, Mannheim, GmbH); ERBB2 RT–PCR QuantiTect Primer Assay QT00060746, GAPDH RT–PCR QuantiTect Primer Assay QT00079247, ITGB8 RT–PCR QuantiTect Primer Assay cat. no. QT00038507, MCAM-MUC18 RT–PCR QuantiTect Primer Assay cat. no. QT00079842, MITF RT–PCR QuantiTect Primer Assay cat. no. QT00037737, MMP2 RT–PCR QuantiTect Primer Assay cat. no. QT00088396, PAK2 RT–PCR QuantiTect Primer Assay cat. no. QT01677172, PTEN RT–PCR QuantiTect Primer Assay cat. no. QT01676969, RRN18S QuantiTect Primer Assay QT00199367 (all from Qiagen, Stanford, CA); TFAP2A RT–PCR, ACATTCCGATCCCAATGAG CA and TGTTTTGTAGCCAGGAGCATGTTT; TFAP2C RT–PCR, AACAG ACCCACACACTTAGCCATT and GCGGACACAAAAACCAACCA; TGFB RT–PCR GCAACAATTCCTGGCGATACCT and AGCCCTCAATTTCCCC TCCA; VEGFA RT–PCRCTATGTCCTCACACCATTGAAACCA and GGAA GGTCAACCACTCACACACA. miR-214 genomic locus: TGGGCAAAAC ACAGTGAAAA and TGACGCGTGGAAGTATCAAA; UBE2E1 genomic locus: GGTGGGAAGTATTGCCACTCA and GTGAAACCCCAATTTATGT AGCGTAT.

Transient transfections of pre-miRs, anti-miRs, siRNAs or cDNAs

To obtain transient anti-miR, pre-miR or siRNA expression, cells were plated in 6-well plates at 30–50% confluency and transfected 24 h later using RNAiFect (Qiagen, Stanford, CA) reagent, according to the manufacturer's instructions, with 100 nM anti-miR, 75 nM pre-miR or 170 nM siRNA. For transient cDNA overexpression, cells were plated in 6-well plates at 90% confluency and transfected 24 h later using Lipofectamine^{TM}2000 (Invitrogen Life Technologies) reagent, according to the manufacturer's instruction. Cells were tested for miR or gene overexpression/knockdown 24 or 48 h later.

Plasmid construction and generation of stable cell lines

The human miR-214 gene was amplified from genomic DNA and cloned into pWPT (Addgene, Cambridge, MA) or pLemiR-tRFP (Open Biosystems) vectors to obtain pWPT-miR-214 and pLemiR-214 (still containing tRFP) vectors. For the preparation of the miR-214 sponges two different 292 nts long sequences, containing eight bulged target sites specific for miR-214 with linkers in-between, were designed as described in Krol *et al* (2010) synthesized by DNA2.0 (CA, USA) and cloned in the 3′UTR of the GFP gene in a pLenti-CMV-GFP-Puro vector (Addgene) generating the pLenti-sponge1 and -sponge3 vectors. The pLenti-CMV-GFP-Puro empty vector was used as control (pLenti-empty). All stable cell lines were generated via lentiviral infection. Lentiviruses were produced by calcium phosphate transfection of 20 μg vector plasmid together with 15 μg packaging (pCMVdR8.74) and 6 μg envelope (pMD2.G-VSVG) plasmids in 293T cells, according to Trono's lab protocol (http://tronolab.epfl.ch). Supernatant was harvested 48 h post-transfection, filtered with 0.45 μm filters, diluted and used to infect 3.5×10^5 cells in 6-well plates, in presence of 8 μg/ml Polybrene (Sigma-Aldrich, St Louis, MO). Luciferase reporter vectors containing the full-length or partial (PTEN, PAK-2, ITGB8) 3′UTR of the indicated miR-214 target genes were generated following PCR amplification of the 3′UTR from human genomic DNA and cloning into the Firefly Luciferase reporter pMIR-REPORT^{TM} vector (Ambion). When indicated the 3′UTRs were mutagenized at the miR-214 recognition site using the QuickChange Site-Directed Mutagenesis kit (Stratagene, Cedar Creek, TX), according to the manufacturer's instructions. miR-214-sensor was obtained by annealing, purifying and cloning short oligonucleotides containing three perfect miR-214 binding sites into the *Spe*I and *Hin*dIII sites of the pMIR-REPORT vector.

RNA isolation and qRT–PCR for miRNA or mRNA detection

Total RNA was isolated from cells or tumours using TRIzol® Reagent (Invitrogen Life Technologies). qRT–PCRs for miR detection were performed with the indicated TaqMan MicroRNA Assays (Applied Biosystems) on 10 ng total RNA, according to the manufacturer's instructions. For mRNA detection, 1 μg of DNAse-treated RNA (DNA-free^{TM} kit, Ambion) was retrotranscribed with RETROscript^{TM} reagents (Ambion) and qRT–PCRs were carried out using gene-specific primers, using a 7900HT Fast Real Time PCR System. Quantitative normalization was performed on the expression of the RNU44 small nucleolar RNA or of GAPDH, for miR or mRNA detection, respectively. The relative expression levels between samples were calculated using the comparative delta *C*T (threshold cycle number) method ($2^{-\Delta\Delta CT}$) with a control sample as the reference point (Bookout and Mangelsdorf, 2003).

Motility assay

For the wound healing motility assay, cells were grown to confluency in 6-well plates, serum starved for 24 h, then a cross wound was made on the monolayer using a pipette tip. Cells were rinsed with PBS buffer and placed in complete growth medium. Photographs in different regions of the wound (at least 10 fields) were taken at $t = 0$ h and at $t = 18$ h, using Olympus IX70 microscope. The distance covered by the migrating cells is inversely proportional to the size of the wound; motility was quantitated by calculating the reciprocal of the wound size measured using the ImageJ software (http://rsbweb.nih.gov/ij/) (Orso *et al*, 2008).

Migration, invasion and transendothelial migration transwell assays

To measure migration 3.5×10^4 MC-1 or 7.5×10^4 MA-2 and WK-Mel or 1.2×10^5 1300-Mel, SK-Mel-187 and GR4-Mel or 2×10^5 A375P or 10^5 4T1 and MDA-MB-231 were seeded in serum-free media in the upper chambers of cell culture inserts (transwells) with 8.0 μm pore size membrane (24-well format, Becton Dickinson, NJ). To measure invasion of MC-1 and MA-2 cells and of 1300-Mel and SK-Mel-187, the previously mentioned inserts were pre-coated with 4 or 2 μg/well growth factor reduced Matrigel (Becton Dickinson), respectively, and the cells seeded as indicated above. For 4T1 and MDA-MB-231 cells, invasion assays were performed using BioCoat^{TM} Matrigel Invasion Chambers with 8.0 μm pore size membrane (Becton Dickinson). For migration and invasion, the lower chambers were filled with complete growth media. After 18–20 h, the migrated cells present on the lower side of the membrane were fixed in 2.5% glutaraldehyde, stained with 0.1% crystal violet and photographed using an Olympus IX70 microscope (Orso *et al*, 2008). For transendothelial migration assay, 10^5 HUVECs–GFP were seeded in complete medium in the upper part of transwell inserts with 5.0 μm pore size membrane (24-well format, Costar, Corning Incorporated, NY) coated by fibronectin at 5 μg/cm^2, and grown for 72 h, till confluency. Then, 5×10^4 cells were labelled with CellTracker^{TM} Orange CMRA (Molecular Probes, Invitrogen Life Technologies), according to the manufacturer's instructions and seeded in HUVEC's complete medium onto the HUVEC–GFP monolayer on the upper side of the transwell. After 20 h, the HUVEC–GFP monolayer was photographed using Zeiss Axiovert200M microscope. Then, HUVECs and non-transmigrated cells were removed and the red-fluorescent (CMRA) cells that migrated on the lower side of the membrane were fixed in 4% paraformaldheyde and photographed using Zeiss AxioObserver microscope with ApoTome Module. Migration, invasion and transendothelial migration were evaluated by measuring the area occupied by migrated cells using the ImageJ software (http://rsbweb.nih.gov/ij/).

Adhesion assays

To test adhesion, 5×10^4 cells/well were seeded onto 5 μg/ml collagen IV or 10 μg/ml fibronectin or 5 μg/ml laminin (all from Sigma-Aldrich) pre-coated 96-well plates, for 1 h at 37°C. Cells were then washed thoroughly to remove non-adherent cells, fixed with methanol and stained with haematoxylin and eosin (Diff-Quik, Medion Diagnostics, Dudingen, CH). Wells were photographed using Olympus IX70 microscope and the area occupied by the adherent cell was measured using the ImageJ software (http://rsbweb.nih.gov/ij/) (Orso *et al*, 2008).

Proliferation assays

In all, 5×10^3 cells/well were plated in 96-well plates in complete medium and starved for 24 h. Complete medium was then added and cells were allowed to grow for 1, 2, 3 and 5 days, fixed with 2.5% glutaraldehyde and stained with 0.1% crystal violet. The dye was solubilized using 10% acetic acid and optical density measured directly in plates using a Microplate Reader Mithras LB940 (Berthold Technologies, GmbH) at 570 nm wavelength (Kueng *et al*, 1989).

Anchorage-independent growth assays

In all, 5×10^4 cells were resuspended in 8 ml of complete DMEM containing 0.45% Difco Noble Agar (Becton Dickinson) and plated in 6 cm bacterial dishes. Medium was changed every 3 days. After 20 days, the dishes were stained with nitroblue tetrazolium (Sigma-Aldrich), photographed with Nikon SMZ1000 stereomicroscope and colonies were counted using the ImageJ software (http://rsbweb.nih.gov/ij/) (Hynes *et al*, 1990).

Anoikis *analysis*

Cells were plated on a 2% agarose pad in serum-free medium for 72 h, collected, washed in PBS buffer, resuspended in 10 mM Hepes, 150 mM NaCl, 5 mM $CaCl_2$ buffer containing FITC-conjugated Annexin-V (Bender MedSystems, GmbH) and 200 nM tetramethylrhodamine-methyl-ester (TMRM, Molecular Probes, Invitrogen, CA) and incubated at 37°C for 15 min. Flow cytometry analysis of apoptosis was carried out by using a FACSCalibur flow cytometer (Becton Dickinson). Data acquisition was performed using CellQuest software (Becton Dickinson) and data analysis with WinMDI software (version 2.8, Scripps Institute, CA). Results were displayed in bidimensional plots, with gates indicating the percentages of healthy and apoptotic populations (Rasola and Geuna, 2001).

In vivo tumour and metastasis assays

All experiments performed with live animals complied with ethical animal care. Seven-week-old female CD1 nude mice (Charles River Laboratories, Wilmington, MA) were subcutaneously injected in the two flanks with 8×10^6 A375P, MA-2, MC-1 cells or with 10^6 WK-Mel, GR4-Mel, 1300-Mel, SK-Mel-173, SK-Mel-197 (in PBS). Tumour growth was monitored every 3 days. Mice were dissected 4 weeks after injection and tumours were weighted. For experimental metastasis assays, 5×10^5 A375P, MA-2 or MC-1 cells (in PBS) were injected into the tail vein of 7-week-old female CB.17 SCID mice (Charles River Laboratories). Mice were dissected 7 (MA-2 and MC-1) or 9 (A375P) weeks later and lung macrometastases counted in fresh total lungs using a Nikon SMZ1000 stereomicroscope. Spontaneous metastases were evaluated in 14-week-old female immunocompetent BALB/c mice injected with 5×10^5 4T1 cells (in PBS) transduced with pLemiR-214 or pLemiR-empty vectors, expressing turbo red-fluorescent protein (tRFP), in the fourth left mammary gland fat pad and dissected 3 weeks later. Red-fluorescent metastatic foci were counted in the fresh total lungs using a Leica MZ16F fluorescence stereomicroscope. For all metastasis studies, lungs were formalin fixed, cut in small pieces and paraffin embedded, sectioned and haematoxylin and eosin (H&E) stained. Micrometastases were evaluated on specimens, with an Olympus BH2 microscope, on at least three different sections.

In vivo extravasation assay

In all, 1.6×10^6 A375P, MA-2 or MC-1 cells, previously labelled with CellTracker™ Orange CMRA (Molecular Probes, Invitrogen Life Technologies) and resuspended in PBS were injected into the tail vein of 7-week-old female CD1 nude mice (Charles River Laboratories). After 2 or 48 h, mice were sacrificed and 4% paraformaldehyde was injected into the trachea. Total lungs were dissected and photographed using a Leica MZ16F fluorescence stereomicroscope and red-fluorescent (CMRA) cells were counted 48 h following injections using the ImageJ software (http://rsbweb.nih.gov/ij/). Lungs were included in freezing resin (*OCT Killik*, Bio-Optica, IT) and cryostat-cut in 6 μm thick sections. For immunofluorescent stainings for blood vessels, samples were acetone fixed for 10 min, blocked in 5% bovine serum albumin (Sigma-Aldrich) for 1 h, incubated with anti-Von Willebrandt Factor (vWF) primary antibody (1:50 dilution) for 1 h and anti-rabbit Alexa-Fluor-488 secondary antibody for 30 min and counterstained with DAPI (Sigma-Aldrich) for 5 min. Specimens were examined and photographed using a Zeiss AxioObserver microscope with the ApoTome Module.

Luciferase assays

In all, 5×10^4 cells were cotransfected with 50 ng of the pMIR-REPORT™ (Ambion) Firefly luciferase constructs containing the 3′UTRs of the indicated miR-214 potential target genes and 20 ng of pRL-TK Renilla Luciferase normalization control (Promega, Madison, WI), using Lipofectamine2000 (Invitrogen Life Technologies). Lysates were collected 48–72 h after transfection and Firefly and Renilla luciferase activities were measured with a Dual-Luciferase Reporter System (Promega).

Protein preparation and immunoblotting

Total protein extracts were obtained using a boiling buffer containing 0.125 M Tris/HCl, pH 6.8 and 2.5% sodium dodecyl sulphate (SDS). In all, 25 or 50 μg proteins were separated by SDS polyacrylamide gel electrophoresis (PAGE) and electroblotted onto polyvinylidene fluoride membranes (Bio-Rad, Hercules, CA). Membranes were blocked in 5% non-fat milk Tris-buffered saline (TBS)–Tween buffer (137 mM NaCl, 20 mM Tris/HCl, pH 7.6, 0.1% Tween-20) for 1 h at 37°C, then incubated with appropriate primary and secondary antibodies in 1% milk TBS–Tween buffer, respectively, overnight at 4°C and for 1 h at room temperature and visualized by enhanced chemiluminescence (ECL®, Amersham Biosciences, Piscataway, NJ).

Proteomic analysis

The expression profile of a panel of 119 soluble receptors expressed by non-hematopoietic cells present in the Human Soluble Receptor Array Non-Hematopoietic Panel (R&D Systems, Minneapolis, MN) was evaluated in total protein extracts of MA-2 cells 72 h after transfection of pre-control or pre-miR-214, according to the manufacturer's instructions.

Ingenuity pathway analysis systems

The Ingenuity Pathways Knowledge Base (http://www.ingenuity.com) is currently the world's largest database of knowledge on biological networks, with annotations organized by experts. We exploited this database to look for functional network connections among the miR-214-modulated genes.

Collection and analyses of human melanoma samples

Archival melanoma tumour samples (13 *in situ* melanomas, 57 primary melanomas and 18 cutaneous metastases) were collected from the Ist. Dermatologic Clinic of the University of Torino and institutional approvals were obtained for all samples. As reference, seven healthy skin samples were included in the analysis. Tumour tissue harvested from patients was quickly frozen or OCT embedded and stored at −80°C, or it was formalin fixed and paraffin embedded (FFPE). Total RNA from frozen and/or OCT-embedded samples was isolated via TRIzol Reagent (Invitrogen Life Technologies), according to the manufacturer's guidelines. Briefly, each sample was homogenized in the denaturing lysis solution and an acid-phenol:chloroform extraction followed. RNA extraction from FFPE samples was performed using the miRNeasy FFPE Kit (Qiagen, Stanford, CA), according to the manufacturer's guidelines. Briefly, samples were treated with the lysis buffer with proteinase K, then incubated at 80°C to reverse formalin crosslinking. Genomic DNA was then removed using gDNA Eliminator spin columns, and the concentrated RNA was purified using RNeasy MinElute spin columns. miR-214 and miR-210 expression was evaluated by qRT–PCR as described above, starting from 10 ng of total RNA. Quantitative normalization was performed on the expression of the RNU44 small nucleolar RNA. Relative expression was calculated using as reference the median expression of miR-214 and miR-210 in the healthy skin samples. Two-tailed Mann–Whitney non-parametric statistical test was used to assess significant differences with a P-value <0.05 considered significant.

Analysis of human melanoma data sets

Expression data for human primary melanomas, nevi and normal skin were obtained from the GEO series associated with Talantov *et al* (2005), Accession GSE3189, log-transformed and variance stabilized by adding a constant equal to 16 before taking the logarithm. The samples were clustered using Pearson

correlation-based hierarchical clustering. Clustering and heatmap were obtained using Bioconductor (Gentleman *et al*, 2004).

Analysis of miR-214 genomic locus

Genomic DNA was isolated from melanoma cell lines using the Qiagen QIAmp DNA Mini kit (Qiagen, Valencia, CA). PCRs were performed using MyiQ Single Color Real time PCR Detection System (Bio-Rad) in 96-well plates, with reaction mixture (25 μl) containing 20 ng of DNA and 12.5 μl of ABsolute Blue QPCR SYBR Green Mix (Thermo Scientific, Waltham, MA). Triplicate reactions were run with specific primers for all samples using the PCR protocol: 95°C for 15 min, 40 cycles of 95°C for 15 s, 55°C 30 s and 72°C for 30 s, followed by melting curve analysis to ensure amplification specificity. Under the selected conditions, only single peaks were detected in the melting curve. The products of the PCRs were also run on a 2% agarose gel to confirm the correct size of the amplified product. To determine the genetic load, the ΔΔCT method was used according to Pfaffl (2001) and assuming 100% efficiency in the amplification from normal human genomic DNA (Promega). *UBE2E1* housekeeping gene was used as reference. This gene has not been found genetically altered in melanomas (Lazar *et al*, 2009).

Statistical analyses

Unless otherwise noted, data are presented as mean ± s.e.m. and two-tailed Student's *t*-test was used for comparison, with $*P<0.05$; $**P<0.01$; $***P<0.001$ considered to be statistically significant. NS indicates a not statistically significant *P*-value.

Supplementary data

Supplementary data are available at *The EMBO Journal* Online (http://www.embojournal.org).

Acknowledgements

This work was supported by grants from the University of Torino (Local Research Funding 2007/DT, 2008/DT), Regione Piemonte Ricerca Scientifica Applicata (CIPE2004/DT), Compagnia di San Paolo (DT), Torino, PRIN 2008 (DT), AIRC 2010 (IG 10104 DT) and FIRB giovani 2008 (RBFR08F2FS-002 FO). FO and DC are fellows of the Regione Piemonte. We thank Lei Xu and Richard Hynes for giving us the A375P cells and its metastatic variants; Paola Circosta and Alessandro Cignetti for providing several melanoma cell lines; Helen Hurst for the pSP(RSV)-NN and pSP(RSV)-TFAP2C vectors; Mike DiPersio for the anti-ITGA3 antibody and the pCMVzeo-ITGA3 vector; Luca Primo for preparing HUVECs–GFP cells; Jacek Krol for advices with sponges; Roberto Chiarle for help with the tumour samples; Nancy Hynes, Pier Paolo Pandolfi and Richard Hynes for critical reading of the manuscript.

Conflict of interest

The authors declare that they have no conflict of interest.

References

Bar-Eli M (2001) Gene regulation in melanoma progression by the AP-2 transcription factor. *Pigment Cell Res* **14:** 78–85

Bartel DP (2009) MicroRNAs: target recognition and regulatory functions. *Cell* **136:** 215–233

Bauer R, Imhof A, Pscherer A, Kopp H, Moser M, Seegers S, Kerscher M, Tainsky MA, Hofstaedter F, Buettner R (1994) The genomic structure of the human AP-2 transcription factor. *Nucleic Acids Res* **22:** 1413–1420

Benvenuti S, Comoglio PM (2007) The MET receptor tyrosine kinase in invasion and metastasis. *J Cell Physiol* **213:** 316–325

Berger AJ, Davis DW, Tellez C, Prieto VG, Gershenwald JE, Johnson MM, Rimm DL, Bar-Eli M (2005) Automated quantitative analysis of activator protein-2alpha subcellular expression in melanoma tissue microarrays correlates with survival prediction. *Cancer Res* **65:** 11185–11192

Blenkiron C, Goldstein LD, Thorne NP, Spiteri I, Chin SF, Dunning MJ, Barbosa-Morais NL, Teschendorff AE, Green AR, Ellis IO, Tavare S, Caldas C, Miska EA (2007) MicroRNA expression profiling of human breast cancer identifies new markers of tumor subtype. *Genome Biol* **8:** R214

Bookout AL, Mangelsdorf DJ (2003) Quantitative real-time PCR protocol for analysis of nuclear receptor signaling pathways. *Nucl Recept Signal* **1:** e012

Bosher JM, Totty NF, Hsuan JJ, Williams T, Hurst HC (1996) A family of AP-2 proteins regulates c-erbB-2 expression in mammary carcinoma. *Oncogene* **13:** 1701–1707

Bosher JM, Williams T, Hurst HC (1995) The developmentally regulated transcription factor AP-2 is involved in c-erbB-2 overexpression in human mammary carcinoma. *Proc Natl Acad Sci USA* **92:** 744–747

Circosta P, Granziero L, Follenzi A, Vigna E, Stella S, Vallario A, Elia AR, Gammaitoni L, Vitaggio K, Orso F, Geuna M, Sangiolo D, Todorovic M, Giachino C, Cignetti A (2009) T cell receptor (TCR) gene transfer with lentiviral vectors allows efficient redirection of tumor specificity in naive and memory T cells without prior stimulation of endogenous TCR. *Hum Gene Ther* **20:** 1576–1588

Croce CM (2009) Causes and consequences of microRNA dysregulation in cancer. *Nat Rev Genet* **10:** 704–714

Cruz-Munoz W, Khokha R (2008) The role of tissue inhibitors of metalloproteinases in tumorigenesis and metastasis. *Crit Rev Clin Lab Sci* **45:** 291–338

Decembrini S, Bressan D, Vignali R, Pitto L, Mariotti S, Rainaldi G, Wang X, Evangelista M, Barsacchi G, Cremisi F (2009) MicroRNAs couple cell fate and developmental timing in retina. *Proc Natl Acad Sci USA* **106:** 21179–21184

Desgrosellier JS, Cheresh DA (2010) Integrins in cancer: biological implications and therapeutic opportunities. *Nat Rev Cancer* **10:** 9–22

DiPersio CM, Shah S, Hynes RO (1995) alpha 3A beta 1 integrin localizes to focal contacts in response to diverse extracellular matrix proteins. *J Cell Sci* **108**(Pt 6)**:** 2321–2336

Duffy MJ, McKiernan E, O'Donovan N, McGowan PM (2009) Role of ADAMs in cancer formation and progression. *Clin Cancer Res* **15:** 1140–1144

Eckert D, Buhl S, Weber S, Jager R, Schorle H (2005) The AP-2 family of transcription factors. *Genome Biol* **6:** 246

Eskandarpour M, Kiaii S, Zhu C, Castro J, Sakko AJ, Hansson J (2005) Suppression of oncogenic NRAS by RNA interference induces apoptosis of human melanoma cells. *Int J Cancer* **115:** 65–73

Fei J, Lan F, Guo M, Li Y, Liu Y (2008) Inhibitory effects of anti-miRNA oligonucleotides (AMOs) on A549 cell growth. *J Drug Target* **16:** 688–693

Filipowicz W, Bhattacharyya SN, Sonenberg N (2008) Mechanisms of post-transcriptional regulation by microRNAs: are the answers in sight? *Nat Rev Genet* **9:** 102–114

Flynt AS, Li N, Thatcher EJ, Solnica-Krezel L, Patton JG (2007) Zebrafish miR-214 modulates Hedgehog signaling to specify muscle cell fate. *Nat Genet* **39:** 259–263

Friedman RC, Farh KK, Burge CB, Bartel DP (2009) Most mammalian mRNAs are conserved targets of microRNAs. *Genome Res* **19:** 92–105

Gadea G, Sanz-Moreno V, Self A, Godi A, Marshall CJ (2008) DOCK10-mediated Cdc42 activation is necessary for amoeboid invasion of melanoma cells. *Curr Biol* **18:** 1456–1465

Gentleman RC, Carey VJ, Bates DM, Bolstad B, Dettling M, Dudoit S, Ellis B, Gautier L, Ge Y, Gentry J, Hornik K, Hothorn T, Huber W, Iacus S, Irizarry R, Leisch F, Li C, Maechler M, Rossini AJ, Sawitzki G *et al* (2004) Bioconductor: open software development for computational biology and bioinformatics. *Genome Biol* **5:** R80

Gershenwald JE, Sumner W, Calderone T, Wang Z, Huang S, Bar-Eli M (2001) Dominant-negative transcription factor AP-2 augments SB-2 melanoma tumor growth *in vivo*. *Oncogene* **20:** 3363–3375

Gupta GP, Massague J (2006) Cancer metastasis: building a framework. *Cell* **127:** 679–695

Hilger-Eversheim K, Moser M, Schorle H, Buettner R (2000) Regulatory roles of AP-2 transcription factors in vertebrate development, apoptosis and cell-cycle control. *Gene* **260:** 1–12

Hornebeck W, Emonard H, Monboisse JC, Bellon G (2002) Matrix-directed regulation of pericellular proteolysis and tumor progression. *Semin Cancer Biol* **12:** 231–241

Huang S, Jean D, Luca M, Tainsky MA, Bar-Eli M (1998) Loss of AP-2 results in downregulation of c-KIT and enhancement

of melanoma tumorigenicity and metastasis. *EMBO J* **17:** 4358–4369

Hynes NE, Taverna D, Harwerth IM, Ciardiello F, Salomon DS, Yamamoto T, Groner B (1990) Epidermal growth factor receptor, but not c-erbB-2, activation prevents lactogenic hormone induction of the beta-casein gene in mouse mammary epithelial cells. *Mol Cell Biol* **10:** 4027–4034

Inui M, Martello G, Piccolo S (2010) MicroRNA control of signal transduction. *Nat Rev Mol Cell Biol* **11:** 252–263

Iyer V, Pumiglia K, DiPersio CM (2005) Alpha3beta1 integrin regulates MMP-9 mRNA stability in immortalized keratinocytes: a novel mechanism of integrin-mediated MMP gene expression. *J Cell Sci* **118**(Pt 6)**:** 1185–1195

Jeanes A, Gottardi CJ, Yap AS (2008) Cadherins and cancer: how does cadherin dysfunction promote tumor progression? *Oncogene* **27:** 6920–6929

John B, Enright AJ, Aravin A, Tuschl T, Sander C, Marks DS (2004) Human microRNA targets. *PLoS Biol* **2:** e363

Juan AH, Kumar RM, Marx JG, Young RA, Sartorelli V (2009) Mir-214-dependent regulation of the polycomb protein Ezh2 in skeletal muscle and embryonic stem cells. *Mol Cell* **36:** 61–74

Karjalainen JM, Kellokoski JK, Mannermaa AJ, Kujala HE, Moisio KI, Mitchell PJ, Eskelinen MJ, Alhava EM, Kosma VM (2000) Failure in post-transcriptional processing is a possible inactivation mechanism of AP-2alpha in cutaneous melanoma. *Br J Cancer* **82:** 2015–2021

Kobayashi H, Boelte KC, Lin PC (2007) Endothelial cell adhesion molecules and cancer progression. *Curr Med Chem* **14:** 377–386

Krol J, Busskamp V, Markiewicz I, Stadler MB, Ribi S, Richter J, Duebel J, Bicker S, Fehling HJ, Schubeler D, Oertner TG, Schratt G, Bibel M, Roska B, Filipowicz W (2010) Characterizing light-regulated retinal microRNAs reveals rapid turnover as a common property of neuronal microRNAs. *Cell* **141:** 618–631

Kueng W, Silber E, Eppenberger U (1989) Quantification of cells cultured on 96-well plates. *Anal Biochem* **182:** 16–19

Lazar V, Ecsedi S, Szollosi AG, Toth R, Vizkeleti L, Rakosy Z, Begany A, Adany R, Balazs M (2009) Characterization of candidate gene copy number alterations in the 11q13 region along with BRAF and NRAS mutations in human melanoma. *Mod Pathol* **22:** 1367–1378

Lee YB, Bantounas I, Lee DY, Phylactou L, Caldwell MA, Uney JB (2009) Twist-1 regulates the miR-199a/214 cluster during development. *Nucleic Acids Res* **37:** 123–128

Liang S, Sharma A, Peng HH, Robertson G, Dong C (2007) Targeting mutant (V600E) B-Raf in melanoma interrupts immunoediting of leukocyte functions and melanoma extravasation. *Cancer Res* **67:** 5814–5820

Longo N, Yanez-Mo M, Mittelbrunn M, de la Rosa G, Munoz ML, Sanchez-Madrid F, Sanchez-Mateos P (2001) Regulatory role of tetraspanin CD9 in tumor-endothelial cell interaction during transendothelial invasion of melanoma cells. *Blood* **98:** 3717–3726

Ma L, Young J, Prabhala H, Pan E, Mestdagh P, Muth D, Teruya-Feldstein J, Reinhardt F, Onder TT, Valastyan S, Westermann F, Speleman F, Vandesompele J, Weinberg RA (2010) miR-9, a MYC/MYCN-activated microRNA, regulates E-cadherin and cancer metastasis. *Nat Cell Biol* **12:** 247–256

Melnikova VO, Bar-Eli M (2008) Transcriptional control of the melanoma malignant phenotype. *Cancer Biol Ther* **7:** 997–1003

Mitchell K, Svenson KB, Longmate WM, Gkirtzimanaki K, Sadej R, Wang X, Zhao J, Eliopoulos AG, Berditchevski F, Dipersio CM (2010) Suppression of integrin alpha3beta1 in breast cancer cells reduces cyclooxygenase-2 gene expression and inhibits tumorigenesis, invasion, and cross-talk to endothelial cells. *Cancer Res* **70:** 6359–6367

Mueller DW, Bosserhoff AK (2009) Role of miRNAs in the progression of malignant melanoma. *Br J Cancer* **101:** 551–556

Neufeld G, Kessler O (2008) The semaphorins: versatile regulators of tumour progression and tumour angiogenesis. *Nat Rev Cancer* **8:** 632–645

Nguyen DX, Bos PD, Massague J (2009) Metastasis: from dissemination to organ-specific colonization. *Nat Rev Cancer* **9:** 274–284

Orso F, Penna E, Cimino D, Astanina E, Maione F, Valdembri D, Giraudo E, Serini G, Sismondi P, De Bortoli M, Taverna D (2008) AP-2alpha and AP-2gamma regulate tumor progression via specific genetic programs. *FASEB J* **22:** 2702–2714

Parkin DM, Bray F, Ferlay J, Pisani P (2005) Global cancer statistics, 2002. *CA Cancer J Clin* **55:** 74–108

Pfaffl MW (2001) A new mathematical model for relative quantification in real-time RT-PCR. *Nucleic Acids Res* **29:** e45

Primo L, di Blasio L, Roca C, Droetto S, Piva R, Schaffhausen B, Bussolino F (2007) Essential role of PDK1 in regulating endothelial cell migration. *J Cell Biol* **176:** 1035–1047

Rasola A, Geuna M (2001) A flow cytometry assay simultaneously detects independent apoptotic parameters. *Cytometry* **45:** 151–157

Segura MF, Belitskaya-Levy I, Rose AE, Zakrzewski J, Gaziel A, Hanniford D, Darvishian F, Berman RS, Shapiro RL, Pavlick AC, Osman I, Hernando E (2010) Melanoma MicroRNA signature predicts post-recurrence survival. *Clin Cancer Res* **16:** 1577–1586

Segura MF, Hanniford D, Menendez S, Reavie L, Zou X, Alvarez-Diaz S, Zakrzewski J, Blochin E, Rose A, Bogunovic D, Polsky D, Wei J, Lee P, Belitskaya-Levy I, Bhardwaj N, Osman I, Hernando E (2009) Aberrant miR-182 expression promotes melanoma metastasis by repressing FOXO3 and microphthalmia-associated transcription factor. *Proc Natl Acad Sci USA* **106:** 1814–1819

Sempere LF, Christensen M, Silahtaroglu A, Bak M, Heath CV, Schwartz G, Wells W, Kauppinen S, Cole CN (2007) Altered microRNA expression confined to specific epithelial cell subpopulations in breast cancer. *Cancer Res* **67:** 11612–11620

Steeg PS (2006) Tumor metastasis: mechanistic insights and clinical challenges. *Nat Med* **12:** 895–904

Swart GW, Lunter PC, Kilsdonk JW, Kempen LC (2005) Activated leukocyte cell adhesion molecule (ALCAM/CD166): signaling at the divide of melanoma cell clustering and cell migration? *Cancer Metastasis Rev* **24:** 223–236

Talantov D, Mazumder A, Yu JX, Briggs T, Jiang Y, Backus J, Atkins D, Wang Y (2005) Novel genes associated with malignant melanoma but not benign melanocytic lesions. *Clin Cancer Res* **11:** 7234–7242

Ueda T, Volinia S, Okumura H, Shimizu M, Taccioli C, Rossi S, Alder H, Liu CG, Oue N, Yasui W, Yoshida K, Sasaki H, Nomura S, Seto Y, Kaminishi M, Calin GA, Croce CM (2010) Relation between microRNA expression and progression and prognosis of gastric cancer: a microRNA expression analysis. *Lancet Oncol* **11:** 136–146

Valastyan S, Reinhardt F, Benaich N, Calogrias D, Szasz AM, Wang ZC, Brock JE, Richardson AL, Weinberg RA (2009) A pleiotropically acting microRNA, miR-31, inhibits breast cancer metastasis. *Cell* **137:** 1032–1046

Valastyan S, Weinberg RA (2009) MicroRNAs: crucial multi-tasking components in the complex circuitry of tumor metastasis. *Cell Cycle* **8:** 3506–3512

Volinia S, Calin GA, Liu CG, Ambs S, Cimmino A, Petrocca F, Visone R, Iorio M, Roldo C, Ferracin M, Prueitt RL, Yanaihara N, Lanza G, Scarpa A, Vecchione A, Negrini M, Harris CC, Croce CM (2006) A microRNA expression signature of human solid tumors defines cancer gene targets. *Proc Natl Acad Sci USA* **103:** 2257–2261

Watanabe T, Sato T, Amano T, Kawamura Y, Kawamura N, Kawaguchi H, Yamashita N, Kurihara H, Nakaoka T (2008) Dnm3os, a non-coding RNA, is required for normal growth and skeletal development in mice. *Dev Dyn* **237:** 3738–3748

Worley LA, Long MD, Onken MD, Harbour JW (2008) Micro-RNAs associated with metastasis in uveal melanoma identified by multiplexed microarray profiling. *Melanoma Res* **18:** 184–190

Xiao F, Zuo Z, Cai G, Kang S, Gao X, Li T (2009) miRecords: an integrated resource for microRNA-target interactions. *Nucleic Acids Res* **37** (Database Issue)**:** D105–D110

Xie S, Luca M, Huang S, Gutman M, Reich R, Johnson JP, Bar-Eli M (1997) Expression of MCAM/MUC18 by human melanoma cells leads to increased tumor growth and metastasis. *Cancer Res* **57:** 2295–2303

Xu L, Shen SS, Hoshida Y, Subramanian A, Ross K, Brunet JP, Wagner SN, Ramaswamy S, Mesirov JP, Hynes RO (2008) Gene expression changes in an animal melanoma model correlate with aggressiveness of human melanoma metastases. *Mol Cancer Res* **6:** 760–769

Yang H, Kong W, He L, Zhao JJ, O'Donnell JD, Wang J, Wenham RM, Coppola D, Kruk PA, Nicosia SV, Cheng JQ (2008) MicroRNA expression profiling in human ovarian cancer: miR-214 induces cell survival and cisplatin resistance by targeting PTEN. *Cancer Res* **68:** 425–433

Yin G, Chen R, Alvero AB, Fu HH, Holmberg J, Glackin C, Rutherford T, Mor G (2010) TWISTing stemness, inflammation and proliferation of epithelial ovarian cancer cells through MIR199A2/214. *Oncogene* **29:** 3545–3553

Zhang L, Huang J, Yang N, Greshock J, Megraw MS, Giannakakis A, Liang S, Naylor TL, Barchetti A, Ward MR, Yao G, Medina A, O'Brien-Jenkins A, Katsaros D, Hatzigeorgiou A, Gimotty PA, Weber BL, Coukos G (2006) microRNAs exhibit high frequency genomic alterations in human cancer. *Proc Natl Acad Sci USA* **103:** 9136–9141

Biscontin *et al. BMC Molecular Biology* 2010, **11**:44
http://www.biomedcentral.com/1471-2199/11/44

BMC Molecular Biology

METHODOLOGY ARTICLE Open Access

New miRNA labeling method for bead-based quantification

Alberto Biscontin[1], Silvia Casara[1], Stefano Cagnin[1], Lucia Tombolan[1], Angelo Rosolen[2], Gerolamo Lanfranchi*[1] and Cristiano De Pittà*[1]

Abstract

Background: microRNAs (miRNAs) are small single-stranded non-coding RNAs that act as crucial regulators of gene expression. Different methods have been developed for miRNA expression profiling in order to better understand gene regulation in normal and pathological conditions. miRNAs expression values obtained from large scale methodologies such as microarrays still need a validation step with alternative technologies.

Results: Here we have applied with an innovative approach, the Luminex® xMAP™ technology validate expression data of differentially expressed miRNAs obtained from high throughput arrays. We have developed a novel labeling system of small RNA molecules (below 200 nt), optimizing the sensitive cloning method for miRNAs, termed miRNA amplification profiling (mRAP). The Luminex expression patterns of three miRNAs (miR-23a, miR-27a and miR-199a) in seven different cell lines have been validated by TaqMan miRNA assay. In all cases, bead-based meas were confirmed by the data obtained by TaqMan and microarray technologies.

Conclusions: We demonstrate that the measure of individual miRNA by the bead-based method is feasible, high speed, sensitive and low cost. The Luminex® xMAP™ technology also provides flexibility, since the central reaction can be scaled up with additional miRNA capturing beads, allowing validation of many differentially expressed miRNAs obtained from microarrays in a single experiment. We propose this technology as an alternative method to qRT-PCR for validating miRNAs expression data obtained with high-throughput technologies.

Background

MicroRNAs (miRNAs) are endogenous 18-24 nucleotides (nt) long noncoding RNAs (ncRNA) that control gene expression by targeting mRNAs and triggering either translation repression or degradation. The degree of complementarity between a miRNA and its mRNA target determines, at least in part, the regulatory mechanism [1]. Recently, a third less understood mechanism of small RNAs interference on gene expression involves heterochromatin silencing [2]. Many miRNAs are highly conserved among animals and plants [3] and it is estimated that up to 33% of all mRNA coding genes are negatively regulated by miRNAs [4,5]. miRNAs exhibit temporally and spatially regulated expression patterns during diverse developmental and physiological processes and clearly animals cannot survive without miRNAs [6,7]. Most of the miRNAs that have been characterized so far in animals seem to regulate developmental processes, including larval stage transitions and neuronal development in *C. elegans* [8], growth control and apoptosis in *Drosophila melanogaster* [9] or haematopoietic differentiation in mammals. Many miRNAs have been found to display unique tissue [10], developmental stage [11] or disease-specific patterns [12]. These observations imply that each tissue is characterized by a specific set of miRNAs that contribute to the definition of the features of that tissue. Hundreds of novel conserved and non-conserved microRNAs have been identified by bioinformatic analyses, suggesting that the total number of human miRNAs could reach 1,000 [13]. According to recent computational predictions, as many as 200 mRNAs can be regulated by a single miRNA, which implies that over one third of protein-coding genes in humans are regulated by miRNA [14,15].

So, the ability to monitor changes in miRNAs expression is important for understanding gene regulation both

* Correspondence: gerolamo.lanfranchi@unipd.it, cristiano.depitta@unipd.it
Department of Biology and CRIBI Biotechnology Centre, Università degli Studi di Padova, Via U. Bassi, 58/B, 35121 Padova, Italy
Full list of author information is available at the end of the article

in physiological and pathological conditions. Several methodologies have been adapted for profiling miRNA expression: northern blotting with radiolabeled probes [16,17], cloning [18,19], massive parallel signature sequencing (MPSS) [20], quantitative PCR-based amplification of precursor [21] or mature miRNAs [22], SAGE-based techniques [23], bead-based profiling methods [24,25] and oligonucleotide microarray [26]. Microarray technology has been successfully used for evaluating variations of miRNA expression during development [27,28], differentiation [29], oncogenesis [30-32], disease progression [33,34] and for the primary identification of new miRNAs that were predicted by bioinformatic approaches [35,36]. However, at present, no standard methodology exists for hybridization-based profiling of miRNAs and, as a consequence, comparison of expression data from different experiments can be difficult. To solve these problems it will be necessary to develop quality procedures for miRNA microarrays. Furthermore, miRNA expression obtained from high throughput arrays has to be validated with alternative technologies. Quantitative real-time PCR (qRT-PCR) has become the golden standard of miRNA quantification because it offers the highest sensitivity from small amounts of starting material and it is able to detect as less as 1-nt difference between miRNAs. Another interesting method is the Luminex® xMAP™ system that is a multiplexed microsphere-based suspension array platform capable of performing and reporting up to 100 different analyses in a single reaction vessel [37,38]. In particular, oligonucleotide-capturing probes complementary to miRNAs of interest are coupled to carboxilated 5-micron polystirene beads impregnated with variable mixtures of two fluorescent dyes, each representing a single miRNA. Using this technique Lu and colleagues [24] were able to differentiate tumours that were instead inaccurately classified by mRNA profiles. Recently, a study performed with Luminex miRNA platform, identified new markers of human breast cancer subtype [39]. When compared to glass-slide microarrays, the bead-based miRNA arrays show many advantages such as easy of use, low cost, superior statistical performance, faster hybridization kinetics (solution hybridization) and higher flexibility in array preparation. Furthermore, the Luminex bead array system has been used in a wide range of multianalyte applications throughout the drug discovery and diagnostics fields and it is also widely adopted for quantitative multiplexed protein expression analysis [40,41].

In this study we have applied the Luminex® xMAP™ technology in a novel approach to validate expression data of differentially expressed miRNAs obtained from high throughput arrays. We have developed an innovative system for labeling of small RNA molecules (below 200 nt) optimizing the sensitive cloning method for miRNAs, termed mRAP, developed by Takada and Mano to define mouse miRNA transcriptional signature [19,42,43]. The expression patterns of three miRNAs (miR-23a, miR-27a and miR-199a) measured by our Luminex approach in seven different cell lines were validated by TaqMan miRNA assay. In all cases, the two technologies gave super imposable results. Our data demonstrate that bead-based detection of individual miRNA is a feasible approach, associated to high speed and low cost. The Luminex® xMAP™ technology is also feasible for multiplexing, since several beads prepared to capture different miRNAs can be added in the same reaction allowing the validation of many differentially expressed miRNAs obtained from large-scale approaches in a single experiment.

Results and Discussion

miRNA expression in rhabdomyosarcoma cell lines

Rhabdomyosarcomas (RMS) are rare but very aggressive tumours of childhood that arise as a consequence of regulatory disruption of the growth and differentiation pathways of myogenic precursor cells [44]. Based on morphology, two major RMS subtypes can be identified: embryonal RMS (ERMS) and alveolar (ARMS). To better understand the global function of miRNA in RMS, we analyzed the expression profile of 7 different RMS cell lines (3 ARMS and 4 ERMS) using the *mirVana* miRNA Probe Set V1 (Ambion) that is a collection of about 400 amino-modified DNA oligonucleotides [45]. Briefly, the miRNA population from a single cell line was compared to a reference sample consisting of a pool of the seven small RNA samples (< 200 nt) mixed in equal amounts. The miRNA microarray platform was able to distinguish *PAX3-FKHR* positive (RH4, RH30) and negative RMS (RD, CCA, SMS-CTR, RH36, RH18) cell lines through the expression pattern of about 120 miRNAs (data not shown). Since the translocation positive RMS patients fared worse than the negative counterpart [46] our results demonstrated the potential of miRNA expression profiling to classify different RMS subtypes, in agreement to previous gene expression studies [47-49], and set the basis for a further functional characterization of selected miRNAs implicated in RMS pathogenesis and in the different clinical behaviour and aggressiveness of the two RMS subtypes. We decided to study miRNAs with the greatest difference in expression between *PAX3-FKHR* positive and negative RMS. So expression levels for three discriminant miRNAs (miR-23a, miR-27a and miR-199a) were validated by xMAP™ technology and TaqMan qRT-PCR.

Testing the hybridization specificity and sensitivity between targets and capture probes coupled to microspheres

To prepare the capture probes, 21-23 bases-long oligonucleotides with sequence complementary to each of the

three differentially expressed miRNAs (miR-23a, miR-27a and miR-199a) in RMS cell lines, were synthesized and coupled to different color-coded microspheres in separate reaction tubes and then mixed for multiplexed assays. The targets were oligonucleotides complementary to capture probes and tagged with biotin at their 5'-end. Capture probes (approximately 5,000 beads for each probe) were mixed in the same tube with targets at various amounts ranging from 15 amol to 300 fmol. Phycoerythrin (PE)-coniugated streptavidin was added to the reaction mixture to detect bound targets that were biotynilated. The signal of each target hybridized to its specific capture probe coupled to microspheres was determined by the fluorescence intensity of phycoerytrin. At least 100 microspheres of each set were analyzed by the Bio-Plex™ system to obtain a median fluorescence intensity value (MFI) that was representative of the whole population of each set of beads. As shown in Figure 1A, the hybridization signal for miR-199a with capture probe varied with the amounts of added target in a logarithmic trend, reaching a plateau when the targets were present at the highest concentrations. Furthermore, the specificity of hybridization did not change while increasing from 1 to 3 the number of different microspheres in the reaction. We have evaluated the stability of conjugated microspheres at regular intervals during 80 days after conjugation. The hybridization signal is stable up to 35 days. As shown in Figure 1A, the hybridization signal for the miR-199a slightly decreased with the distance from conjugation, but the hybridization between the capture probe and the corresponding target remained specific and proportional. Furthermore, our data show that it is better to use microspheres conjugated in the same day to correctly detect miRNA expression values. We have also represented the curve in a log-scale (Figure 1B) highlighting the linearity range of our technique: the lower limit of sensitivity is 0.073 fmol and the upper is 18.75 fmol. We have obtained comparable results with either miR-23a or miR-27a. We measured the specificity of our technique by testing the variation in hybridization signal intensity when miR-27a and miR-199a are captured with probes that contain one or two mismatches in their complementary sequences (see Table 1). We have evaluated the signal of each target (biotynilated oligonucleotides perfectly complementary to mature miRNA sequence) hybridized to the correspondent capture probes with perfect match, one or two mismatches. As described above, capture probes were mixed in the same tube with targets at various amounts (from 15 amol to 300 fmol). Figure 2 shows that for both miRNAs we obtain a significant decrease of hybridization fluorescence intensity with capture probes containing a single mismatch. The signal drop is even greater with two mismatches: 62% for miR-27a and 85% for miR-199a.

We have also determined the expression levels of above cited miRNAs, using the capture probes with perfect match, one or two mismatches in complex RNA populations obtained from seven RMS cell lines (RD, CCA, SMS-CTR, RH36, RH18, RH4, RH30) in comparison to a reference sample (Pool). As shown in Figure 3, we observe a decreasing trend in fluorescence signal for the capture probes with two mismatches. These experiments show that the specificity of a capture probe is proportional to the number of mismatches present in its sequence and that this specificity guarantee the correct quantification of miRNA expression levels in complex RNA populations.

A new application of mRAP method for miRNA labeling

We have developed a new sensitive miRNA labeling method based on the mRAP strategy recently developed by Mano and Takada for miRNA cloning [40,41]. This new procedure is described schematically in Figure 4. Small RNA molecules (< 200-nt) purified by PureLink™ miRNA Isolation Kit (Invitrogen) were polyadenylated with Poly(A) polymerase (PAP). Complementary DNAs corresponding to the miRNAs were then synthesized with the use of reverse transcriptase and a RT primer, named Oligo-dT_{15}-T7, complementary to the poly(A) sequences added to the miRNA. This RT reaction was allowed for 30 minutes in order to synthesize cDNA molecules of about 200 nt. We have used a degenerated oligo(dT) to reduce the length of the neo-synthesized poly(A) tails to 15 nucleotides. Given that some reverse transcriptases possess terminal deoxynucleotidyl transferase activity, the synthesized cDNA strands frequently result with small poly(C) overhangs at their 3' ends. After annealing a long 5'-adptor, named SMART-16attB1-T3, to such poly(C) overhangs, PCR was used to amplify the miRNA-derived cDNAs. Using a T3-biotinylated forward primer, we have obtained biotinylated cDNA that was detected with Phycoerythrin (PE)-coniugated streptavidin after hybridization reaction. Every step of this protocol was quality checked by Agilent Bioanalyzer 2100 and the resulting electropherograms are represented in Figure 4. Electropherogram analysis of the RT products have revealed two major bands of ~30 and ~40 nt that correspond to the 5'-adaptor (SMART-16attB1-T3) and the oligo-dT_{15}-T7 primer respectively. The electropherograms also evidence the action of degenerated oligo(dT) that reduces the length of neo-synthesized cDNAs to 100-110 nucleotides by shortening the poly(A) to 15 nt (Figure 4).

We have decided to block PCR reaction during the exponential phase at 22 cycles, to avoid distortion of the actual concentration of miRNAs in the sample under consideration. We have demonstrated that PCR cycles between 20 and 25 are sufficient to achieve a good level of

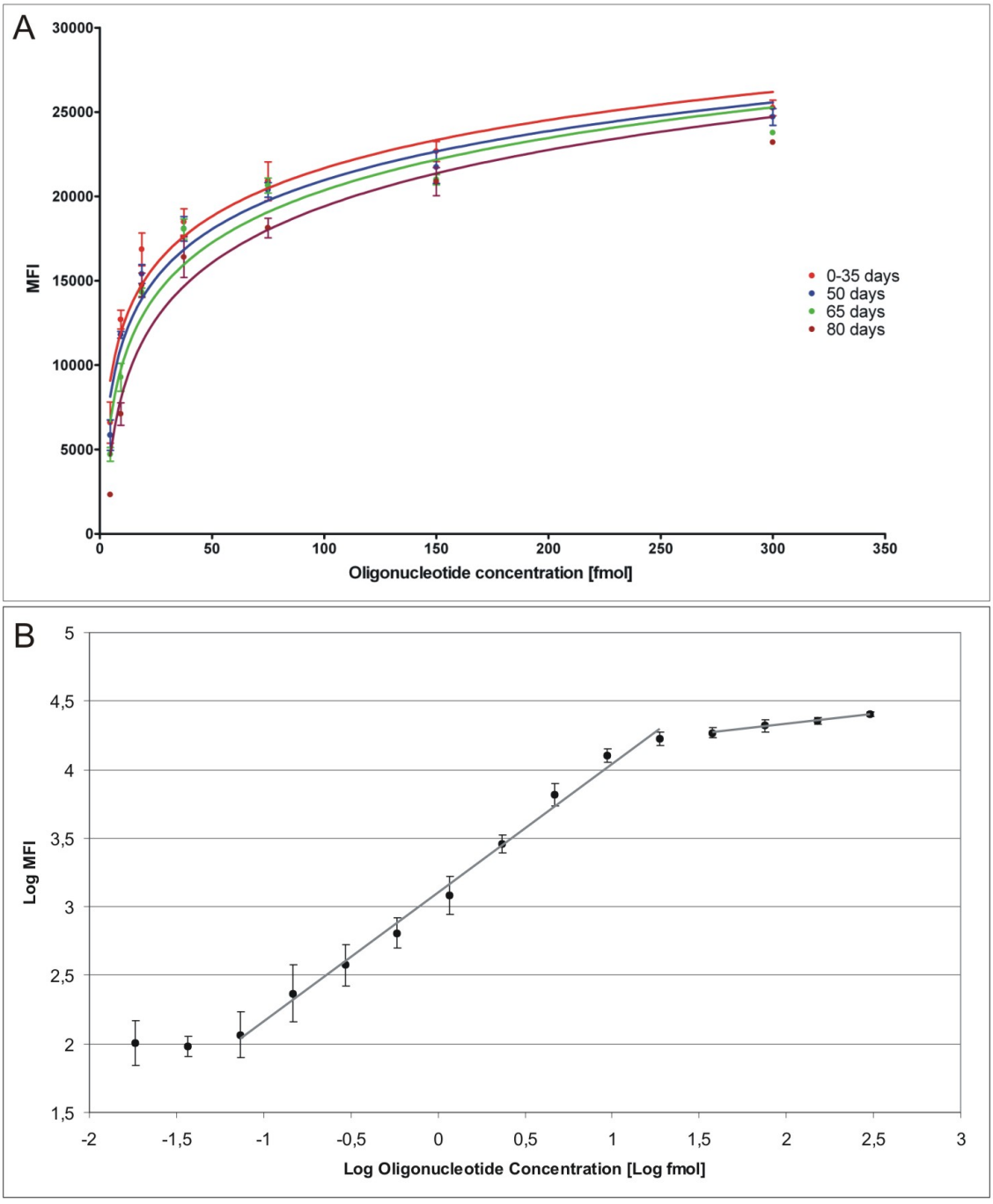

Figure 1 Stability of conjugated microspheres and sensitivity of hybridization. **A**) Increasing amounts of miR-199a target oligonucleotide (from 15 amol to 300 fmol) show higher fluorescence levels reaching a plateau when the target is present at high concentrations. The curve shows a logarithmic trend. We observed a slightly decrease of the hybridization signal at 50, 65 and 80 days after conjugation. **B**) Calibration curve (0-35 days) of miR-199a in a log-scale from 15 amol to 300 fmol. The two lines show the linear and plateau range of fluorescence levels representing by two different slopes: 0.94 and 0.15 respectively with $R^2 = 0.99$. The linearity range of our technique is comprised between a lower value of 0.073 fmol and an upper value of 18.75 fmol. Mean value of expression and 95% confidence intervals are associated to each fluorescence value (MFI corresponds to Median Fluorescence Intensity).

Table 1: Capture probes

ID	Nucleotide sequence (5'-3')	Lenght (nt)
miR-23a	GGAAATCCCTGGCAATGTGAT	21
miR-27a	GCGGAACTTAGCCACTGTGAA	21
miR-27a-1MM	GCGGAACT**A**AGCCACTGTGAA	21
miR-27a-2MM	GCGGAA**G**TTAGCCACTG**A**GAA	21
miR-199a	GAACAGGTAGTCTGAACACTGGG	23
miR-199a-1MM	GAACAGGTAGTCTGAA**G**ACTGGG	23
miR-199a-2MM	GA**T**CAGGTAGT**G**TGAACACTGGG	23
Spike 18	CATTGCCACAATCAAGACTAAGA	23

Nucleotide sequence of capture probes synthesized with 5'-amino linker and a C12 spacer. Basepair mismatches (named MM) are in bold and underlined

amplification without reaching the plateau phase in which the expression differences would be invalidated (Figure 5A).

Finally, to verify the presence of miRNAs within the labeled cDNA population we have identified, by PCR, three specific miRNAs (miR-1, miR-206 and miR-450) using the sequence of each miRNA as forward primer, and the sequence for T7 promoter, which is common to all labeled molecules, as reverse primer. The result of PCR amplification of the three miRNAs is shown in Figure 5B.

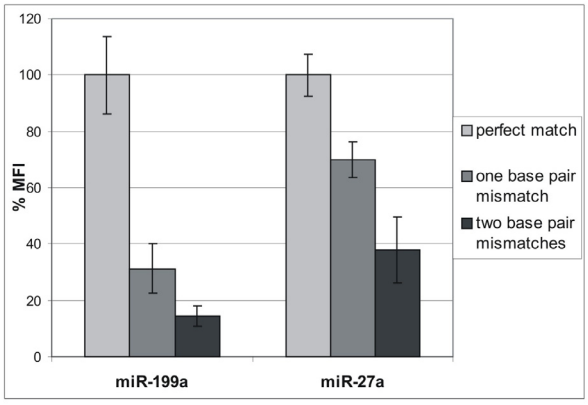

Figure 2 Specificity of hybridization between capture probes and miRNA targets. Biotynilated miR-199a and miR27a (bottom panel) were captured in solution by the corresponding probes with exactly matching sequences (light grey boxes) or with one (dark grey boxes) or two mismatched bases (black boxes). The fluorescence signal obtained by the hybridization of both the perfectly matching probes was set to 100%. The hybridization signal between both capture probes and the corresponding miRNA target shows a statistically significant decrease (p-value < 0.05) when one or two mismatches are introduced into the capture sequence. Hybridization experiments were obtained with 18.75 fmol of biotynilated targets that fall in the linearity range of our method as shown in Figure 1B. Mean value of expression and 95% confidence intervals are associated to each fluorescence value (%MFI corresponds to the percentage of Median Fluorescence Intensity).

Validation of differentially expressed miRNAs by Luminex® xMAP™ technology

Using the xMAP™ assay described above we have determined the expression levels of miR-23a, miR-27a and miR-199a in seven RMS cell lines (RD, CCA, SMS-CTR, RH36, RH18, RH4, RH30) in comparison to a reference sample consisting of a pool of small RNA from each cell line mixed in equal amounts.

To evaluate the validity and feasibility of an assay, it is necessary to compare data with that obtained by other established technologies such as, in this case, microarray and qRT-PCR. As shown in Figure 6, the trends of expression levels measured for all the miRNAs by the three technologies (microarray, xMAP™ and qRT-PCR) were very similar. Although the actual values of the relative miRNA hybridization signals in the seven RMS cell lines were not exactly the same for the three technologies, up-regulated miRNAs (miR-23a and miR-27a) in *PAX3-FKHR* positive RMS samples (RH4, RH30) detected originally by microarray were also up-regulated as detected by xMAP™ and qRT-PCR, and signals for miRNAs down-regulated in *PAX3-FKHR* negative RMS samples (RD, CCA, SMS-CTR, RH36, RH18) resulted consistently low by all three independent technologies. To better understand which are the techniques that provide the most similar results we have applied non-parametric Spearman correlation to the following paired comparisons for each tested miRNAs: $xMAP_{TM}$ *vs.* microarray, $xMAP_{TM}$ *vs.* qRT-PCR and qRT-PCR *vs.* microarray. It is interesting to note that data obtained with xMAP™ technology seem to be more similar to those defined by microarray (Spearman correlation: miR-199a = 0.64, miR-23a = 0.64, miR-27a = 0.84) respect to qRT-PCR (Spearman correlation: miR-199a = 0.67, miR-23a = 0.53, miR-27a = 0.81). From this comparison we could observe that the PCR amplification step introduced in xMAP™ labeling method does not affect miRNA expression levels whereas miRNA expression data obtained from < 200-nt RNA molecules

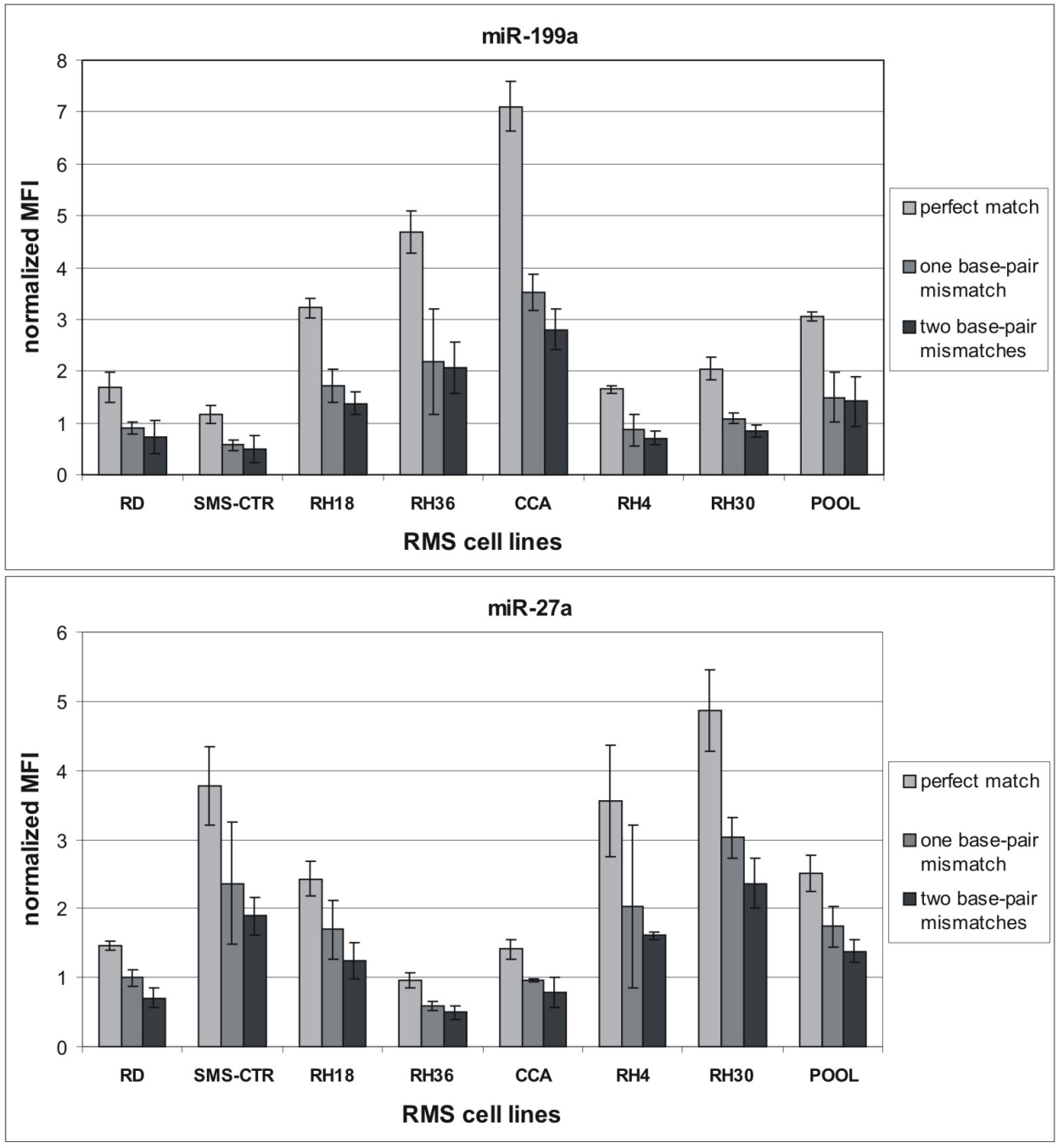

Figure 3 Specificity of hybridization between capture probes and miRNA targets in complex RNA populations. miR-199a (top panel) and miR27a (bottom panel) were captured from labeled total RNA populations prepared from 7 different RMS cell lines (RD, SMS-CTR, RH18, RH36, CCA, RH4, RH30) and a pool these RNA preparations mixed in equal amounts (POOL) with capture probes with exactly matching sequences (light grey boxes) or with one (dark grey boxes) or two mismatched bases (black boxes). The hybridization signal in all complex RNA mixtures between both capture probes and the corresponding miRNA target in comparison to the reference pooled sample shows a statistically significant decrease (p-value < 0.05) when one or two mismatches are introduced into the capture sequence. Mean value of expression and 95% confidence intervals are associated to each fluorescence value (normalized MFI represents the average of the ratio between the value of fluorescence of miRNAs and the spike).

(microarray and xMAP™) differ slightly from those obtained from total RNA (qRT-PCR). This is particularly evident by non-parametric Spearman correlation for qRT-PCR *vs*. microarray (miR-199a = 0.94, miR-23a = 0.42, miR-27a = 0.70) with the exception of miR-199a.

Conclusions

We have described a new method that makes use of xMAP™ technology for the quantitative determination of single miRNAs. This approach quantifies miRNA expression levels based on hybridization of small RNA popula-

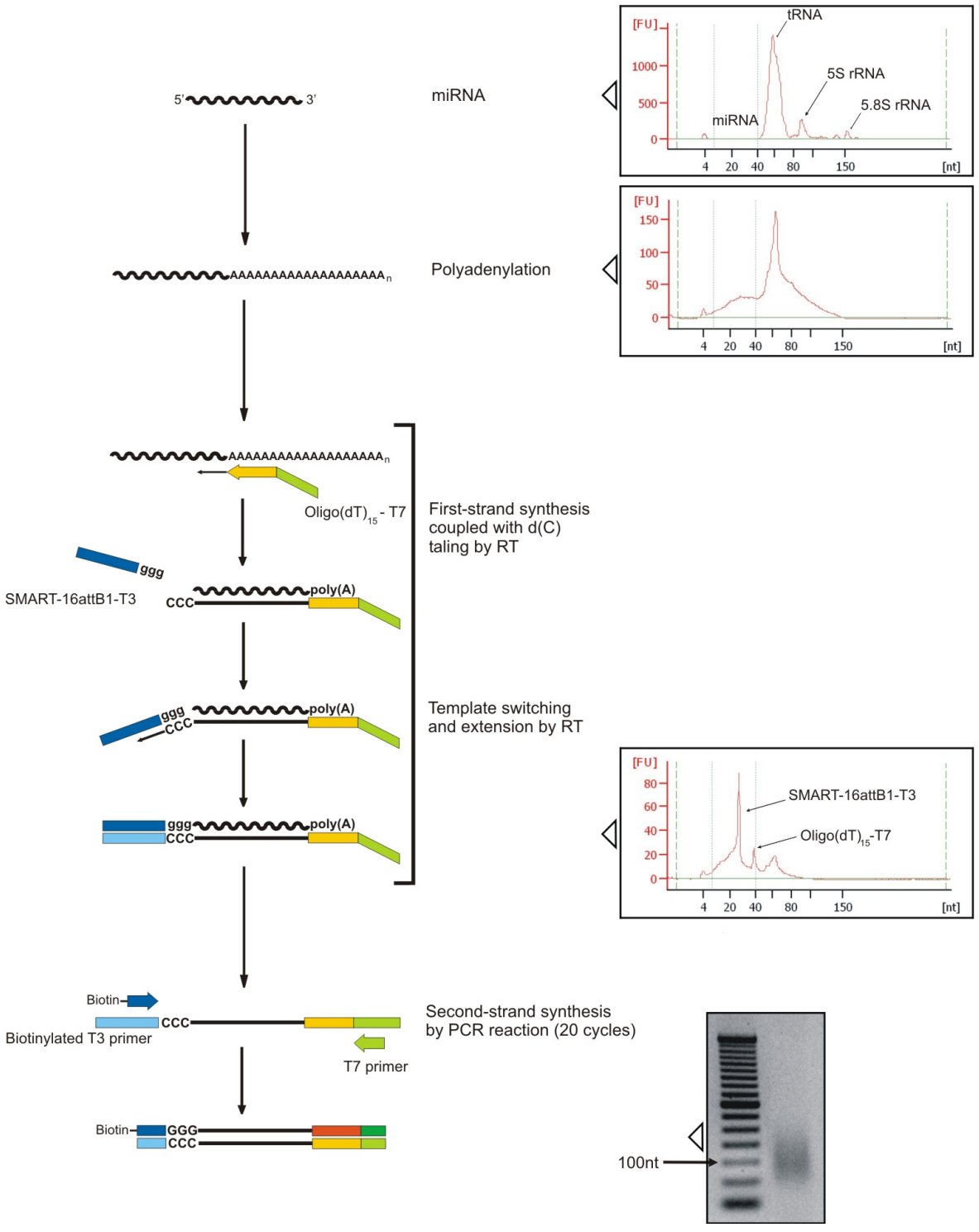

Figure 4 Schematic representation of miRNA labeling method for bead based quantification. All protocol steps and quality checking with Agilent Bioanalyzer 2100 and gel electrophoresis (2% agarose) are schematically represented: starting material (RNA < 200 nt), the result of polyadenylation reaction with PAP, the synthesis of first-strand cDNA (peaks are associated to Oligo-dT15-T7 and SMART-16attB1-T3 primers) and the second-strand synthesis by PCR amplification.

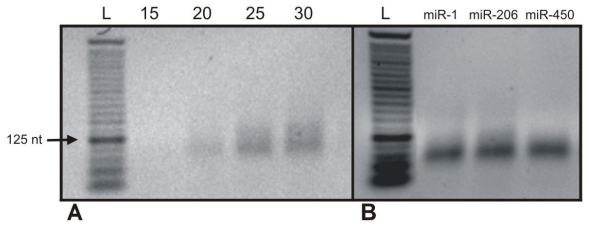

Figure 5 Second-strand synthesis by PCR reaction. **A**)Determination of the optimal PCR amplification cycle: the 2% agarose gel shows the amplification products of RH30 first-strand cDNA stopped at 15, 20, 25 and 30 PCR cycles. **B**) Presence of specific miRNAs in the labeled cDNA population: the 2.25% agarose gel shows PCR amplification products of three specific miRNAs (miR-1, miR-206 and miR-450) performed by using the sequence of each miRNA as forward primer, and the sequence for T7 promoter, which is common to all labeled molecules, as reverse primer.

tions to the probes designed for miRNAs of interest that are coupled to different color-coded microspheres. A flow-cytometer is used to simultaneously measure the hybridization signal associated with the surface of the microspheres and to categorize the color-coded microspheres. The method allows to obtain up to 100 independent measures. This xMAP™ method offers affordable cost, speed, and high flexibility with capability for multiplexed assays that are increasingly needed. It is valuable for applications such as diagnostic detection of disease miRNAs from clinical samples and validation of differentially expressed miRNAs obtained from microarray analysis.

We have evaluated the stability of conjugated microspheres demonstrating that they are stable for about one month. We have also tested the specificity of hybridization between targets and capture probes showing that the introduction of a single mismatch in the sequence of capture probes significantly hampers its hybridization capacity (Figures 2 and 3). These data have demonstrated the specificity of our capture probes to correctly identify and quantify the expression levels of miRNAs. We have developed a new sensitive small RNAs labeling protocol introducing some changes on mRAP strategy for miRNA cloning. This protocol has been applied successfully to validate the expression levels of three miRNAs that were found differentially expressed in positive and negative *PAX3/FKHR* alveolar rhabomyosarcomas by microarray experiments. To demonstrate the reliability of this method, the transcriptional levels of these miRNAs were also determined by qRT-PCR with TaqMan probes. The most significant information which emerges comparing the data obtained by the three different technologies (microarray, xMAP™ and qRT-PCR) is represented by the general overlapping of the expression profiles obtained. It is interesting to note that small differences in miRNAs expression data could depend on the approaches used for total RNA purification rather than on different labeling protocols. In fact, microarray and xMAP™ data obtained from labeling < 200-nt RNA molecules, are more similar compared to qRT-PCR data obtained from labeling total RNA, as demonstrated by the Spearman non parametric correlation.

We think that the xMAP™ technology associated with our new labeling protocol could become an alternative and equally reliable method in the study of expression of a limited number of miRNAs respect to qRT-PCR with TaqMan probes. The comparison of the two experimental approaches (see Table 2) shows that the xMAP™ technique is less expensive and more flexible allowing the simultaneous analysis of a larger number of miRNAs from the same sample. In addition, xMAP™ does not need for specific reverse transcription reactions for each miRNA and provides at least 100 independent measures for each miRNA, improving the statistical power. Moreover, xMAP™ expression data can be normalized respect to a spike fluorescence signal added in known quantities in the early stages of the labeling reaction, allowing the control over all stages of the reaction. In this way there is no need of an endogenous control, like in qRT-PCR, whose representativeness is sample-dependent.

Probably, a negative aspect of xMAP™ technology is represented by the use of enriched total RNA (< 200 nt) that requires higher amounts of starting material respect to qRT-PCR. To avoid the enrichment step of < 200 nt RNA molecules, we propose the use of LNA capture-probe oligonucleotides that increase the affinity of the oligonucleotide for its complementary RNA target leading to a significant enhance in stability and specificity of the duplex.

We think that the technology we have developed could be an alternative method to qRT-PCR for validating miRNAs expression data obtained with a large scale technology such as microarray and it could have a wide application in clinical, pharmaceutical, agricultural and environmental studies.

Methods

Cell culture

Human alveolar RMS (ARMS) cell lines, positive for *PAX3-FKHR* translocation (RH4, RH30), negative for *PAX3-FKHR* translocation (RH18) and human embryonal RMS (ERMS) cells (RD, RH36, CCA, SMS-CTR) were maintained in modified Eagle's medium (DMEM) containing 10% fetal calf serum, penicillin (100 U/ml), and streptomycin (100 μg/ml) (Invitrogen) at 37°C, 5% CO2 in a humidified incubator.

The human RMS cell lines RH30 and RD were purchased from ATCC (Manassas, VA); RH4 and RH18 were a gift of Dr P.J. Houghton (St Jude Children's Hospital,

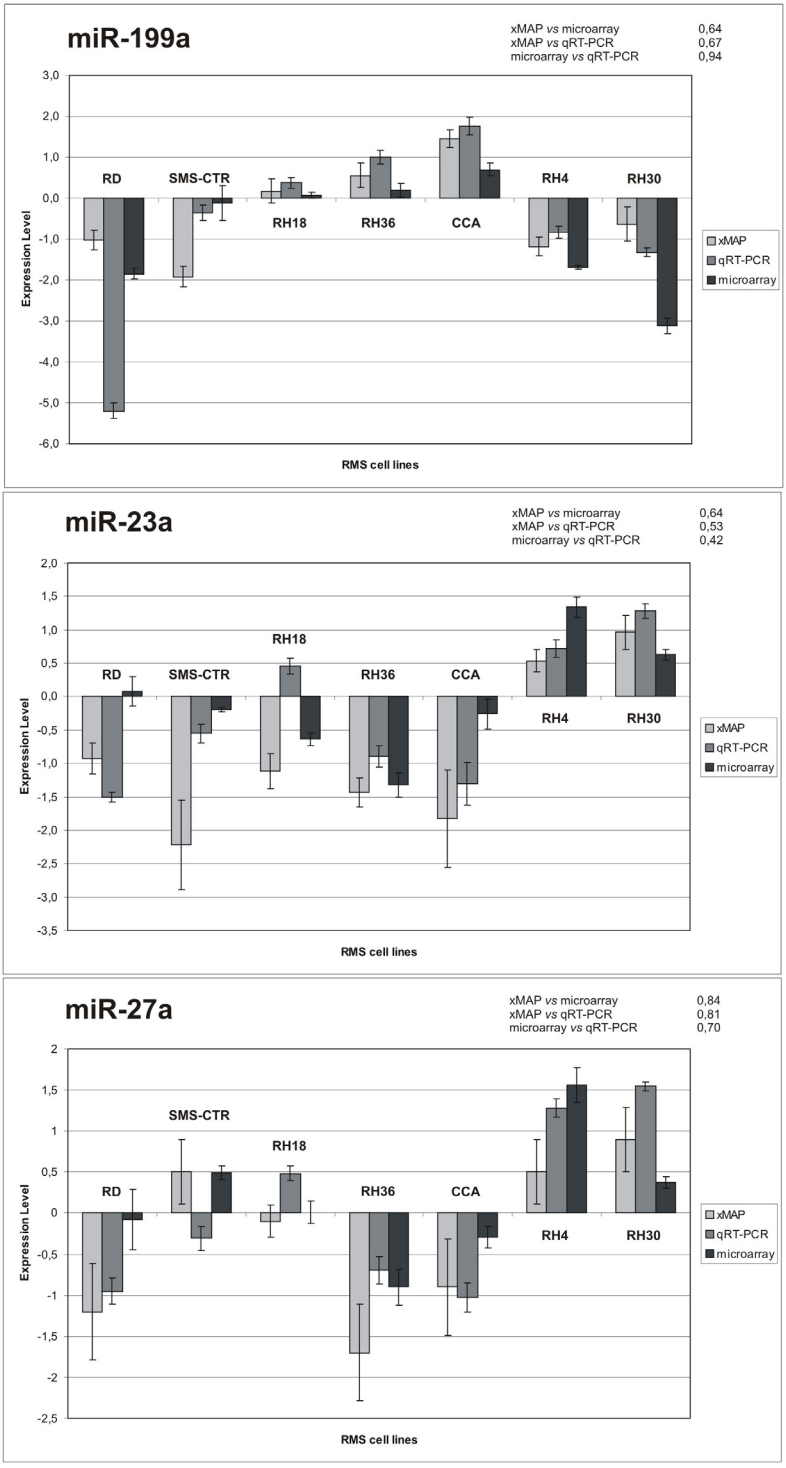

Figure 6 Comparison of three different techniques used to define miRNA expression profiles in seven RMS cell lines. Expression levels of miR-199a, miR-23a and miR-27a in seven RMS cell lines obtained with three methods (xMAP™, qRT-PCR and microarray) are represented. Mean value of expression and 95% confidence intervals are associated to each miRNA. The Figure also indicate, for each tested miRNAs, non-parametric Spearman correlations for the following paired comparisons: xMAP™ *vs*. microarray, xMAP™ *vs*. qRT-PCR and qRT-PCR *vs*. microarray.

Table 2: Comparison of xMAP™ and qRT-PCR techniques

	xMAP™	qRT-PCR
< 200 nt RNA molecules enrichment	YES	NO
RT step	YES	YES
Amplification	YES	YES
Endogenous control	NO	YES
Control spike	YES	NO
Multiplexing	YES	NO
Liquid-phase hybridization	YES	NO
No. of measures	100	1
Custom-tailored assay	YES	NO
Cost	Low	High

Memphis, TN); SMS-CTR, RH36, CCA were obtained from Dr M. Tsokos (NCI, Bethesda, MD).

Isolation of small RNA molecules

Total RNA was prepared from seven cell lines of human rhabdomyosarcoma using a modified TRIzol (Life Technologies Corporation, Carlsbad, CA, USA) protocol for small RNA enrichment. A pellet of about 6×10^6 - 9×10^6 cells was dissolved in 1 ml of TRIzol and the supernatant, containing total RNA, was purified by PureLink™ miRNA Isolation Kit (Life Technologies Corporation) that was specifically designed to enrich total RNA preparation for < 200-nt RNA molecules. RNA quantity and quality were assessed by Nanodrop (NanoDrop Technologies, Wilmington, DE, USA) spectrophotometry and microelectrophoresis using Small RNA Nano LabChip by Agilent 2100 bioanalyzer (Agilent Technologies, Palo Alto, CA, USA) respectively.

miRNA expression profiling and statistical analysis of data

microRNA expression profiling was carried out using the "mirVana Probe Set V1" (Ambion) that is a collection of about 400 amine-modified DNA oligonucleotides representing a panel of the human, mouse and rat microRNAome in the miRNA Registry (miRBase - Release 9). The probes are 42-46 nucleotides (nt) long, with 18-24 nt segment targeting a specific miRNA, and the remaining sequence serving as spacer. We analyzed the expression profiles of 7 different rhabdomyosarcoma cell lines: 3 ARMS (RH4, RH30, RH18) and 4 ERMS (RD, RH36, CCA, SMS-CTR). The miRNA population from each cell line was compared to a reference sample consisting of a pool of the 7 total RNA samples mixed in equal amounts. Two replicates of each experiment were performed using different microarray slides, in which sample and reference RNAs, labeled either with Cy3 or Cy5 fluorochromes, were crossed in both combinations (dye-swapping procedure). miRNAs were labeled with the mirVana Labeling Kit (Ambion) and amine-reactive dyes (GE Healthcare) as recommended by the manufacturer's protocol [45]. Normalization of expression levels of all spot replicates was performed by MIDAW [50]. Principal component analysis, cluster analysis and profile similarity searching were performed with tMev software [51]. One and two class Significance Analysis of Microarray (SAM) allowed to identify differentially expressed miRNAs [52].

Capture probe and its coupling to microspheres

A sequence of 21-23 nt complementary for each tested miRNAs (listed in the Table 1) was chosen as capture probe and synthesized with 5'-amino linker and a C12 spacer (PRIMM, Milan, Italy). Capture-probe oligonucleotides were covalently linked to carboxylated fluorochrome microspheres (Bio-Rad Laboratories, Hercules, CA, USA) in water-soluble carbodiimide. Specifically, 1×10^6 carboxylated microspheres were pelleted in a microcentrifuge for 5 minutes at 12,000×g and then supernatant was carefully removed. The dry microspheres were dissolved in 20 μl of a buffer containing 0.1 M MES (Sigma-Aldrich, St. Louis, MO, USA) at pH 4.5. The amino-substituted capture probe was dissolved in molecular biology grade water at a concentration of 100 μM and 0.5 μl of the solution (containing 0.05 nmole of capture probe oligonucleotides) was added to the beads for the coupling reaction. The coupling reaction was performed by adding 2.5 μl of a freshly made solution of 10 mg/ml 1-ethyl-3-(3-dimethylaminopropyl) carbodiimide hydrochloride (EDC) (Pierce, Thermo Scientific, Wilmington, DE, USA) in molecular biology grade water. The mixture of microspheres, capture probes, and EDC was vortexed briefly and incubated at room temperature for 30 minutes in the dark. Occasionally, the reaction was mixed by finger flicking the tube to keep the microspheres in suspension. A second incubation steps was done adding a freshly-made solution of 10 mg/mL EDC in molecular biology grade water. After the coupling reac-

tion, 500 μl of 0.02% Tween 20 (Sigma-Aldrich) was added to the microspheres. The solution was mixed well by vortex and centrifuged for 6 minutes at 12,000×g. The supernatant containing free-capture-probe oligonucleotides and excess EDC was carefully removed. The coupled microspheres were washed in 500 μl of 0.1% SDS (Sigma-Aldrich) by vortex and centrifuged for 5 minutes at 12,000×g. Finally, the supernatant was removed and the capture-probe conjugated microspheres were resuspended in 20 μl of TE pH 8.0 and stored at 4°C in a dark box (stable for at least 6 months). The microspheres were diluted in TE buffer and counted using a Bürker chamber under the microscope at 100× magnification.

miRNA labeling

At the beginning, 1 μg of small RNA molecules (< 200-nt) and 200 pg of a synthetic pre-labeling control RNA (5'-UCUUAGUCUUGAUUGUGGCAAUG-3', PRIMM) were mixed in order to control target preparation efficiency and to normalize expression data. The mixture was polyadenylated using Poly(A) Tailing Kit (Ambion) according to the manufactures' instructions. The reaction was precipitated with NaOAc 3 M pH 5.5 (1/10 volume) and absolute ethanol (4 volumes) overnight at -20°C. The polyadenylated RNA molecules were resuspended in 15 μl of H_2O RNase free and then volume was reduced to 3.2 μl by vacuum (VR-1, Heto-Holten, Denmark). miRNAs labeling was performed by mRAP modified protocol in which miRNA-derived cDNAs were flanked by synthesized oligomers at each end. The SMART (switching mechanism at the 5'-end of RNA templates of reverse transcriptase) oligo sequence (SMART-16attB1-T3: 5'-TACAAAAAAGCAGGCTAATTAACCCTCAC-TAAAggg-3') and the overhang of the oligo-dT_{15}-T7 primer (5'-GTGAATTGTTAATACGACTCACTATAG-GCGC $[dT]_{15}$N-3') were used for first strand synthesis. First strand cDNA synthesis was performed from 500 ng of small RNA in a 10 μl reaction. Then, the reaction was diluted 1:2 and incubated at 72°C for 7 min. Second strand reaction mix was added to 3.0 μl of diluted first strand cDNA to give a final concentration of 1X BD Advantage 2 PCR reaction buffer (Clontech Laboratories, Mountain View, CA, USA), 0.2 mM dNTPs, 100 nM primers (T3-biotinylated forward primer: 5' - biotAAT-TAACCCTCACTAAAGGG-3' and T7 reverse primer: 5'- TAATACGACTCACTATAGG-3') and 1X of Advantage 2 DNA polymerase mix (Clontech Laboratories) in a total volume of 25 μl. This second strand reaction mixture was incubated for 22 cycles of the following steps: 15 sec 95°C, 20 sec 51°C and 20 sec 72°C. Only those ss cDNAs having a SMART anchor sequence at the 5'-end were used as template and exponentially amplified. The second strand reaction was precipitated in sodium acetate-ethanol solution and dissolved in 11 μl TE buffer pH 8.0 (10 mM TrisHCl pH 8.0, 1 mM EDTA). Biotinylated cDNA quantity was assessed by Nanodrop spectrophotometer (Nanodrop Technologies) and stored at -20°C until hybridization with microspheres. Labelled target produced by a single PCR reaction was sufficient for two hybridization reactions.

Hybridization of targets to capture probes coupled to microspheres

The microspheres of each probe set were resuspended by vortexing for approximately 20 seconds. A microsphere mixture was prepared by diluting coupled stocks to 150 microspheres of each set/μl in 1.5× TMAC Hybridization Buffer (5 M tetramethylammonium chloride, 0.15% Sarkosyl; 75 mM Tris-HCl pH 8.0; and 6 mM EDTA, pH 8.0), followed by vortex mixing for approximately 20 seconds. Two μg of biotinylated DNA target in 17 μL of TE buffer pH 8.0 was added to 33 μl of microsphere mixture (approximately 5,000 beads per color) in the wells of a 96-well plate. 17 μl of TE buffer pH 8.0 were added to background wells. Each well reaction was mixed gently by pipetting up and down several times and the labeled DNA was denatured by heating at 95-100°C for 3 min. The hybridization mixture was incubated at 48°C for 17 h, covering the plate to prevent evaporation, in a Eppendorf microplate incubator with shaking speed of 700 rpm. After incubation, the hybridization mixture was spun down for 3 min at 3,000×g to pellet the microspheres. Supernatant was carefully removed with a pipette without disturbing the microspheres. During centrifugation, fresh reporter mix was prepared by diluting streptavidin-conjugated R-phycoerythrin (Invitrogen) to 3 mg/ml in 1× TMAC Hybridization Buffer and 75 μl of reporter mix were added to the microspheres. The solution was gently mixed by pipetting and incubated in the dark at 48°C for 15 minutes in a Eppendorf microplate incubator. 50 μl of each sample were transferred to a Multiscreen HTS plate (Millipore) and analyzed on the BioPlex™ (Luminex® 100™, BioRad) machine at hybridization temperature.

Bead-based detection

Each set of microspheres was distinguished by assigned colour code (different percentage of red and orange) inside the microspheres. In our experiments we have used four different probe sets (regions: 1, 21, 51 e 57). The fluorescence associated to the surface of each bead, corresponding to the amounts of bound miRNAs, was detected and measured by the laser detector. The Bio-Plex™ (Luminex® 100™, Bio-Rad Laboratories) system detects fluorescent dyes with an excitation wavelength of -532 nm and emission wavelength -580 nm. For each experiment, 100 events of each subset of microspheres were analyzed on the Bio-Plex™ system to obtain a

median fluorescence intensity value (MFI) that was representative of the whole population of each set of beads.

Computational analyses (data processing and quality control)

To eliminate bead-specific background, the reading of every bead for every samples was first processed by subtracting the average readings of that particular bead in the absence of target miRNAs. Samples with median fluorescence intensity values smaller than background signals were removed. Every samples was assayed in three wells. Each of the three wells contained 4 probes: miR-23a, miR-27a, miR-199a and one pre-labeling control (Spike-18). Expression data were scaled according to the pre-labeling control in order to normalize readings from different probe/bead sets for the same sample and to normalize for the labeling efficiency. Technical replicate samples for each probe were summarized by their mean profile and expression data (test/control) were log2 transformed. The error associated to each probe is obtained by quadratic propagation from standard deviation.

qRT-PCR TaqMan

TaqMan® MicroRNA Assays incorporate a target-specific stem-loop, reverse transcription primer. The stem-loop structure provides specificity only for the mature miRNA target and forms a RT primer/mature miRNA-chimera that extends the 5'-end of the miRNA. The resulting longer RT amplicon presents a template amenable to standard real-time PCR using TaqMan Assays [22]. In brief, according to the manufacture's instructions (Applied Biosystems), each 15 μl RT reaction contained purified 10 ng of total RNA, 3.0 μl of 5× stem-loop RT primer, 1× RT buffer, 0.25 mM each of dNTPs, 50 U MultiScribe™ reverse transcriptase and 3.8 U RNase inhibitor. The reactions were incubated in a Mastercycler EP gradient S (Eppendorf) in 0.2 ml PCR tubes for 30 min at 16°C, 30 min at 42°C, followed by 5 min at 85°C, and then held at 4°C. RT products were diluted two times with H_2O prior to setting up PCR reaction. Each real-time PCR for each miRNA assay (10 μl volume) was carried out in triplicate, and each 10 μl reaction mixture included 1 μl of diluted RT product, 5 μl of 2 × TaqMan® Universal PCR Master Mix and 0.5 μl of 20× TaqMan® MicroRNA Assay. The reaction was incubated in a 7500 Real-Time PCR System (Applied Biosystems) in 96- well plates at 95°C for 10 min, followed by 40 cycles of the following steps: 95°C for 15 sec and 60°C for 1 min. The threshold cycle (CT) is defined as the fractional cycle number at which the fluorescence exceeds the fixed threshold of 0.2. To evaluate differences in miRNA expression, a relative quantification method was chosen where the expression of the miRNA target is standardized by a non-regulated small non-coding RNA used as reference.

Consequently, three replicates of each sample and endogenous control were amplified. U6B small nuclear (RNU6B) was used as endogenous control because the level of this small RNA remains essentially constant from sample to sample. To calculate the relative expression ratio, the $2^{-\Delta\ \Delta Ct}$ (RQ, relative quantification) method implemented in the 7500 Real Time PCR System software [53] was used. This method determines the change in expression of a nucleic acid sequence (target) in a test sample relative to the same sequence in a calibrator sample.

Authors' contributions

AB performed small RNA molecules isolation, capture probes coupling to microspheres, miRNA labeling method, bead-based detection with BioPlex and computational analyses (data processing and quality control). SC performed RMS cell lines culture, small RNA molecules isolation, microarray experiments and qRT-PCR validation. SC participated in conceiving the study and in development of miRNA labelling method. LT performed RMS cell lines culture and participated in total RNA extraction. AR provided RMS cell lines and revised the manuscript. GL supervised the study, participating in the design and coordination of the work, the interpretation of the results and revision of the manuscript. CDP conceived and supervised the study, participating in the design and coordination of the work, the interpretation of data and manuscript writing. All Authors read and approved the final version of the manuscript declaring that they have no potential conflicts of interests.

Acknowledgements

This work was supported by Associazione Italiana per la Ricerca sul Cancro (AIRC) and Biotech Action III bis (CIPE 3/06 DGR 4073 19/12/2006 Veneto Region). The authors wish to thank Emanuele Papini, Paola Cecchini and Regina Tavano (Dept. Biomedical Sciences and C.R.I.B.I. Biotechnology Centre-University of Padova, Italy) for technical support in bead-based detection with BioPlex. We are also grateful to Angelica Zin for RMS cell lines.

Author Details

[1]Department of Biology and CRIBI Biotechnology Centre, Università degli Studi di Padova, Via U. Bassi, 58/B, 35121 Padova, Italy and [2]Clinica di Oncoematologia Pediatrica, Azienda Ospedaliera-Università degli Studi di Padova, Vi Giustiniani 3, 35128 Padova, Italy

Received: 21 December 2009 Accepted: 16 June 2010
Published: 16 June 2010

References

1. Engels BM, Hutvagner G: **Principles and effects of microRNA-mediated post-transcriptional gene regulation.** *Oncogene* 2006, **25:**6163-6169.
2. Lippman Z, Martienssen R: **The role of RNA interference in heterochromatic silencing.** *Nature* 2004, **431:**364-370.
3. Zhang B, Wang Q, Pan X: **MicroRNAs and their regulatory roles in animals and plants.** *J Cell Physiol* 2007, **210:**279-289.
4. Harfe BD: **MicroRNAs in vertebrate development.** *Curr Opin Genet Dev* 2005, **15:**410-415.
5. Xi Y, Shalgi R, Fodstad O, Pilpel Y, Ju J: **Differentially regulated micro-RNAs and actively translated messenger RNA transcripts by tumor suppressor p53 in colon cancer.** *Clin Cancer Res* 2006, **12:**2014-2024.
6. Bartel DP: **MicroRNAs: genomics biogenesis, mechanism, and function.** *Cell* 2004, **116:**281-297.
7. Stefani G, Slack FJ: **Small non-coding RNAs in animal development.** *Nat Rev Mol Cell Biol* 2008, **9:**219-230.
8. Lee RC, Ambros V: **An extensive class of small RNAs in Caenorhabditis elegans.** *Science* 2001, **294:**862-864.
9. Jaubert S, Mereau A, Antoniewski C, Tagu D: **MicroRNAs in Drosophila: the magic wand to enter the Chamber of Secrets?** *Biochimie* 2007, **89:**1211-1220.
10. Landgraf P, Rusu M, Sheridan R, Sewer A, Iovino N, Aravin A, Pfeffer S, Rice A, Kamphorst AO, Landthaler M, Lin C, Socci ND, Hermida L, Fulci V, Chiaretti S, Foà R, Schliwka J, Fuchs U, Novosel A, Müller RU, Schermer B,

Bissels U, Inman J, Phan Q, Chien M, Weir DB, Choksi R, De Vita G, Frezzetti D, Trompeter HI, *et al.*: **A mammalian microRNA expression atlas based on small RNA library sequencing.** *Cell* 2007, **129:**1401-1414.
11. Pasquinelli AE, Ruvkun G: **Control of developmental timing by microRNAs and their targets.** *Annu Rev Cell Dev Biol* 2002, **18:**495-513.
12. Rana TM: **I lluminating the silence: understanding the structure and function of small RNAs.** *Nat Rev Mol Cell Biol* 2007, **8:**23-36.
13. Bentwich I, Avniel A, Karov Y, Aharonov R, Gilad S, Barad O, Barzilai A, Einat P, Einav U, Meiri E, Sharon E, Spector Y, Bentwich Z: **Identification of hundreds of conserved and nonconserved human microRNAs.** *Nat Genet* 2005, **37:**766-770.
14. Lewis BP, Shih IH, Jones-Rhoades MW, Bartel DP, Burge CB: **Prediction of mammalian microRNA targets.** *Cell* 2003, **115:**787-798.
15. Wang X, El Naqa IM: **Prediction of both conserved and nonconserved microRNA targets in animals.** *Bioinformatics* 2008, **24:**325-332.
16. Reinhart BJ, Slack FJ, Basson M, Pasquinelli AE, Bettinger JC, Rougvie AE, Horvitz HR, Ruvkun G: **The 21-nucleotide let-7 RNA regulates developmental timing in *Caenorhabditis elegans*.** *Nature* 2000, **403:**901-906.
17. Valoczi A, Hornyik C, Varga N, Burgyan J, Kauppinen S, Havelda Z: **Sensitive and specific detection of microRNAs by northern blot analysis using LNA-modified oligonucleotide probes.** *Nucleic Acids Res* 2004, **32:**e175.
18. Berezikov E, Cuppen E, Plasterk RH: **Approaches to microRNA discovery.** *Nat Genet* 2006, **38(Suppl):**S2-7.
19. Takada S, Berezikov E, Yamashita Y, Lagos-Quintana M, Kloosterman WP, Enomoto M, Hatanaka H, Fujiwara S, Watanabe H, Soda M, Choi YL, Plasterk RH, Cuppen E, Mano H: **Mouse microRNA profiles determined with a new and sensitive cloning method.** *Nucleic Acids Res* 2006, **34:**e115.
20. Mineno J, Okamoto S, Ando T, Sato M, Chono H, Izu H, Takayama M, Asada K, Mirochnitchenko O, Inouye M, Kato I: **The expression profile of microRNAs in mouse embryos.** *Nucleic Acids Res* 2006, **34:**1765-1771.
21. Schmittgen TD, Jiang J, Liu Q, Yang L: **A high-throughput method to monitor the expression of microRNA precursors.** *Nucleic Acids Res* 2004, **32:**e43.
22. Chen C, Ridzon DA, Broomer AJ, Zhou Z, Lee DH, Nguyen JT, Barbisin M, Xu NL, Mahuvakar VR, Andersen MR, Lao KQ, Livak KJ, Guegler KJ: **Real-time quantification of microRNAs by stem-loop RT-PCR.** *Nucleic Acids Res* 2005, **33:**e179.
23. Cummins JM, He Y, Leary RJ, Pagliarini R, Diaz LA Jr, Sjoblom T, Barad O, Bentwich Z, Szafranska AE, Labourier E, Raymond CK, Roberts BS, Juhl H, Kinzler KW, Vogelstein B, Velculescu VE: **The colorectal microRNAome.** *Proc Natl Acad Sci USA* 2006, **103:**3687-3692.
24. Lu J, Getz G, Miska EA, Alvarez-Saavedra E, Lamb J, Peck D, Sweet-Cordero A, Ebert BL, Mak RH, Ferrando AA, Downing JR, Jacks T, Horvitz HR, Golub TR: **MicroRNA expression profiles classify human cancers.** *Nature* 2005, **435:**834-838.
25. Jay C, Nemunaitis J, Chen P, Fulgham P, Tong AW: **miRNA profiling for diagnosis and prognosis of human cancer.** *DNA Cell Biol* 2007, **26:**293-300.
26. Yin JQ, Zhao RC, Morris KV: **Profiling microRNA expression with microarrays.** *Trends Biotechnol* 2008, **26:**70-76.
27. Rosa A, Brivanlou AH: **MicroRNAs in early vertebrate development.** *Cell Cycle* 2009 in press.
28. Kloosterman WP, Plasterk RH: **The diverse functions of microRNAs in animal development and disease.** *Dev Cell* 2006, **11:**441-450.
29. Asli NS, Pitulescu ME, Kessel M: **MicroRNAs in organogenesis and disease.** *Curr Mol Med* 2008, **8:**698-710.
30. Esquela-Kerscher A, Slack FJ: **Oncomirs: microRNAs with a role in cancer.** *Nature Rev Cancer* 2006, **6:**259-269.
31. Croce CM: **Causes and consequences of microRNA dysregulation in cancer.** *Nat Rev Genet* 2009, **10:**704-714.
32. Drakaki A, Iliopoulos D: **MicroRNA Gene Networks in Oncogenesis.** *Curr Genomics* 2009, **10:**35-41.
33. Latronico MV, Condorelli G: **MicroRNAs and cardiac pathology.** *Nat Rev Cardiol* 2009, **6:**419-29.
34. Pauley KM, Chan EK: **MicroRNAs and their emerging roles in immunology.** *Ann N Y Acad Sci* 2008, **1143:**226-239.
35. Bentwich I, Avniel A, Karov Y, Aharonov R, Gilad S, Barad O, Barzilai A, Einat P, Einav U, Meiri E, Sharon E, Spector Y, Bentwich Z: **Identification of hundreds of conserved and nonconserved human microRNAs.** *Nat Genet* 2005, **37:**766-770.
36. Li SC, Pan CY, Lin WC: **Bioinformatic discovery of microRNA precursors from human ESTs and introns.** *BMC Genomics* 2006, **7:**164.
37. Earley MC, Vogt RF Jr, Shapiro HM, Mandy FF, Kellar KL, Bellisario R, Pass KA, Marti GE, Stewart CC, Hannon WH: **Report from a workshop on multianalyte microsphere assays.** *Cytometry* 2002, **50:**239-42.
38. **Luminex xMAP Technology** [http://www.luminexcorp.com/technology/index.html]
39. Blenkiron C, Goldstein LD, Thorne NP, Spiteri I, Chin SF, Dunning MJ, Barbosa-Morais NL, Teschendorff AE, Green AR, Ellis IO, Tavaré S, Caldas C, Miska EA: **MicroRNA expression profiling of human breast cancer identifies new markers of tumor subtype.** *Genome Biol* 2007, **8:**R214.
40. Taylor JD, Briley D, Nguyen Q, Long K, Iannone MA, Li MS, Ye F, Afshari A, Lai E, Wagner M, Chen J, Weiner MP: **Flow cytometric platform for high-throughput single nucleotide polymorphism analysis.** *BioTechniques* 2001, **30:**661-666. 668-669
41. Prabhakar U, Eirikis E, Davis HM: **Simultaneous quantification of proinflammatory cytokines in human plasma using the LabMAP assay.** *Journal of immunological methods* 2002, **260:**207-218.
42. Mano H, Takada S: **mRAP, a sensitive method for determination of microRNA expression profiles.** *Methods* 2007, **43:**118-122.
43. Takada S, Mano H: **Profiling of microRNA expression by mRAP.** *Nature protocols* 2007, **2:**3136-3145.
44. Merlino G, Helman LJ: **Rhabdomyosarcoma-working out the pathways.** *Oncogene* 1999, **18:**5340-348.
45. Shingara J, Keiger K, Shelton J, Laosinchai-Wolf W, Powers P, Conrad R, Brown D, Labourier E: **An optimized isolation and labeling platform for accurate microRNA expression profiling.** *RNA* 2005, **11:**1461-1470.
46. Anderson J, Gordon T, McManus A, Mapp T, Gould S, Kelsey A, McDowell H, Pinkerton R, Shipley J, Pritchard-Jones K: **Detection of the *PAX3-FKHR* fusion gene in paediatric Rhabdomyosarcoma: a reproducible predictor of outcome?** *Br J Cancer* 2001, **85:**831-35.
47. De Pittà C, Tombolan L, Albiero G, Sartori F, Romualdi C, Jurman G, Carli M, Furlanello C, Lanfranchi G, Rosolen A: **Gene expression profiling identifies potential relevant genes in alveolar rhabdomyosarcoma pathogenesis and discriminates *PAX3-FKHR* positive and negative tumors.** *Int J Cancer* 2006, **118:**2772-81.
48. Romualdi C, De Pittà C, Tombolan L, Bortoluzzi S, Sartori F, Rosolen A, Lanfranchi G: **Defining the gene expression signature of rhabdomyosarcoma by meta-analysis.** *BMC Genomics* 2006, **7:**287.
49. Davicioni E, Finckenstein FG, Shahbazian V, Buckley JD, Triche TJ, Anderson MJ: **Identification of a PAX-FKHR gene expression signature that defines molecular classes and determines the prognosis of alveolar rhabdomyosarcomas.** *Cancer Res* 2006, **66:**6936-46.
50. Romualdi C, Vitulo N, Del Favero M, Lanfranchi G: **MIDAW: a web tool for statistical analysis of microarray data.** *Nucleic Acids Res* 2005:W644-9.
51. Saeed AI, Bhagabati NK, Braisted JC, Liang W, Sharov V, Howe EA, Li J, Thiagarajan M, White JA, Quackenbush J: **TM4 microarray software suite.** *Methods in Enzymology* 2006, **411:**134-93.
52. Tusher VG, Tibshirani R, Chu G: **Diagnosis of multiple cancer types by shrunken centroids of gene expression.** *Proc Natl Acad Sci USA* 2001, **98:**5116-121.
53. Livak KJ, Schmittgen TD: **Analysis of relative gene expression data using real-time quantitative PCR and the 2(-Delta Delta C(T)) Method.** *Methods* 2001, **25:**402-408.

doi: 10.1186/1471-2199-11-44
Cite this article as: Biscontin *et al.*, New miRNA labeling method for bead-based quantification *BMC Molecular Biology* 2010, **11**:44